STUDY OF THE MECHANISMS UNDERLYING HIPPOCAMPAL NEURON SYNAPTOGENESIS

THE ROLES OF NEUROTROPHIN SIGNALING AND MICRORNAS

APPROVED BY SUPERVISORY COMMITTEE

Luis F. Parada, Ph.D.

Gang Yu, Ph.D., Committee Chair

Kimberly Huber, Ph.D.

Jane Johnson, Ph.D.

Dedicated To My Mother, Li Zhang

and My Husband, Peng Yi

ACKNOWLEDGEMENTS

My pursuing for the Ph.D. degree has been a long and challenging journey, and it is definitely not possible without the supports and helps from many people. My sincere gratitude goes to my mother, my husband, all my friends, my great collegues and supervisor for their love, support, and patience over the past years.

This dissertation would not have been possible without the great guidance from my esteemed mentor, Dr. Luis Parada. I was honored to have the opportunity to work in his laboratory. His comments and suggestions throughout my graduate studies have always been extremely perceptive, encouraging and helpful. Not only does he inspire me as an insightful scientist, but also as a very kind and pleasant person.

I would like to sincerely thank my thesis committee members, Dr. Gang Yu, Dr. Kimberly Huber, and Dr. Jane Johnson at UT Southwestern Medical Center at Dallas, for all their excellent advice and supports throughout my graduate studies.

My thanks also go to Dr. Bryan Luikart, who gave me a warm welcome and encouragement when I joined the lab. He is a marvelous friend and collaborator who taught me techniques and had wonderful discussions with me.

My graduate studies would not have been the same without my wonderful colleagues and close friends. I am grateful to everyone in the Parada lab and especially to Dr. Douglas Benson, Jian Chen, Yanjiao Li, Dr. Yun Li, Dr.Lu Lin, Dr. Jing Zhou and Shawna Kennendy for their kindness in all respects everyday.

Finally, I would give my thanks to my family for always being there: My mother always believes in me and gave me unconditional support. My husband, who shares my joy when I am happy, consoles me when I am sad, encourages me when I am depressed, takes care of me when I am sick and stands by me no matter what happens.

STUDY OF THE MECHANISMS UNDERLYING HIPPOCAMPAL NEURON SYNAPTOGENESIS

THE ROLES OF NEUROTROPHIN SIGNALING AND MICRORNAS

by

WEI ZHANG

DISSERTATION

Presented to the Faculty of the Graduate School of Biomedical Sciences
The University of Texas Southwestern Medical Center at Dallas
In Partial Fulfillment of the Requirements
For the Degree of

DOCTOR OF PHILOSOPHY

The University of Texas Southwestern Medical Center at Dallas
Dallas, Texas
July, 2010

STUDY OF THE MECHANISMS UNDERLYING HIPPOCAMPAL NEURON SYNAPTOGENESIS

THE ROLES OF NEUROTROPHIN SIGNALING AND MICRORNAS

Wei Zhang, Ph.D.

The University of Texas Southwestern Medical Center at Dallas, 2010

Mentor: Luis F. Parada, Ph.D.

ABSTRACT

Synapse formation requires contacts between dendrites and axons. Although this process is often viewed as axon mediated, dendritic filopodia may be actively involved in mediating synaptogenic contacts. Brain-derived neurotrophic factor (BDNF) increases the density of dendritic filopodia and the conditional deletion of tyrosine receptor kinase B (TrkB) reduces synapse density *in vivo* (Luikart et al., 2005). Here, we report that TrkB associates with dendritic growth cones and

filopodia, mediates filopodial motility, and does so via the phosphoinositide 3 kinase (PI3K) pathway. We used genetic and pharmacological manipulations of mouse hippocampal neurons to assess signaling downstream of TrkB. Conditional knock-out of two downstream negative regulators of TrkB signaling, Pten (phosphatase with tensin homolog) and Nf1 (neurofibromatosis type 1), enhanced filopodial motility. This effect was PI3K-dependent and correlated with synapse density. Phosphatidylinositol 3,4,5- trisphosphate (PIP3) was preferentially localized in filopodia and this distribution was enhanced by BDNF application. Thus, intracellular control of filopodial dynamics converged on PI3K activation and PIP3 accumulation, a cellular paradigm conserved for chemotaxis in other cell types. Our results suggest that filopodial movement is not random, but responsive to synaptic guidance cues.

In order to further elucidate the mechanisms of BDNF-TrkB-PI3K pathway downstream signaling involved in regulating dendritic filopodial motility, we used a pharmacological approach as well as a gene expression approach to show that Rac1 and RhoA may play a role in this pathway. Rac1 positively regulated dendritic filopodial motility while RhoA had a negative effect. Our data suggest that BDNF-TrkB signaling might function to regulate the balance between Rac1 and RhoA, thus controlling dendritic filopodial motility.

The developing nervous system is shaped by highly orchestrated programs of gene expression. This tight regulation is regulated by various transcriptional and post-transcriptional events that control individual gene expression. The recent discovery of small, non-coding RNAs has greatly expanded our understanding of the mechanisms that regulate gene expression at the post-transcriptional level. Here, I characterized the expression pattern of one neuronal microRNA, miR-381, and used *in vitro* cultured hippocampal neurons to show that miR-381 regulates neurite growth, as overexpression of miR-381 promotes neuronal dendritic branching. The effect of miR-381 on neuronal dendritic branching might be through a net regulation of multiple target genes.

TABLE OF CONTENTS

LIST OF PUBLICATIONS

1. Yi P, **Zhang W (co-first author)**, Zhai Z, Miao L, Wang Y, Wu M. Bcl-rambo beta, a special splicing variant with an insertion of an Alu-like cassette, promotes etoposide- and Taxol-induced cell death. FEBS Lett. 2003 Jan 16;534(1-3):61-8.
2. Xu BE, Stippec S, Lenertz L, Lee BH, **Zhang W**, Lee YK, Cobb MH. WNK1 activates ERK5 by an MEKK2/3-dependent mechanism. J Biol Chem. 2004 Feb 27;279(9):7826-31. Epub 2003 Dec 16.
3. Kwon CH, Luikart BW, Powell CM, Zhou J, Matheny SA, **Zhang W**, Li Y, Baker SJ, Parada LF. Pten regulates neuronal arborization and social interaction in mice. Neuron. 2006 May 4;50(3):377-88.
4. Orvedahl A, Alexander D, Tallóczy Z, Sun Q, Wei Y, **Zhang W**, Burns D, Leib DA, Levine B. HSV-1 ICP34.5 confers neurovirulence by targeting the Beclin 1 autophagy protein. Cell Host Microbe. 2007 Mar 15;1(1):23-35.
5. Luikart BW, **Zhang W (co-first author)**, Wayman GA, Kwon CH, Westbrook GL, Parada LF. Neurotrophin-dependent dendritic filopodial motility: a convergence on PI3K signaling. J Neurosci. 2008 Jul 2;28(27):7006-12.

LIST OF FIGURES

LIST OF TABLES

LIST OF ABBREVIATIONS

ANOVA Analysis of Variance

BDNF Brain-Derived Neurotrophic Factor

CaMKII Calmodulin-dependent protein Kinase II

CB Cerebellum

CDC42 Cell division cycle 42

CKO Conditional knockout

CNS Central Nervous System

CTX Cerebral cortex

DIV Day *in vitro*

DMEM Dulbecco's Modified Eagle's Medium

ERK Extracellular signal-regulated kinase

GAP GTPase-activating protein

GEFs Guanine-nucleotide exchange factors

GFAP Glial Fibrillary Acidic Protein

GFP Green Fluorescent Protein

MAPK Mitogen-Activated Protein Kinase

NF1 Neurofibromatosis type 1

Nf1-/- Nf1 homozygous mutant

NGF Nerve Growth Factor

NT3/4 Neurotrophin 3/4

P0 Postnatal day 0

PBS Phosphate-buffered saline

PI3K Phosphatidylinositol-3-Kinase

PLCγ Phospholipase C γ

PNS Peripheral Nervous System

PSD95 Postsynaptic density protein 95

Rac1 Ras-related C3 botulinum toxin substrate 1

RasGAP Ras GTPase Activating Protein

RhoA Ras homolog gene family, member A

Syn Synaptophysin

TRK Tyrosine Receptor Kinase

WT Wild Type

CHAPTER I

INTRODUCTION

1.1 The neuron, synapse, synapse formation and plasticity.

Neurons are the construction bricks of the nervous system. They are connected to each other through a specific structure called the synapse, through which one neuron can connect to thousands of others. The human brain contains roughly 10^{11} neurons and up to 10^{15} synapses in total (Pelvig et al., 2008). This complicated neuronal network enables us to be able to think, behave and respond to the outside world. In addition, the synapse connection between neurons is dynamic. Neuronal activities elicit new synapse formation, strengthening or eliminating existing synapses, which are the basis for us to learn and memorize things. To understand the mechanisms of learning and memory is the Holy Grail of neuroscience research. At the cell biological level, understanding how synapses are formed and how their dynamics is achieved are the most essential questions to be answered.

All neurons share similar structures, including soma, dendrites and axons (Figure 1.1A). The soma, also called the “cell body”, is the central part of the neuron. It contains the cell nucleus, and therefore is where most protein synthesis occurs. The dendrites of a neuron are cellular extensions with many branches, which in shape and structure are similar to a dendritic tree. The dendrite is where the

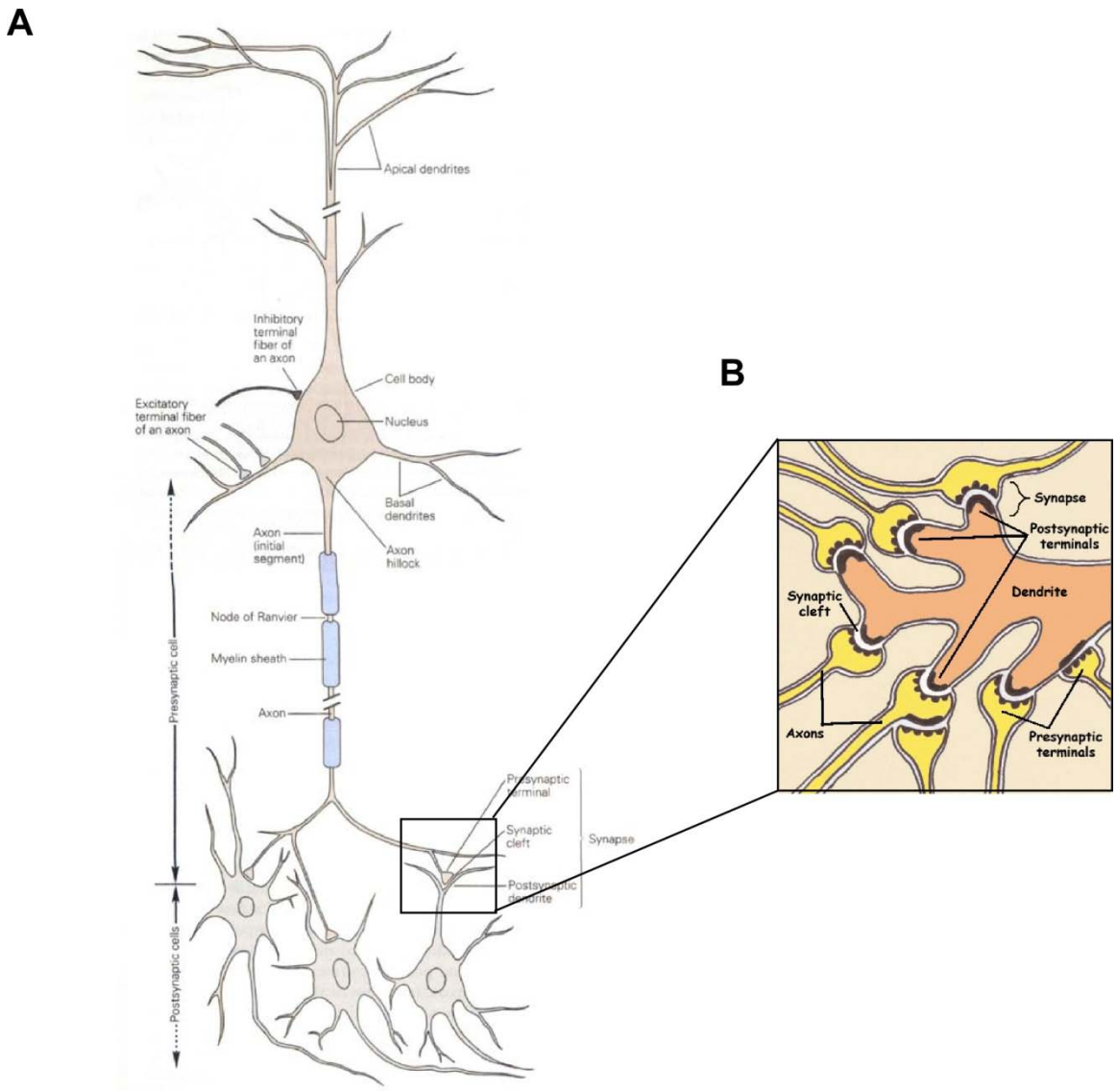

Figure 1.1. Structure of neuron and synapses. (Adapted and modified from *Principle of Neural Science*) A. The structure of a neuron. **B,** The structure of synapses, which are formed between axon boutons and dendritic spines.

majority of the input to the neuron occurs. The axon of a neuron is a cable-like projection that carries nerve signals away from the soma.

A synapse is usually defined by the presence of a presynaptic active zone with synaptic vesicles, a synaptic cleft and a postsynaptic density (PSD) (Figure 1.1B). In the mature brain, most excitatory synapses are formed between axonal boutons and dendritic spines. An electrical pulse is passed from the axon of a presynaptic neuron to the dendrite of a postsynaptic neuron in a uni-directional manner through synapses (Colonnier, 1968; Harris et al., 1992). Most synapses are formed in the early stage of brain development, but synapses can still be formed or eliminated throughout adult life.

The plasticity of the neuronal network in the central nervous system (CNS) is achieved at two levels. First, the strength of an existing synapse can be changed upon repetitive stimuli, for example by a process termed long-term potentiation (LTP). Second, new synapses can be formed or existing synapses can be eliminated, which hugely increases the memory storage capacity of the brain. The dynamics of synapse formation is believed to be mostly due to dendritic spine plasticity (Holtmaat and Svoboda, 2009).

1.2 Dendritic spines and filopodia.

Dendritic spines are specialized protrusions emerging from dendrites, where the majority of excitatory inputs are received by postsynaptic neurons (Nimchinsky et al., 2002). Dendritic spines are first formed in the early postnatal stage and subsequently become functional synapses. Dendritic spines are continuously shaped upon experience and maintained into adulthood. Abnormal spine structures are often associated with neurological disorders such as Down syndrome, Rett syndrome and Fragile X syndrome (Kaufmann and Moser, 2000). Structurally, the hallmark of a dendritic spine is the postsynaptic density (PSD), a unique electron-dense thickening. Various components have been discovered within the PSD, including cell recognition/adhesion molecules, neurotransmitter receptors, ion channels etc.

How dendritic spines are formed and how their plasticity in adult life is regulated are also intriguing questions in neuroscience research. It is believed that dendritic spines originally come from another motile structure within the dendrite called dendritic filopodia. Dendritic filopodia are long, thin and mostly PSD-free protrusions abundantly present in the developing neurons. Dendritic filopodia are highly motile and flexible structures, the average lifetime of which is in the range of minutes to hours (Dailey and Smith, 1996; De Roo et al., 2008; Zuo et al., 2005). During development, dendritic filopodia repeatedly make transient contacts with axons of other neurons. They can pull the axon towards the dendrite, and after the proper choice is made, the filopodia are morphologically and

functionally transformed into spines and then form synapses (De Roo et al., 2008; Maletic-Savatic et al., 1999; Marrs et al., 2001; Trachtenberg et al., 2002; Zuo et al., 2005). However, this process is not always efficient. It has been shown that only 10%-20% of filopodia can eventually form a spine. During early brain development, filopodial motility represents a major advantage because it increases the probability of them reaching a partner and forming a contact. Reduced dendritic filopodial motility often results in reduced synapse formation. For example, it has been shown that elimination of EphBs results in decreased filopodial motility without affecting spine motility, but still causes a reduced rate of synaptogenesis (Kayser et al., 2008).

The mechanisms underlying dendritic filopodia formation, maturation, and the decision to become a dendritic spine are largely unknown. The regulators of dendritic filopodia can be categorized into two classes: (1) Those that potentiate filopodial motility but inhibit spine formation, including Telencephalin, Ezrin, SynGAP and Plk-2 (Furutani et al., 2007; Kumar et al., 2005; Matsuno et al., 2006; Pak and Sheng, 2003; Vazquez et al., 2004). These proteins maintain dendritic filopodia but slow spine maturation, and can cause spine-to-filopodia reversion. (2) Those that promote filopodial motility and also enhance spine formation, which include CamKII, Syndecan-2 and Paralemmin-1 (Arstikaitis et al., 2008; Ethell and Yamaguchi, 1999; Jourdain et al., 2003; Lin et al., 2007). Here, I provide evidence demonstrating that neurotrophin signaling, particularly

the BDNF-TrkB pathway, promotes dendritic filopodial motility and enhances spine/synapse formation (Luikart et al., 2008).

1.3.Neurotrophin and Trk receptor tyrosine kinases.

The neurotrophin family is one of the most important regulators of nervous system development. Neurotrophins belong to a class of growth factors, secreted proteins that signal neurons to survive, differentiate and grow. Various studies show that neurotrophins can regulate neuron survival, development and function. Neurotrophins are usually secreted from target tissue and act to prevent the associated neurons from programmed cell death, thus allowing the neurons to survive. In addition, they have been shown to regulate synapse plasticity at multiple levels upon neuronal activity. Neuronal activity can elicit neurotrophin synthesis, secretion and signaling, which in turn modulates postsynaptic responsiveness, synaptic morphology, presynaptic neurotransmitter release, and membrane excitability (Figure 1.2) (Poo, 2001).

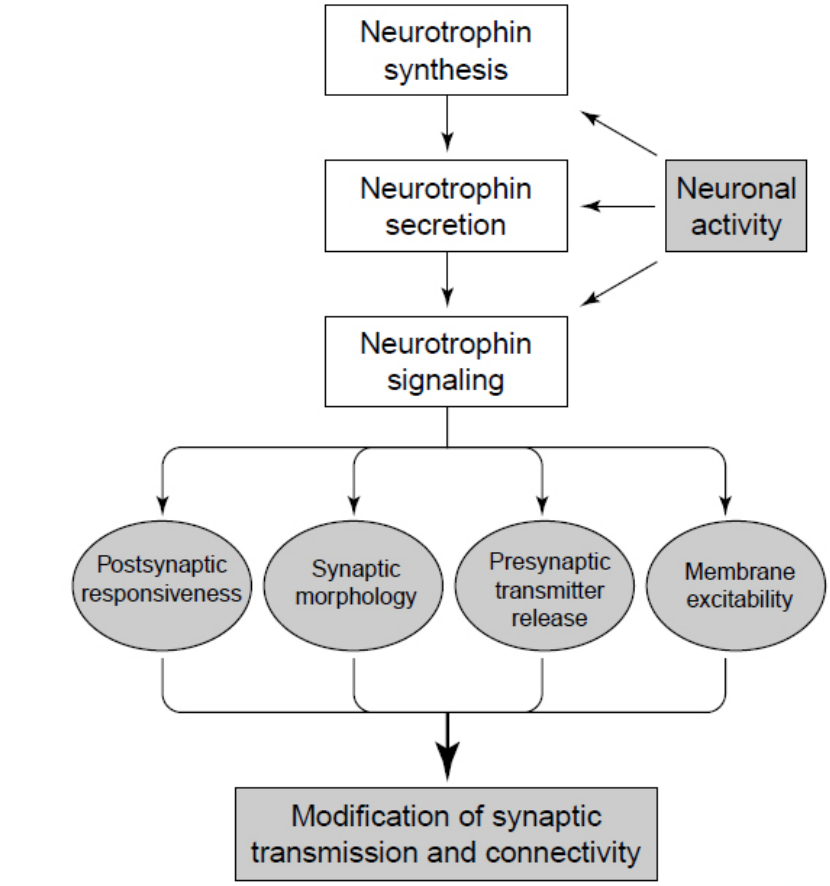

Figure 1.2. Regulation of neurotrophins by neuronal activity and their effects on the synapse. Neurotrophins are regulated by neuronal activity at the level of neurotrophin synthesis, secretion and signaling, which in turn modulate postsynaptic responsiveness, synaptic morphology, presynaptic neurotransmitter release, and membrane excitability.

There are four major members in the neurotrophin family: Nerve growth factor (NGF), brain-derived neurotrophic factor (BDNF), neurotrophin-3 (NT-3), and neurotrophin-4 (NT-4). There are two classes of receptors for neurotrophins: p75NTR and the tyrosine kinases receptors (Trks) (Figure 1.3). p75NTR is a non-specific neurotrophin receptor that binds to all the neurotrophin family members. Trk receptors (TrkA, B and C) tend to bind specifically to only a subset of neurotrophin members (Figure 1.3). NGF binds only to TrkA, BDNF and NT-4 bind only to TrkB, and NT-3 binds to the TrkB and TrkC receptors (Reichardt, 2006).

NGF is secreted by a neuron's target and is essential for the survival and maintenance of both sympathetic and sensory neurons. Upon NGF binding to its high affinity receptor TrkA, the NGF:TrkA complex is internalized into the responsive neurons and trafficked to the cell body, a process thought to be important for the long-distance signaling of neurons (Reichardt, 2006).

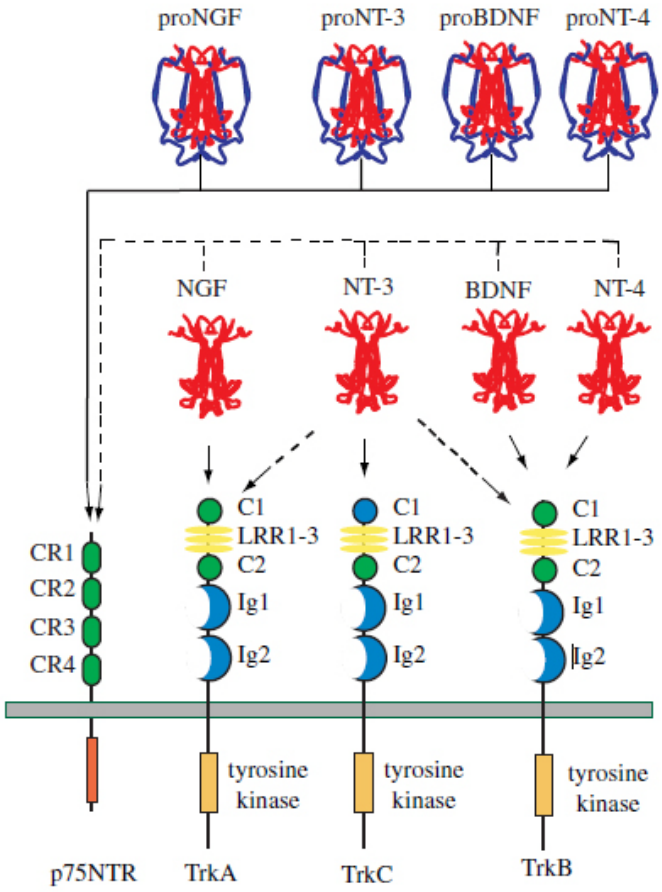

Figure 1.3. Neurotrophins and their receptors. There are four major members in the neurotrophin family: Nerve growth factor (NGF), brain-derived neurotrophic factor (BDNF), neurotrophin-3 (NT-3), and neurotrophin-4 (NT-4). There are two classes of receptors for neurotrophins, p75 and the tyrosine kinases receptors (Trk) (Figure 1.11). p75 is a non-specific neurotrophin receptor that binds to all the neurotrophin members with low affinity. On the contrary, Trk receptors (TrkA, B and C) bind only a subset of neurotrophin members specifically: NGF binds to TrkB only, BDNF and NT-4 bind to TrkB only, and NT-3 binds to both the TrkB and TrkC receptors.

Brain-derived neurotrophic factor (BDNF) is a neurotrophic factor found mostly in the brain, but also in the peripheral nervous system (PNS). It helps to support the survival of existing neurons and facilitates the growth and differentiation of new neurons and synapses through axonal and dendritic sprouting. In the brain, it is active in the hippocampus, cortex, cerebellum and basal forebrain, which are all essential for learning and memory. It is thought to be an important regulator of synapse formation and plasticity (Poo, 2001).

Neurotrophin-3 (NT-3) was the third neurotrophic factor to be characterized, after NGF and BDNF. NT-3, given its ability to activate two of the Trk receptors (TrkB and TrkC), is unique in the number of neurons it can potentially stimulate. Mice without NT-3 have been shown to have loss of proprioceptive neurons and subsets of mechanoreceptive sensory neurons. Neurotrophin-4 (NT-4), also known as NT4, NT5, NTF4, and NT-4/5 is the fourth member of the neurotrophin family, and like BDNF, signals predominantly through the TrkB receptor tyrosine kinase (Reichardt, 2006).

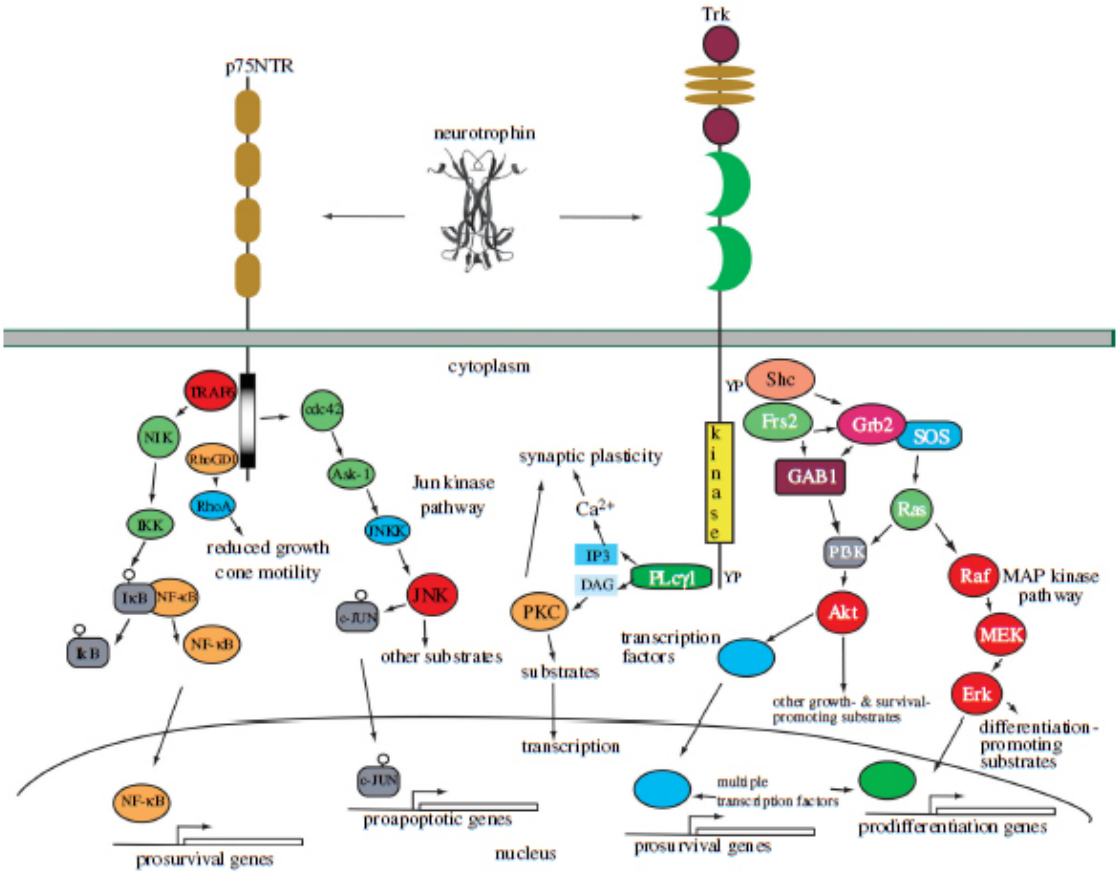

Figure 1.4. Neurotrophins signaling pathways. Binding of neurotrophins to p75 activates the NFκB pathway via TRAP6, and also activate the CDC42 and the JNK pathways to turn on pro-apoptotic genes. Binding of neurotropins to their high affinity Trk receptors activates a number of signaling pathways as well, including PLC-γ pathway, Akt and MAPK pathway.

Binding of neurotrophins to p75NTR has two distinct effects on neurons. p75NTR is able to activate the NFκB pathway via TRAP6, which can facilitate neuron survival. On the other hand, p75 can also activate CDC42 and the JNK pathway to turn on pro-apoptotic genes. Therefore, the effect of p75 on neuronal survival results from the balance between these two opposing pathways (Skaper, 2008). Binding of neurotrophins to their high affinity Trk receptors results in dimerization of the receptors, and subsequent activation of three main signalingpathways, including the Ras-mitogen-activated protein kinase (MAPK) pathway, the phosphatidylinositol 3-kinase (PI3K)-Akt pathway and the PLCγ-Ca^{2+} pathway (Kaplan and Miller, 2000). The recruitment and phosphorylation of Shc adaptor protein leads to the binding of growth factor receptor-bound protein 2 (GRB2), and subsequent activation of the Ras pathway (Huang and Reichardt, 2003). PI3K is activated upon GAB1, IRS1and IRS2 binding to the Trk receptor. Activated PI3K then generates PI3 and activates PI3-dependent protein kinase 1 (PDPK1). Together with PI3, PDPK1 can activate the protein kinase Akt (also known as Protein kinase B) (Yamada et al., 1997). Finally, phosphorylation of TrkB leads to the recruitment and phosphorylation of PLCγ1. Activated PLCγ1 hydrolyzes phosphatidylinositol-4,5-bisposphate (PtIns(4, 5)P_2) to generate inositol-1,4,5-triphosphate (Ins(1,4,5)P_3) and diacylglycerol (DAG). Ins(1,4,5)P3 promotes the release of Ca^{2+} in the cells and activate Ca^{2+} dependent enzymes

such as CaMK (Kaplan and Miller, 2000). A summary of neurotrophin signaling pathways is illustrated in Figure 1.4.

1.4 Neurotrophin and synapse formation/plasticity.

It has been well described that neurotrophins are important regulatory factors for differentiation and survival of neurons. In addition, neurotrophins also act as synaptic modulators by facilitating synapse formation and synapse plasticity (reviewed by (Poo, 2001)). Neurotrophins and their receptors are highly enriched in neurons of both CNS and PNS. Their expression and activity can be regulated by neuronal activity. Secretion of neurotrophins and subsequent activation of their receptors regulates synapse strength as well as modulates the structure of dendrite and axons in multiple neuron types (Poo, 2001).

The important roles of neurotrophins and their receptors in synapse formation and plasticity are indicated by their unique expression pattern and cellular localizations. BDNF is found enriched in the central nervous system neurons, including in hippocampus and cortex (Kaisho et al., 1991). TrkB was found to be expressed in CNS and PNS neurons in both embryonic and adult stages (Klein et al., 1990; Klein et al., 1989). At cellular level, BDNF accumulates axonally within a vesicular compartment and is transported anterogradely and released by

regulated secretary mechanisms in rat brain (Fawcett et al., 1997) and in cultured cortical neurons (Haubensak et al., 1998). TrkB was found in both soma and dendrite in visual cortex (Cabelli et al., 1996). In adult rat central nervous system, TrkB was observed on the surface of neuronal cell bodies, axons and dendrites in almost all neuron types, including cerebral cortex, hippocampus, dendate gyrus, striatum, septal nuclei, substantia nigra, cerebelar purkinje cells and brainstem sensory nuclei (Yan et al., 1997).

In addition to their expression pattern and cellular localization, the expression and activity of BDNF and TrkB can be regulated by neuronal activity. In cultured rat hippocampal neurons, depolarization with high potassium resulted in an increase in the level of BDNF mRNA (Zafra et al., 1990). In rat hippocampus slice culture, a stimulus that induces LTP in CA1 increases the BDNF expression as well (Patterson et al., 1992). It has been shown that kindling induced by electrical stimulation in the ventral hippocampus leads to a dramatic and transient increase of BDNF mRNA level in dentate gyrus, parietal cortex and piriform cortex (Ernfors et al., 1991). It was also observed that BDNF expression can be up-regulated by light stimuli in rat visual cortex (Castren et al., 1992). On the contrary, BDNF mRNA level is reduced in Alzheimer disease hippocampus and temporal cortex (Connor et al., 1997).

In addition to the mRNA level, the secretion of BDNF from neurons can also be controlled by neuronal activity. In hippocampus, BDNF is released from post-synaptic neurons upon high-frequency stimulation of glutamatergic synapses (Hartmann et al., 2001). BDNF can be transported in an anterogradely direction and transferred into postsynaptic neurons in an activity-dependent manner (Kohara et al., 2001).

Various studies using *in vitro* systems suggesting an essential role of BDNF/TrkB signaling in regulating neuronal morphology and synapse formation in different neuronal types. In central nervous system, BDNF may act as a cue to guide neuronal growth. Using a neuronal culture system, BDNF was observed to be released from a single cells and it acts locally to elicits neighbor neurons dendritic growth (Horch and Katz, 2002). Treating the neurons with BDNF induces structural instability in dendrites and spines, which is thought to be a basis for neuron morphological remodeling and synapses plasticity upon neuronal activity (Horch et al., 1999). BDNF is able to promote dendritic growth in developing visual cortex (McAllister et al., 1995), and function in both sensory and motor neurons in the limb bud to facilitate axon growth (Tucker et al., 2001). Blocking the BDNF-TrkB signaling using TrkB-IgG results in changes of dendritic spine morphology in Purkinje cells (Shimada et al., 1998) and also inhibits the formation of ocular dominance column (Cabelli et al., 1997). In *Xenopus* optic neurons, increasing BDNF levels significantly increased both axon arborization

and synapse number (Alsina et al., 2001). In some case, the low-affinity receptor of neurotrophin p75NTR was involved to mediate dendrites growth together with TrkB, which might be independent on neurotrophins (Hartmann et al., 2004). Depending on different neuronal types or different compartments of the same neuron, neurotrophins can have different effects. For example, in *Xenopus* retinal ganglion cells (RGC), BDNF is able to differentially modulate axonal and dendritic arborization in opposing manners (Lom and Cohen-Cory, 1999).

BDNF/TrkB signaling pathway is also well documented to be an important pathway to regulate synapse plasticity by facilitating synapse strengthening. Application of BDNF in slice cultured hippocampus produces a rapid and dramatic increase of synaptic transmission, as shown by increased frequency and amplitude of excitatory postsynaptic currents (Levine et al., 1995), which subsequently increases the synapse strength at the Schaffer collateral-CA1 synapses (Kang and Schuman, 1995). In TrkB knockout mice, the Ca^{2+}-evoked synaptic transmission, the fast glutamatergic and GABAergic receptor level are impaired in forebrain neurons (Carmona et al., 2003). At the neuromuscular junction, treatment with BDNF potentiates the synapse activity as well (Lohof et al., 1993).

There are many mechanism identified underlying the effect of BDNF/TrkB signaling in the regulation of neuronal morphology, synapse formation and

synapse plasticity. In slice cultured hippocampus, the increase of dendritic spine density upon treatment of BDNF was shown to be through activating the ERK1/2 signaling (Alonso et al., 2004). It has also been shown that BDNF regulates dendritic filopodia growth depending on the proper localization of mRNA in the dendrites (Eom et al., 2003). BDNF can regulates filopodial length and number through a Rho kinase-dependent mechanism, in which actin depolymerizing factor (ADF)/cofilin is required for this effect (Gehler et al., 2004).

For the regulation of synapse plasticity, activation of TrkB signaling at post-synaptic neurons clusters the excitatory and inhibitory neurotransmitter, hence modulates the synapse transmission (Elmariah et al., 2004). In hippocampal slice culture, BDNF enhances neurotransmitter release by increasing the number of docked vesicles at the active zones in the excitatory synapses (Tyler and Pozzo-Miller, 2001). In developing cortical neurons, BDNF signaling was shown to enhance and maintain the expression of AMPA receptor-associated PDZ proteins, which subsequently increases the protein level of AMPA receptor subunits GluR1 and GluR2/3 (Jourdi et al., 2003). In neuromuscular junction, TrkB regulates postsynaptic acetylcholine receptor (AChR) clustering in the muscle cells upon activation by neurotrophins (Gonzalez et al., 1999).

In addition to all the results from *in vitro* system, genetic deletion of BDNF and TrkB provides more solid evidences to support their function in synapse

formation and synapse plasticity. In BDNF knockout mice, LTP was observed to be dramatically reduced in both homo- and heterozygous mice using a slice cultured hippocampus system. This reduced LTP can be restored in these neurons by re-expression of BDNF using virus infection method (Korte et al., 1995; Korte et al., 1996). Furthermore, adding recombinant BDNF protein into the culture can rescue the LTP as well, indicating an acute role of BDNF in hippocampal synaptic function (Patterson et al., 1992).

Using electron microscopy, TrkB knockout animals that survived until postnatal day 13 were shown to have a reduced number of hippacampal Schaffer collateral excitatory synapses (Martinez et al., 1998). However, the straight knockout of TrkB animal is overall unhealthy, so it is possible that the defects in synapse number seen in these animals are due to a second effect. This problem was solved by generating a serial of conditional knockout TrkB knockout animals. Deletion of TrkB in cerebellum leads to reduced amounts of GABAergic synapses in the inhibitory interneurons (Rico et al., 2002). Deleting TrkB specifically in either pre- or post-synaptic neurons or both in the hippocampus neurons revealed that TrkB has an autonomous role in regulating synapse numbers and it is required in both pre- and post-synaptic neurons (Luikart et al., 2005).

CHAPTER II

MATERIALS AND METHODS

Mice.

TrkB$^{flox/flox}$, *Nf-1*$^{flox/flox}$, and *Pten*$^{flox/flox}$ mice have all been described previously (Kwon et al., 2006a; Luikart et al., 2005; Zhu et al., 2001). Mutant mice were generated by crossing parents that were homozygous for the loxP alleles. All mouse procedures were approved by institutional animal care and advisory committees at the University of Texas Southwestern Medical Center and Oregon Health & Sciences University.

Constructs.

TrkB cDNAs including point mutations were PCR cloned from previously described adenoviral genomic DNA or plasmids (Atwal et al., 2000) (sense, ACCATGTCGCCCAGGTGGCAT; TrkB wild type (WT), TrkB Y490F, and TrkB K538N antisense, GTCGACCCTAGGATGTCCAGGAA; TrkB Y785F and TrkB Y785/490F antisense, GTCGACCCTAGGATGTCCAGGTA). PCR products were cloned into pGEM-T easy (Promega), removed with *Eco*RI/*Sal*I, and cloned into the same sites of pEYFP-N1 (Clontech).

All the mCherry fused small GTPases and their mutants were generated by first cloning mCherry cDNA into pCMV plasmid using XbaI and EcoRI to get a pCMV-mCherry, and then cloning wildtype Rac1, RhoA or CDC42 and their constitutive active mutant, dominant negative mutant forms with EcoRI and

BamHI into pCMV-mCherry. The point mutation for the constitutive active mutant and dominant active mutant was introduced by the 5' primer of the small GTPases. The 5' primer for the small GTPases are listed below:

RhoA-forward-EcoRI	CGG AAT TCA TGG CTG CCA TCA GGA AGA AAC TGG TG
RhoA(V14)-forward-EcoRI	CGG AAT TCA TGG CTG CCA TCA GGA AGA AAC TGG TGA TTG TTG GTG ATG TAG C
RhoA(N19)-forward-EcoRI	CGG AAT TCA TGG CTG CCA TCA GGA AGA AAC TGG TGA TTG TTG GTG ATG GAG CTT GTG GTA AGA ATT G
Rac1-forward-EcoRI	CGG AAT TCA TGC AGG CCA TCA AGT GTG TGG TGG TG
Rac1(V12)-forward-EcoRI	CGG AAT TCA TGC AGG CCA TCA AGT GTG TGG TGG TGG GAG ACG TAG C
CDC42-forward-EcoRI	CGG AAT TCA TGC AGA CAA TTA AGT GTG TTG TTG TTG
CDC42(V12)-forward-EcoRI	CGG AAT TCA TGC AGA CAA TTA AGT GTG TTG TTG TTG GTG ATG TTG C
CDC42(N17)-forward-EcoRI	CGG AAT TCA TGC AGA CAA TTA AGT GTG TTG TTG TTG GTG ATG GTG CTG TTG GTA AAA ATT G

To generate the miR-381 over-expression construct, the stem loop sequence of miR-381 is cloned into a pCMV (Clontech) plasmid with DraI and BglII sites. The primer sequence is listed below:

Forward: CGG TTT AAA ACA CAG AGC TTT ATT C

Reverse: CGA GAT CTT ATA CAA GGA ATA AAG

To generate the miR-381 sponge construct, two complementary long single stranded DNAs were designed with 6 tandem miR-381 binding sites separated with a spacer sequence, which is flanked by DraI and BglII. The two single stranded DNAs were annealed and ligated into the pCMVU6 (gift from Eric Olson lab) backbone with DraI and BglII. The sense single stranded DNA sequence is below (181bp):

5'-CGG TTT AAA ACA GAG AGC TTT ATT CCT TGT ATA TTT TAC AGA GAG CTT TAT TCC TTG TAT ATT TTA CAG AGA GCT TTA TTC CTT GTA TAT TTT ACA GAG AGC TTT ATT CCT TGT ATA TTT TAC AGA GAG CTT TAT TCC TTG TAT ATT TTA CAG AGA GCT TTA TTC CTT GTA TAA GAT CTC G-3'

To generate the BDNF3'UTR fusion luciferase reporter, ~2.9kb BDNF'UTR (from mouse BDNF transcripti variant 1) was subcloned to the 3' end of a CMV promoter driven luciferase reporter plasmid. The primer sequence used is listed below:

Forward: TGGATTTATGTTGTATAGATTATATTG

Reverse: TAGAACCTGTATTTACAATAGGCTTC

Small GTPases activity assay.

Small GTPases activity is determined using Active GTPase Pull-Down and Detection Kits from Thermo Scientific Inc. Cell lysates were obtained using standard cell lysate buffer and then incubated with either Pak1 p21-binding domain (Pak1-PBD) conjugated beads to pull down Rac1 and CDC42, or Rhotekin Rho-binding domain (Rhotekin-RBD) conjugated beads to pull down RhoA. The pulled down proteins sample will be analyzed using western blotting with antibody against Rac1, RhoA and CDC42.

Cell line, Primary cell culture and live imaging.

COS7 cells and NG108 cells lines have been used and cultured according to the standard protocol. These cell lines were transfected using lipofactamine 2000 (Invitrogen). Serum-containing dissociated hippocampal cultures were prepared from postnatal day 1 (P1) to P3 mouse pups and transfected at 4–6 d *in vitro* (DIV) using calcium phosphate as described previously (Luikart et al., 2005). Live imaging at 10–11 DIV was performed using the 63x objective of the LSM510 confocal microscope equipped with a motorized stage, objective heater (temperature control mini, 37.5°C), stage heater (temperature control, 37°C), and humidified climate control chamber (temperature overheat, 1.5°C, CTI controller 3700, 5% CO2). With these settings, the neurons were maintained at an actual

temperature of 37°C. All imaging was performed without changing cell-culture media. Images of up to eight cells were captured per imaging session using LSM510 software with the MultiTime Module at a resolution of 640x480, an electronic zoom of 2.5x, and a scan speed of 2.56_m/s. For each neuron, a Z-stack of seven images (Z-step, 0.6 μm) was captured using 1–4% argon laser power with a pinhole of 2.4 μm. Thus, protrusions appeared in at least two images of the stack, and the entire dendritic region remained in the plane of the Z-stack. All equipment was from Zeiss.

Organotypic hippocampal slice cultures.

Slice cultures were prepared from P5 Sprague Dawley rats and transfected using the Helios Gene Gun (Biorad) as described previously. Live imaging was performed using the 63x water-immersion objective with an Axioskop 2 FS microscope (Zeiss) equipped with a motorized stage (Applied Scientific Instrumentation), inline solution heater (Warner Instruments; bath temp, 35°C), spinning disk unit (Solamere Technology), and an XR/Mega10 CCD camera (Stanford Photonics). Imaging was performed in a solution containing (in mM) 125 NaCl, 25 $NaHCO_3$, 2.5 KCl, 1.25 NaH_2PO_4, 2.0 $CaCl_2$, 1.0 $MgCl_2$, and 25 D-glucose, bubbled with 95% O_2/5% CO_2. Images of a single field of view were captured per imaging session using QED In Vivo software. For each neuron, a Z-stack of 20–30 images (Z-step, 0.4 μm) was captured using a 33 ms exposure time

and signal averaging of four images. Thus, protrusions appeared in at least two images of the stack and the entire dendritic region remained in the plane of the Z-stack.

Imaging quantification.

We imaged the cultures at a time (10 DIV) when spine formation has not yet occurred and filopodia are the predominant dendritic protrusion. We thus defined filopodia as any dendritic protrusion under 10 μm in length. We quantified filopodial turnover as the average of the sum of new filopodia appearing and the number of filopodia eliminated per dendrite length every 5 min for a total of 30 min. This measurement was performed manually using the manual object counting feature of MetaMorph. Filopodial motility was calculated as the average of the absolute value of the sum of changes in filopodial lengths per dendrite length every 5 min for a total of 30 min. The length of each filopodia was measured by manual tracing using MetaMorph. The relative fluorescence of dendritic versus filopodial pleckstrin homology (PH)-green fluorescent protein (GFP) was quantitated by manually tracing the parent dendrite and the filopodia arising from this dendrite, and using the color profiler plugin for Image J. The fluorescence index was defined as filopodial 488/568 ratio divided by the dendritic 488/568 ratio. Measurements were performed by an investigator blind to experimental conditions.

Immunocytochemistry.

Neurons were prefixed with 4% paraformaldehyde in PBS at a 1:1 ratio with cell culture media (37°, 2 min) followed by a change into 37°C 4% paraformaldehyde for 5 min. Using this protocol, we observed minimal filopodial collapse; however, no fixation protocol completely maintained filopodia as observed in living cells. After fixation, cells were washed for 5 min with PBS, 5 min with 0.3% Triton X-100 in PBS, and blocked with 6% NGS in PBS for 30 min. Primary antibodies were applied overnight at 4°C in blocking solution. All antibodies were used at the following concentrations: postsynaptic density-95 (PSD-95; Affinity Bioreagents; MA1-046) at 1:400; synaptophysin (Zymed; 18-0130) at 1:800; and anti-TrkB at 1:100 (a gift from David Kaplan, Hospital for Sick Children, Toronto, Ontario, Canada). Secondary Cy3 anti-mouse and Cy5 anti-rabbit antibodies were applied for 30 min (The Jackson Laboratory). Cells were washed 3x5 min after each antibody application.

Northern blotting

20μg of total RNA was resolved on 15% urea/polyacrylamide gels and transferred to Hybond membrane (Amersham). RNA was crosslinked by UV cross-linking (1000 μJ). Membranes were prehybridized in hybridization buffer (5xSSC, 20 mM Na_2HPO_4 pH 7.2, 7% SDS, 2x Denhardt's solution) for at least 2 h at 50° C.

Small RNAs were detected using P^{32} end-labeled antisense DNA oligonucleotides (5'-ACAGAGAGCTTGCCCTTGTATA-3') in hybridization buffer overnight at 50° C. U6 probe was used as loading controls. Membranes were washed 4x in non-stringent wash solution (3x SSC, 25 mM NaH_2PO_4 pH 7.5, 5%SDS, 10x Denhardt's solution) followed by one wash in stringent wash solution (1xSSC, 1%SDS). The membrane was exposed to phosphorimager plates.

miR-381 Real-time PCR

Total RNA from neuronal cultures was isolated using TRIZOL and treated with DNase to remove genomic DNA. Real-time PCR was performed using a miR-381 specific Real-time PCR kit from Applied Biosystems.

In-situ hybridization

In-situ hybridizations were performed in 10-mm cryosections from adult mouse brain. Sections were fixed in 4% paraformaldehyde and acetylated in acetic anhydride/triethanolamine, followed by washes in PBS. Sections were then pre-hybridized in hybridization solution (50% formamide, 5X SSC, 0.5 mg/mL, yeast tRNA, 1 x Denhardt's solution) at 25°C below the predicted Tm value of the LNA probe for 30 min. Probes (3 pmol) (LNA miRCURY probe; Exiqon) were DIG-labeled (DIG Oligonucleotide Tailing Kit; Roche Applied Sciences) and

hybridized to the sections for 1 h at the same temperature as pre-hybridization. After post-hybridization washes in 0.1X SSC at 55°C, the *in-situ* hybridization signals were detected using the tyramide signal amplification system (Invitrogen) with Alexa 488 according to the manufacturer's instructions. Immunostaining with various neuronal markers was performed after the post-hybridization washes with Alexa 555. For double *in-situ* hybridization, GFAP, beta-tubulin III and claudin 11 antisense probes will be biotin labeled and hybridized to the section together with DIG-miR-381 probe. DIG and biotin will then be detected by immunostaining with secondary antibodies conjugated with Alexa 488 and 555, respectively. Slides were mounted in Vectashield with DAPI (Vector Inc.) and analyzed with an LSM510 Meta confocal microscope.

CHAPTER III

NEUROTROPHIN-DEPENDENT DENDRITIC FILOPODIAL MOTILITY: A CONVERGENCE ON PI3K SIGNALING.

** Work described in this chapter was performed in collaboration with Bryan Luikart and is published as “Neurotrophin-dependent dendritic filopodial motility: a convergence on PI3K signaling”. J Neurosci. 2008 Jul 2;28(27):7006-12.

Introduction

The establishment of appropriate synaptic connections between neurons during development is a prerequisite for normal nervous system function, beginning with contact between presynaptic elements and motile dendritic filopodia (Dailey and Smith, 1996; Fiala et al., 1998; Niell et al., 2004; Ziv and Smith, 1996). Neural activity in developing networks must involve extracellular cues that guide filopodial motility. Activity-dependent release of BDNF, a 13.5 kDa neurotrophin, is an attractive candidate for this purpose. *In vitro* application of BDNF elicits filopodia and spine formation (Dasgupta and Gutmann, 2003; Eom et al., 2003; Ji et al., 2005). Furthermore, conditional ablation of the high affinity BDNF receptor, tyrosine receptor kinase B (TrkB), reduces synaptic density indicating its participation in hippocampal synapse formation *in vivo* (Luikart et al., 2005). Thus, the interaction of BDNF with TrkB could drive activity-dependent synaptic morphogenesis (Cohen-Cory, 2002; Patapoutian and Reichardt, 2001; Poo, 2001). TrkB activation drives signaling through the phospholipase Cγ (PLCγ), phosphoinositide 3 kinase (PI3K), and Ras pathways. These signaling pathways

are highly regulated and mediate context-dependent cellular responses including differentiation, survival, growth, and synaptic potentiation. For example, the neurofibromatosis type 1 (Nf1) tumor suppressor functions as a Ras GTPase-activating protein (GAP) that negatively regulates Ras signaling (Zhu et al., 2001). The loss of Nf1 results in neurotrophin-independent survival of neurons (Vogel et al., 1995). The lipid phosphatase, phosphatase with tensin homolog (Pten) opposes PI3K signaling by catalyzing the conversion of phosphatidylinositol 3,4,5-trisphosphate (PIP3) into phosphatidylinositol 4,5-bisphosphate (PIP2). Pten overexpression inhibits neurotrophin-dependent growth and differentiation (Musatov et al., 2004), whereas conditional deletion of Pten in the hippocampus and cortex results in neuronal hypertrophy and behavioral abnormalities reminiscent of human autism (Kwon et al., 2006a). These observations and the fact that mutations in BDNF, TrkB, Pten, and Nf1 are associated with impaired cognitive function in humans could indicate a convergence on a common mechanism (Butler et al., 2005; North et al., 1997; Yeo et al., 2004). Despite extensive knowledge of downstream TrkB signaling, the molecular pathways underlying dendritic filopodial motility and synapse formation are unknown. To identify the signaling pathways involved in TrkB-mediated synapse formation, we imaged dendritic filopodia and synapses in hippocampal neuronal cultures. To alter molecules involved in TrkB signaling, we over-expressed TrkB mutant cDNAs, and used cre-mediated knockdown of TrkB, Pten, or Nf1 in neurons

cultured from loxP-generated germline alleles. We also used pharmacological inhibitors to complement the genetic studies. Deletion of TrkB, Pten, or Nf1 all caused abnormal dendritic filopodial motility, and altered excitatory synapse formation by a common PI3K-dependent mechanism.

Results

TrkB containing puncta traffic to dendritic growth cones and filopodia in hippocampal neurons

We hypothesized that TrkB plays an important role in regulating synaptogenesis, therefore we first examined TrkB subcellular localization dynamics in hippocampal neurons. We generated a C-terminal yellow fluorescent protein (YFP)-tagged TrkB. To reduce the signaling contribution by the endogenous TrkB receptor, we used primary cultured neurons from homozygous $TrkB^{loxP}$ mice and cotransfected Cre-dsRed, to knockout TrkB in the neurons, and TrkB-YFP. We found that DsRed and YFP colocalized in a diffuse pattern throughout the neurons. As shown in Figure 3.1, YFP and dsRed labeled the whole dendritic structure including the dynamic structures: growth cones and dendritic filopodias. We then performed live cell imaging for the transfected neurons at the stage of DIV10. We found that TrkB-YFP concentrated in the highly motile puncta and these TrkB-YFP puncta were transported in both anterograde and retrograde

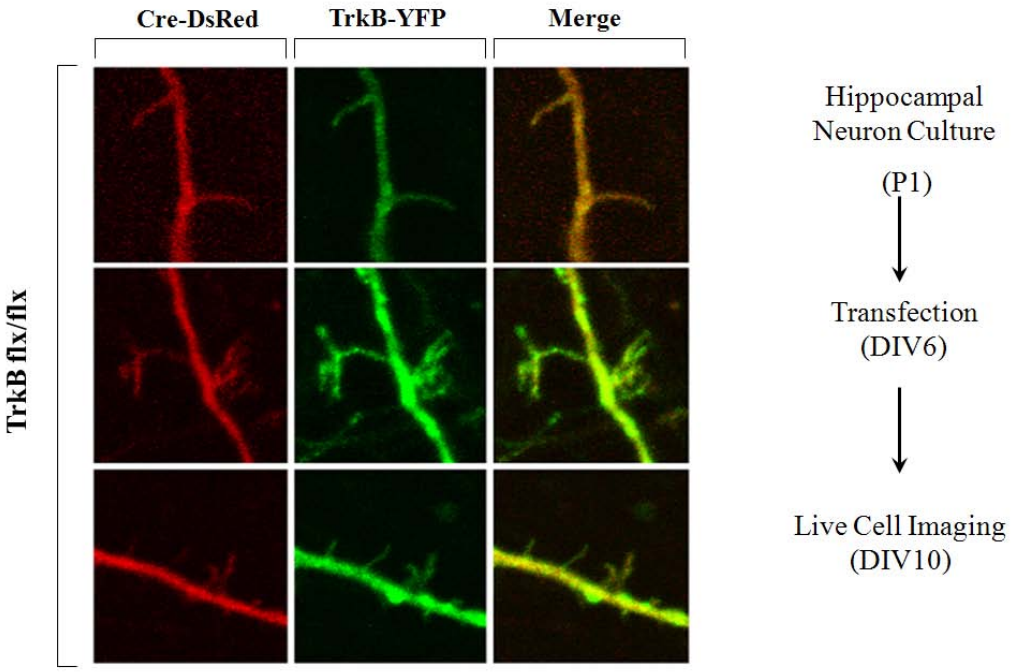

Figure 3.1. Transfection of Cre-DsRed and TrkB-YFP into TrkB flx/flx neurons. Transfection of Cre-DsRed and TrkB-YFP into in vitro cultured hippocampal neurons at DIV 6. DsRed and YFP label the entire neuron structure including growth cones and filopodia structures.

directions in the shafts of the primary dendrites (Figure 3.2 A and B). To be certain that those puncta were indeed representing TrkB, we performed immunocytochemistry using TrkB antibody. As shown in Figure 3.3, TrkB immunostaining shows the same pattern as the TrkB-YFP, which is enriched in puncta structure.

The TrkB-YFP puncta were not stable, traveling anterogradely at 1.008±0.082μm/s and retrogradely at 0.988±0.071μm/s (mean±SEM; n=50 and 51 puncta from 6 cells, respectively). Puncta movement appeared to be saltatory with brief pauses in movement followed by rapid transport. We also found that the TrkB-YFP puncta traveled in and out of dendritic growth cones and filopodia at a slower velocity (Figure 3.2 C and D). In secondary dendrites with growth cones and filopodia, the TrkB-YFP puncta moved at 0.015±0.002μm/s (mean±SEM; n=85 from 3 cells). The movement of TrkB-YFP puncta was reduced in dendritic growth cones and filopodia compared to that in primary dendrites, which suggests that TrkB is trafficking to and from these dynamic structures. The velocities measured for TrkB motility in the primary dendrite are within the ranges defined as active transport by kinesin and dynein (Hill et al., 2004).

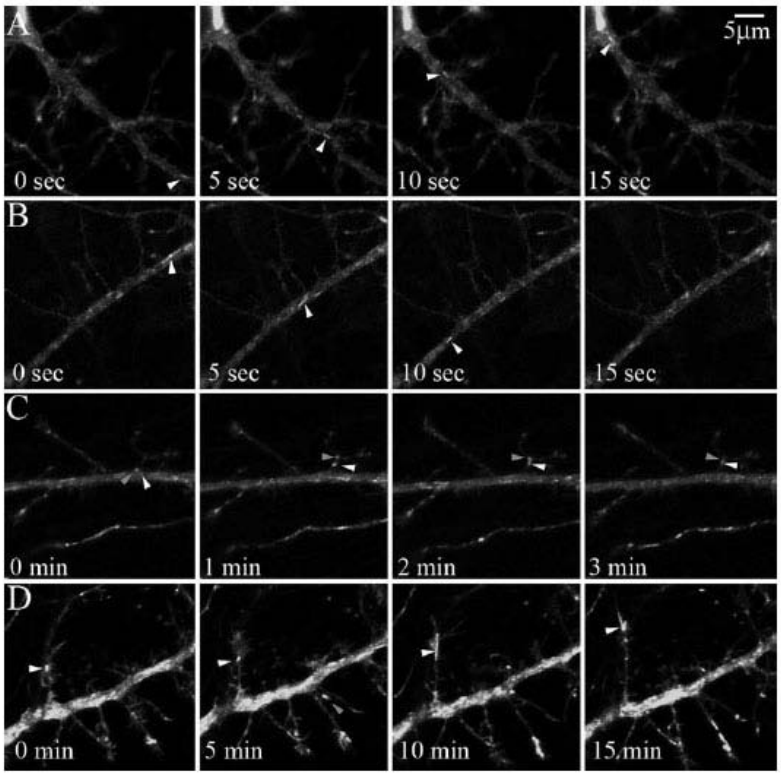

Figure 3.2. TrkB-YFP puncta are rapidly transported within primary dendrites and stable in dendritic growth cones and filopodia. ***A***,***B***,We observed TrkB puncta being rapidly transported in both the retrograde (***A***, arrowheads) and anterograde (***B***, arrowheads) directions. Within primary dendrites, TrkB puncta traveled at an average velocity of 1.008±0.082µm/s in the anterograde and 0.988±0.071µm/s in the retrograde direction (mean±SEM; *n*=50 and 51 puncta from 6 cells, respectively). ***C***, ***D***, At longer time intervals (1 and 5 min), we observed that TrkB puncta were less mobile in immature dendritic branches, growth cones, and filopodia (arrowheads). In these structures, TrkB puncta moved at an average velocity of 0.015±0.002µm/s (mean±SEM; *n*=85 puncta from 3 cells).

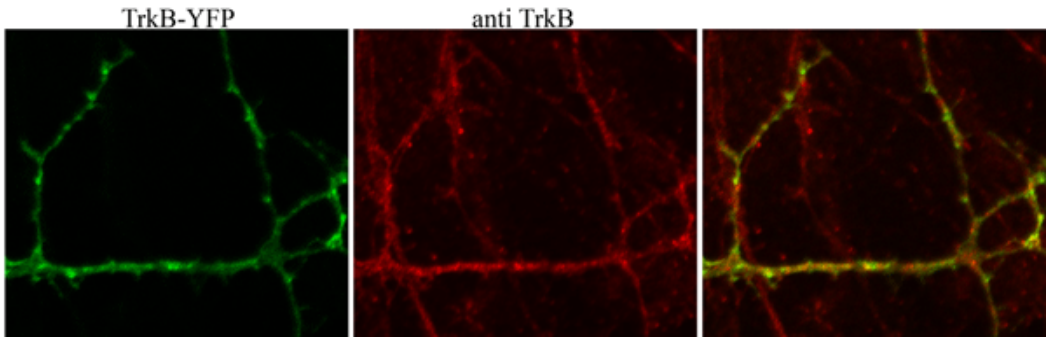

Figure 3.3. TrkB Immunocytochemistry. Cultures transfected with TrkB-YFP were fixed and immunohistochemistry for TrkB performed. We found that the TrkB-YFP puncta were immunopositive confirming that the GFP signal corresponds to TrkB expression. Further we saw a similar pattern of punctate staining in neighboring non-transfected neurons.

TrkB signaling mediates filopodial motility

TrkB can activate various downstream signaling pathways including the PI3K, MAPK, and PLC-γ pathways (Figure 3.4). TrkB, a receptor tyrosine kinase, phosphorylates and activates various substrates using different tyrosine residues in the intracellular domain. Y490 is used to phosphorylate the substrate that activates the PI3K and MAPK pathways, whereas Y785 is used to activate the PLC-γ pathway (Figure 3.4). Therefore, one can easily mutate these different tyrosine residues to block different downstream signaling pathways. We used this strategy to generate different point mutation forms of TrkB fused with YFP at the C-terminal. We obtained the original cDNAs of the TrkB point mutation forms from Dr. David Kaplan's lab (Atwal et al., 2000).

To examine the roles of different downstream pathways in TrkB signaling, we used TrkB mutant cDNAs that disrupt specific downstream pathways, fused in frame with an enhanced-YFP (Atwal et al., 2000). These YFP-fused mutants also allowed us to study neuronal structure dynamics. The relative activity of the mutant proteins was first assessed by transfection of the TrkB-YFP fusion proteins into NG108 cells in the presence of BDNF (50 ng/ml, 10min) (Figure 3.5).

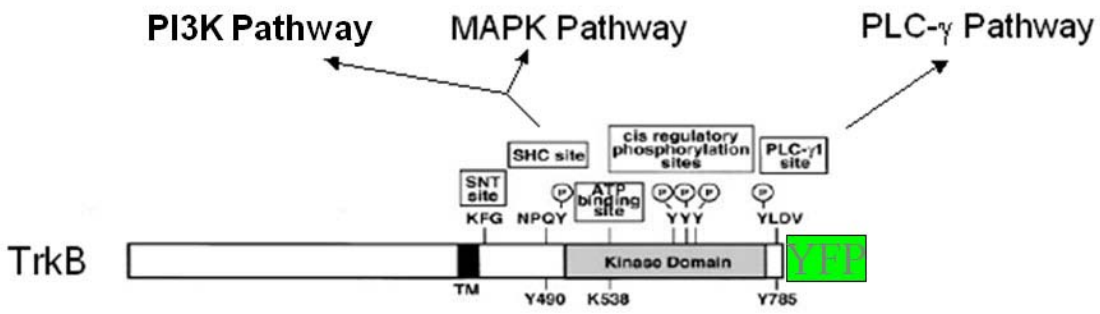

Figure 3.4. TrkB activated signaling pathway. TrkB phosphorylates and activates different substrates using different tyrosine residue in the intracellular domain. Y490 is used to phosphorylate the substrate that activates the PI3K and MAPK pathways, whereas Y785 is used to activate the PLC-γ pathway.

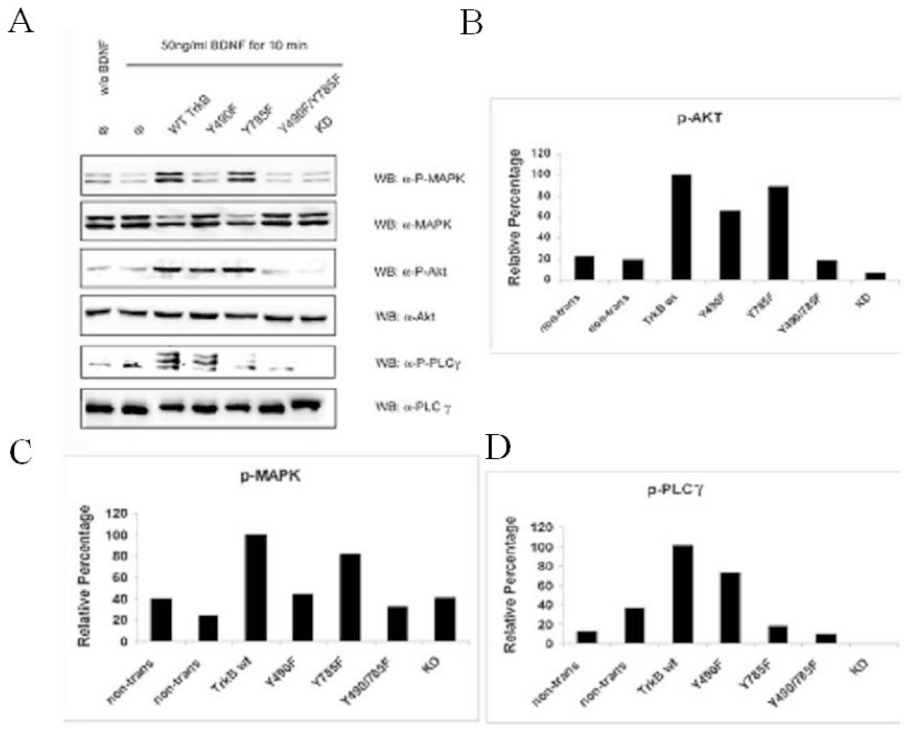

Figure 3.5. TrkB mutants block specific downstream signaling pathways. (A) TrkB-YFP increased phosphorylation of mitogen-activated protein kinase (MAPK), AKT, and PLC-γ, whereas a kinase dead receptor, incapable of binding ATP (TrkB K538N-YFP), did not support phosphorylation of these downstream effectors. Mutation of the TrkB Shc/FRS-2 binding site (TrkB Y490F-YFP) selectively inhibited phosphorylation of extracellular signal regulated kinase (ERK) and AKT, whereas mutation of the PLC-γ binding site (TrkB Y785F-YFP) abolished PLC-γ phosphorylation and the double mutant TrkB Y490F/Y785F abolished all BDNF-induced phosphorylation. **(B-D)** Quantification of the biochemistry assay in **(A).**

As anticipated, TrkB-YFP increased phosphorylation of mitogen-activated protein kinase (MAPK), AKT, and PLC-γ, whereas a kinase dead receptor incapable of binding ATP (TrkB K538N-YFP), did not support phosphorylation of these downstream effectors. Mutation of the TrkB Shc/FRS-2 binding site (TrkB Y490F-YFP) selectively inhibited phosphorylation of ERK and AKT, whereas mutation of the PLC-γ binding site (TrkB Y785F-YFP) abolished PLC-γ phosphorylation. The double mutant TrkB Y490F/Y785F abolished all BDNF-induced phosphorylation (Figure 3.5).

To test whether TrkB puncta in dendritic growth cones and filopodia influence structural dynamics, we analyzed filopodial motility (Fig. 3.6, Table 3.1), which is enhanced by BDNF (50 ng/ml). Overexpression of wild-type TrkB cDNA (TrkB-YFP) increased filopodial motility, whereas the kinase dead receptor reduced filopodial motility below the level of wildtype cells, consistent with a dominant negative activity (Table 3.1). Overexpression of the kinase dead receptor also resulted in decreased filopodial density (0.31/μm TrkB-YFP vs 0.09/μm TrkB K538N; $p<0.00004$) and increased filopodial length (2.66 μm TrkB-YFP vs 5.04 μm TrkB K538N; $p<0.0004$. To examine which signaling pathways were responsible for the effects of TrkB on dendritic filopodia, we expressed the TrkB mutants in cre-dsRed-positive $TrkB^{flox/flox}$ hippocampal neurons so that we could blunt background effects of the wildtype receptor. We

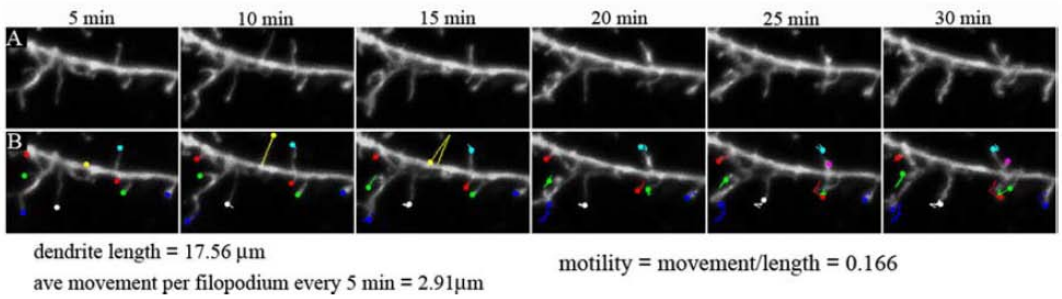

Figure 3.6. Dendritic filopodial motility quantification. **(A)** Time-lapse images of dendrites from neurons expressing GFP. **(B)** Filopodial motility was calculated as the average of the absolute value of the sum of changed filopodial lengths per dendrite length every 5 min for a total of 30 min. The colored dots represent the tip of each filopodia and the corresponding line shows the distance the filopodia travels over time. For this example, the dendritic segment is 17.56 µmlong. The average distance each filopodia moves every 5 min is 2.91µm, and the motility is 0.166 (2.91/17.56).

	Motility mean ± variance (*n*)	*p* value	% of control	Implicated pathway
GFP	0.218 ± 0.008 (27)			
GFP + BDNF (50 ng/ml)	0.386 ± 0.019 (11)	$6.11 \times 10^{-4**}$	177%	PLCγ, ERK, PI3K
TrkB WT	0.354 ± 0.015 (8)	$2.76 \times 10^{-2*}$	162%	PLCγ, ERK, PI3K
TrkB Y490/785F	0.178 ± 0.017 (7)	9.75×10^{-1}	82%	PLCγ, ERK, PI3K
TrkB K538N	0.094 ± 0.004 (7)	$4.93 \times 10^{-2*}$	43%	PLCγ, ERK, PI3K
TrkB Y490F	0.215 ± 0.011 (10)	1.00	99%	ERK, PI3K
TrkB Y785F	0.346 ± 0.027 (8)	$4.66 \times 10^{-2*}$	158%	Not PLCγ
GFP + DMSO	0.246 ± 0.017 (24)			
TrkB WT + DMSO	0.468 ± 0.010 (7)	$1.76 \times 10^{-4**}$	190%	PLCγ, ERK, PI3K
Nf1 KO + DMSO	0.368 ± 0.012 (12)	$2.87 \times 10^{-2*}$	150%	ERK, PI3K
Pten KO + DMSO	0.474 ± 0.018 (14)	$2.32 \times 10^{-6**}$	193%	PI3K
TrkB WT + PD98059 (10 μM)	0.409 ± 0.025 (9)	$4.19 \times 10^{-3**}$	166%	Not ERK
Nf1 KO + PD98059 (10 μM)	0.356 ± 0.010 (13)	5.56×10^{-2}	144%	Not ERK
Pten KO + PD98059 (10 μM)	0.439 ± 0.009 (11)	$1.11 \times 10^{-4**}$	178%	Not ERK
TrkB WT + LY294002 (10 μM)	0.154 ± 0.004 (12)	1.83×10^{-1}	63%	PI3K
Nf1 KO + LY294002 (10 μM)	0.194 ± 0.025 (13)	7.97×10^{-1}	79%	PI3K
Pten KO + LY294002 (10 μM)	0.156 ± 0.004 (15)	1.39×10^{-1}	63%	PI3K

Table 3.1. PI3K mediates dendritic filopodial motility. (Legend is on the next page)

Table 3.1. PI3K mediates dendritic filopodial motility.

The average filopodial motility values for all genetic and pharmacological manipulations performed on the dissociated hippocampal neurons are shown. Compared with the GFP control, both the application of exogenous BDNF and the overexpression of TrkB WT enhanced filopodial motility, implicating the PLCγ, Erk, and PI3K pathways in motility regulation. Expression of TrkB Y785F, but not TrkB Y490F, supported enhanced motility, indicating that the PI3K or ERK pathways (not PLCγ) are primarily responsible for this effect. The expression of the kinase dead point mutation (TrkB K538N) resulted in a reduction of filopodial motility indicating the dominant negative role of this receptor. Compared with control, the overexpression of TrkB WT, knock-out of Nf1, and knock-out of Pten all supported an increase in filopodial motility. In the presence of the Erk inhibitor PD98059 these genetic manipulations still caused an increase in filopodial motility. However, in the presence of the PI3K inhibitor LY294002, this increase was completely abolished. Together, these results indicate that PI3K signaling mediates enhanced dendritic filopodial motility (statistics using a one-way ANOVA and Dunnett's *post hoc* test against either the GFP or GFP+DMSO control).

**Significant at the 5% level; **significant at the 1% level.*

found that, whereas introduction of the PLCγ signaling mutant caused a similar enhancement of filopodial motility compared with TrkB-YFP, overexpression of the Ras/MAPK/PI3K signaling-deficient TrkB cDNA did not support the enhancement of motility (Table 3.1). These data confirm TrkB activity in filopodial motility and refine its signaling requirement for the Ras pathway.

TrkB Y490 has two major bifurcating effector pathways: PI3K and Raf/ERK (Atwal et al., 2000). To distinguish between these downstream pathways, we used specific pharmacological inhibitors (Alessi et al., 1995; Eberwine et al., 2001; Vlahos et al., 1994). The ERK inhibitor [2-(2-amino-3-methyoxyphenyl)-4*H*-1-benzopyran-4-one (PD98059), 10 μM] had no effect on TrkB-mediated filopodial motility, whereas blockade of PI3K signaling (LY294002 [2-(4-morpholinyl)-8-phenyl-4*H*-1-benzopyran-4-one], 10μM) completely prevented TrkB-mediated enhancement of filopodial motility (Table 3.1). Thus, consistent with the TrkB mutant studies, the Ras and PI3K pathways are critical, whereas Raf/ERK signaling is dispensable.

To examine the *in vivo* relevance of our observations, we turned to genetic systems using mouse conditional knock-outs. The Nf1 tumor suppressor encodes a Ras-GAP that is a known negative regulator of Trk family receptor signaling (Dasgupta and Gutmann, 2003). The Pten tumor suppressor negatively regulates

PI3K signaling (Wu et al., 1998). Thus, elimination of either of these two tumor suppressors results in constitutive activation of the Ras and PI3K pathways, respectively. We reasoned that if reduction of TrkB activity diminished filopodial motility, then genetic activation of the Ras/PI3K pathway should have an opposing effect. We cultured hippocampal neurons from *Nf1*$^{flox/flox}$ and *Pten*$^{flox/flox}$ mice to examine the consequence of genetic ablation on filopodial motility (Backman et al., 2001; Zhu et al., 2001). GFP-cre mediated recombination of either Nf1 or Pten resulted in increased filopodial motility (Table 3.1). Thus, genetic activation of the PI3K pathway demonstrates its role in filopodial motility downstream of TrkB. We next examined the activity of pharmacological inhibitors on genetically modified neurons. The PI3K antagonist eliminated the enhanced filopodial motility that resulted from Nf1 or Pten ablation. Conversely, ERK pathway inhibition had no discernible effect when compared with Nf1 or Pten knock-out neurons (Table 3.1). Thus, both our pharmacologic and genetic data converge to identify a requirement for PI3K activity in mediating neuronal filopodial motility.

Synaptic marker density correlates with filopodial motility

Filopodial motility and turnover can be associated with synapse formation (Ziv and Smith, 1996). We therefore examined whether the observed changes in filopodial motility correlated with synapse number as assessed by

immunocytochemical overlap of presynaptic and postsynaptic proteins (synaptophysin and PSD-95). TrkB overexpression increased synaptic density when compared with neurons expressing GFP alone (0.287 ± 0.023 synapses/μm^2 vs 0.218 ± 0.021 synapses/μm^2, respectively; $p<0.05$ using a two-tailed two-sample equal-variance Student's *t* test). Consistent with our observations using TrkB mutant cDNAs in filopodial motility, the PI3K deficient mutant, but not the PLCγ deficient mutant, resulted in decreased PSD-95/synaptophysin overlap (Fig. 3.7). Thus, changes in synapse density paralleled changes in filopodial motility in a TrkB-dependent manner. These data were further validated in similar studies using conditional Pten and Nf1 neurons in which synaptic density was enhanced. We next examined synapse formation *in vivo*. In the CNS dendritic spines are considered to reflect synaptic density. Using the Golgi technique, we examined dendritic spine density in the dentate gyrus of mice with conditional hippocampal ablation of TrkB (Luikart et al., 2005), Pten (Kwon et al., 2006a), and Nf1 (Zhu et al., 2001). We found that TrkB ablation resulted reduced dendritic spines, whereas Pten and Nf1 abated brains exhibited increased numbers of spines. Thus, *in vivo*, TrkB and downstream effector activity governs normal dendritic spine formation (Figure 3.8).

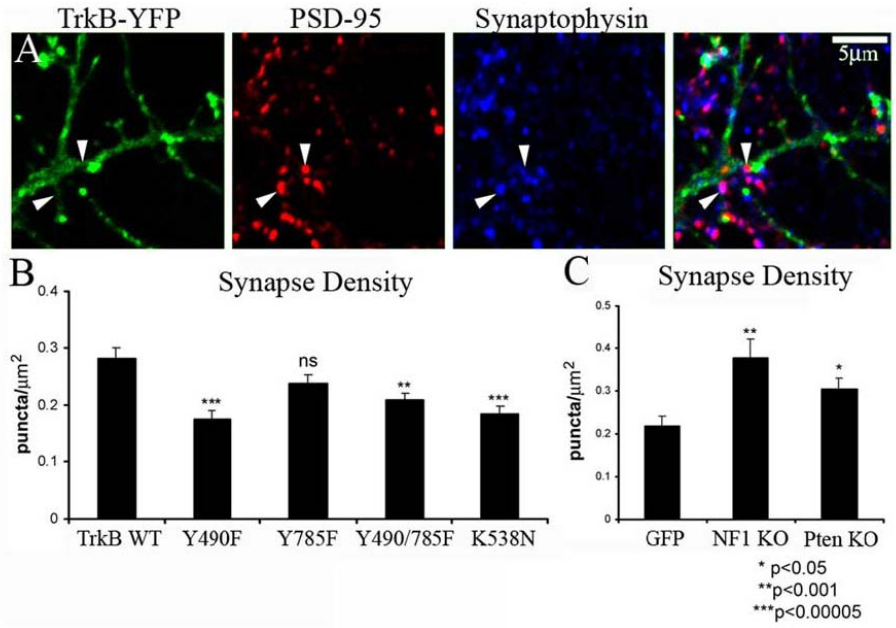

Figure 3.7. Synapse density in TrkB, Nf1, and Pten mutant hippocampal neurons. (A) Immunohistochemistry for PSD-95 (red) and synaptophysin (blue) in neurons expressing the TrkB-YFP fusion protein (green). Synapses were identified for quantification as points at which the red, green, and blue signals overlapped (**A**, arrowheads). Synaptic density was measured for TrkB-YFP (WT; *n*=80 neurons), TrkB Y490F-YFP (*n*=79), TrkB Y785F-YFP (*n*=77), TrkB Y490/785F-YFP (*n*=78), and TrkB K538N-YFP (KD, *n*=77). The Y490F, Y490/785F, and K538N mutations resulted in a significant decrease in synapse number when compared with TrkB-YFP. **(B)** However, TrkB Y785F-YFP was not significantly different from TrkB-YFP. Synapse density was measured for neurons from Nf1 flox and Pten flox animals transfected with GFP or GFP-cre. **(C)** The deletion of both Nf1 (*n*=30 neurons) and Pten (*n*=30) resulted in a significant increase in synaptic density when compared with GFP (*n*=34; *p* values calculated using two-sample equal variance *t* test).

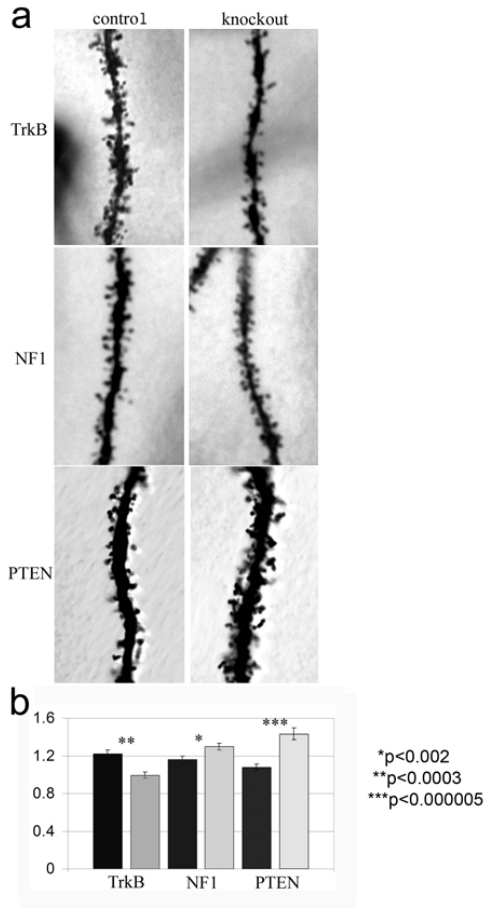

Figure 3.8. Spine Density in TrkB, NF1 and Pten mutant dentate gyrus granule neurons *in vivo*. Representative images of Golgi stained dendrites from the outer molecular layer of $TrkB^{flx/flx}$ x SynapsinI-cre, $NF1^{flx/flx}$ x GFAP-cre, and $Pten^{flx/flx}$ x NSE-cre animals **(a)**. For the TrkB x SynapsinI-cre there is a 22.8% reduction in granule neuron dendritic spine density (n = 24 control dendrites and n = 44 KO dendrites) (consistent with previously published results for the CA1 region (Luikart et al., 2005)). For the NF1 x GFAP-cre there was a 10.6% increase in spine density (n = 33 control dendrites and n = 38 KO dendrites). The 24.9% increase in Pten x NSE-cre animals has been previously published (Kwon et al., 2006) (n = 27 control dendrites and n = 24 KO dendrites). **(b)** (p-values calculated using two-sample equal variance t-test).

Accumulation of PIP3 in filopodia

PI3K and Pten direct the spatial accumulation of PIP3 and, thus, actin polymerization in *Dictyostelium discoideum* during chemotaxis (Iijima and Devreotes, 2002). To test whether a similar focal accumulation of PIP3 accompanies filopodial motility, we examined the cellular localization of the PIP3 indicator, PH-GFP (Jin et al., 2000). For these experiments, we used biolistic gene transfer into organotypic hippocampal cultures. We used the ratio of PH-GFP and monomeric Cherry fluorescent protein (mCherry) as a measure of PIP3 accumulation. To address whether this ratio was altered between filopodia and the parent dendrite, we defined the fluorescence index as the filopodial GFP/cherry ratio divided by the dendritic GFP/cherry ratio. We found a significant accumulation of PH-GFP in dendritic filopodia (1.349±0.0261) compared with GFP (1.028±0.0236, mean±SEM; $p < 1.0 \times 10^{-5}$) (Fig. 3.9). Treatment of slice cultures with BDNF produced a 1.682±0.0442-fold increase in filopodial PH-GFP (mean±SEM; $p<1.0 \times 10^{-5}$, BDNF-treated versus untreated slices) (Fig. 3.9). Thus, PI3K activity downstream of TrkB increased PIP3 within dendritic filopodia indicating activity of the receptor within this dynamic structure.

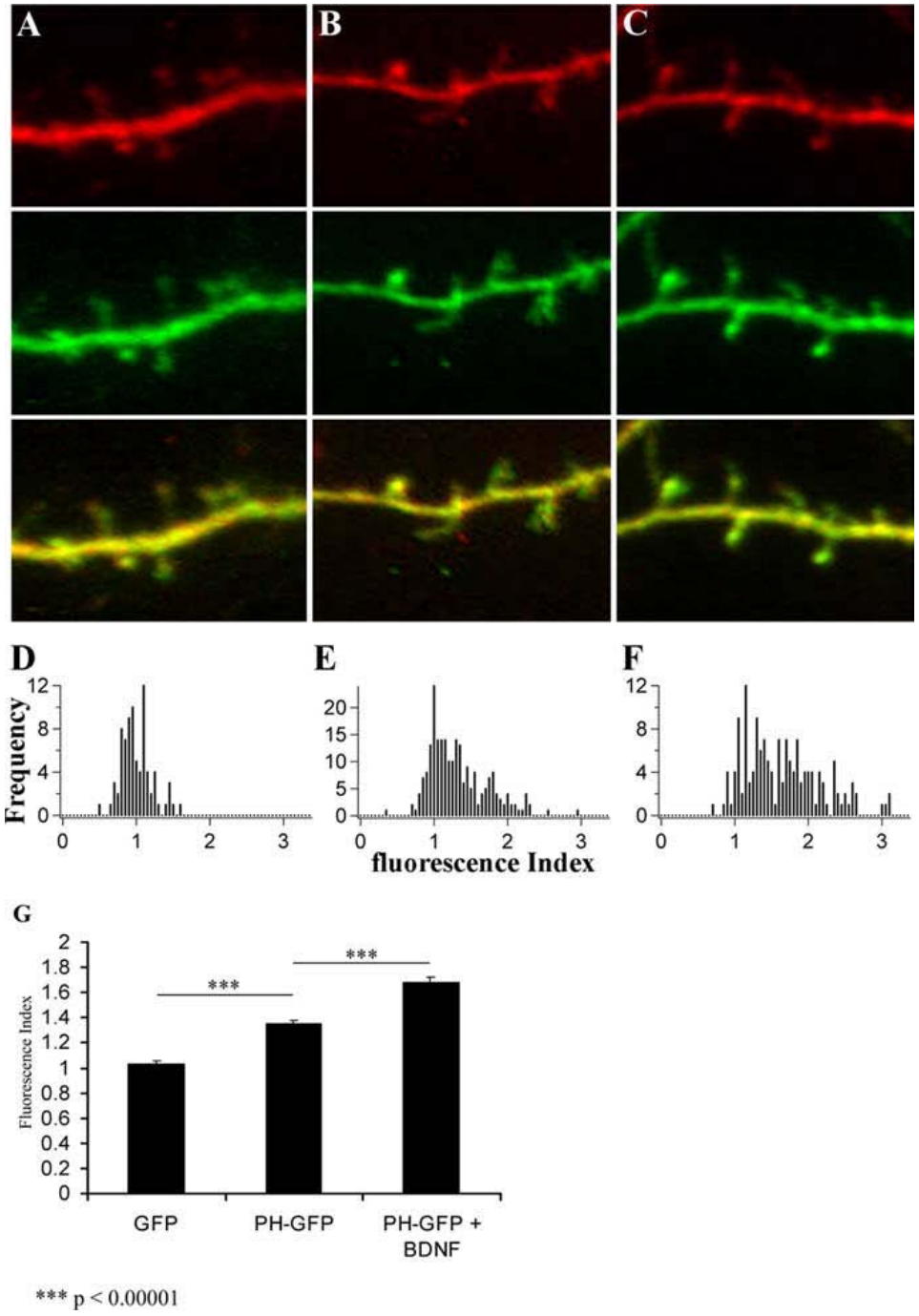

Figure 3.9. BDNF-dependent accumulation of PH-GFP in dendritic filopodia.

(Legend is on the next page)

Figure 3.9. BDNF-dependent accumulation of PH-GFP in dendritic filopodia. **(A-C)**, Representative images of dendritic segments expressing GFP and mCherry **(A),** PH-GFP and mCherry **(B),** and PH-GFP and mCherry from BDNF-treated (50 ng/ml for 4–6 h) slices **(C).** The distribution of GFP fluorescence in filopodia relative to dendrites was quantified as the filopodial 488/568 ratio divided by the dendritic 488/568 ratio (fluorescence index). Thus, numbers>1 indicate increased relative GFP fluorescence in the filopodia versus dendrites. **D–F**, The distribution of these values was plotted for GFP (**D**; *n*=79 filopodia), PH-GFP (**E**; *n*=230 filopodia), and BDNF treated PH-GFP (**F**; *n*=151 filopodia). The equal distribution of GFP and mCherry between dendrites and filopodia is indicated by the distribution of the fluorescence index around 1. The shift in this distribution toward numbers>1 in the PH-GFP condition indicates accumulation of PIP3 in dendritic filopodia. Application of BDNF further increased the filopodial PIP3 levels when compared with untreated cells (*p* values calculated using the Newman–Keuls test).

Discussion

TrkB localization

TrkB is necessary for the normal development of synaptic connectivity of the hippocampus *in vivo* (Luikart et al., 2005). We first examined the cellular localization of TrkB-YFP in primary hippocampal cultures during synaptogenesis. In agreement with the study by Gomes et al. (Gomes et al., 2006), TrkB was trafficked in anterograde and retrograde directions through both dendrites and axons. Furthermore, once in filopodia and dendritic growth cones, TrkB receptors appeared to stabilize. Using antibodies specific to the extracellular domain of TrkB, Gomes et al. (2006) (Gomes et al., 2006) reported that puncta in dendritic growth cones and filopodia are exposed to the extracellular environment. Therefore, it appears that these receptors are poised to transduce signals in response to extracellular BDNF. Our calculated velocity of TrkB puncta movement in dendrites was faster than that observed by Gomes et al. (Gomes et al., 2006) in axons. This difference is not unexpected as we performed live imaging at 37°C whereas they recorded at room temperature. Our results demonstrate that TrkB is associated with dendritic growth cones and filopodia, and is thus in position to regulate dynamics of those structures.

PI3K signaling and filopodial motility

Our results demonstrate that PI3K is the mediator of TrkB-dependent filopodial motility. The mechanism by which PI3K activity is linked to cytoskeletal dynamics has been studied in cellular chemotaxis (Sasaki and Firtel, 2006; Song and Poo, 2001; Van Haastert and Devreotes, 2004). In response to extracellular guidance molecules, the cellular distribution of PI3K and Pten regulates the spatial distribution of PIP3 in *Dictyostelium* (Huang et al., 2003; Iijima and Devreotes, 2002). Accumulation of PIP3 results in actin polymerization and forward movement of the cell. In dendritic filopodia, the accumulation of PIP3 and the regulation of motility by Pten and PI3K suggests that filopodial dynamics use an analogous mechanism. Trk receptors form complexes with components of the PI3K signaling cascade (Howe et al., 2001) and associate with dendritic filopodia. BDNF application results in filopodial PIP3 accumulation, increased motility, and increased filopodial number. BDNF is a synaptically released molecule with limited diffusion capability *in vivo*, suggesting that its dendritic growth promoting properties are likely localized. Furthermore, the molecular machinery underlying BDNF enhancement of filopodial motility has been conserved in chemotaxis indicating that it may elicit directional movements of dendritic filopodia. This chemoattractive aspect of BDNF has been documented for growing axons (Song and Poo, 2001). However, this is the first study to link spatially restricted TrkB signaling to PI3K activation, PIP3 accumulation, and dendritic filopodial motility.

Although it is unclear how PI3K activity and PIP3 accumulation may lead to actin polymerization, it is ultimately the activation of Rac, Rho, and Cdc42 that mediate actin dynamics (Etienne-Manneville and Hall, 2002) and dendritic growth (Threadgill et al., 1997). PI3K is required for Rac activation and critical for the activation of Rac by Ras (Cantrell, 2001; Innocenti et al., 2003). T-cell lymphoma invasion and metastasis 1 (Tiam1), the Rac1-GEF (guanine-nucleotide exchange factor) that mediates activity-dependent dendritic elaboration, is regulated directly by TrkB, PIP3, and calcium through NMDA receptor activation (Fleming et al., 2004; Innocenti et al., 2003; Miyamoto et al., 2006). Thus, an attractive model would place Tiam1 as the nexus for neurotrophin and glutamate regulation of dendritic growth.

Filopodial motility and synapse formation

The enhancement of filopodial motility resulting from the overexpression of TrkB, or reduction of Pten and Nf1, correlated with increased synaptic density. In our studies, enhancement of motility correlates positively with ultimate stabilization of synaptic contacts. BDNF-dependent activation of TrkB promoted dendritic filopodial motility and synapse formation via the activation of PI3K. For synaptogenesis to occur, there must not only be contact between neurons, but also

stabilization of contacts and accumulation of synaptic proteins (Akins and Biederer, 2006). Although our data addresses the molecular pathways by which TrkB mediates enhanced filopodial motility and synapse formation, it does not address mechanisms by which TrkB may contribute to the stabilization of synaptic contacts. Nonetheless, it appears that Trk signaling does contribute to stabilization (Hu et al., 2005; Vaillant et al., 2002). The PI3K pathway has been highly conserved throughout evolution, mediating chemoattractive responses in *Dictyostelium*, neutrophil chemotaxis, wound healing, and tumor cell metastasis (Merlot and Firtel, 2003; Van Haastert and Devreotes, 2004). This paradigm suggests that BDNF not only enhances filopodial motility, but may use chemoattractive molecular pathways allowing for directed movement of filopodia toward sites of BDNF release. BDNF synthesis and secretion is regulated by neuronal activity (Hartmann et al., 2001; Kohara et al., 2001; Patterson et al., 1992). Thus, filopodial motility may not be random, but influenced by extracellular cues allowing for the activity-dependent sculpting of neuronal connectivity during development and activity-dependent remodeling of synaptic connectivity in the adult (Luikart and Parada, 2006). Indeed, recent evidence suggests that filopodia are not distributed randomly with respect to mature synaptic boutons (Nagerl et al., 2007; Toni et al., 2007). Although BDNF is an attractive candidate to mediate this extracellular targeting, other neuromodulators also influence PI3K-dependent and -independent pathways that are important for

dendritic development. For example, glutamate and GABA influence dendritic development through non-PI3K pathways. Thus, a variety of extracellular influences likely converge on intracellular pathways mediating directional growth and movement. The modulation of dendritic development and synapse formation can have global consequences on CNS function. Accordingly, human mutations in the TrkB, Pten, and Nf1 genes cause cognitive impairment (Butler et al., 2005; North et al., 1997; Yeo et al., 2004). Our data provide a putative link between the function of these genes and normal synaptic development.

CHAPTER IV

NEUROTROPHIN-TRKB SIGNALING CONTROLS DENDRITIC FILOPODIAL MOTILITY THROUGH SMALL GTPASES RAC1 AND RHOA

Introduction

Previous study in our lab (Luikart et al., 2005) and the data in chapter 3 demonstrated that activity-dependent release of brain-derived neurotrophic factor (BDNF) plays an important role in regulating the dendritic filopodial motility in developing hippocampal neurons, where BDNF functions through its high affinity receptor, TrkB, and activates the downstream PI3K signaling pathway (Luikart et al., 2008). PI3K then catalyzes Phosphatidylinositol 4,5-trisphosphate (PIP2) to Phosphatidylinositol 3,4,5-trisphosphate (PIP3) (Toker and Cantley, 1997). We showed that PIP3 was preferentially localized in filopodia and this distribution was enhanced by BDNF application. We concluded that the intracellular control of filopodial dynamics converged on PI3K activation and PIP3 accumulation, a cellular paradigm conserved for chemotaxis in other cell types. However, the mechanism by which PI3K and PIP3 control filopodial dynamics is still unknown.

Possible candidates that act at the downstream of TrkB-PI3K signaling include small GTPase family of proteins, which have long been shown to be the essential regulators of cell dynamic structure formation and motility (Rossman et al., 2005). The most important small GTPases that regulate cell dynamic structure include RhoA, Rac1 and CDC42. Small GTPases cycle between inactive (GDP-bound) and active (GTP-bound) conformation (Figure 4.1). When they are active, Rac1, CDC42, and RhoA alter the cytoskeleton to mediate various cellular processes,

including cell morphological changes, cell migration, filopodia formation, and dynamics (Ridley et al., 2003; Rossman et al., 2005). The exchange reactions of bound GDP for GTP by small GTPases are regulated by guanine-nucleotide exchange factors (GEFs). On the contrary, the exchange reaction of bound GTP for GDP, carried out by small GTPases, is regulated by GTPase activating proteins (GAPs) (Ridley et al., 2003; Rossman et al., 2005). GEFs and GAPs are important regulators of the action of small GTPases. RhoA, Rac1 and CDC42 have been shown to regulate neuronal morphology and dynamics in various neuronal cell types. For instance, Rac1 was shown to regulate neurotrophin-3 (NT3)-activated Schwann cell migration through a GEF family protein, Tiam1 (Yamauchi et al., 2005).

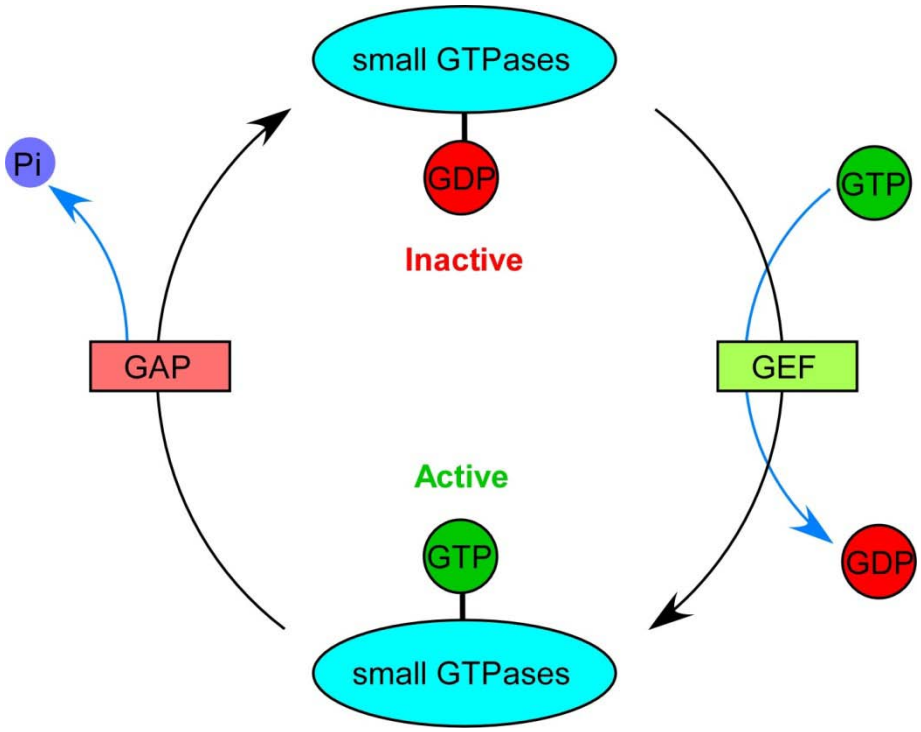

Figure 4.1. Small GTPases cycle. Small GTPases cycle between inactive (GDP-bound) and active (GTP-bound) conformation. The exchange reactions of bound GDP for GTP by small GTPases are regulated by guanine-nucleotide exchange factors (GEFs). Likewise, the exchange reaction of bound GTP for GDP by small GTPases are regulated by GTPase activating proteins (GAPs).

Small GTPases are considered as final effectors that receive upstream signals and then directly regulate cytoskeleton and cell motility. It has also been shown that TrkC, another neurotrophin family member that activates similar signaling pathways as TrkB, regulates Schwann cell morphology and migration through activation of a small GTPase, Rac1 (Yamauchi et al., 2005). It has also been shown that in different neuron types, small GTPases receive the signal from excitatory synaptic activity induced by L-glutamine or BDNF and regulate neuron morphology and motility. Rac1 and CDC42 have been shown to positively regulate cell morphology and motility, whereas RhoA negatively regulate cell morphology and motility (Figure 4.2). Therefore, we hypothesize that in hippocampal neurons, BDNF-induced neuronal filopodial motility change is also carried out by small GTPases. This hypothesis is supported by the studies of selective elimination of Rac1 in excitatory neurons, where it was demonstrated that not only the spine structure is disrupted but also the synapse plasticity in hippocampal neurons is impaired, leading to a hippocampus-dependent special learning defect (Haditsch et al., 2009).

Here I provided evidence that the small GTPases Rac1 and RhoA, are important regulators of hippocampal neuron dendritic filopodial motility. I showed that Rac1 increases but RhoA decreases hippocampal neuron dendritic filopodial motility. The action of Rac1 and RhoA can be considered as the

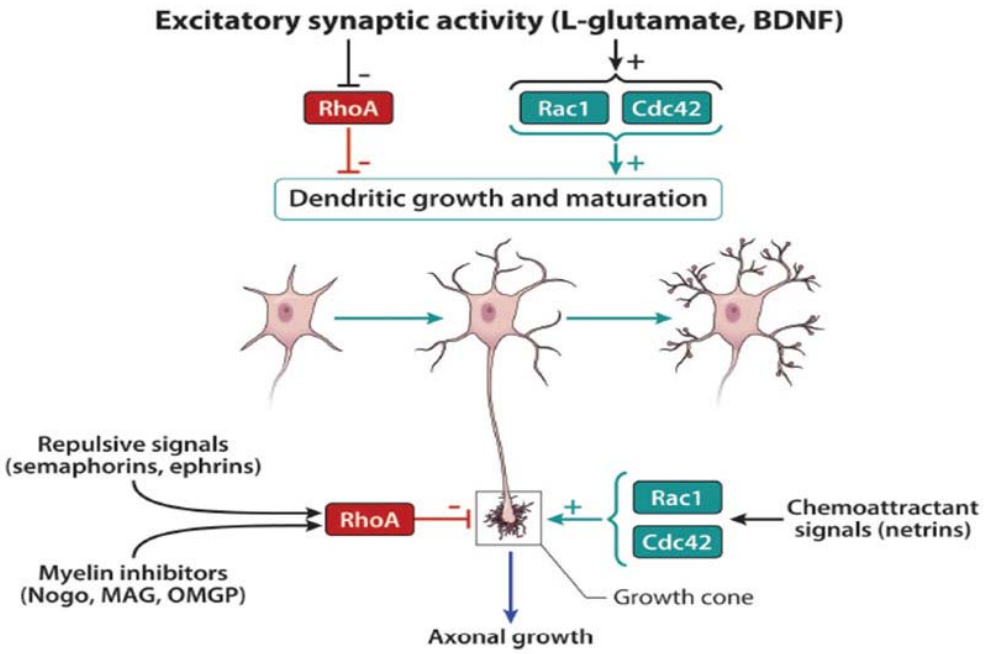

Figure 4.2. Small GTPases are important regulators of neuron morphology. It has been shown that in different neuron types, small GTPases receive the signaling coming from excitatory synaptic activity induced by L-glutamine or BDNF and regulate neuron morphology and motility. Rac1 and CDC42 have been shown to positively regulate cell morphology and motility, whereas RhoA negatively regulates cell morphology and motility (Adpated form Neurology).

downstream mechanism for BDNF-TrkB signaling regulated hippocampal neuron dendritic filopodial motility.

Results

Making mcherry fusion small GTPase dominant negative (DN) and constitutive active (CA) mutant forms

The activity of small GTPases depends on their choice to bind GDP or GTP. When binding to GDP they are inactive, whereas they become active when binding to GTP. There are certain point mutations that can mimic their active or inactive status. I sought to study the function of active or inactive small GTPases by introducing such mutations to Rac1, RhoA and CDC42. The V14 mutation in RhoA, and the V12 mutation in Rac1 and CDC42 are constitutively active forms, that mimic the GTP-bound form of small GTPases. Similarly, the N19 mutation in RhoA and the N17 mutation in Rac1 and CDC42 are the dominant negative forms, that mimic the GDP-bound forms of small GTPases (Figure 4.3A). The point mutations were introduced by designing mutated DNA sequences in the 5' primers (See chapter 2 for the primer sequences). In order to visualize the neuronal structure, especially the dendritic filopodia structure, I

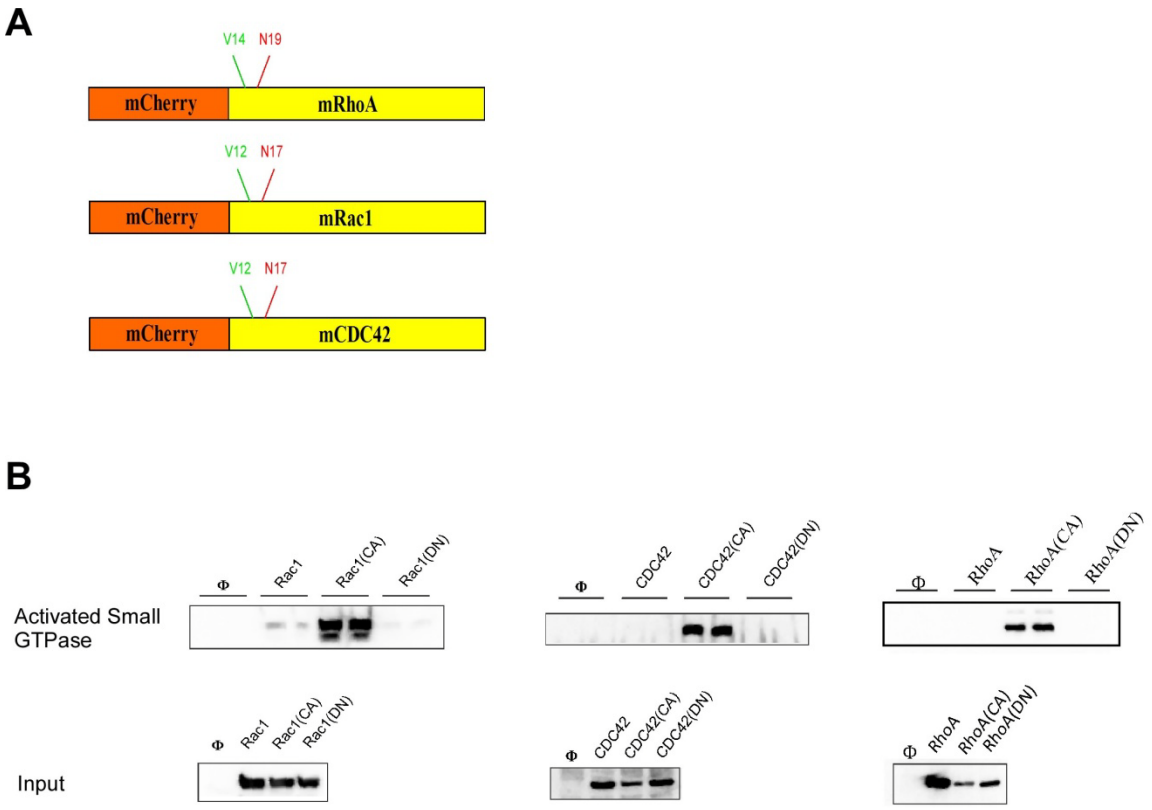

Figure 4.3. Making mCherry fusion small GTPase dominant negative (DN) and constitutive active (CA) mutant forms. (A). Strategy to generate the DN or CA form of small GTPases. MCherry is fused at the N-terminus of each mutant. The V14 mutation in RhoA or the V12 mutation in Rac1 and CDC42 are the constitutively active forms; N19 mutation in RhoA or N17 mutation in Rac1 and CDC42 are the dominant negative forms. **(B).** Small GTPase activity assays confirm that all of the CA mutants can bind to their substrates but the DN mutants cannot.

chosed to fuse a mCherry to the N-terminus of all the mutated small GTPases (Figure 4.3A).

Small GTPases activity assay twas performed to confirm that these small GTPase mutant-mCherry fusion proteins can function as they are designed to. I transfected the wildtype small GTPases and the mutant forms into NG108 cells, a neuronal cell line. The transfected cells were then lysed and the lysates were used for pull-down experiments with small GTPase substrate-conjugated beads, followed by western blottings with small GTPase antibodies. Pak1 p21-binding domain conjugated beads were used to pull down Rac1 and CDC42, where Rhotekin Rho-binding domain conjugated beads were used to pull down RhoA. As shown in Figure 4.3B, wildtype Rac1, CDC42 and RhoA show minimal binding to their substrates, and the dominant negative form of these small GTPases does not bind to the substrates at all, whereas the constitutive active form of the three small GTPases can strongly bind substrate (Figure 4.3B).

mCherry fusion small GTPases label intact neuronal dendritic structures

I then want to examine whether these fusion proteins can label the intact neuronal dendritic structure, including the dendritic filopodia. I cultured primary hippocampal neurons from neonatal mice and transfected the mCherry

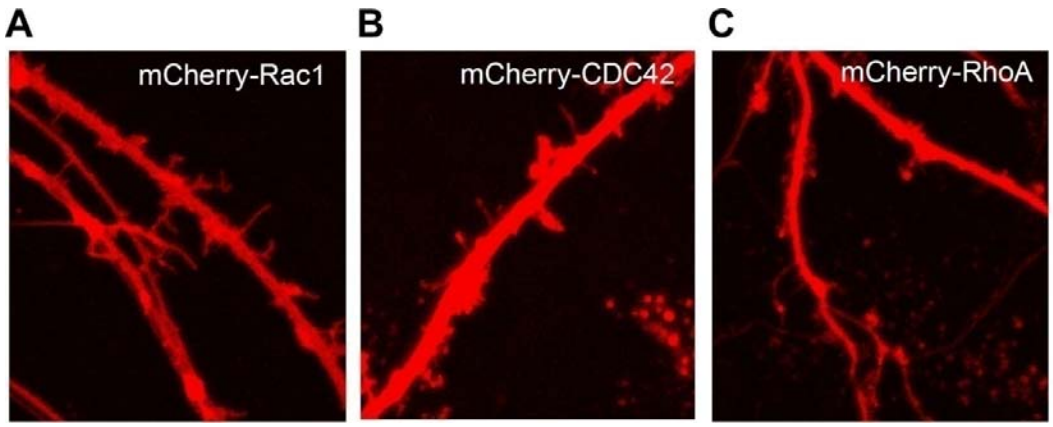

Figure 4.4. mCherry fusion small GTPases label the intact neuronal dendritic structures. The mCherry fusion Rac1, CDC42, and RhoA are localized throughout the intact neuronal dendritic structure, including the dendrite, the filopodia structure, and the growth cone.

fusion wildtype small GTPases into the neurons at 10DIV. As shown in Figure 4.4A-C, the mCherry fusion proteins are localized throughout the intact neuronal dendritic structure, including the dendrite, the filopodia structure, and the growth cone, which enable us to study the dendritic morphology dynamics in these neurons.

Rac1 positively but RhoA negatively regulates dendritic filopodial motility

To investigate whether Rac1, RhoA and CDC42 regulate dendrtic filopodia motility, the wildtype small GTPases, their dominant negative and constitutive active mutant forms were transfected into primary cultured hippocampal neurons at 10DIV. Following transfection, live cell imagings were performed using confocal microscopy to record dendritic filopodia dynamics. As shown in Figure 4.5, compared to mCherry only transfected neurons, the neurons transfected with constitutively active form of Rac1 (mCherry-Rac1-CA) might have slightly higher dendritic filopodial motility. The neurons transfected with dominant negative form of RhoA (mCherry-RhoA-DN) also might have a slightly higher dendritic filopodial motility. The majority of the neurons transfected with Rac1 CA mutant or RhoA DN mutant showed increased dendritic filopodial motility based on live cell imaging. However, there are a few neurons that are unhealthy, thus showed a decreased filopodial motility on the contrary, which might be why the error bars in Figure 4.5B are very big. This might be because that

overexpression of Rac1 or RhoA mutants in some neurons severely disrupted cytoskeleton and these neurons are overall unhealthy and probably dying. My later experiments using a working condition of Rac1 or RhoA inhibitor gave much more consistent results.These data suggested that Rac1 might positively but RhoA might negatively regulate dendritic filopodial motility in hippocampal neurons.

Rac1 inhibition completely blocks TrkB-induced dendritic filopodial motility increase

I next wanted to test whether TrkB-induced dendritic filopodial motility increase occurs via regulation of Rac1 activity. I transfected wildtype TrkB into primary cultured hippocampal neurons followed by application of a Rac1 inhibitor.

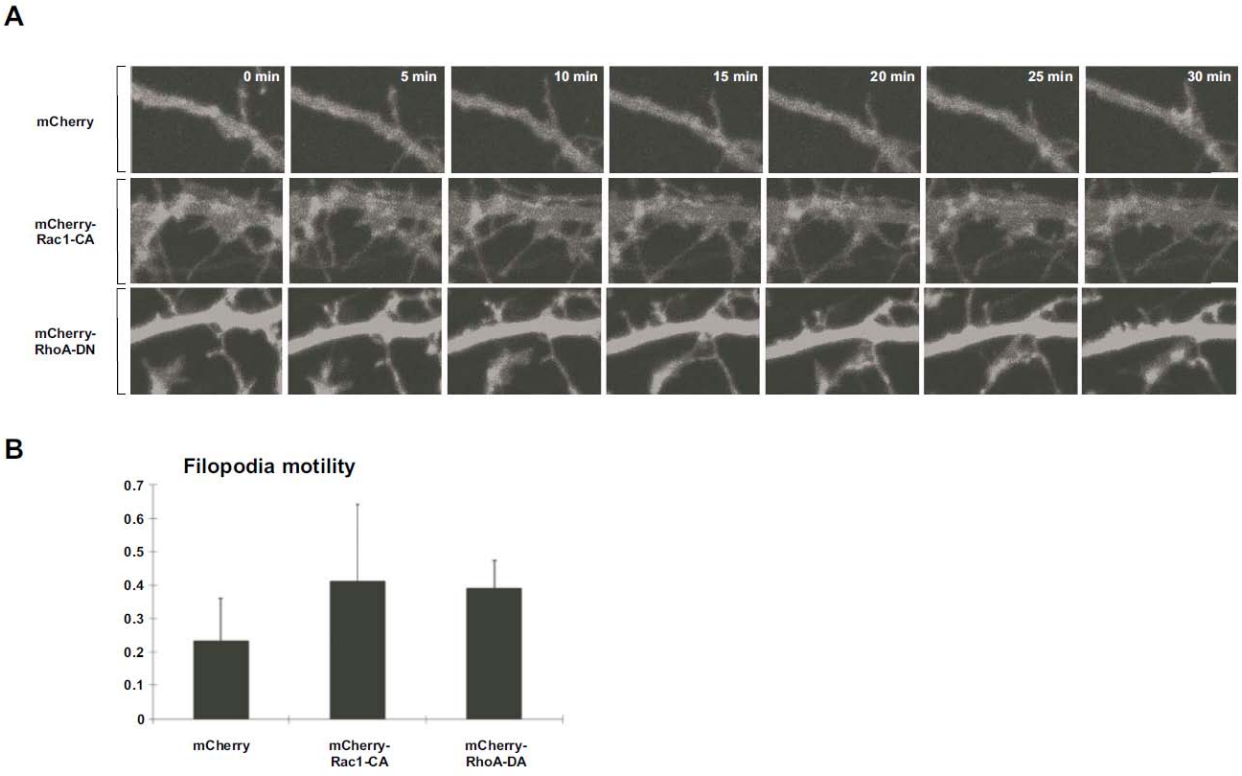

Figure 4.5 Rac1 positively but RhoA negatively regulates dendritic filopodial motility. (A). Compared to mCherry only transfected neurons, constitutively active form of Rac1 (mCherry-Rac1-CA) transfected neurons have a higher dendritic filopodial motility. The neurons transfected with dominant negative form of RhoA (mCherry-RhoA-DN) also have a higher dendritic filopodia motility. **(B).** Quantification of the filopodial motility of mCherry only, mCherry-Rac1-CA and mCherry-RhoA-DN transfected hippocampal neurons.

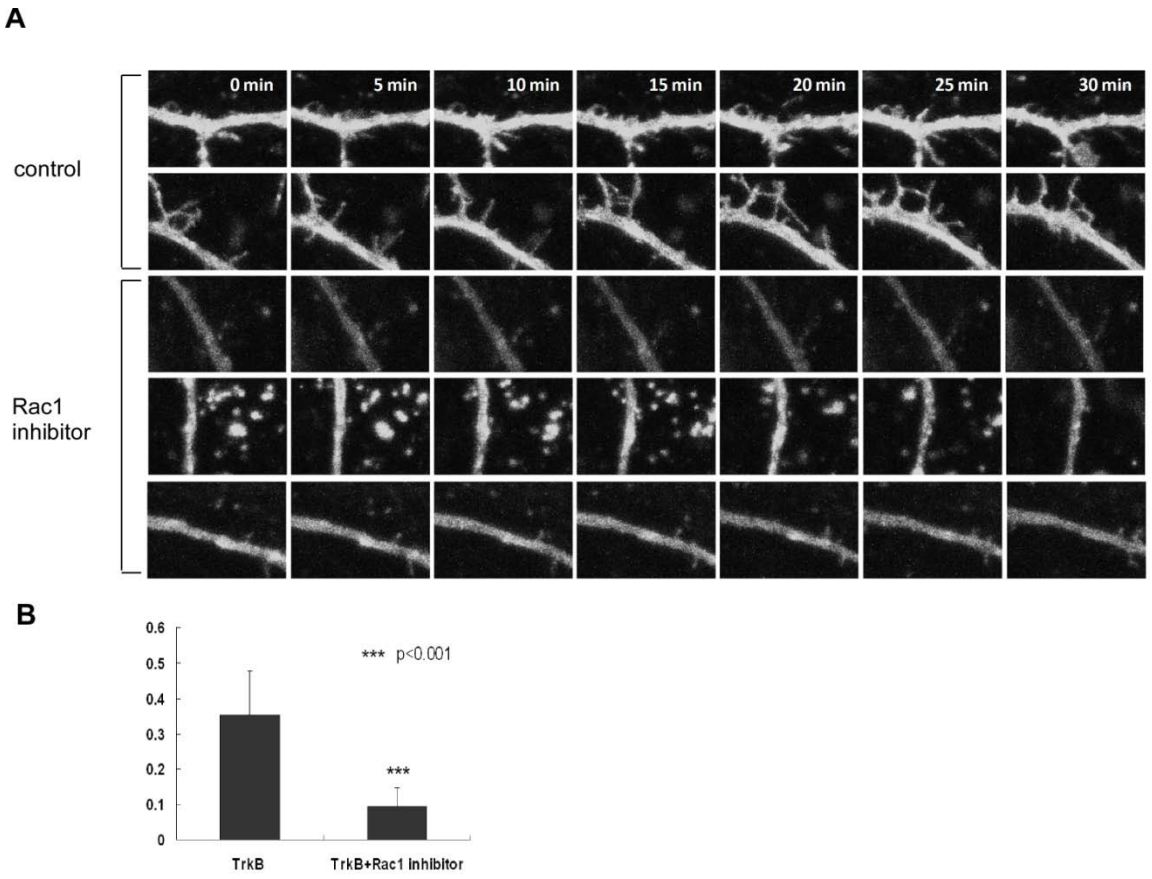

Figure 4.6. Inhibition of Rac1 abolished the dendritic filopodia motility increase induced by TrkB overexpression. (A). Compared to the neurons transfected with the wildtype TrkB alone, Rac1 inhibitor-treated neurons have dramatically decreased dendritic filopodial motility. **(B).** Quantification of the filopodial motility shows that Rac1 inhibitor treatment decreases the filopodial motility by about 3-fold.

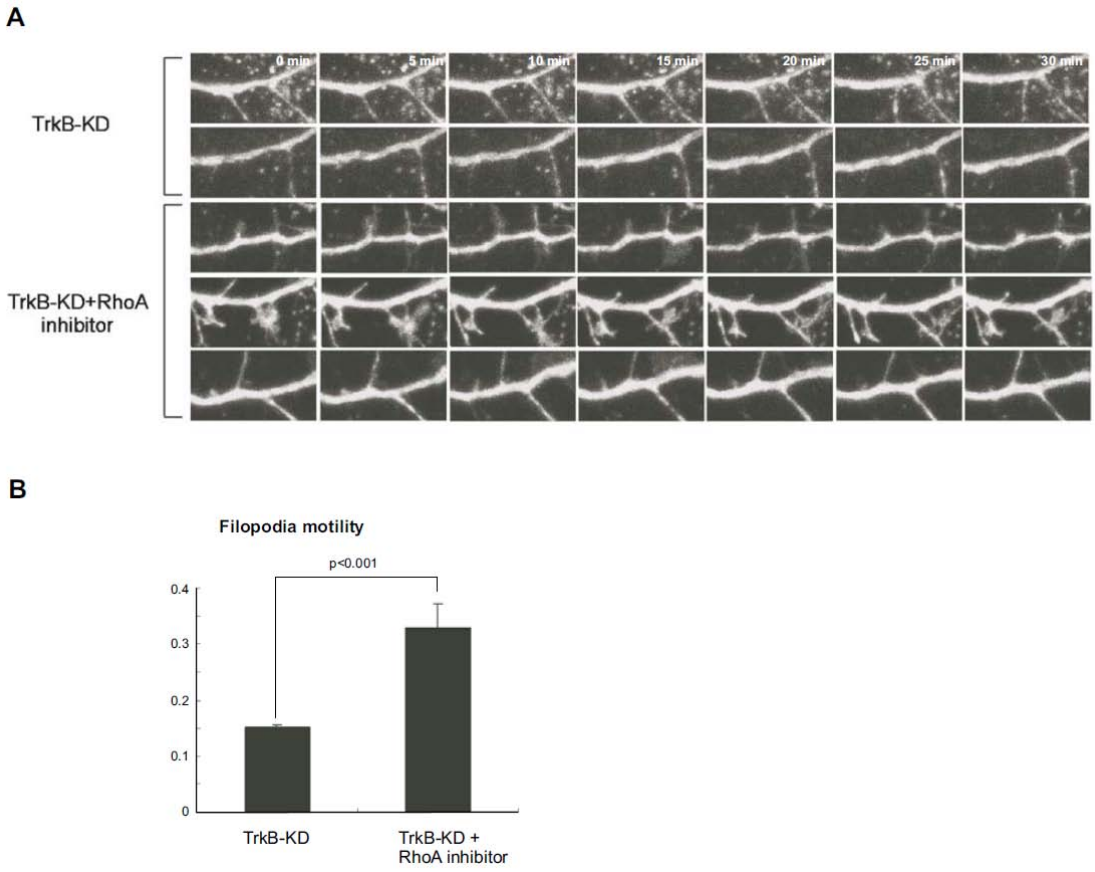

Figure 4.7. Inhibition of RhoA increases dendritic filopodial motility even when TrkB signaling is blocked. (A). Compared to the neurons transfected with the TrkB kinase dead form alone, RhoA inhibitor-treated neurons have dramatically increased dendritic filopodial motility. **(B).** Quantification of the filopodial motility shows that RhoA inhibitor treatment increases the filopodial motility by up to 2-fold.

Dendritic filopodial motility was then recorded using confocal microscopy. As shown in chapter 3, wildtype TrkB overexpression induced a roughly 2 folds increase of dendritic filopodial motility compared to control. If TrkB signaling induced dendritic filopodial motility increase is solely dependent on small GTPase Rac1 activity, I expect that the 2 folds increase of the dendritic motility induced by TrkB overexpression will be completely abolished by application of Rac1 inhibitor. Indeed, the filopodial motility was found to be dramatically reduced in Rac1 inhibitor-treated hippocampal neurons compared to the TrkB transfected only neurons (Figure 4.6A). The filopodial motility was reduced by about 3-fold in Rac1 inhibitor-treated TrkB transfected neurons (Figure 4.6B). These data support the hypothesis that the small GTPase Rac1 functions downstream of TrkB signaling, and that TrkB increases dendritic filopodial motility through activation of Rac1.

RhoA inhibition increases dendritic filopodial motility even when TrkB signaling is blocked

As shown in Figure 4.5, RhoA negatively regulates dendritic filopodial motility. To determine if RhoA functions downstream of TrkB, I again

used the inhibitors but this time in combination with TrkB knockdown. In chapter 3, I found that TrkB dominant negative kinase dead form overexpression leads to a 50% reduction of filopodial motility. If RhoA functions downstream of the TrkB signaling, I expect that overexpression of RhoA dominant negative will bypass the reduction of TrkB kinase dead form induced filopodial motility reduction. For this purpose, I overexpressed the TrkB dominant negative kinase dead form in primary cultured hippocampal neurons and then added a RhoA inhibitor (Cytoskeleton). Live cell imaging was performed to record the dendrtic filopodia motility. As expected, compared to the neurons transfected with the TrkB kinase dead form alone, RhoA inhibitor-treated neurons had dramatically increased dendritic filopodial motility (Figure 4.7A). Quantification of filopodial motility showed that RhoA inhibitor treatment increased filopodial motility by up to 2-fold (Figure 4.7B). In addition, the hippocampal neurons were also treated with a Rho kinase inhibitor (Calbiochem), which inhibits the Rho kinase downstream of RhoA, following knock down of TrkB by the TrkB kinase dead form. Similar to RhoA inhibitor treated neurons, filopodial motility in RhoA kinase inhibitor-treated neurons was also increased about 2-fold (Figure 4.8A and B) compared to TrkB kinase dead form alone transfected neurons.

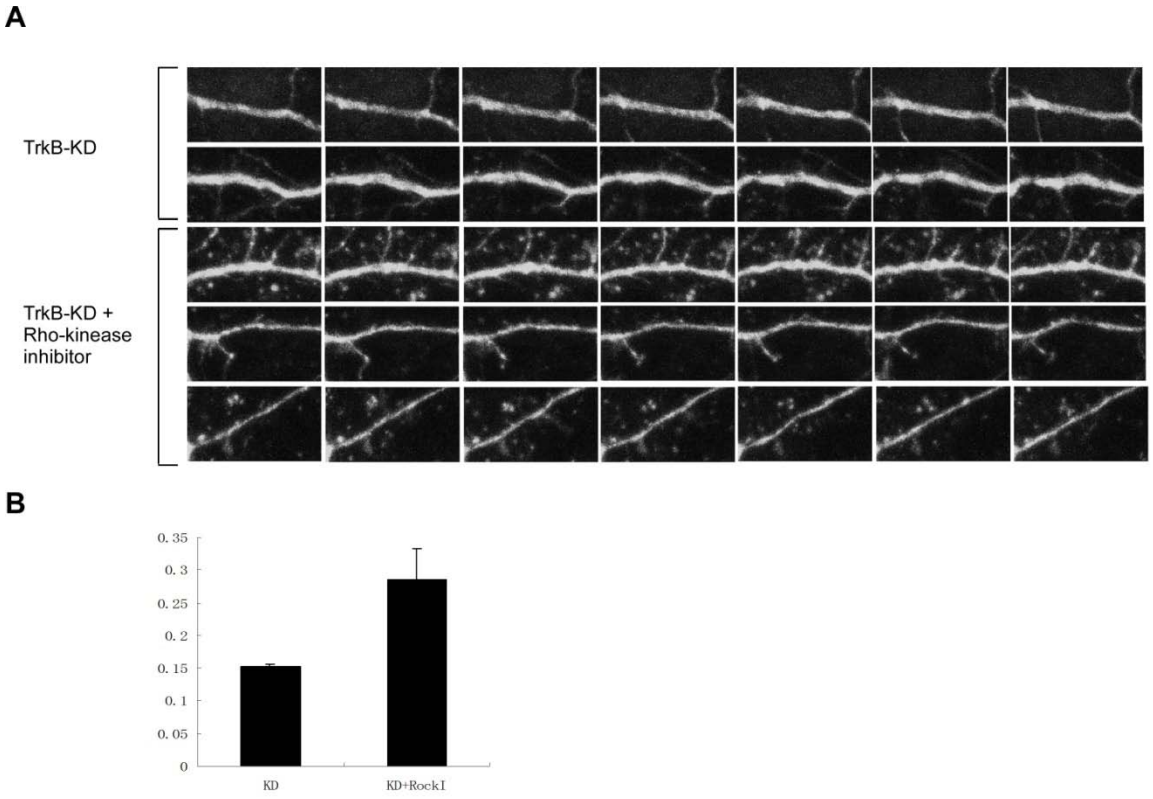

Figure 4.8. Inhibition of RhoA kinase increases dendritic filopodial motility. **(A).** Filopodial motility in RhoA kinase inhibitor-treated neurons is increased. **(B).** Quantification shows that filopodial motility in RhoA kinase inhibitor-treated neurons is increased up to 2-fold.

Discussion

Here I demonstrated that small GTPases Rac1 positively but RhoA negatively regulates dendritic filopodial motility. The other important small GTPase CDC42 does not have any effect on dendritic filopodial motility. I overexpressed wildtype TrkB combined with Rac1 inhibitor treatment in cultured hippocampal neurons and found that Rac1 inactivation completely abolished wildtype TrkB overexpression induced dendritic filopodial motility increase. In addition, inhibition of RhoA or Rho kinase by their inhibitors rescues the TrkB kinase dead form overexpression induced dendritic filopodial motility decrease.

There is no direct evidence showing that TrkB direct binds Rac1/ RhoA and subsequently regulates their activity. The fact that TrkB signaling and Rac1/RhoA both regulate dendritic filopodial motility suggests that either BDNF/TrkB signaling and Rac1/RhoA function in the same pathway, or they function in parallel and regulate dendritic filopodial motility additively or synergically. As shown in Figure 4.9, there are three possibilities about the relations between BDNF/TrkB signaling and Rac1/RhoA.

Possibility 1: Rac1/RhoA acts at the upstream of the BDNF/TrkB signling;

Possibility 2: Rac1/RhoA acts at the downstream of the BDNF/TrkB signling;

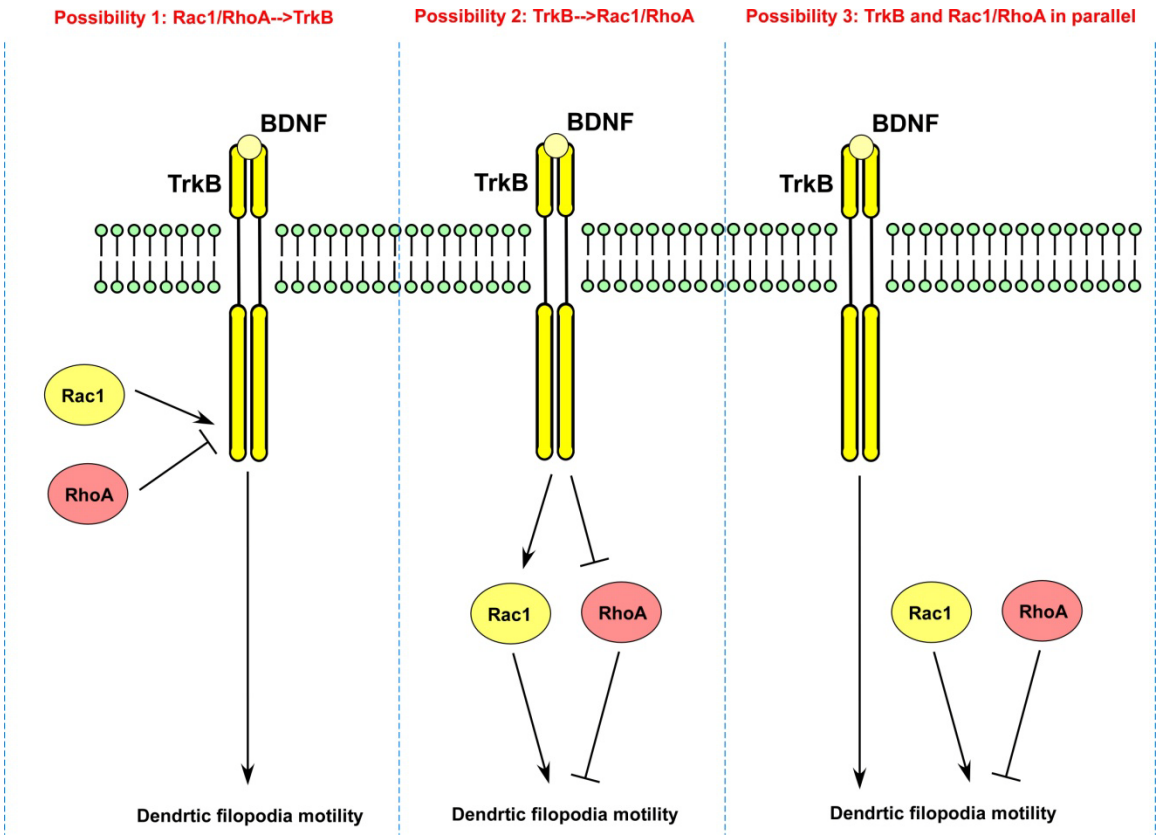

Figure 4.9. Three possibilities about the relations between BDNF/TrkB signaling and Rac1/RhoA. Possibility 1: Rac1/RhoA acts at the upstream of the BDNF/TrkB signling; Possibility 2: Rac1/RhoA acts at the downstream of the BDNF/TrkB signling; Possibility 3: Rac1/RhoA acts in parallel with BDNF/TrkB signaling and function additively or synergically.

Possibility 3: Rac1/RhoA acts in parallel with BDNF/TrkB signaling and function additively or synergically.

If the first possibility is true, when I overexpress TrkB while inhibiting Rac1, I will not see Rac1 inhibition has any effect on TrkB overexpression induced dendritic filopodial motility increase. Similarly, I will not see that RhoA inactivation increases the dendritic filopodial motility when TrkB kinase dead form is overexpressed. Therefore, our experiment data argue against this possibility. As for the third possibility, if the BDNF/TrkB functions in parallel with Rac1/RhoA, when I overexpress wildtype TrkB and inhibit Rac1, I will expect that inhibition may only decrease TrkB overexpression induced dendrtic filopodial motility to a certain degree but not completely abolish the effect of TrkB on filopoidla motility. Out data also argue against this possibility.The second possibility is best supported by our experiment data.

The activity of small GTPases is usually regulated by GAPs and GEFs. There is no evidence showing TrkB itself has a GAP or GEF activity. Therefore, the direct GAPs and GEFs need to be identified to link the TrkB signaling to the Rac1/RhoA activity. Interestingly, it has been shown that one GEF, Tiam1, can directly interact with TrkB and be activated by TrkB upon BDNF binding. Tiam1 is phosphorylated by TrkB at Tyr-829 and then activate Rac1, leading to lamellipodia formation in Cos-7 cells and increased neurite outgrowth in cortical

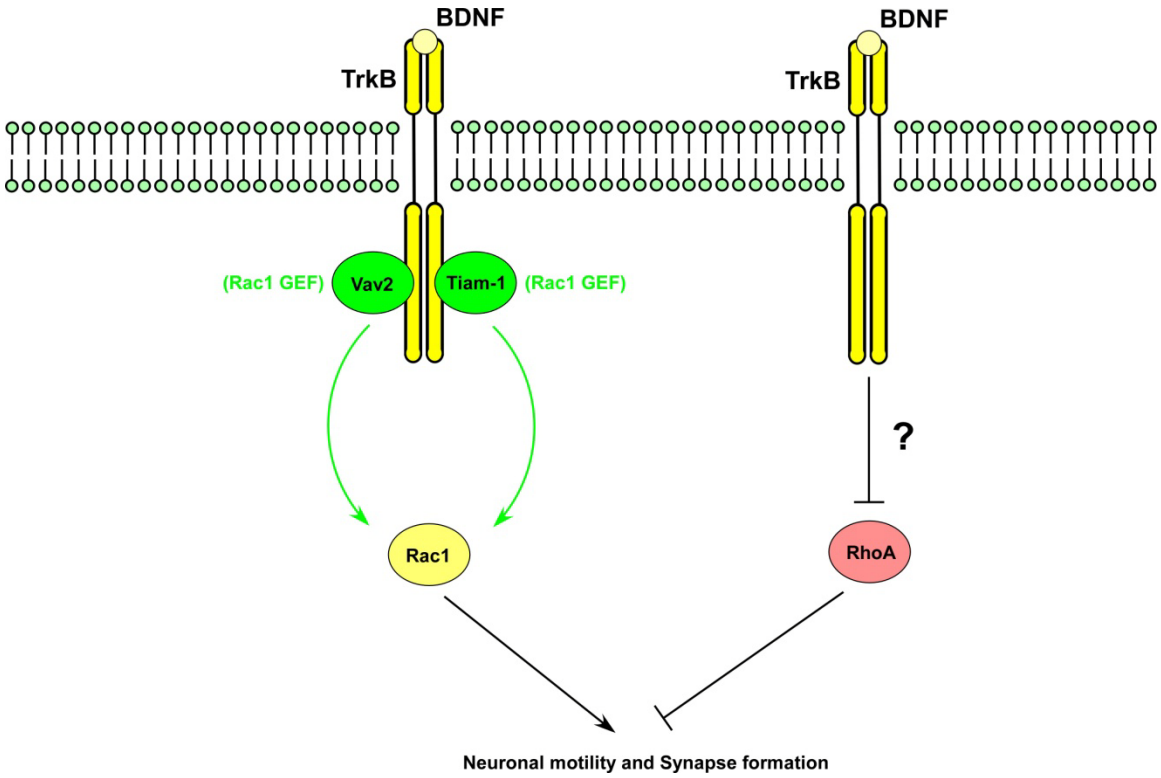

Figure 4.10. Possible mechanism that link BDNF/TrkB signaling and Rac1/RhoA. One GEF, Tiam1, was shown to directly interact with TrkB and be activated by TrkB upon BDNF binding, and then activate Rac1. Another Rac1 GEF, Vav2, has been found to regulate Rac1 activity in hippocampal neurons and then control the dendritic dynamic structure formation. It is also possible that BDNF/TrkB signaling can inhibit RhoA, which is a negative regulator for the dendritic filopodia motility.

neurons (Miyamoto et al., 2006). Similarly, in Schwann cells, Tiam1 is activated by NT3/TrkC signaling and activate Rac1, regulating the Schwann cells migration (Yamauchi et al., 2005). Recently, another Rac1 GEF, Vav2, has been found to regulate Rac1 activity in hippocampal neurons and then control the dendritic dynamic structure formation (Personal communication with Cowan C. group) (Figure 4.10). It will be interesting to examine if these Rac1 GEFs are also essential for the Rac1/RhoA function in regulating the dendritic filopodia motility in hippocampal neurons.

In Summary, evidence is provided to show that small GTPases Rac1 positively and RhoA negatively regulate the dendritic filopodia motility in cultured hippocampal neurons. I showed that inhibition of Rac1 abolished TrkB overexpression induced dendritic filopodial motility increase, whereas inhibition of RhoA or Rho kinase rescued the TrkB kinase dead mutant overexpression induced dendritic filopodial motility decrease. These data suggested Rac1/RhoA might serve as the downstream machinery for the dendritic filopodial motility regulation by BDNF/TrkB signaling.

Future Experimental Design

Specific Aim 1. To determine whether BDNF/TrkB regulates Rac1/RhoA activity.

Rationale:

I have provided evidence that Rac1 inhibition can abolish TrkB induced dendritic filopodial motility increase, suggesting Rac1 may act at the downstream of the BDNF/TrkB signaling in the hippocampal neurons. However, to confirm that they are functioning in the same pathway, I need to show direct evidence that activation of BDNF/TrkB signaling would change the activity of Rac1 or RhoA in the whole cells or in the dendrtic filopodial structure. Biochemical Rac1/RhoA activity assay may be used for this purpose. Immunocytochemistry can be used to determine the subcellular change of Rac1/RhoA in the neurons.

Experiment 1. To examine whether TrkB overexpression regulates Rac1/RhoA activity.

Small GTPase assay will be used to test the activity of Rac1 and RhoA. Neuronal cell lines or other cell lines (such as Cos7) will be used for the assay. Cells will be transfected with wildtype TrkB or control plasmid. The cells will then be lysed and the lysate will be subjected to the pull-down experiments with Rac1 or RhoA

substrate-conjugated beads. The pulled-down proteins will be analyzed by western blottings using antibodies against Rac1 or RhoA. Pak1 p21-binding domain conjugated beads will be used to pull down Rac1, whereas Rhotekin Rho-binding domain conjugated beads were used to pull down RhoA. It is possible that when TrkB is overexpressed, the activity of Rac1 will be increased and/or the activity of RhoA will be decreased. In fact, this experiment has been tried once on neuronal cell line NG108. However, due to a relatively high background activity of Rac1 and RhoA, I was not able to tell a difference between control and TrkB transfected cells (data not shown). To reduce the basal activity, one may consider swiching to another cell line (such as Cos7) or starving the cells before/during the transfection by serum deprivation and then performing the small GTPases assay on these cells.

Experiment 2. To determine if TrkB signaling activation leads to the subcellular localization change of Rac1/RhoA.

One possible reason that I did not see the activity change of Rac1/RhoA upon TrkB signaling activation could be that instead of the activity change, the subcellular localization of Rac1/RhoA is changed in the neurons. For example, it is possible that activation of TrkB signaling results in accumulation of Rac1 in dendritic filopodia structure and/or RhoA moves out of the dendritic filopodia. To test this possibility, I can overexpress TrkB or add BDNF in cultured

hippocampal neurons, and then perform immunocytochemistry to examine the subcellular localization of Rac1 and RhoA. The immunostained neurons can be analyzed using con-focal microscopy and the relative fluorescence intensity in the dendritic filopodia structure will be used as a read-out.

Specific Aim 2. To determine whether Rac1/RhoA functions at the downstream of the BDNF/TrkB→PI3K signaling for the regulation of dendritic filopodial motility.

Rationale:

Our data suggests that BDNF/TrkB regulate dendritic filopodial motility through Rac1/RhoA. Our previous data (chapter 3) showed that BDNF/TrkB activation leads to PI3K activation and then control dendritic filopodial motility. It will be interesting to investigate whether or not PI3K and Rac1/RhoA also work in a linear signaling pathway in the context of dendritic filopodial motility control. Some studies showed that TrkB may directly bind Rac1 GEF (e.g. Vav2 and Tiam1) and then activate Rac1 in hippocampal neurons. It will be critical to distinguish whether PI3K is required for the Rac1 activation or PI3K and the Rac1 GEF work in a parallel manner.

Experiment 1. To test whether Rac1 inhibition abolishes PI3K induced dendrtic filopodia motility increase.

For this purpose, I will generate a constitutive active PI3K construct by introducing a CAAX motif at the C-terminus on the PI3K p110α subunit. This CAAX motif will tether p110α subunit to the plasma membrane and leads to its activation independent on its upstream signaling. I will first examine if overexpression of this p110a-CAAX will increase the dendritic filopodia motility in cultured hippocampal neurons similar as TrkB overexpression. If this result is positive, I will apply Rac1 inhibitor on the p110α-CAAX transfected hippocampal neurons to see if the inactivation of Rac1 will abolish the dendritic filopodia motility increase. If Rac1 inhibitor treatment blocked the action of p110a-CAAX, it will suggest Rac1 functions at the downstream of PI3K. If not, it will suggest that they act in a parallel pathway.

Alternatively, different mouse models can be used for this experiment. As we have shown in chapter 3, Nf1 knockout mice and Pten knockout mice have increased PI3K activity and increased dendritic filopodial motility. I can use the hippocampal neurons isolated from these mouse lines for *in vitro* culture and then apply the Rac1 inhibitor on these neurons to determine whether inactivation of Rac1 will inhibit the dendritic filopodia motility increase in Nf1 or Pten knockout neurons.

CHAPTER V

MICRORNA MIR-381 REGULATES DENDRITIC MORPHOLOGY IN HIPPOCAMPAL NEURONS

Introduction

Neuronal dendritic morphogenesis has been a focus of the neuroscience field for decades. It is intriguing to understand how neurons acquire elaborate dendritic structures and how these structures can be dynamically re-modeled upon neuronal activity. Important dendrite characterstics include dendritic branching, extension, spine and synapse formation. Dendritic branching and extension affect the field the dendrite can cover, which determines the extent to which the dentrite is able to connect to presynaptic neurons (MacNeil and Masland, 1998; Wassle and Boycott, 1991), while dendritic spines are the structural basis for excitatory synapses to be formed (Yuste and Denk, 1995). Dendritic morphology has a huge impact on the function of a certain type of neurons and its remodeling plays an essential role in neuronal plasticity upon activation. Abnormalities in dendrite morphogenesis are often seen in patients with mental disorders such as autism, Down's syndrome, Angelman's syndrome, Rett's syndrome, fragile X syndrome and schizophrenia (Bagni and Greenough, 2005; Bourgeron, 2009; Dindot et al., 2008; Garey et al., 1998; Kaufmann and Moser, 2000; Kelleher and Bear, 2008; Pardo and Eberhart, 2007; Ramocki and Zoghbi, 2008; Walsh et al., 2008).

Many regulators of dendritic morphogenesis have been identified to date. Using *Drosophila* genetics and mouse models, it has been shown that dendritic structure can be regulated by various transcription factors (Gaudilliere et al., 2004; Hand et

al., 2005), secreted proteins (Jossin and Goffinet, 2007; Rosso et al., 2005), adhesion molecules (Fuerst et al., 2009), cytoskeletal regulators (Chen and Firestein, 2007; Newey et al., 2005), motor proteins (Hoogenraad et al., 2005; Zheng et al., 2008), neurotrophins (McAllister et al., 1997; McAllister et al., 1995) and local translation molecules (Bagni and Greenough, 2005; Vessey et al., 2008). The role that local translation control plays in dendrite morphogenesis is of great interest because it provides a mechanism for dendrites to fine tune their local structures according to neuronal activity inputs. Various RNA binding proteins have been shown to control local protein translation in dendrites, including Pumilio, Nanos and Staufen 1 (Vessey et al., 2008; Ye et al., 2004). In addition, recent discovery of microRNAs provides another mechanism for local translational control in neuronal dendrites.

MicroRNAs (miRNAs) are a family of small, non-coding RNAs that are transcribed as a pre-microRNA (pre-miRNA) and then processed into a short double-stranded RNA (21-23bp) by the proteins Drosha and Dicer, and subsequently is loaded onto the RISC complex where it binds to target mRNAs at the 3'UTR. This binding leads to either degradation of the target mRNA or inhibits translation (Ambros, 2004; Bartel, 2004; He and Hannon, 2004). Many miRNAs have been discovered in the vertebrate nervous system (Kim et al., 2004; Krichevsky et al., 2003; Lagos-Quintana et al., 2002), and recent studies demonstrated the crucial roles of miRNAs in early brain development

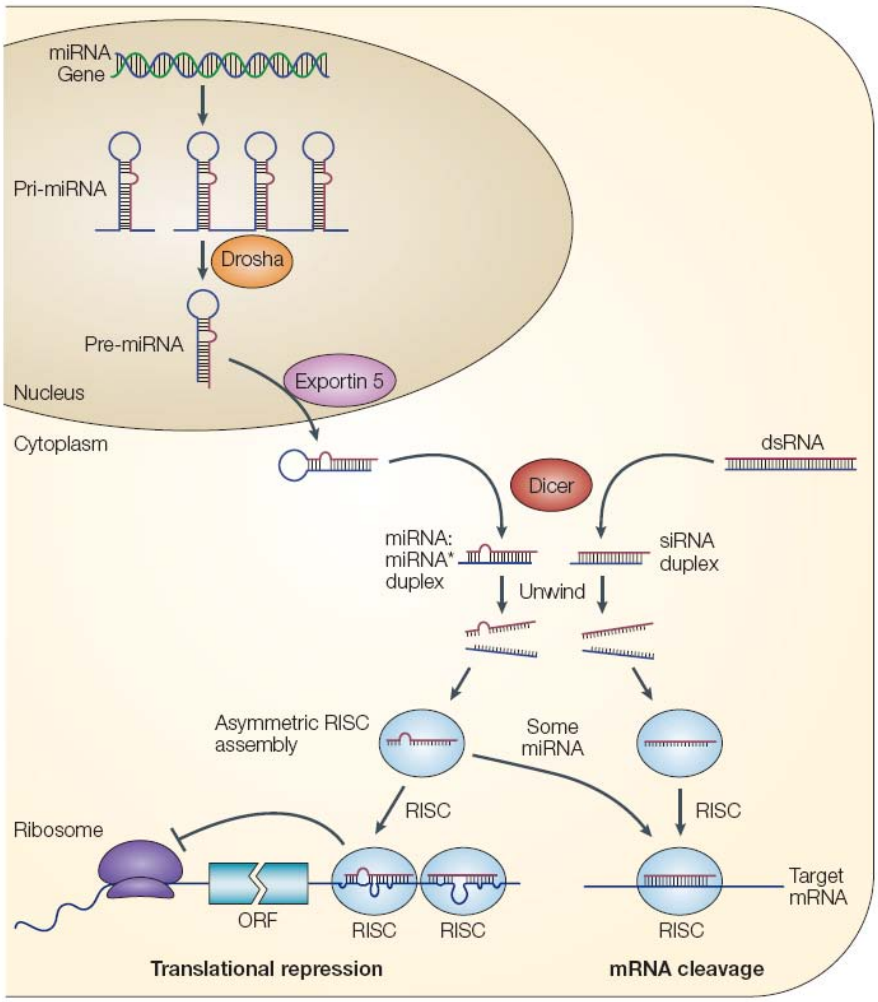

Figure 5.1. MicroRNA biosynthesis and function mechanism overview. (Adapted from (He and Hannon, 2004)). MicroRNAs (miRNAs) are a family of small, non-coding RNAs that are transcribed as a pre-microRNA (pre-miRNA), exported by Exportin 5 to the cytosol, then processed into a short double-stranded RNA (21-23bp) by the proteins Drosha and Dicer, and subsequently is loaded onto the RISC complex where it binds to target mRNAs at the 3'UTR. This binding leads to either degradation of the target mRNA or inhibits translation when the sequence is perfect match or non-perfect match, repectively.

(Giraldez et al., 2005; Schratt et al., 2006), as well as neuronal maturation and synapse development at later stages of brain development (Krichevsky et al., 2003; Miska et al., 2004; Sempere et al., 2004). The overall contribution of miRNAs to neurons of the central nervous system (CNS) was further assessed by deletion of Dicer, which is required for processing of all miRNAs, in excitatory neurons (CamK II-cre mediated deletion. Inactivation of Dicer in excitatory neurons leads to an array of phenotypes in both cortical and hippocampal neurons including microcephaly, reduced dendritic branching, and large increases in dendritic spine length (Davis et al., 2008).

MicroRNAs have been found to be processed within or translocated into neuronal dendrites. Such miRNAs might have important functions in terms of regulating dendrite morphogenesis and local dendrite remodeling. One of these miRNAs, miR-134, is found to be expressed in the hippocampus and its expression increases as the brain matures. Using *in-situ* hybridization, miR-134 is shown to localize in the neuronal dendrite and enriched in the synapto-dendritic compartment. MiR-134 is able to inhibit the local translation of LIM-domain kinase 1 (Limk1) mRNA, through which miR-134 negatively regulates the size of dendritic spines but not other aspects of dendrite morphogenesis such as dendrite branching and outgrowth (Schratt et al., 2006).

MiR-134 belongs to a huge cluster of miRNAs at the Dlk1-Gt12 domain in the mouse genome (chromosome 12 distal region). There are another 45 miRNAs in this cluster but none of them have been characterized and studied individually in great detail. It was shown that most of the miRNAs in this cluster are transcribed together as a large RNA and then processed into individual miRNAs (Seitz et al., 2004). Therefore, they should share the same expression pattern, although the repertoire of target genes varies and thus they serve different functions in a neuron. This miRNA cluster is conserved throughout mammalian species (human cluster is in 14q32), thus indicating its important role in mammalian brain development (Seitz et al., 2004). Recently, these miRNAs were found to be regulated by the neuronal transcription factor Myocyte enhancing factor 2 (Mef2), in an activity-dependent manner in hippocampal neurons (Fiore et al., 2009). Interestingly, the miRNAs in the Dlk1-Gt12 domain are epigenetically imprinted, they can be transcribed from maternal alleles but not paternal ones (Seitz et al., 2004).

Here I describe how another miRNA from the Dlk1-Gt12 cluster, miR-381, is specifically expressed in the brain in different regions. Similar to miR-134, its expression is increased as the brain matures. Using *in- vitro* cultured mouse hippocampal neurons, I were able to show that miR-381 positively regulates neuronal dendrite branching, as over-expression of miR-381 in hippocampal

neurons increases the number of dendritic branches, while inhibition of miR-381 has the opposite effect.

Results

miR-381 is one of the microRNAs in the Dlk1-Gt12 domain:

miR-381 is located in the Dlk1-Gt12 domain miRNA cluster (Figure 5.2A), which contains at least 46 miRNAs and is conserved across the mammalian genome (Figure 5.2B). MiR-134 is one of the miRNAs in this cluster, which has been previously shown to possess a unique neuronal expression pattern and to play an important role in neuron and dendritic spine development (Schratt et al., 2006) (Figure 5.2A). Based on bioinformatic prediction, the pre-miRNA of miR-381 is 77 base pairs long and forms a hairpin structure, which is then processed into a 22 bp mature miRNA (Figure 5.2C). The seeding region (2-7 bp of a microRNA used to bind its target mRNA) of miR-381 has a sequence of 7 bp (3'-gaacaua-5') (Figure 5.2D, blue region).

Expression of miR-381 in mouse brain

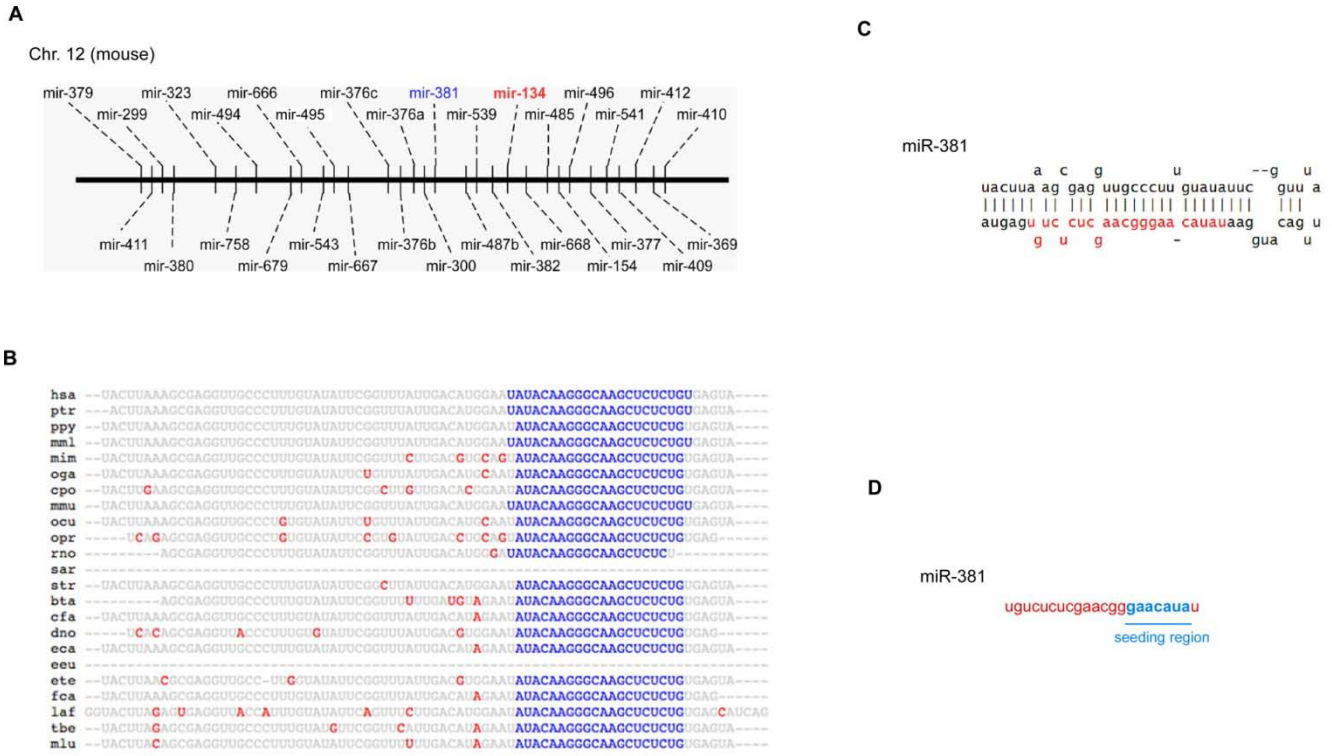

Figure 5.2. miR-381 is a microRNA in the Dlk1-Gt12 domain. (A). miR-381(blue) is located in the genome very closely to a microRNA cluster called the Dlk1-Gt12 domain, which contains at least 30 microRNAs and is conserved between the mouse and human genome. miR-134 (red), one of the microRNAs in this cluster, has been previously shown to have a unique neuronal expression (Schratt et al., 2006). (**B).** The pre-miRNA of mir-381 is 77 base pairs long and forms a hairpin structure, which is then processed into a 22bp mature miRNA (red). **(C)**. miR-381 is conserved throughout mammalian species. **(D).** The seeding region of miR-381 (blue).

Northern blotting was performed to determine the expression pattern of miR-381. P^{32} labeled mature miR-381 complement sequence (22bp) was used as a probe. Different tissues were collected including brain, skeletal muscle, stomach, heart, spleen, bladder, lung, colon, intestine, liver, thymus and kidney from adult mice (2 months old) and their total RNA was isolated. I found that miR-381 was expressed with the predicted size (22bp) only in the brain tissue but not detected in any other tissues (Figure 5.3A). In addition, different regions of the brain were then analyzed to determine whether miR-381 expression is restricted to specific brain areas. Cortex, cerebellum and hippocampus were dissected and then the total RNA was isolated. Using northern blotting, I found that miR-381 was detected in all of these regions in adult mice (2 months old) (Figure 5.3B), indicating that miR-381 might play a general role in the brain. Furthermore, to determine at which stages miR-381 is expressed, brain tissues from mice at different ages were subjected to northern blotting for miR-381. As shown in Figure 5.3C, miR-381 is expressed weakly in P1 and P7 brain and then increased as the brain further develops. It is known that neurons continue to develop and pattern after birth, so I expect that miR-381 may play a role during neuron morphogenesis and patterning after the first week of birth.

Over-expression of miR-381 increases dendritic branch number

To investigate whether miR-381 plays a role in neuronal dendrite morphogenesis, I first examined whether dendrite morphology is altered when miR-381 is over-expressed. I cloned pre-miR-381 hairpin (77bp) from mouse genomic DNA and used CMV promoter to drive pre-miR-381 expression in neurons (Figure 5.4A). First, to ensure that this construct can correctly express mature miR-381 in the cells, I transfected pCMV-miR-381 into Cos7 cells and then performed northern blots for miR-381. As shown in Figure 5.4B, miR-381 is expressed in Cos7 cells and with the correct expected size (22bp). I then co-transfected a GFP expression plasmid and pCMV-miR-381 into 5DIV primary cultured hippocampal neurons. GFP transfection enables us to label the entire

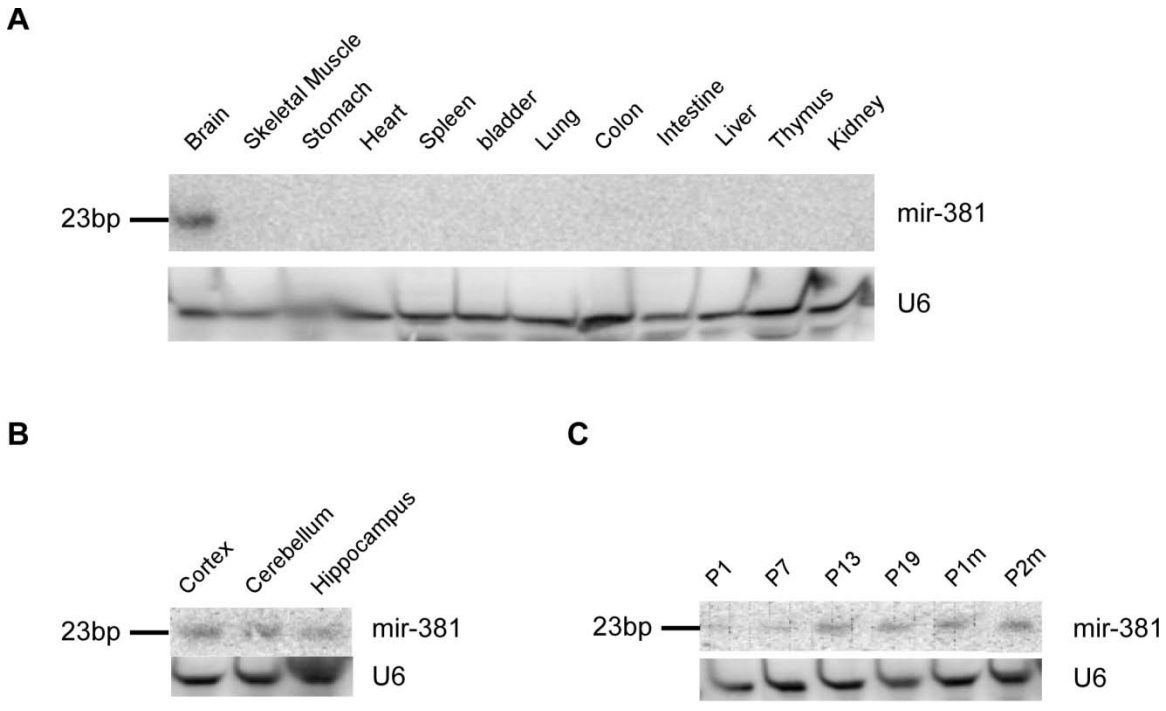

Figure 5.3. Expression pattern of miR-381. (A) miR-381 is only expressed in brain tissue and not detected in any other tissues. **(B)** miR-381 is expressed in cortex, cerebellum and hippocampus. **(C)** miR-381 is expressed weakly in P1 and P7 brain and then increases as the mice develop.

structure of hippocampal neurons, where Axons and dendrites were distinguished based on well established morphologic characteristics. Transfection of GFP and pCMV were used as a negative control. After 5 days in culture, neuronal dendrite morphology was examined by confocal microscopy (Fig. 5.4C) and the total dendrite length, primary dendrite length, dendritic branch number, and number of primary dendrites per neuron were counted and analyzed using MetaMorph software. I found that the total dendrite length was increased in miR-381 over-expressed neurons by more than 20% ($p<0.02$) (Fig. 5.4D), however the primary dendrite length is not changed significantly (Fig. 5.4G). This result suggests that the total dendrite increase in length is due to the dendritic branch numbers increasing rather than each dendrite outgrowth lengthening. Indeed, the total branch number and the primary dendrite number per neuron are increased in miR-381 over-expressed neurons (For total branch number, mean of 18.1 compared to mean of 13.2 in control, $p<0.001$; For primary dendrite number per neuron, mean of 5.2 per neuron compared to mean of 4.1 per neuron in control, $p<0.05$) (Figs. 5.4E and 5.4F). Over-expression of another miRNA, miR-495 does not have an effect on dendrite branching (Figure 5.4C-5.4G), suggesting the dendrite branching increase I observed is not due to a non-specific effect of double-stranded RNA expression in neurons. Therefore, I concluded that miR-381 positively regulates neuronal dendrite branching in hippocampal neurons.

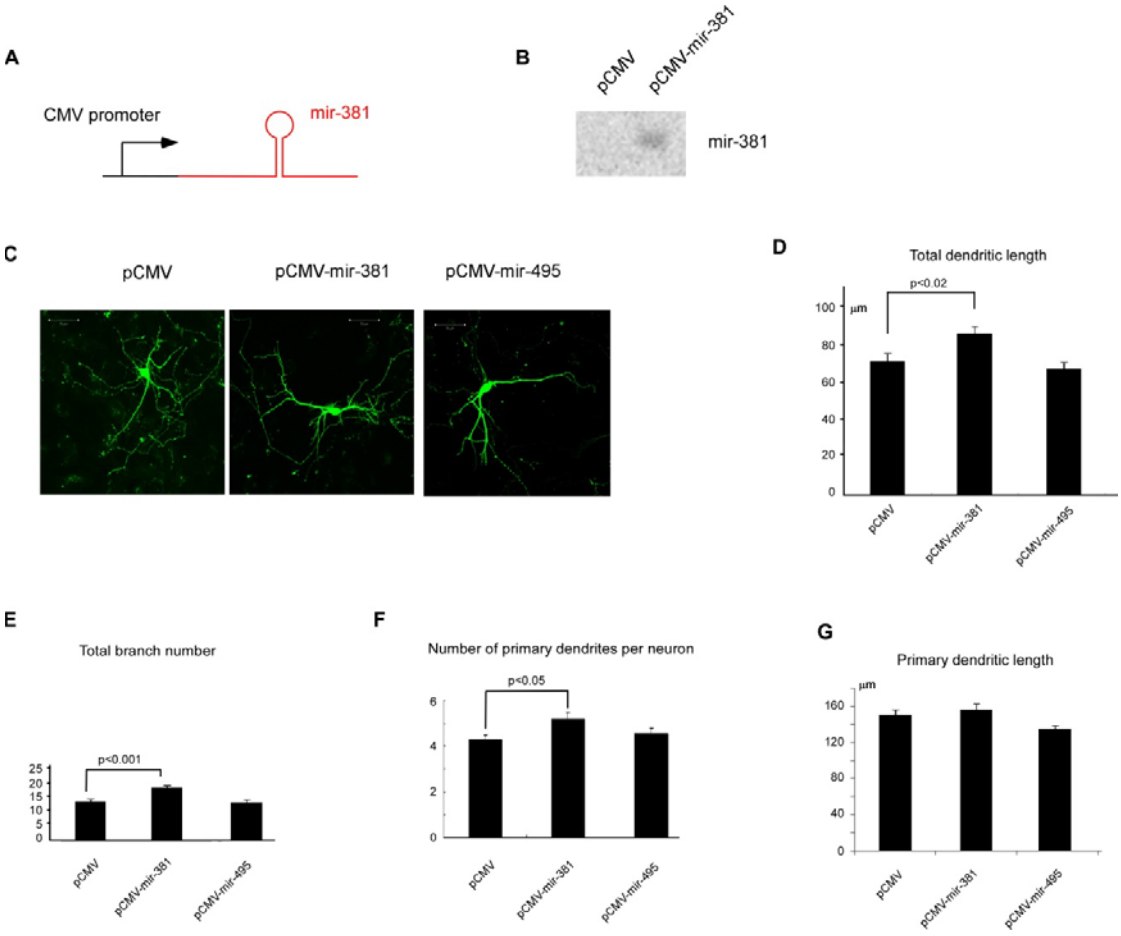

Figure 5.4. Over-expression of miR-381 increases dendritic branch number. **(A)** CMV promoter driven miR-381 expression. **(B)** pCMV-miR-381 can express mature miR-381 in NG108 cells. **(C)** Representative picture of miR-381, miR-495 and GFP co-transfected hippocampal neurons. Total dendrite length is increased in miR-381 over-expressed neurons but not in miR-495 overexpressed neurons. **(D)** The primary dendrite length is not changed **(G).** Total branch number **(E)** and primary dendrite number per neuron **(F)** is increased in miR-381 over-expressed neurons but not miR-495 over-expressed neurons. (Neurons counted in these experiments: pCMV, n=42; pCMV-miR-381, n=36; pCMV-miR-495, n=34.)

Inhibition of miR-381 decreases dendritic branch number

By an over-expression experiment in hippocampal neurons, I demonstrated that expression of miR-381 is sufficient to increase the number of neuronal dendrite branches. I then wanted to examine if miR-381 is required for neuronal dendrite branching. For this purpose, I sought to inhibit miR-381 in a hippocampal neuronal culture to see if it will affect neuronal dendrite branching. To accomplish this, I used a technique called a "microRNA sponge" (Ebert et al., 2007). A short RNA with a cluster of miR-381 binding sites (6 in total) was transcribed under the control of a pol III promoter, known as U6 (Figure 5.5A). This short RNA traps most of the endogenous miR-381 inside neurons, thus preventing it from binding to its native target mRNAs. I then co-transfected a GFP expression plasmid and pCMVU6-miR-381-sponge into 5DIV primary cultured hippocampal neurons. GFP and pCMVU6 were transfected as a negative control. After 5 days, neuron morphology was examined (Figure 5.5B) using confocal microscopy, and dendrite length and numbers were counted and analyzed. I found that inhibition of miR-381 had the opposite effect on dendritic morphology compared to over-expression of miR-381. The total dendritic length (Fig. 5.5C) and the number of dendrites (Fig. 5.5D) were found decreased when miR-381 was inhibited (For total dendritic length, average 480μm compared to 652μm in control, $p<0.001$; For dendrite number, average

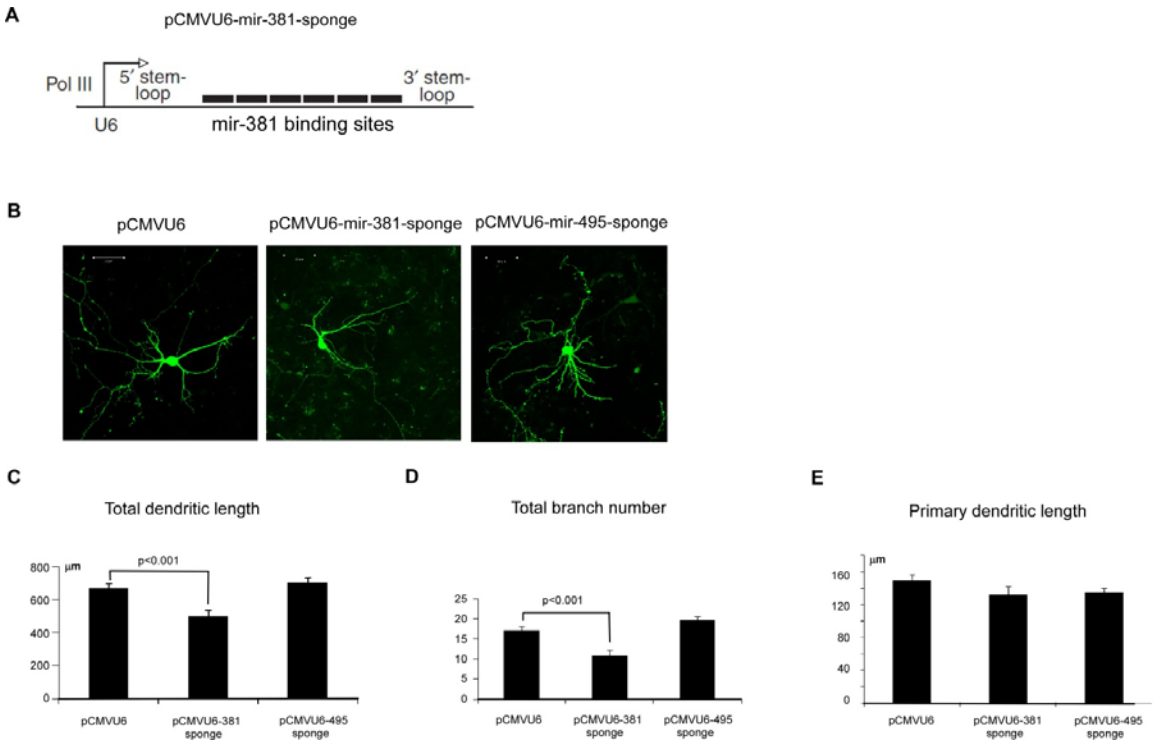

Figure 5.5. Inhibition of mir-381 decreases dendritic branch number. (A) U6 promoter driven miR-381 sponge expression. **(B)** Representative picture of mir-381 sponge, miR-495 sponge and GFP co-transfected hippocampal neurons. Total dendrite length **(C)** and total branch number **(D)** are decreased in miR-381 sponge expressing neurons but not in miR-495 sponge expressing neurons. **(E)** The primary dendrite length is not changed. (Neurons counted in these experiments: pCMVU6, n=38; pCMVU6-miR-381-sponge, n=35; pCMVU6-miR-495-sponge, n=33.)

10.1 compared to 16.8 in control, $p<0.001$), but the primary dendrite length was not changed significantly (Figure 5.5E), confirming miR-381 as a positive regulator of neuronal dendrite branching. As a control, over-expression of miR-495 sponge in the neurons does not affect dendrite branching (Figure 5.5B-5.5E). Combined with the miR-381 over-expression experiments, I concluded that miR-381 is both sufficient and required for hippocampal neurons to establish proper dendritic trees.

Discussion

Here I characterize the expression pattern of one of the miRNAs in the Dlk1-Gt12 domain miRNA cluster, miR-381, specifically in various brain regions in mice. I show that miR-381 expression increases after birth. I used *in- vitro* cultured hippocampal neurons to show that miR-381 is a positive regulator of neuronal dendrite branching, and that the effect of miR-381 on dendrite branching is both sufficient and required.

Although I demonstrate that miR-381 is a brain-specific miRNA that is expressed in various brain regions, I do not provide evidence to support that miR-381 is solely neuron-specific. It may however be expressed in other cell types such as

glial cells. This is particularly important to understanding the mechanism of miR-381 regulated dendritic branching because it has been shown that dendritic morphogenesis can be regulated in a neuron non-autonomous fashion (Murai et al., 2003). However, there is indirect evidence supporting the notion that miR-381 is specifically expressed in neurons. First, miR-381 belongs to a large cluster of miRNA, the Dlk1-Gt12 domain. This cluster of miRNAs is transcribed as one large RNA and then processed into different miRNAs. Therefore, all miRNAs in this cluster should share the same expression pattern. One of the miRNAs in this cluster, miR-134, has been characterized in great detail, showing that it is specifically expressed in neurons (Schratt et al., 2006). Second, the Dlk1-Gt12 cluster of miRNAs has been shown to be controlled by a transcription factor, Mef2 (Fiore et al., 2009), which is well-known as a neuron-specific transcription factor in the brain (Lyons et al., 1995). Direct evidence may come from *in-situ* hybridization of miR-381 in cultured hippocampal neurons or from brain sections which are co-stained with cell type specific markers, such as the neuronal marker class III beta-tubulin III (Tuj1) or the glial marker GFAP etc.

The phenotype I observed when I over-expressed or inhibited miR-381 is restricted to dendrite branching but not other aspects of dendritic structure, such as individual dendrite outgrowth, dendritic spine formation etc. This result suggests that miR-381 determines how widely the dendrite structure can cover locally rather than how far the dendritc tree can reach. There are similar regulators

identified that behaves the similar manner. For example, using *Drosophila* RNAi screening, several transcription factors were found to specifically regulate dendrite lateral branching positively (*sna* and *knirps*) or negatively (*gcm2, pcaf*) (Parrish et al., 2006). It will be interesting to find out whether the function of these genes is also conserved in mammals and whether there are genetic interactions between these genes and miR-381.

Our data suggests that miR-381 increases its expression during the postnatal stages (Figure 5.3C). At this stage, neurons in the brain undergo maturation and remodeling, however here is not where the neurons become specified. Given this expression pattern, I speculate miR-381 would have a role in neuronal morphogenesis. Indeed, by over-expression or inhibition of miR-381 in cultured hippocampal neurons, I were able to show that miR-381 positively regulates neuronal dendrite branching, a crucial process for neurons to branch out and form proper networks. Interestingly, the transcription factor Mef2, which is shown to regulate Dlk-Gt12 cluster miRNA expression, has a similar expression pattern as miR-381 during development. Mef2 starts to be expressed in neurons after they exit the cell cycle and begin to differentiate (Lyons et al., 1995). Deletion of Mef2c in mouse brain was shown to result in disorganized neuronal structure and to present an autistic phenotype (Li et al., 2008; Lipton et al., 2009). It would be

interesting to investigate whether or not miR-381 contributes to the function of mef2 in neuronal development, specifically at the level of dendritic morphogenesis.

miR-381 belongs to the miR-154 family, which consists of 13 miRNAs. These miRNAs share a similar secondary structure and seeding region. In the miR-154 family, the seeding region of miR-381 has only one base pair difference between that of another miRNA, miR-300 (3'-GAACAUA-5' in miR-381 compared to 3'-GAACGUA-5' in miR-300). This similarity may cause a partial overlapping of target genes between miR-381 and miR-300, which might mean a partial functional redundancy between miR-381 and miR-300. Therefore, the dendritic phenotype I observed in miR-381 over-expression and miR-381 sponge inhibition experiments may also partially be due to gain-of-function or loss-of-function of miR-300 or both miR-300 and miR-381. One could also examine the expression pattern of miR-300 in the brain to see if the timing, cell types and sub-cellular localization miR-300 expression also overlap with miR-381. If they share the same expression pattern, to draw a safe conclusion about the unique function of miR-381, more specific experiments need to be done, such as genetic deletion of miR-381 without affecting miR-300. On the other hand, redundancy is often seen in higher species, where genes are co-regulated and can be substituted with one

another. To study these redundant genes, one would have to delete all the genes in order to see a clear phenotype. In this study, over-expression experiments and miRNA sponge experiments actually provide us a chance to manipulate the redundant miRNAs together to study their functions.

To fully understand the mechanisms of miR-381 regulated dendritic branching, the target gene(s) of miR-381 need to be defined. However, to look for miRNA target genes has proven to be rather difficult. Also, one miRNA might have multiple target genes and the function of such a miRNA can be through a net effect of various target genes. The most popular way nowadays to find miRNA target genes is through bioinformatic prediction. Originally, I chose to study miR-381 because it is predicted by "TargetScan" to target Brain-derived neurotrophic factor (BDNF), one of the favorite molecules studied in our lab. However, when I co-transfected a luciferase reporter with the 3'UTR from BDNF and miR-381 in neuronal cell lines, I found that over-expression of miR-381 fails to reduce luciferase reporter activity as predicted (Figure 5.6), suggesting that the prediction of BDNF as a miR-381 target gene might be a false positive. In addition, BDNF is also a positive regulator of neuronal dendrite branching, which opposes the theory that BDNF is a true target gene of miR-381. Therefore, further effort will be

needed to define the target gene(s) for miR-381 to interpret the dendrite branching phenotype.

Currently, there are multiple search tools used for miRNA target gene prediction. Each of them uses different algorithms to calculate the binding energy and to produce an eclectic repertoire of target genes. The genes that are predicted by more than one search tool are found to have a higher chance to be true miRNA target genes. I used three different online search tools to predict the miR-381 target genes, including Microcosm, Microrna.org and Targetscan (http://www.ebi.ac.uk/enright-srv/microcosm/, http://www.microrna.org/microrna/, and http://www.targetscan.org/ respectively). I found 25 target genes that are predicated by at least 2 search engines (Table 5.1), among which 2 genes are predicted by all three, including Kif1B and Myst4

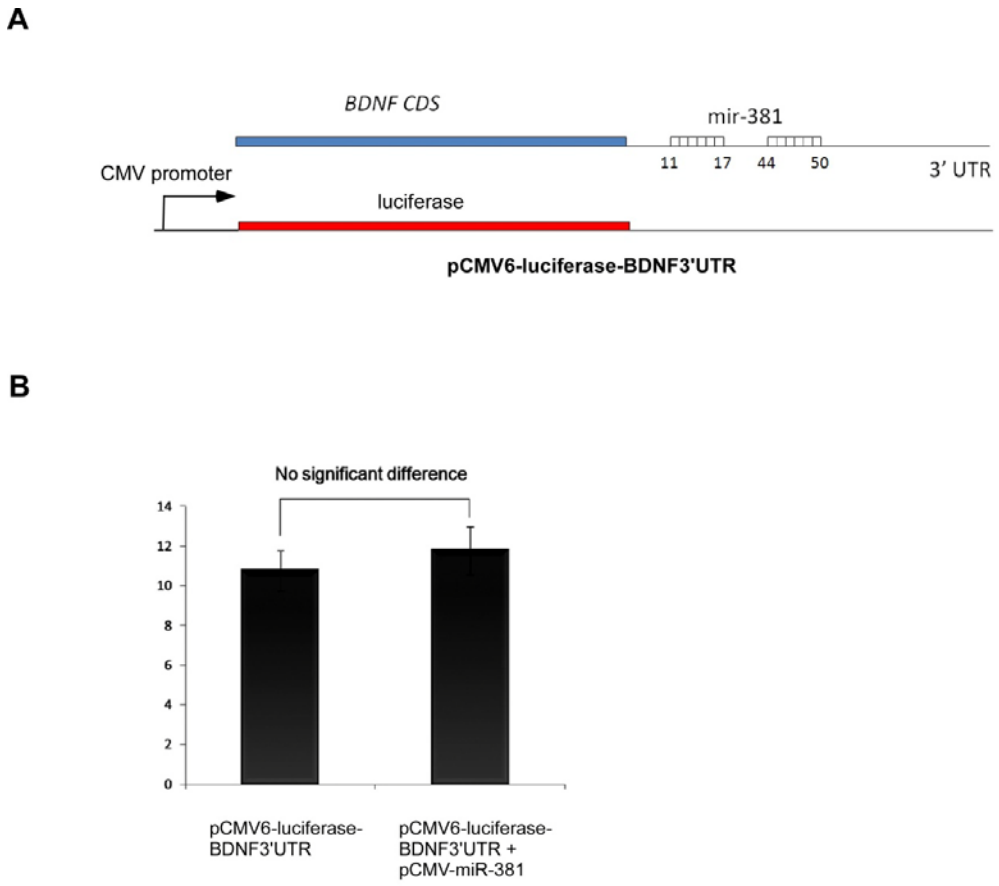

Figure 5.6. Over-expression of miR-381 does not affect BDNF 3'UTR activity. **(A).** Experimental strategy: to use the BDNF 3'UTR sequence to control luciferase reporter activity. **(B).** There is no significant difference in luciferase activity between miR-381 transfected and non-transfected cells.

(Table 5.1 denoted with *). 10 of the genes have been shown to be expressed in the brain and 9 of them have a known function pertaining to neuronal development, differentiation or synaptic activity regulation (Table 5.1). Among these genes, two motor genes are of great interest, KIF11 and KIF1B. KIF1B is predicted as a miR-381 target gene by all the search tools. Motor proteins such as kinesin have been shown to regulate dendrite morphogenesis in mice. KIF5 can bind to an adaptor protein GRIP1 to transport EphB receptor in the dendrites, which is shown to be essential for dendritic outgrowth and branching (Hoogenraad et al., 2005). It is possible that other kinesins can use similar mechanisms to regulate different aspects of dendrite morphogenesis. Indeed, inhibition of KIF11 by its inhibitor monastrol in neurons leads to an increase in their dendritic outgrowth (Yoon et al., 2005). Therefore, it will be particularly interesting to investigate if KIF11 and KIF1B can serve as major target genes for miR-381 to regulate dendritic branching.

The miRNA cluster in Dlk1-Gt12 domain is conserved throughout the mammalian species, indicating their important roles in mammalian brain development and function. miR-134 is found to specifically regulate dendritic spine development and maturation. Here I show that miR-381 is important for dendritic branching. I also studied miR-495 in this cluster in the same setting

Gene Symbol	Gene Name	Brain expression	Known brain function
ACTG1	actin, gamma 1	Yes	hearing, mutation causes hearing impairment
AFF4	AF4/FMR2 family, member 4	not known	n.a.
EDEM3	ER degradation enhancer, mannosidase alpha-like 3	not known	n.a.
FGFR2	fibroblast growth factor receptor 2	Yes	prefrontal cortex development
GPR158	G protein-coupled receptor 158	not known	n.a.
ID2	inhibitor of DNA binding 2	Yes	neuronal differentiation
JAG2	jagged 2	Yes	neuronal differentiation
KIF1B*	kinesin family member 1B	Yes	n.a.
KPNA6	karyopherin (importin) alpha 6	not known	n.a.
LRRC4	leucine rich repeat containing 4	Yes	neuronal differentiation and neurite outgrowth
MYST4*	MYST histone acetyltransferase (monocytic leukemia) 4	Yes	cerabelum development
KIF11	Kinesin family member 11	Yes	neuronal outgrowth and dendrite branching
NUFIP2	nuclear fragile X mental retardation protein interacting protein 2	not known	n.a.
PLAG1	pleiomorphic adenoma gene 1	not known	n.a.
PPP1R14C	protein phosphatase 1, regulatory (inhibitor) subunit 14C	not known	n.a.
RYBP	RING1 and YY1 binding protein	Yes	nervous system development
SEMA6D	sema domain, transmembrane domain (TM), and cytoplasmic domain, (semaphorin) 6D	not known	n.a.
SLC24A3	solute carrier family 24 (sodium/potassium/calcium exchanger), member 3	Yes	neuronal activity
SMARCB1	SWI/SNF related, matrix associated, actin dependent regulator of chromatin, subfamily b, member 1	not known	n.a.
SNX14	sorting nexin 14	not known	n.a.
STX12	syntaxin 12	Yes	synaptic vesicle exocytosis
XPO7	exportin 7	not known	n.a.
ZFHX3	zinc finger homeobox 3	not known	n.a.
ZNF148	zinc finger protein 148	not known	n.a.
ZNF509	zinc finger protein 509	not known	n.a.

Table 5.1. Predicted target genes for miR-381. Three different online search engines used to predict miR-381 target genes, including Microcosm, Microrna.org and Targetscan. 25 genes were predicted by at least 2 search engines. 2 genes were predicted by all three, including Kif1B and Myst4 (*). 10 of the genes have been shown to be expressed in the brain and 9 of them have a known function on neuronal development, differentiation or synaptic activity.

but I did not find that it affects dendritic branching (Figure 5.4 and Figure 5.5). MiR-495 may regulate other aspects of neuronal morphogenesis which I did not examine, such as dendrite spine formation, synapse formation and their function regulation. It is possible that all the miRNAs in this cluster play slightly different roles in neuronal morphogenesis or functions. The net effects of all these miRNAs may provide the mammalian neurons greater flexibility to remodel their structure to fulfill their functional needs. Therefore, it will be worth investigating other miRNAs in this cluster to determine their roles in neuronal morphogenesis and function. Interestingly, the Dlk1-Gt12 is a Single Nucleotide Polymorphism (SNP) rich locus. In mice, there are about 347 SNPs defined in this region. The human cluster has a similar number of SNPs. This SNP enrichment could indicate that these miRNAs might serve to code for the individual differences seen in neuronal structure and activity in mammals, especially in humans. Although there is no SNP within the miR-381 coding region itself, there are 6 SNPs flanking miR-381, which may affect the expression of miR-381 in neurons in a subtle manner.

In summary, here I characterize a brain specific miRNA, miR-381, which has previously never been studied in detail. I show that miR-381 is expressed in different brain regions and its expression increases as the brain matures. Using *in-vitro* cultured hippocampal neurons, I were able to discover that miR-381 is a positive regulator of neuronal dendrite branching, providing another level of

regulation of dendritic morphogenesis. To fully understand the detailed mechanism of how miR-381 controls dendritic branching, it will require identification of all the miR-381 target genes.

Future experimental design

Specific Aim 1: To further characterize miR-381 expression and localization in neurons.

Rationale:

I have shown that miR-381 is a brain-specific microRNA expressed in different brain regions, and its expression increases as the brain matures. However I did not provide evidence showing in which brain cell types that miR-381 is expressed. Knowledge of this will be essential because it will indicate whether or not the miR-381 induced dendritic branching phenotype is neuron-autonomous or not. I will use in-situ hybridization for miR-381 on brain section or in neuronal culture for this purpose.

In addition, it has been shown that some of the miRNAs in the Dlk1-Gt12 domain are regulated by Mef2 upon neuronal activation. It would be interesting to know if

miR-381 is also regulated the same way, which might provide an additional mechanism to link neuronal activity and dendritic structure remodeling.

Experiment 1: Using *in-situ* hybridization to determine the expression of cell types and the sub-cellular localization of miR-381 in hippocampal neurons.

To precisely determine the expression pattern of miR-381, *in-situ* hybridization may give a better resolution of what cell types and the sub-cellular localization of miR-381. Both brain sections and cultured hippocampal cells can be used for the *in-situ* hybridization. Brain sections are more suitable to determining cell type, while the cultured monolayer cell system is better for studying staining of sub-cellular localization.

P14 mice brain will be used for brain section *in-situ* hybridization. The brain will be dissected and flash frozen in liquid nitrogen. 10μm cryosections of brain will be fixed in 4% PFA and hybridized with a DIG-labeled LNA miR-381 probe. The section will be further stained with anti-DIG together with multiple neuronal cell type markers including Tuj1 (neuron), GFAP (glial) and claudin 11 (oligodendrocyte).

Similarly, the cultured hippocampal neurons can be used for *in-situ* hybridization. Neurons will also be fixed by 4% PFA and hybridized with a DIG labeled LNA

miR-381 probe. Neurons will then be stained with anti-DIG together with multiple neuronal cell types markers including Tuj1 (neuron), GFAP (glial) and claudin 11 (oligodendrocyte). To determine the sub-cellular localization, synapsin (synapses, dendritic spines), MAP2 (dendrites), tau (axons), PSD-95 (synapse), Golgi marker, Mitochondrial marker, and DAPI (nucleus) antibodies will be used.

One potential problem here might be that some antibodies will not work after the hybridization with miR-381 probe because of the 55-60^{0}C heating. In that case, for the experiment to determine miR-381 expressing cell types, I will consider double *in-situ* hybridization instead. MiR-381 probe will be labeled with DIG and the other neuronal marker probes (GFAP, beta tubulin III and claudin 11) will be labeled with biotin. DIG and biotin will then stained with secondary antibodies with different fluorophores. For the sub-cellular localization experiments, it is known that Golgi marker, mitochondrial marker (MitoTracker) and synapsin antibody will work at this condition. Other structures will have to be determined by the neuronal morphology using light microscopy.

Determining the sub-cellular localization of miR-381 is crucial because it will be the first clue about how miR-381 functions to regulate dendritic branching. For example, another miRNA in the Dlk1-Gt12 domain, miR-134, was detected in the dendrite-synaptosome. It was subsequently found to regulate local dendritic spine morphogenesis (Schratt et al., 2006).

Experiment 2: To determine if the expression of miR-381 is regulated by neuronal activity.

An illustration of this experiment is shown in Figure 5.7. E18 mouse hippocampi will be dissected and cultured in dishes. Cultured hippocampal cells will be treated with cytosine arabinoside to remove glial cells to obtain a glial-free neuronal culture. I will then treat the neurons with either KCl or BDNF to mimic neuronal activity. 5DIV neuronal cultures will be treated with 16mM KCl for 1, 2 or 6 hours. For BDNF treatment, the 5DIV neurons will be treated with 40ng/ml BDNF for 1, 2 or 6 hours. The total RNA will then be extracted from these neurons and subjected to

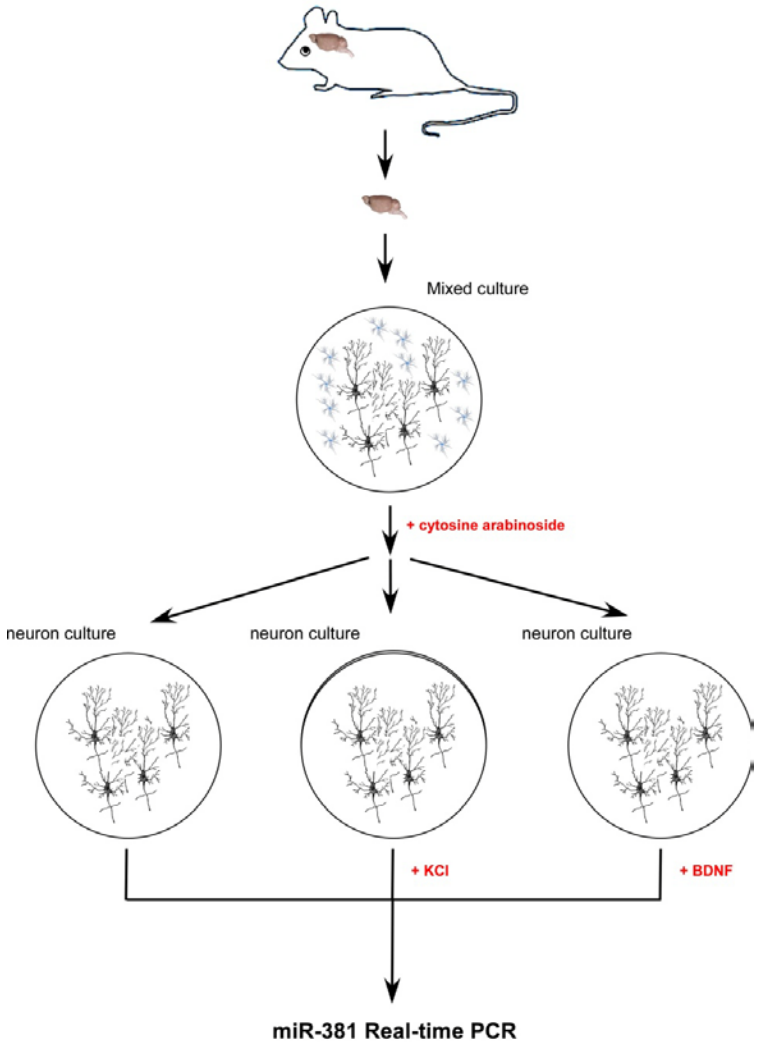

Figure 5.7. *In- vitro* culture experiment for miR-381 Real-time PCR. Hippocampus dissected from E18 mouse brain and cultured in poly d-lysine treated plate (mixed culture). Cells are treated with cytosine arabinoside to remove glial cells. The cultured hippocampal neurons will be treated with KCl or BDNF to study neuronal activity regulation of miR-381 expression.

miR-381 real-time PCR. I expect that the quantity of miR-381 will increase upon sustained KCl or BDNF treatment.

Specific Aim 2: Further characterization of neuronal phenotypes of loss-of-function and gain-of-function related to miR-381.

Rationale: I have characterized the gain-of-function or loss-of-function dendritic phenotype of miR-381 in cultured hippocampal neurons. However, I did not characterize the function of miR-381 in the context of the whole brain. Because of the partial redundancy between miR-300 and miR-381, further specific genetic experiments are required to distinguish the unique functions of miR-381 and miR-300. Therefore, mouse lines with a genetic deletion of miR-381 must be generated in order to answer these questions. In addition, I can also generate miR-381 transgenic mice or miR-381 sponge transgenic mice to study the function of miR-381 in-vivo.

Experiment 1: Generating a miR-381 knock-out mouse.

The genetic locus of miR-381 is shown in Figure 5.8A. The 5' neighbor gene of miR-381 is miR-300 and the 3' neighbor gene is miR-487b. I will be generating a loxP flanked miR-381 allele. ES cells will be targeted with the alleles as shown in Figure 5.8A. ES cell will be positively selected for neomycin and negatively based on Diphteria Toxin A (DTA). Target ES cells will be transfected with an FLP expression plasmid to remove the neo cassette. These ES cells will be then be used to produce miR-381 floxed mice.

(1) Germline deletion of miR-381:

The complete deletion of miR-381 can be achieved by crossing male miR-$381^{flox/flox}$ mice to Sox2-cre or CAG-cre female mice. F2 generation from these crosses will be used to evaluate the function of miR-381 after I confirm that miR-381 is successfully deleted from the animal using either Northern blotting or Real-time PCR. Since miR-381 is maternally imprinted, the $miR381^{flox}$/+ mice can be used for analysis, in which maternal derived miR-381^{flox} mice will be a miR-381 knockout while paternal derived miR-381^{flox} mice will be used for a heterozygous control.

(2) GFAP-cre, CamKII-cre, Synapsin-cre or Nse (Neuron-specific enolase) -cre^{CK1} mediated deletion of miR-381:

If I can confirm that miR-381 is a neuron-specific miRNA, I can use several neuronal cre lines to delete miR-381 in order to study the function of miR-381 in

hippocampal neurons more specifically. GFAP-cre (Zhuo et al., 2001) will delete miR-381 in the entire hippocampus including the pyramidal and granule neurons as well as astrocytes. Nse-cre ^{CK1} will delete miR-381 in most of the neuronal regions in the nervous system (Kwon et al., 2006b). CamKII-cre (T-50 line) (Tsien et al., 1996) will delete miR-381 in the neurons of Ammon's Horn and the dentate gyrus. Synapsin 1-cre (Zhu et al., 2001) will delete miR-381 in all the pyramidal and granule neurons.

Experiment 2: Generating a miR-381 transgenic mouse.

I chose to use a cre-mediated expression system to over-express miR-381 in a cell type specific manner. As shown in Figure 5.8B, I will knock-in a miR-381 hairpin sequence at the 3' end of the lacZ gene into the Rosa26 locus. I can then use a Pol II promoter of the Rosa26 locus to drive lacZ and miR-381 fusion mRNA and the miR-381 hairpin will be processed into mature miR-381 afterward. To achieve cell-type-specific expression, I will add three polyA sites flanked by two loxP sites at the 5' end of the lacZ gene. In contrast to most of the Rosa26 knock-in construct designs, I will use three polyA sequences instead of repetitive stop codons to make sure that there is no RNA (rather than protein translation) transcribed when loxP sites are not recombined by cre. Similar to Experiment 1, ES cells will be targeted and used for generating the chimeric mice. F2 mice will be used for over-expression experiments. Sox2-cre/CAG-cre female mice will be

used to generate germ-line deletion and GFAP-cre, Synapsin 1-cre, CamKII-cre or Nse-cre ^{CK1} will be used to express miR-381 in different neuronal types in the hippocampus.

Experiment 3: Generating a miR-381 sponge transgenic mouse.

I will use the same strategy as in Experiment 2 to generate a miR-381 sponge transgenic mouse (Figure 5.8C). The miR-381 sponge construct I used in this manuscript (Fig. 5.5A) will be modified and targeted to the Rosa26 locus. I will also introduce a loxP flanked triple polyA sequence at the 5' end of the miR-381 sponge. The breeding strategy will be the same as in Experiment 2.

Experiment 4: Histologic analysis of the miR-381 KO, miR-381 or miR-381 sponge transgenic mouse.

(1) Morphologic analysis of hippocampal neurons *in-vitro*:

Hippocampal neuron cultures will be prepared from all the mouse models described above. 10DIV neurons will be fixed with 4% PFA and stained with several antibodies to show different neuronal structures. Tuj1 (whole neuron structure), tau (axon) and MAP2 (dendrite) antibodies will be used to show the basic neuronal structure. Synaptophysin and PSD95 antibodies will be used to show a presynaptic-postsynatptic pair, which is an indicator of mature synapses. Images will be analyzed using MetaMorph. The quantification of dendrite length,

branching and synapse number will be compared among the different mouse models. I expect to see similar phenotypes as those seen in the miR-381/miR-381 sponge transfection experiment.

(2) Histologic analysis of hippocampal brain sections.

Hippocampi from different mouse models will be dissected and flash frozen. 10μm sections will be used for immuno-histochemical analysis. The same antibodies as (2) will be used to show the neuronal structures. Images will be analyzed using MetaMorph as well.

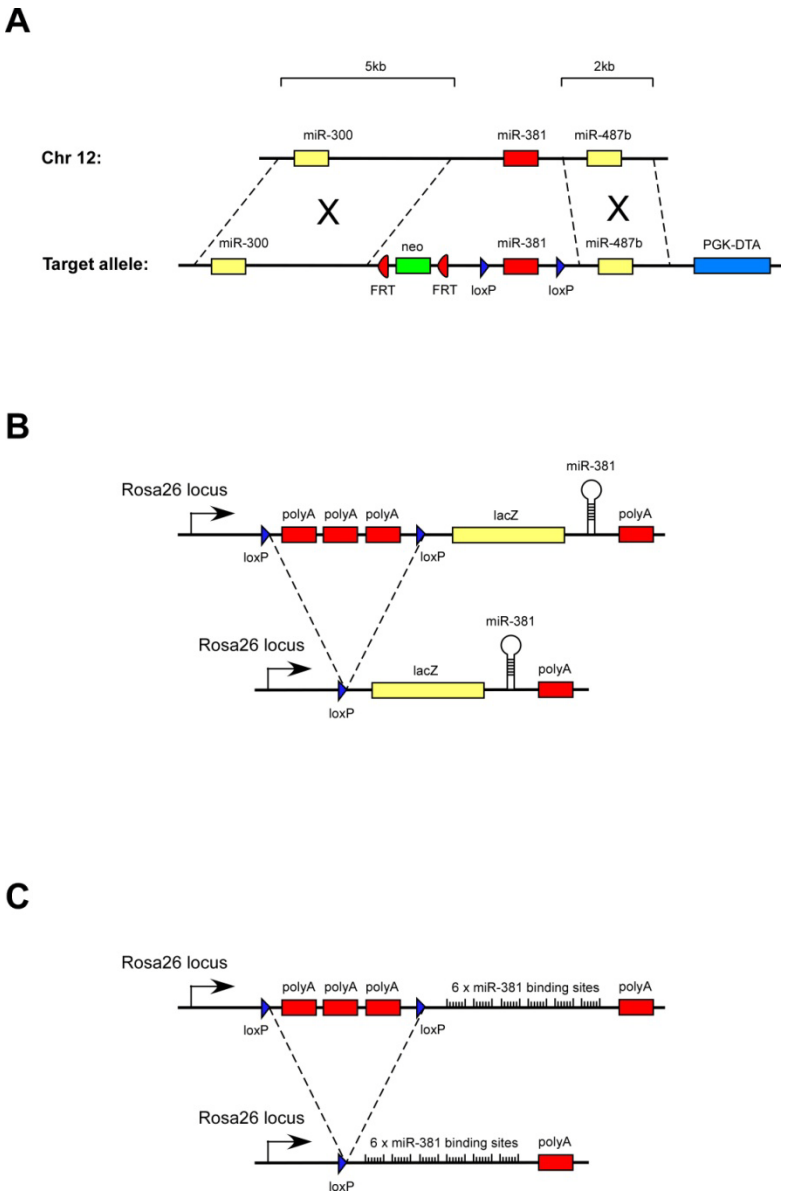

Figure 5.8. Targeting strategy for miR-381 mutant mice. (A). miR conditional knockout strategy. **(B).** miR-381 transgenic strategy. **(C).** miR-381 sponge transgenic strategy.

Discussion of mouse genetic studies.

Many miRNA deletions (especially for those miRNAs that are enriched in adult stage) shows no obvious developmental phenotypes but they fail to respond to stress or injuries (van Rooij et al., 2007; Wang et al., 2008; Williams et al., 2009). It is possible that miR-381 deletion or over-expression in mice also have a similar phenotype. If this is the case, I will induce some stress such as ischemic stroke in mouse to see if miR-381 deletion or miR-381 over-expression will have a different response to stress compared to wild type. It has been shown that ischemic stroke will trigger neuron stem cell proliferation, migration and differentiation (Liu et al., 2009). It will be interesting to examine if deletion or over-expression of miR-381 will block or facilitate the brain recovery after the ischemic stroke.

Specific Aim 3: Mechanistic study of miR-381 regulated neuronal dendrite branching.

Rationale: To better understand the mechanism of the miR-381 mediated dendritic branching phenotype, the target gene(s) of miR-381 needs to be defined. There are several approaches that can be used to search for the target genes. First, bioinformatic prediction provides an easy way to generate a list of miRNA

target genes, which can be further tested using western blotting and the luciferase reporter assay. However, this mode of prediction has been shown to produce a lot of false-positives. Second, microarray analysis is a high throughput method used to define genes whose expression is regulated by a miRNA. Although miRNA binding to an mRNA often leads to translation inhibition, some binding of miRNA with a perfect seeding region match also leads to mRNA degradation. Thus, microarray analysis is good for finding such genes. It should be noted that genes found by microarray analysis can be regulated by miRNA both directly and indirectly. Further biochemical experiments are needed to distinguish these two possibilities. Third, recently there are some biochemical pull-down assays that have been developed to directly isolate miRNA-bound mRNA. However, it is possible that this method cannot identify all the target genes for a miRNA. Therefore, combining all these approaches may increase our chances of identifying the true target gene(s) for miR-381.

Experiment 1: Candidate gene study.

Candidate genes can be predicted by several bioinformatic software programs. The target genes predicted by multiple programs have a better chance to be the true target of a miRNA. The target genes predicted by at least two software programs are listed in Table 5.1, in which two motor proteins, KIF11 and KIF1B,

are of great interest. To test if these genes are true target genes, I can use two methods in neurons. First, use western blot to examine if their expression is decreased when miR-381 is over-expressed in neuronal cells. Second, I will clone the 3'UTR of a potential target gene and ligate it to the 3' end of a luciferase reporter. A luciferase assay will be used to test if miR-381 over-expression will decrease luciferase activity. In addition, if the luciferase assay result is as expected, I will mutate the miR-381 binding site(s) at 3'UTR of the potential target gene to see if the luciferase activity reduction is miR-381 binding dependent.

Experiment 2: microarray analysis to search for miR-381 target genes.

Two sources of RNA can be used for microarray analysis. First, cultured hippocampal neurons transfected/infected with miR-381 or a miR-381 sponge can be used for this purpose. Second, the neurons isolated from miR-381 KO mice and miR-381 or miR-381 sponge transgenic mice can also be used. Total RNA will be isolated from neurons, amplified and labeled with biotin using the Ambion cRNA amplification kit. The labeled cRNA will be used for microarray analysis using the Illuminar microarray system. An RNA quantity with a profile that is miR-381 sponge/miR-381 KO > control > miR-381 over-expression would be a potential target gene for miR-381.

Experiment 3: biochemistry approach to pull down miR-381 target genes.

Figure 5.9 shows the procedure of this experiment (Modified from (Andachi, 2008)). Total cell lysate will be derived from either cultured hippocampal neurons or the hippocampus of a wild type mouse. Treatment with the strong detergent SDS at low temperature will destabilize the RISC complex protein and make the reverse transcription easier to start. First strand cDNA will be synthesized using the reverse transcription reaction. Double stranded DNA will

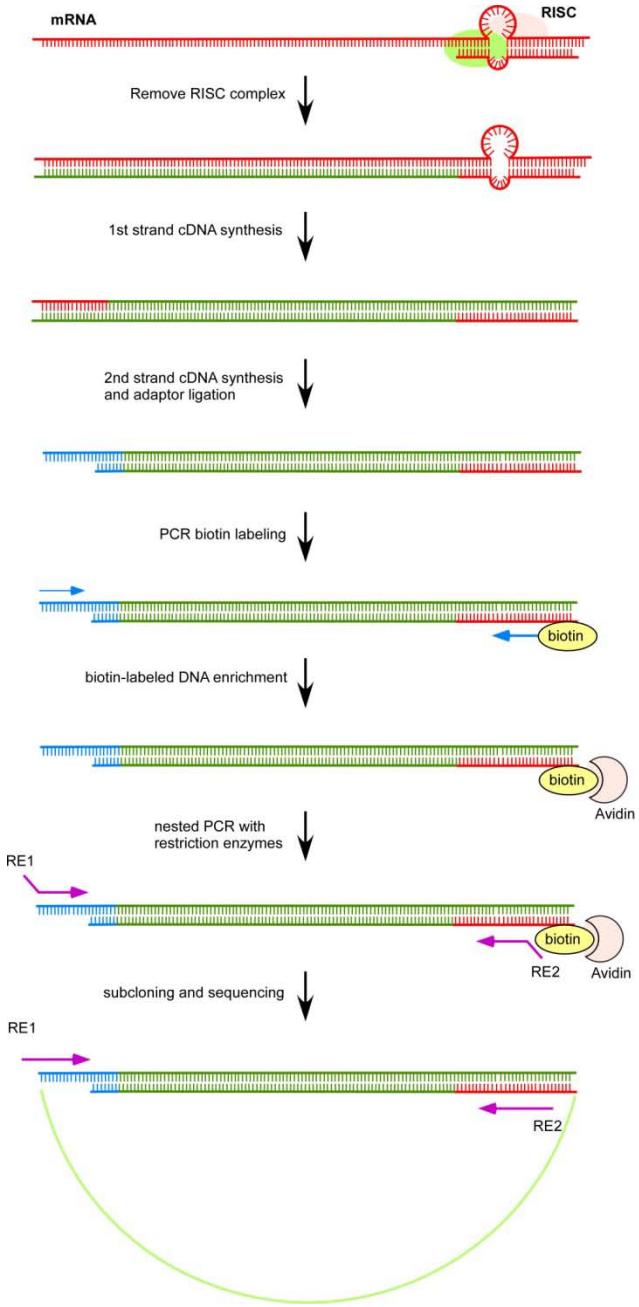

Figure 5.9. Strategy to clone miR-381 target genes. This method is modified from (Andachi, 2008).

be synthesized using a random primer with an adaptor sequence and a biotin-labeled miR-381 specific reverse primer. The miR-381 specific double stranded DNA will be enriched using an avidin pull-down, which will be used for a second round of amplification by a nest PCR using primers with flanking restriction enzyme sites. These DNA will then be sub-cloned and sequenced to identify the potential target genes.

CHAPTER VI

CONCLUSION AND PERSPECTIVE

The focus of my graduate study is to understand the mechanism of synapse formation, especially neurotrophin regulated synapse formation and plasticity. Previous study in our lab showed that deletion of BDNF receptor TrkB results in reduction of dendritic spine density in hippocampus neurons. *In vitro* culture experiment showed that the function of BDNF/TrkB signaling pathway is cell autonomous. However, how cell-automous BDNF/TrkB signaling regulates synaptogenesis is still elusive. There are studies showing that dendritic filopodia motility is a key factor that determines how well the excitatory synapses can be formd at the dendritic spines (Ziv and Smith, 1996). Chapter 3 and chapter 4 my thesis showed that BDNF/TrkB signaling regulates dendritic filopodia motility, and defined the downstream signaling pathways that are responsible for this regulation. TrkB regulates different downstream signaling pathways using different amino acids in its cytosolic domain. In chapter 3, I used various mutation forms of TrkB to selectively block downstream pathways and found that the downstream PI3K signaling pathway but not the PLCγ pathway is required for the function of TrkB for dendritic filopodia motility regulation. The experiments using chemical inhibitors of different molecules and using different genetic models (such as Pten KO or Nf1 KO mice) also confirm this conclusion. We found that Phosphatidylinositol 3,4,5- trisphosphate (PIP3) was preferentially localized in filopodia and this distribution was enhanced by BDNF application. We proposed that the intracellular control of filopodial dynamics by BDNF/TrkB

signaling converged on PI3K activation and PIP3 accumulation. In chapter 4, we try to take a further step forward on the mechanism of BDNF/TrkB regulated dendritic filopodia motility. We used the same *in vitro* cultured hippocampal neurons system and showed that the small GTPases, Rac1 and RhoA, can positively and negatively control the dendritic filopodia motility, respectively. We proposed that BDNF/TrkB signaling induced dendritic filopodia motility increase is through regulating the Rac1/RhoA activity. We showed that Rac1 inactivation can completely abolish TrkB overexpression induced dendritic filopodia motility increase. We also showed that inactivation of RhoA and Rho kinase can rescue TrkB kinase dead form induced dendritic filopodia motility decrease. These data favor the possibility that Rac1 and RhoA function at the downstream of BDNF/TrkB signaling pathway, and they may act as the end point for the dynamics structure control in the dendritic filopodia.

In chapter 5, I switch the gear to a microRNA, miR-381, to show that it plays an important role in dendritic branching in hippocampal neurons. Originally I studied this microRNA because it was predicted to target BDNF 3'UTR. However, using a luciferase assay, I found that BDNF is not a true target of miR-381, but we found a surprising function of miR-381 in dendritic branching. We showed that miR-381 is a positive regulator for dendritic branching, and its function is both required and sufficient. Since miR-381 is a brain-specific microRNA and its expression increase as the brain matures, we expect that miR-381 plays an

essential role in neuronal dendritic morphogenesis and remodeling after birth. Further mechanism of miR-381 awaits the identification of miR-381 target genes in the future.

Our data in chapter 3 pinpoint the downstream signaling pathway of BDNF/TrkB to PI3K pathway in term of regulating the synapse formation and dendrtic filopodia motility for the first time. It has been known for a long time that activity-dependent BDNF release is essential for local synapse structure remodeling, which is considered as a basis for learning and memory in mammals. Defect in BDNF signaling has been linked to various mental disorders. For example, in human, mutations in BDNF gene lead to poorer episodic memory (Egan et al., 2003),obsessive-compulsive disorder (OCD) (Hall et al., 2003), and biopolar disorder (Geller et al., 2004). It will be interesting to investigate whether the disregulation of dendritic filopodia motility may serve as the mechanism of these various neuronal disorders.

BDNF/ TrkB, PI3K and Rac1/RhoA are generally expressed in neurons or other cell types. Therefore, they cannot be considered as perfect pharmaceutical targets to treat diseases. However, there are numerous regulators of Rac1 and RhoA, the GAPs and GEFs, many of which have specific expression pattern. If we can

determine that BDNF/TrkB→Rac1/RhoA signaling pathway is essential for the neuronal disorders such as OCD and the bipolar disorder, to look for a neuron-type-specific GAP/GEF may enable us to find a better drug target for treating these disorders.

The study of microRNA miR-381 is of great interest as well. It provided another layer of mechanism (post-transcriptional regulation) for the neuronal and dendritic morphogenesis. It will be interesting to study how the regulation of neuronal structure by microRNAs can be incorporated into other idenditified mechanisms. For example, BDNF has been shown to promote dendrite outgrowth and branching (Tolwani et al., 2002), which might be partially through regulating some microRNAs function locally such as miR-381. Mouse genetic studies will tell us if these microRNAs are also important at the brain-function level and if they are also related to neuronal diseases. MicroRNAs can serve as better drug targets because one can easily inhibit or overexpress them in a sequence-specific manner using cell-permeable antisense/sense oligos (Poller et al.), and then regulate multiple target genes at the same time. We will look forward to seeing more translational studies about microRNAs, especially in the neuroscience field in the future.

BIBLOGRAPHY

Akins, M.R., and Biederer, T. (2006). Cell-cell interactions in synaptogenesis. Curr Opin Neurobiol *16*, 83-89.

Alessi, D.R., Cuenda, A., Cohen, P., Dudley, D.T., and Saltiel, A.R. (1995). PD 098059 is a specific inhibitor of the activation of mitogen-activated protein kinase kinase in vitro and in vivo. J Biol Chem *270*, 27489-27494.

Alonso, M., Medina, J.H., and Pozzo-Miller, L. (2004). ERK1/2 activation is necessary for BDNF to increase dendritic spine density in hippocampal CA1 pyramidal neurons. Learn Mem *11*, 172-178.

Alsina, B., Vu, T., and Cohen-Cory, S. (2001). Visualizing synapse formation in arborizing optic axons in vivo: dynamics and modulation by BDNF. Nat Neurosci *4*, 1093-1101.

Ambros, V. (2004). The functions of animal microRNAs. Nature *431*, 350-355.

Andachi, Y. (2008). A novel biochemical method to identify target genes of individual microRNAs: identification of a new Caenorhabditis elegans let-7 target. RNA *14*, 2440-2451.

Arstikaitis, P., Gauthier-Campbell, C., Carolina Gutierrez Herrera, R., Huang, K., Levinson, J.N., Murphy, T.H., Kilimann, M.W., Sala, C., Colicos, M.A., and El-Husseini, A. (2008). Paralemmin-1, a modulator of filopodia induction is required for spine maturation. Mol Biol Cell *19*, 2026-2038.

Atwal, J.K., Massie, B., Miller, F.D., and Kaplan, D.R. (2000). The TrkB-Shc site signals neuronal survival and local axon growth via MEK and P13-kinase. Neuron *27*, 265-277.

Backman, S.A., Stambolic, V., Suzuki, A., Haight, J., Elia, A., Pretorius, J., Tsao, M.S., Shannon, P., Bolon, B., Ivy, G.O., *et al.* (2001). Deletion of Pten in mouse brain causes seizures, ataxia and defects in soma size resembling Lhermitte-Duclos disease. Nat Genet *29*, 396-403.

Bagni, C., and Greenough, W.T. (2005). From mRNP trafficking to spine dysmorphogenesis: the roots of fragile X syndrome. Nat Rev Neurosci *6*, 376-387.

Bartel, D.P. (2004). MicroRNAs: genomics, biogenesis, mechanism, and function. Cell *116*, 281-297.

Bourgeron, T. (2009). A synaptic trek to autism. Curr Opin Neurobiol *19*, 231-234.

Butler, M.G., Dasouki, M.J., Zhou, X.P., Talebizadeh, Z., Brown, M., Takahashi, T.N., Miles, J.H., Wang, C.H., Stratton, R., Pilarski, R., *et al.* (2005). Subset of individuals with autism spectrum disorders and extreme macrocephaly associated with germline PTEN tumour suppressor gene mutations. J Med Genet *42*, 318-321.

Cabelli, R.J., Allendoerfer, K.L., Radeke, M.J., Welcher, A.A., Feinstein, S.C., and Shatz, C.J. (1996). Changing patterns of expression and subcellular localization of TrkB in the developing visual system. J Neurosci *16*, 7965-7980.

Cabelli, R.J., Shelton, D.L., Segal, R.A., and Shatz, C.J. (1997). Blockade of endogenous ligands of trkB inhibits formation of ocular dominance columns. Neuron *19*, 63-76.

Cantrell, D.A. (2001). Phosphoinositide 3-kinase signalling pathways. J Cell Sci *114*, 1439-1445.

Carmona, M.A., Martinez, A., Soler, A., Blasi, J., Soriano, E., and Aguado, F. (2003). Ca(2+)-evoked synaptic transmission and neurotransmitter receptor levels are impaired in the forebrain of trkb (-/-) mice. Mol Cell Neurosci *22*, 210-226.

Castren, E., Zafra, F., Thoenen, H., and Lindholm, D. (1992). Light regulates expression of brain-derived neurotrophic factor mRNA in rat visual cortex. Proc Natl Acad Sci U S A *89*, 9444-9448.

Chen, H., and Firestein, B.L. (2007). RhoA regulates dendrite branching in hippocampal neurons by decreasing cypin protein levels. J Neurosci *27*, 8378-8386.

Cohen-Cory, S. (2002). The developing synapse: construction and modulation of synaptic structures and circuits. Science *298*, 770-776.

Colonnier, M. (1968). Synaptic patterns on different cell types in the different laminae of the cat visual cortex. An electron microscope study. Brain Res *9*, 268-287.

Connor, B., Young, D., Yan, Q., Faull, R.L., Synek, B., and Dragunow, M. (1997). Brain-derived neurotrophic factor is reduced in Alzheimer's disease. Brain Res Mol Brain Res *49*, 71-81.

Dailey, M.E., and Smith, S.J. (1996). The dynamics of dendritic structure in developing hippocampal slices. J Neurosci *16*, 2983-2994.

Dasgupta, B., and Gutmann, D.H. (2003). Neurofibromatosis 1: closing the GAP between mice and men. Curr Opin Genet Dev *13*, 20-27.

Davis, T.H., Cuellar, T.L., Koch, S.M., Barker, A.J., Harfe, B.D., McManus, M.T., and Ullian, E.M. (2008). Conditional loss of Dicer disrupts cellular and tissue morphogenesis in the cortex and hippocampus. J Neurosci *28*, 4322-4330.

De Roo, M., Klauser, P., Mendez, P., Poglia, L., and Muller, D. (2008). Activity-dependent PSD formation and stabilization of newly formed spines in hippocampal slice cultures. Cereb Cortex *18*, 151-161.

Dindot, S.V., Antalffy, B.A., Bhattacharjee, M.B., and Beaudet, A.L. (2008). The Angelman syndrome ubiquitin ligase localizes to the synapse and nucleus, and maternal deficiency results in abnormal dendritic spine morphology. Hum Mol Genet *17*, 111-118.

Ebert, M.S., Neilson, J.R., and Sharp, P.A. (2007). MicroRNA sponges: competitive inhibitors of small RNAs in mammalian cells. Nat Methods *4*, 721-726.

Eberwine, J., Miyashiro, K., Kacharmina, J.E., and Job, C. (2001). Local translation of classes of mRNAs that are targeted to neuronal dendrites. Proc Natl Acad Sci U S A *98*, 7080-7085.

Egan, M.F., Kojima, M., Callicott, J.H., Goldberg, T.E., Kolachana, B.S., Bertolino, A., Zaitsev, E., Gold, B., Goldman, D., Dean, M., *et al.* (2003). The BDNF val66met polymorphism affects activity-dependent secretion of BDNF and human memory and hippocampal function. Cell *112*, 257-269.

Elmariah, S.B., Crumling, M.A., Parsons, T.D., and Balice-Gordon, R.J. (2004). Postsynaptic TrkB-mediated signaling modulates excitatory and inhibitory neurotransmitter receptor clustering at hippocampal synapses. J Neurosci *24*, 2380-2393.

Eom, T., Antar, L.N., Singer, R.H., and Bassell, G.J. (2003). Localization of a beta-actin messenger ribonucleoprotein complex with zipcode-binding protein modulates the density of dendritic filopodia and filopodial synapses. J Neurosci *23*, 10433-10444.

Ernfors, P., Bengzon, J., Kokaia, Z., Persson, H., and Lindvall, O. (1991). Increased levels of messenger RNAs for neurotrophic factors in the brain during kindling epileptogenesis. Neuron *7*, 165-176.

Ethell, I.M., and Yamaguchi, Y. (1999). Cell surface heparan sulfate proteoglycan syndecan-2 induces the maturation of dendritic spines in rat hippocampal neurons. J Cell Biol *144*, 575-586.

Etienne-Manneville, S., and Hall, A. (2002). Rho GTPases in cell biology. Nature *420*, 629-635.

Fawcett, J.P., Aloyz, R., McLean, J.H., Pareek, S., Miller, F.D., McPherson, P.S., and Murphy, R.A. (1997). Detection of brain-derived neurotrophic factor in a vesicular fraction of brain synaptosomes. J Biol Chem *272*, 8837-8840.

Fiala, J.C., Feinberg, M., Popov, V., and Harris, K.M. (1998). Synaptogenesis via dendritic filopodia in developing hippocampal area CA1. J Neurosci *18*, 8900-8911.

Fiore, R., Khudayberdiev, S., Christensen, M., Siegel, G., Flavell, S.W., Kim, T.K., Greenberg, M.E., and Schratt, G. (2009). Mef2-mediated transcription of the miR379-410 cluster regulates activity-dependent dendritogenesis by fine-tuning Pumilio2 protein levels. EMBO J *28*, 697-710.

Fleming, I.N., Batty, I.H., Prescott, A.R., Gray, A., Kular, G.S., Stewart, H., and Downes, C.P. (2004). Inositol phospholipids regulate the guanine-nucleotide-exchange factor Tiam1 by facilitating its binding to the plasma membrane and regulating GDP/GTP exchange on Rac1. Biochem J *382*, 857-865.

Fuerst, P.G., Bruce, F., Tian, M., Wei, W., Elstrott, J., Feller, M.B., Erskine, L., Singer, J.H., and Burgess, R.W. (2009). DSCAM and DSCAML1 function in self-avoidance in multiple cell types in the developing mouse retina. Neuron *64*, 484-497.

Furutani, Y., Matsuno, H., Kawasaki, M., Sasaki, T., Mori, K., and Yoshihara, Y. (2007). Interaction between telencephalin and ERM family proteins mediates dendritic filopodia formation. J Neurosci *27*, 8866-8876.

Garey, L.J., Ong, W.Y., Patel, T.S., Kanani, M., Davis, A., Mortimer, A.M., Barnes, T.R., and Hirsch, S.R. (1998). Reduced dendritic spine density on cerebral cortical pyramidal neurons in schizophrenia. J Neurol Neurosurg Psychiatry *65*, 446-453.

Gaudilliere, B., Konishi, Y., de la Iglesia, N., Yao, G., and Bonni, A. (2004). A CaMKII-NeuroD signaling pathway specifies dendritic morphogenesis. Neuron *41*, 229-241.

Gehler, S., Shaw, A.E., Sarmiere, P.D., Bamburg, J.R., and Letourneau, P.C. (2004). Brain-derived neurotrophic factor regulation of retinal growth cone filopodial dynamics is mediated through actin depolymerizing factor/cofilin. J Neurosci *24*, 10741-10749.

Geller, B., Badner, J.A., Tillman, R., Christian, S.L., Bolhofner, K., and Cook, E.H., Jr. (2004). Linkage disequilibrium of the brain-derived neurotrophic factor Val66Met polymorphism in children with a prepubertal and early adolescent bipolar disorder phenotype. Am J Psychiatry *161*, 1698-1700.

Giraldez, A.J., Cinalli, R.M., Glasner, M.E., Enright, A.J., Thomson, J.M., Baskerville, S., Hammond, S.M., Bartel, D.P., and Schier, A.F. (2005). MicroRNAs regulate brain morphogenesis in zebrafish. Science *308*, 833-838.

Gomes, R.A., Hampton, C., El-Sabeawy, F., Sabo, S.L., and McAllister, A.K. (2006). The dynamic distribution of TrkB receptors before, during, and after synapse formation between cortical neurons. J Neurosci *26*, 11487-11500.

Gonzalez, M., Ruggiero, F.P., Chang, Q., Shi, Y.J., Rich, M.M., Kraner, S., and Balice-Gordon, R.J. (1999). Disruption of Trkb-mediated signaling induces disassembly of postsynaptic receptor clusters at neuromuscular junctions. Neuron *24*, 567-583.

Haditsch, U., Leone, D.P., Farinelli, M., Chrostek-Grashoff, A., Brakebusch, C., Mansuy, I.M., McConnell, S.K., and Palmer, T.D. (2009). A central role for the small GTPase Rac1 in hippocampal plasticity and spatial learning and memory. Mol Cell Neurosci *41*, 409-419.

Hall, D., Dhilla, A., Charalambous, A., Gogos, J.A., and Karayiorgou, M. (2003). Sequence variants of the brain-derived neurotrophic factor (BDNF) gene are strongly associated with obsessive-compulsive disorder. Am J Hum Genet *73*, 370-376.

Hand, R., Bortone, D., Mattar, P., Nguyen, L., Heng, J.I., Guerrier, S., Boutt, E., Peters, E., Barnes, A.P., Parras, C., *et al.* (2005). Phosphorylation of Neurogenin2 specifies the migration properties and the dendritic morphology of pyramidal neurons in the neocortex. Neuron *48*, 45-62.

Harris, K.M., Jensen, F.E., and Tsao, B. (1992). Three-dimensional structure of dendritic spines and synapses in rat hippocampus (CA1) at postnatal day 15 and

adult ages: implications for the maturation of synaptic physiology and long-term potentiation. J Neurosci *12*, 2685-2705.

Hartmann, M., Brigadski, T., Erdmann, K.S., Holtmann, B., Sendtner, M., Narz, F., and Lessmann, V. (2004). Truncated TrkB receptor-induced outgrowth of dendritic filopodia involves the p75 neurotrophin receptor. J Cell Sci *117*, 5803-5814.

Hartmann, M., Heumann, R., and Lessmann, V. (2001). Synaptic secretion of BDNF after high-frequency stimulation of glutamatergic synapses. EMBO J *20*, 5887-5897.

Haubensak, W., Narz, F., Heumann, R., and Lessmann, V. (1998). BDNF-GFP containing secretory granules are localized in the vicinity of synaptic junctions of cultured cortical neurons. J Cell Sci *111 (Pt 11)*, 1483-1493.

He, L., and Hannon, G.J. (2004). MicroRNAs: small RNAs with a big role in gene regulation. Nat Rev Genet *5*, 522-531.

Hill, D.B., Plaza, M.J., Bonin, K., and Holzwarth, G. (2004). Fast vesicle transport in PC12 neurites: velocities and forces. Eur Biophys J *33*, 623-632.

Holtmaat, A., and Svoboda, K. (2009). Experience-dependent structural synaptic plasticity in the mammalian brain. Nat Rev Neurosci *10*, 647-658.

Hoogenraad, C.C., Milstein, A.D., Ethell, I.M., Henkemeyer, M., and Sheng, M. (2005). GRIP1 controls dendrite morphogenesis by regulating EphB receptor trafficking. Nat Neurosci *8*, 906-915.

Horch, H.W., and Katz, L.C. (2002). BDNF release from single cells elicits local dendritic growth in nearby neurons. Nat Neurosci *5*, 1177-1184.

Horch, H.W., Kruttgen, A., Portbury, S.D., and Katz, L.C. (1999). Destabilization of cortical dendrites and spines by BDNF. Neuron *23*, 353-364.

Howe, C.L., Valletta, J.S., Rusnak, A.S., and Mobley, W.C. (2001). NGF signaling from clathrin-coated vesicles: evidence that signaling endosomes serve as a platform for the Ras-MAPK pathway. Neuron *32*, 801-814.

Hu, B., Nikolakopoulou, A.M., and Cohen-Cory, S. (2005). BDNF stabilizes synapses and maintains the structural complexity of optic axons in vivo. Development *132*, 4285-4298.

Huang, E.J., and Reichardt, L.F. (2003). Trk receptors: roles in neuronal signal transduction. Annu Rev Biochem *72*, 609-642.

Huang, Y.E., Iijima, M., Parent, C.A., Funamoto, S., Firtel, R.A., and Devreotes, P. (2003). Receptor-mediated regulation of PI3Ks confines PI(3,4,5)P3 to the leading edge of chemotaxing cells. Mol Biol Cell *14*, 1913-1922.

Iijima, M., and Devreotes, P. (2002). Tumor suppressor PTEN mediates sensing of chemoattractant gradients. Cell *109*, 599-610.

Innocenti, M., Frittoli, E., Ponzanelli, I., Falck, J.R., Brachmann, S.M., Di Fiore, P.P., and Scita, G. (2003). Phosphoinositide 3-kinase activates Rac by entering in a complex with Eps8, Abi1, and Sos-1. J Cell Biol *160*, 17-23.

Ji, Y., Pang, P.T., Feng, L., and Lu, B. (2005). Cyclic AMP controls BDNF-induced TrkB phosphorylation and dendritic spine formation in mature hippocampal neurons. Nat Neurosci *8*, 164-172.

Jin, T., Zhang, N., Long, Y., Parent, C.A., and Devreotes, P.N. (2000). Localization of the G protein betagamma complex in living cells during chemotaxis. Science *287*, 1034-1036.

Jossin, Y., and Goffinet, A.M. (2007). Reelin signals through phosphatidylinositol 3-kinase and Akt to control cortical development and through mTor to regulate dendritic growth. Mol Cell Biol *27*, 7113-7124.

Jourdain, P., Fukunaga, K., and Muller, D. (2003). Calcium/calmodulin-dependent protein kinase II contributes to activity-dependent filopodia growth and spine formation. J Neurosci *23*, 10645-10649.

Jourdi, H., Iwakura, Y., Narisawa-Saito, M., Ibaraki, K., Xiong, H., Watanabe, M., Hayashi, Y., Takei, N., and Nawa, H. (2003). Brain-derived neurotrophic factor signal enhances and maintains the expression of AMPA receptor-associated PDZ proteins in developing cortical neurons. Dev Biol *263*, 216-230.

Kaisho, Y., Shintani, A., Ono, Y., Kato, K., and Igarashi, K. (1991). Regional expression of the nerve growth factor gene family in rat brain during development. Biochem Biophys Res Commun *174*, 379-385.

Kang, H., and Schuman, E.M. (1995). Long-lasting neurotrophin-induced enhancement of synaptic transmission in the adult hippocampus. Science *267*, 1658-1662.

Kaplan, D.R., and Miller, F.D. (2000). Neurotrophin signal transduction in the nervous system. Curr Opin Neurobiol *10*, 381-391.

Kaufmann, W.E., and Moser, H.W. (2000). Dendritic anomalies in disorders associated with mental retardation. Cereb Cortex *10*, 981-991.

Kayser, M.S., Nolt, M.J., and Dalva, M.B. (2008). EphB receptors couple dendritic filopodia motility to synapse formation. Neuron *59*, 56-69.

Kelleher, R.J., 3rd, and Bear, M.F. (2008). The autistic neuron: troubled translation? Cell *135*, 401-406.

Kim, J., Krichevsky, A., Grad, Y., Hayes, G.D., Kosik, K.S., Church, G.M., and Ruvkun, G. (2004). Identification of many microRNAs that copurify with polyribosomes in mammalian neurons. Proc Natl Acad Sci U S A *101*, 360-365.

Klein, R., Martin-Zanca, D., Barbacid, M., and Parada, L.F. (1990). Expression of the tyrosine kinase receptor gene trkB is confined to the murine embryonic and adult nervous system. Development *109*, 845-850.

Klein, R., Parada, L.F., Coulier, F., and Barbacid, M. (1989). trkB, a novel tyrosine protein kinase receptor expressed during mouse neural development. EMBO J *8*, 3701-3709.

Kohara, K., Kitamura, A., Morishima, M., and Tsumoto, T. (2001). Activity-dependent transfer of brain-derived neurotrophic factor to postsynaptic neurons. Science *291*, 2419-2423.

Korte, M., Carroll, P., Wolf, E., Brem, G., Thoenen, H., and Bonhoeffer, T. (1995). Hippocampal long-term potentiation is impaired in mice lacking brain-derived neurotrophic factor. Proc Natl Acad Sci U S A *92*, 8856-8860.

Korte, M., Griesbeck, O., Gravel, C., Carroll, P., Staiger, V., Thoenen, H., and Bonhoeffer, T. (1996). Virus-mediated gene transfer into hippocampal CA1 region restores long-term potentiation in brain-derived neurotrophic factor mutant mice. Proc Natl Acad Sci U S A *93*, 12547-12552.

Krichevsky, A.M., King, K.S., Donahue, C.P., Khrapko, K., and Kosik, K.S. (2003). A microRNA array reveals extensive regulation of microRNAs during brain development. RNA *9*, 1274-1281.

Kumar, V., Zhang, M.X., Swank, M.W., Kunz, J., and Wu, G.Y. (2005). Regulation of dendritic morphogenesis by Ras-PI3K-Akt-mTOR and Ras-MAPK signaling pathways. J Neurosci *25*, 11288-11299.

Kwon, C.H., Luikart, B.W., Powell, C.M., Zhou, J., Matheny, S.A., Zhang, W., Li, Y., Baker, S.J., and Parada, L.F. (2006a). Pten regulates neuronal arborization and social interaction in mice. Neuron *50*, 377-388.

Kwon, C.H., Zhou, J., Li, Y., Kim, K.W., Hensley, L.L., Baker, S.J., and Parada, L.F. (2006b). Neuron-specific enolase-cre mouse line with cre activity in specific neuronal populations. Genesis *44*, 130-135.

Lagos-Quintana, M., Rauhut, R., Yalcin, A., Meyer, J., Lendeckel, W., and Tuschl, T. (2002). Identification of tissue-specific microRNAs from mouse. Curr Biol *12*, 735-739.

Levine, E.S., Dreyfus, C.F., Black, I.B., and Plummer, M.R. (1995). Brain-derived neurotrophic factor rapidly enhances synaptic transmission in hippocampal neurons via postsynaptic tyrosine kinase receptors. Proc Natl Acad Sci U S A *92*, 8074-8077.

Li, H., Radford, J.C., Ragusa, M.J., Shea, K.L., McKercher, S.R., Zaremba, J.D., Soussou, W., Nie, Z., Kang, Y.J., Nakanishi, N., *et al.* (2008). Transcription factor MEF2C influences neural stem/progenitor cell differentiation and maturation in vivo. Proc Natl Acad Sci U S A *105*, 9397-9402.

Lin, Y.L., Lei, Y.T., Hong, C.J., and Hsueh, Y.P. (2007). Syndecan-2 induces filopodia and dendritic spine formation via the neurofibromin-PKA-Ena/VASP pathway. J Cell Biol *177*, 829-841.

Lipton, S.A., Li, H., Zaremba, J.D., McKercher, S.R., Cui, J., Kang, Y.J., Nie, Z., Soussou, W., Talantova, M., Okamoto, S., *et al.* (2009). Autistic phenotype from MEF2C knockout cells. Science *323*, 208.

Liu, Y.P., Lang, B.T., Baskaya, M.K., Dempsey, R.J., and Vemuganti, R. (2009). The potential of neural stem cells to repair stroke-induced brain damage. Acta Neuropathol *117*, 469-480.

Lohof, A.M., Ip, N.Y., and Poo, M.M. (1993). Potentiation of developing neuromuscular synapses by the neurotrophins NT-3 and BDNF. Nature *363*, 350-353.

Lom, B., and Cohen-Cory, S. (1999). Brain-derived neurotrophic factor differentially regulates retinal ganglion cell dendritic and axonal arborization in vivo. J Neurosci *19*, 9928-9938.

Luikart, B.W., Nef, S., Virmani, T., Lush, M.E., Liu, Y., Kavalali, E.T., and Parada, L.F. (2005). TrkB has a cell-autonomous role in the establishment of hippocampal Schaffer collateral synapses. J Neurosci *25*, 3774-3786.

Luikart, B.W., and Parada, L.F. (2006). Receptor tyrosine kinase B-mediated excitatory synaptogenesis. Prog Brain Res *157*, 15-24.

Luikart, B.W., Zhang, W., Wayman, G.A., Kwon, C.H., Westbrook, G.L., and Parada, L.F. (2008). Neurotrophin-dependent dendritic filopodial motility: a convergence on PI3K signaling. J Neurosci *28*, 7006-7012.

Lyons, G.E., Micales, B.K., Schwarz, J., Martin, J.F., and Olson, E.N. (1995). Expression of mef2 genes in the mouse central nervous system suggests a role in neuronal maturation. J Neurosci *15*, 5727-5738.

MacNeil, M.A., and Masland, R.H. (1998). Extreme diversity among amacrine cells: implications for function. Neuron *20*, 971-982.

Maletic-Savatic, M., Malinow, R., and Svoboda, K. (1999). Rapid dendritic morphogenesis in CA1 hippocampal dendrites induced by synaptic activity. Science *283*, 1923-1927.

Marrs, G.S., Green, S.H., and Dailey, M.E. (2001). Rapid formation and remodeling of postsynaptic densities in developing dendrites. Nat Neurosci *4*, 1006-1013.

Martinez, A., Alcantara, S., Borrell, V., Del Rio, J.A., Blasi, J., Otal, R., Campos, N., Boronat, A., Barbacid, M., Silos-Santiago, I., *et al.* (1998). TrkB and TrkC signaling are required for maturation and synaptogenesis of hippocampal connections. J Neurosci *18*, 7336-7350.

Matsuno, H., Okabe, S., Mishina, M., Yanagida, T., Mori, K., and Yoshihara, Y. (2006). Telencephalin slows spine maturation. J Neurosci *26*, 1776-1786.

McAllister, A.K., Katz, L.C., and Lo, D.C. (1997). Opposing roles for endogenous BDNF and NT-3 in regulating cortical dendritic growth. Neuron *18*, 767-778.

McAllister, A.K., Lo, D.C., and Katz, L.C. (1995). Neurotrophins regulate dendritic growth in developing visual cortex. Neuron *15*, 791-803.

Merlot, S., and Firtel, R.A. (2003). Leading the way: Directional sensing through phosphatidylinositol 3-kinase and other signaling pathways. J Cell Sci *116*, 3471-3478.

Miska, E.A., Alvarez-Saavedra, E., Townsend, M., Yoshii, A., Sestan, N., Rakic, P., Constantine-Paton, M., and Horvitz, H.R. (2004). Microarray analysis of microRNA expression in the developing mammalian brain. Genome Biol *5*, R68.

Miyamoto, Y., Yamauchi, J., Tanoue, A., Wu, C., and Mobley, W.C. (2006). TrkB binds and tyrosine-phosphorylates Tiam1, leading to activation of Rac1 and induction of changes in cellular morphology. Proc Natl Acad Sci U S A *103*, 10444-10449.

Murai, K.K., Nguyen, L.N., Irie, F., Yamaguchi, Y., and Pasquale, E.B. (2003). Control of hippocampal dendritic spine morphology through ephrin-A3/EphA4 signaling. Nat Neurosci *6*, 153-160.

Musatov, S., Roberts, J., Brooks, A.I., Pena, J., Betchen, S., Pfaff, D.W., and Kaplitt, M.G. (2004). Inhibition of neuronal phenotype by PTEN in PC12 cells. Proc Natl Acad Sci U S A *101*, 3627-3631.

Nagerl, U.V., Kostinger, G., Anderson, J.C., Martin, K.A., and Bonhoeffer, T. (2007). Protracted synaptogenesis after activity-dependent spinogenesis in hippocampal neurons. J Neurosci *27*, 8149-8156.

Newey, S.E., Velamoor, V., Govek, E.E., and Van Aelst, L. (2005). Rho GTPases, dendritic structure, and mental retardation. J Neurobiol *64*, 58-74.

Niell, C.M., Meyer, M.P., and Smith, S.J. (2004). In vivo imaging of synapse formation on a growing dendritic arbor. Nat Neurosci *7*, 254-260.

Nimchinsky, E.A., Sabatini, B.L., and Svoboda, K. (2002). Structure and function of dendritic spines. Annu Rev Physiol *64*, 313-353.

North, K.N., Riccardi, V., Samango-Sprouse, C., Ferner, R., Moore, B., Legius, E., Ratner, N., and Denckla, M.B. (1997). Cognitive function and academic performance in neurofibromatosis. 1: consensus statement from the NF1 Cognitive Disorders Task Force. Neurology *48*, 1121-1127.

Pak, D.T., and Sheng, M. (2003). Targeted protein degradation and synapse remodeling by an inducible protein kinase. Science *302*, 1368-1373.

Pardo, C.A., and Eberhart, C.G. (2007). The neurobiology of autism. Brain Pathol *17*, 434-447.

Parrish, J.Z., Kim, M.D., Jan, L.Y., and Jan, Y.N. (2006). Genome-wide analyses identify transcription factors required for proper morphogenesis of Drosophila sensory neuron dendrites. Genes Dev *20*, 820-835.

Patapoutian, A., and Reichardt, L.F. (2001). Trk receptors: mediators of neurotrophin action. Curr Opin Neurobiol *11*, 272-280.

Patterson, S.L., Grover, L.M., Schwartzkroin, P.A., and Bothwell, M. (1992). Neurotrophin expression in rat hippocampal slices: a stimulus paradigm inducing LTP in CA1 evokes increases in BDNF and NT-3 mRNAs. Neuron *9*, 1081-1088.

Pelvig, D.P., Pakkenberg, H., Stark, A.K., and Pakkenberg, B. (2008). Neocortical glial cell numbers in human brains. Neurobiol Aging *29*, 1754-1762.

Poller, W., Hajjar, R., Schultheiss, H.P., and Fechner, H. Cardiac-targeted delivery of regulatory RNA molecules and genes for the treatment of heart failure. Cardiovasc Res *86*, 353-364.

Poo, M.M. (2001). Neurotrophins as synaptic modulators. Nat Rev Neurosci *2*, 24-32.

Ramocki, M.B., and Zoghbi, H.Y. (2008). Failure of neuronal homeostasis results in common neuropsychiatric phenotypes. Nature *455*, 912-918.

Reichardt, L.F. (2006). Neurotrophin-regulated signalling pathways. Philos Trans R Soc Lond B Biol Sci *361*, 1545-1564.

Rico, B., Xu, B., and Reichardt, L.F. (2002). TrkB receptor signaling is required for establishment of GABAergic synapses in the cerebellum. Nat Neurosci *5*, 225-233.

Ridley, A.J., Schwartz, M.A., Burridge, K., Firtel, R.A., Ginsberg, M.H., Borisy, G., Parsons, J.T., and Horwitz, A.R. (2003). Cell migration: integrating signals from front to back. Science *302*, 1704-1709.

Rossman, K.L., Der, C.J., and Sondek, J. (2005). GEF means go: turning on RHO GTPases with guanine nucleotide-exchange factors. Nat Rev Mol Cell Biol *6*, 167-180.

Rosso, S.B., Sussman, D., Wynshaw-Boris, A., and Salinas, P.C. (2005). Wnt signaling through Dishevelled, Rac and JNK regulates dendritic development. Nat Neurosci *8*, 34-42.

Sasaki, A.T., and Firtel, R.A. (2006). Regulation of chemotaxis by the orchestrated activation of Ras, PI3K, and TOR. Eur J Cell Biol *85*, 873-895.

Schratt, G.M., Tuebing, F., Nigh, E.A., Kane, C.G., Sabatini, M.E., Kiebler, M., and Greenberg, M.E. (2006). A brain-specific microRNA regulates dendritic spine development. Nature *439*, 283-289.

Seitz, H., Royo, H., Bortolin, M.L., Lin, S.P., Ferguson-Smith, A.C., and Cavaille, J. (2004). A large imprinted microRNA gene cluster at the mouse Dlk1-Gtl2 domain. Genome Res *14*, 1741-1748.

Sempere, L.F., Freemantle, S., Pitha-Rowe, I., Moss, E., Dmitrovsky, E., and Ambros, V. (2004). Expression profiling of mammalian microRNAs uncovers a subset of brain-expressed microRNAs with possible roles in murine and human neuronal differentiation. Genome Biol *5*, R13.

Shimada, A., Mason, C.A., and Morrison, M.E. (1998). TrkB signaling modulates spine density and morphology independent of dendrite structure in cultured neonatal Purkinje cells. J Neurosci *18*, 8559-8570.

Skaper, S.D. (2008). The biology of neurotrophins, signalling pathways, and functional peptide mimetics of neurotrophins and their receptors. CNS Neurol Disord Drug Targets *7*, 46-62.

Song, H., and Poo, M. (2001). The cell biology of neuronal navigation. Nat Cell Biol *3*, E81-88.

Threadgill, R., Bobb, K., and Ghosh, A. (1997). Regulation of dendritic growth and remodeling by Rho, Rac, and Cdc42. Neuron *19*, 625-634.

Toker, A., and Cantley, L.C. (1997). Signalling through the lipid products of phosphoinositide-3-OH kinase. Nature *387*, 673-676.

Tolwani, R.J., Buckmaster, P.S., Varma, S., Cosgaya, J.M., Wu, Y., Suri, C., and Shooter, E.M. (2002). BDNF overexpression increases dendrite complexity in hippocampal dentate gyrus. Neuroscience *114*, 795-805.

Toni, N., Teng, E.M., Bushong, E.A., Aimone, J.B., Zhao, C., Consiglio, A., van Praag, H., Martone, M.E., Ellisman, M.H., and Gage, F.H. (2007). Synapse formation on neurons born in the adult hippocampus. Nat Neurosci *10*, 727-734.

Trachtenberg, J.T., Chen, B.E., Knott, G.W., Feng, G., Sanes, J.R., Welker, E., and Svoboda, K. (2002). Long-term in vivo imaging of experience-dependent synaptic plasticity in adult cortex. Nature *420*, 788-794.

Tsien, J.Z., Chen, D.F., Gerber, D., Tom, C., Mercer, E.H., Anderson, D.J., Mayford, M., Kandel, E.R., and Tonegawa, S. (1996). Subregion- and cell type-restricted gene knockout in mouse brain. Cell *87*, 1317-1326.

Tucker, K.L., Meyer, M., and Barde, Y.A. (2001). Neurotrophins are required for nerve growth during development. Nat Neurosci *4*, 29-37.

Tyler, W.J., and Pozzo-Miller, L.D. (2001). BDNF enhances quantal neurotransmitter release and increases the number of docked vesicles at the active zones of hippocampal excitatory synapses. J Neurosci *21*, 4249-4258.

Vaillant, A.R., Zanassi, P., Walsh, G.S., Aumont, A., Alonso, A., and Miller, F.D. (2002). Signaling mechanisms underlying reversible, activity-dependent dendrite formation. Neuron *34*, 985-998.

Van Haastert, P.J., and Devreotes, P.N. (2004). Chemotaxis: signalling the way forward. Nat Rev Mol Cell Biol *5*, 626-634.

van Rooij, E., Sutherland, L.B., Qi, X., Richardson, J.A., Hill, J., and Olson, E.N. (2007). Control of stress-dependent cardiac growth and gene expression by a microRNA. Science *316*, 575-579.

Vazquez, L.E., Chen, H.J., Sokolova, I., Knuesel, I., and Kennedy, M.B. (2004). SynGAP regulates spine formation. J Neurosci *24*, 8862-8872.

Vessey, J.P., Macchi, P., Stein, J.M., Mikl, M., Hawker, K.N., Vogelsang, P., Wieczorek, K., Vendra, G., Riefler, J., Tubing, F., *et al.* (2008). A loss of function allele for murine Staufen1 leads to impairment of dendritic Staufen1-RNP delivery and dendritic spine morphogenesis. Proc Natl Acad Sci U S A *105*, 16374-16379.

Vlahos, C.J., Matter, W.F., Hui, K.Y., and Brown, R.F. (1994). A specific inhibitor of phosphatidylinositol 3-kinase, 2-(4-morpholinyl)-8-phenyl-4H-1-benzopyran-4-one (LY294002). J Biol Chem *269*, 5241-5248.

Vogel, K.S., Brannan, C.I., Jenkins, N.A., Copeland, N.G., and Parada, L.F. (1995). Loss of neurofibromin results in neurotrophin-independent survival of embryonic sensory and sympathetic neurons. Cell *82*, 733-742.

Walsh, C.A., Morrow, E.M., and Rubenstein, J.L. (2008). Autism and brain development. Cell *135*, 396-400.

Wang, S., Aurora, A.B., Johnson, B.A., Qi, X., McAnally, J., Hill, J.A., Richardson, J.A., Bassel-Duby, R., and Olson, E.N. (2008). The endothelial-specific microRNA miR-126 governs vascular integrity and angiogenesis. Dev Cell *15*, 261-271.

Wassle, H., and Boycott, B.B. (1991). Functional architecture of the mammalian retina. Physiol Rev *71*, 447-480.

Williams, A.H., Valdez, G., Moresi, V., Qi, X., McAnally, J., Elliott, J.L., Bassel-Duby, R., Sanes, J.R., and Olson, E.N. (2009). MicroRNA-206 delays ALS progression and promotes regeneration of neuromuscular synapses in mice. Science *326*, 1549-1554.

Wu, X., Senechal, K., Neshat, M.S., Whang, Y.E., and Sawyers, C.L. (1998). The PTEN/MMAC1 tumor suppressor phosphatase functions as a negative regulator of the phosphoinositide 3-kinase/Akt pathway. Proc Natl Acad Sci U S A *95*, 15587-15591.

Yamada, M., Ohnishi, H., Sano, S., Nakatani, A., Ikeuchi, T., and Hatanaka, H. (1997). Insulin receptor substrate (IRS)-1 and IRS-2 are tyrosine-phosphorylated

and associated with phosphatidylinositol 3-kinase in response to brain-derived neurotrophic factor in cultured cerebral cortical neurons. J Biol Chem *272*, 30334-30339.

Yamauchi, J., Miyamoto, Y., Tanoue, A., Shooter, E.M., and Chan, J.R. (2005). Ras activation of a Rac1 exchange factor, Tiam1, mediates neurotrophin-3-induced Schwann cell migration. Proc Natl Acad Sci U S A *102*, 14889-14894.

Yan, Q., Radeke, M.J., Matheson, C.R., Talvenheimo, J., Welcher, A.A., and Feinstein, S.C. (1997). Immunocytochemical localization of TrkB in the central nervous system of the adult rat. J Comp Neurol *378*, 135-157.

Ye, B., Petritsch, C., Clark, I.E., Gavis, E.R., Jan, L.Y., and Jan, Y.N. (2004). Nanos and Pumilio are essential for dendrite morphogenesis in Drosophila peripheral neurons. Curr Biol *14*, 314-321.

Yeo, G.S., Connie Hung, C.C., Rochford, J., Keogh, J., Gray, J., Sivaramakrishnan, S., O'Rahilly, S., and Farooqi, I.S. (2004). A de novo mutation affecting human TrkB associated with severe obesity and developmental delay. Nat Neurosci *7*, 1187-1189.

Yoon, S.Y., Choi, J.E., Huh, J.W., Hwang, O., Lee, H.S., Hong, H.N., and Kim, D. (2005). Monastrol, a selective inhibitor of the mitotic kinesin Eg5, induces a distinctive growth profile of dendrites and axons in primary cortical neuron cultures. Cell Motil Cytoskeleton *60*, 181-190.

Yuste, R., and Denk, W. (1995). Dendritic spines as basic functional units of neuronal integration. Nature *375*, 682-684.

Zafra, F., Hengerer, B., Leibrock, J., Thoenen, H., and Lindholm, D. (1990). Activity dependent regulation of BDNF and NGF mRNAs in the rat hippocampus is mediated by non-NMDA glutamate receptors. EMBO J *9*, 3545-3550.

Zheng, Y., Wildonger, J., Ye, B., Zhang, Y., Kita, A., Younger, S.H., Zimmerman, S., Jan, L.Y., and Jan, Y.N. (2008). Dynein is required for polarized dendritic transport and uniform microtubule orientation in axons. Nat Cell Biol *10*, 1172-1180.

Zhu, Y., Romero, M.I., Ghosh, P., Ye, Z., Charnay, P., Rushing, E.J., Marth, J.D., and Parada, L.F. (2001). Ablation of NF1 function in neurons induces abnormal development of cerebral cortex and reactive gliosis in the brain. Genes Dev *15*, 859-876.

Zhuo, L., Theis, M., Alvarez-Maya, I., Brenner, M., Willecke, K., and Messing, A. (2001). hGFAP-cre transgenic mice for manipulation of glial and neuronal function in vivo. Genesis *31*, 85-94.

Ziv, N.E., and Smith, S.J. (1996). Evidence for a role of dendritic filopodia in synaptogenesis and spine formation. Neuron *17*, 91-102.

Zuo, Y., Lin, A., Chang, P., and Gan, W.B. (2005). Development of long-term dendritic spine stability in diverse regions of cerebral cortex. Neuron *46*, 181-189.

APPENDICES

THE JOURNAL OF BIOLOGICAL CHEMISTRY
Vol. 279, No. 9, Issue of February 27, pp. 7826–7831, 2004

Printed in U.S.A.

WNK1 Activates ERK5 by an MEKK2/3-dependent Mechanism*

Received for publication, December 9, 2003
Published, JBC Papers in Press, December 16, 2003, DOI 10.1074/jbc.M313465200

Bing-e Xu, Steve Stippec, Lisa Lenertz‡, Byung-Hoon Lee‡, Wei Zhang, Youn-Kyoung Lee, and Melanie H. Cobb§

From the Department of Pharmacology, The University of Texas Southwestern Medical Center, Dallas, Texas 75390-9041

WNK1 belongs to a unique protein kinase family that lacks the catalytic lysine in its normal position. Mutations in human WNK1 and WNK4 have been implicated in causing a familial form of hypertension. Here we report that overexpression of WNK1 led to increased activity of cotransfected ERK5 in HEK293 cells. ERK5 activation was blocked by the MEK5 inhibitor U0126 and expression of a dominant negative MEK5 mutant. Expression of dominant negative mutants of MEKK2 and MEKK3 also blocked activation of ERK5 by WNK1. Moreover, both MEKK2 and MEKK3 coimmunoprecipitated with endogenous WNK1 from cell lysates. WNK1 phosphorylated both MEKK2 and -3 *in vitro*, and MEKK3 was activated by WNK1 in 293 cells. Finally, ERK5 activation by epidermal growth factor was attenuated by suppression of WNK1 expression using small interfering RNA. Taken together, these results place WNK1 in the ERK5 MAP kinase pathway upstream of MEKK2/3.

More than 500 protein kinases have been recognized in the human genome, ~1.7% of all human genes (1, 2). These enzymes play crucial roles in regulating cellular processes and participate in most, if not all, of the signal transduction pathways in cells. Among them, WNKs[1] (with no lysine (K)) comprise a newly described subfamily with a unique placement of the catalytic lysine responsible for binding to ATP (3). WNKs exist in multicellular organisms including plants, *Caenorhabditis elegans*, *Drosophila,* and mammals but not in unicellular organisms such as *Saccharomyces cerevisiae* (3–8). The well studied plant *Arabidopsis thaliana* has the largest number of WNK family members known with at least nine, some of which are implicated in controlling circadian rhythm (5, 6). In contrast, both *C. elegans* and *Drosophila* have only one WNK in their genomes.

There are at least four mammalian WNK family members with high sequence identity within their catalytic domains (4, 8). Rat WNK1, the first mammalian member of this protein kinase subfamily identified, contains an N-terminal kinase domain followed by an autoinhibitory domain and a long C-terminal tail (3, 9). Disruption of the WNK1 gene in mice leads to lethality before embryonic day 13 (10). Lifton and colleagues (8) showed that mutations in WNK1 and WNK4 could lead to a familial type of human hypertension pseudohypoaldosteronism type II (PHAII). The mutations in WNK1 are large deletions in the first intron that increase its expression up to 5-fold. The WNK4 mutations are missense mutations located in regions near the two coiled-coil domains that are highly conserved among the four WNKs (8). Recently, WNK4 has been shown to inhibit the activity of the sodium chloride cotransporter by reducing its membrane expression (11, 12). This inhibition was reported to be dependent on the catalytic activity of WNK4, and the disease-causing mutation Q562E has less inhibitory effect. WNK1, on the other hand, was found to have no effect on sodium chloride cotransporter activity on its own. However, WNK1 relieved sodium chloride cotransporter inhibition by WNK4 (12). These new findings provide a potential mechanism for regulation of blood pressure by WNKs and suggest an explanation for the finding that loss of WNK regulation causes hypertension.

MAP kinase (MAPK) cascades are involved in many signal transduction pathways including those regulating cell cycle, transcription, apoptosis, and proliferation (13, 14). A typical MAPK cascade consists of a MAPK kinase kinase (MAP3K or MEKK), and a MAPK kinase (MAP2K or MEK) which act in series on a MAPK. There are several MAPK pathways in mammals. One of them, the ERK5 MAPK pathway, contains MEK5 (MAP2K) and MEKK2/3 (MAP3K) as its upstream regulators (15–19). ERK5 contains a long C-terminal tail, and its kinase domain most resembles ERK2. ERK5 can be activated by proliferative stimuli such as epidermal growth factor (EGF), serum, lysophosphatidic acid, neurotrophins, and phorbol ester, as well as by stress stimuli such as sorbitol, H_2O_2, and UV irradiation (20–28). The known ERK5 substrates include the MEF2 family members, MEF2A, -C, and -D, and the ETS-like transcription factor SAP1a (21, 23). The upstream kinase MEK5 contains two alternatively spliced forms, α and β (16). MEK5 is the only known MAP2K in the ERK5 pathway (21). Its sequence similarity to MEK1/2 renders it susceptible to the pharmacological inhibitors PD98059 and U0126, originally identified as selective blockers of MEK1/2 (21, 29, 30).

MEKK2 and MEKK3 are two closely related MAP3Ks with extremely high sequence identity within their catalytic domains, although less so within their N-terminal regulatory domains (31). Both kinases have been shown to interact with MEK5 directly and activate the MEK5-ERK5 pathway (18, 19). A dominant negative mutant of MEKK3 is capable of blocking ERK5 activation by growth factors and H_2O_2 (18, 19).

In the present study, we demonstrate that overexpression of WNK1 in HEK293 cells causes activation of ERK5 but not ERK2. The activation is blocked by the MEK5 inhibitor U0126 and is dependent on MEKK2/3. Furthermore, WNK1 is re-

* This work was supported by Grant GM53032 from the National Institutes of Health and Grant I1243 from the Welch Foundation. The costs of publication of this article were defrayed in part by the payment of page charges. This article must therefore be hereby marked "*advertisement*" in accordance with 18 U.S.C. Section 1734 solely to indicate this fact.

‡ Submitted in partial fulfillment of the requirements for a Ph.D.

§ To whom correspondence should be addressed: University of Texas, Southwestern Medical Ctr., 5323 Harry Hines Blvd., Dallas, TX 75390-9041. Tel.: 214-648-3627; Fax: 214-648-3811; E-mail: mcobb@mednet.swmed.edu.

[1] The abbreviations used are: WNK, with no lysine (K); ERK, extracellular signal-regulated kinase; MAPK, mitogen-activated protein kinase; MEK, mitogen-activated protein kinase/extracellular signal-regulated kinase kinase; MEKK, MEK kinase; EGF, epidermal growth factor; GST, glutathione *S*-transferase; HA, hemagglutinin; KM, kinase-dead mutant.

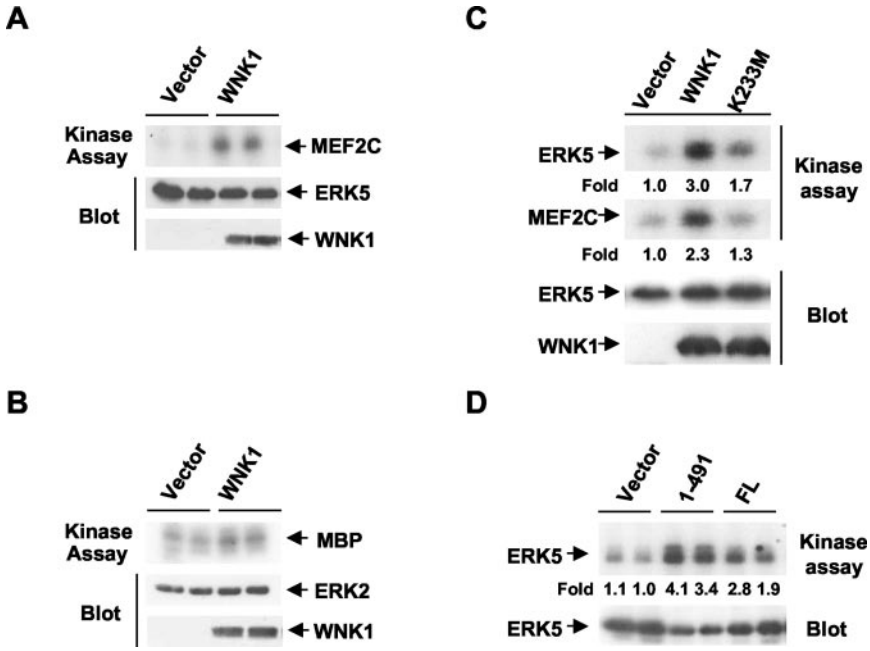

FIG. 1. **Overexpression of WNK1 activates ERK5 in HEK293 cells.** *A*, HEK293 cells were transfected with pCEP4-HA-ERK5 along with empty pCMV5-Myc vector or Myc-WNK1-(1–491). ERK5 was immunoprecipitated using anti-HA, and its activity was assayed with GST·MEF2C-(204–321) as the substrate. The lysates were immunoblotted with anti-HA to detect ERK5 expression and anti-Myc to detect WNK1 expression. This is one of four experiments. *B*, as in *A*, except ERK2 was expressed instead of ERK5. ERK2 activity was assayed using myelin basic protein as the substrate. The lysates were immunoblotted with anti-HA to detect ERK2 expression and anti-Myc to detect WNK1 expression. This is one of three experiments. *C*, HEK293 cells were transfected with pCEP4-HA-ERK5 along with pCMV5-Myc vector, WNK1-(1–491), or WNK1-(1–491) K233M. ERK5 was immunoprecipitated and assayed as above. Fold changes in activity are indicated. The lysates were immunoblotted with anti-HA to detect ERK5 expression and anti-Myc to detect WNK1 expression. This is one of three experiments. *D*, as in *C*, except WNK1 full-length (*FL*) and WNK1-(1–491) were compared. Only ERK5 autophosphorylation and blot are shown. Fold changes in activity are indicated. This is one of four experiments.

quired for activation of ERK5 by EGF. These results place WNK1 in the ERK5 MAPK pathway upstream of MEKK2/3.

MATERIALS AND METHODS

Plasmids, Subcloning, and Mutagenesis—pCEP4-HA-ERK5 and pCEP4-HA-ERK2 were as described by Xu *et al.* (3). pCMV5-Myc-WNK1-(1–491) and full-length WNK1 were described previously (3, 9). pCMV5–3xFlag vector was purchased from Sigma. pCMV5-HA-MEKK2 and -3 were kindly provided by Dr. Gary Johnson (University of Colorado, Denver, CO/University of North Carolina, Chapel Hill, NC) (31). To make FLAG-MEK5α K195M and β K106M, FLAG-MEKK2, and FLAG-MEKK3 constructs, the open reading frames were amplified by PCR and subcloned into pCMV5–3xFlag. To make constructs expressing fusions of MEKK2 and -3, cDNAs encoding residues 1–350 and 1–354 (N constructs) and 332–619 K385M and 350–626 K391M (C constructs) of MEKK2 and MEKK3, respectively, were amplified by PCR and subcloned into pGEX-KG. pCMV5-Myc-TAO2-(1–993) D169A was as described by Chen *et al.* (32). Site-directed mutagenesis was performed using the QuikChange kit (Stratagene) according to the manufacturer's directions.

Proteins and Antibodies—GST·MEF2C-(204–321) and His_6-MEK6 K82M were as described in Refs. 27 and 33. His_6-WNK1-(198–491) was described previously (9). Myelin basic protein was purchased from Sigma. GST·MEKK2/3-N/C proteins were expressed using standard protocols. The anti-HA antibody (12CA5) was from Berkeley Antibody Company. The anti-Myc antibody (9E10) was from the National Cell Culture Center. The monoclonal anti-FLAG antibody was obtained from Sigma. The polyclonal anti-WNK1 antibody Q256 and its preimmune serum were as described by Xu *et al.* (3). The anti-ERK1/2 antibody Y691 was described previously (34). The anti-ERK5 antibody was purchased from Sigma.

Cell Culture, Transfections, and Harvesting—HEK293 cells were maintained, transfected, and harvested as described by Xu *et al.* (35). Lysis buffer with 1% Triton X-100 or Nonidet P-40 was used, except for coimmunoprecipitation experiments, in which case detergent was omitted. HeLa cells were grown in Dulbecco's modified Eagle's medium with 10% fetal bovine serum and 1% L-glutamine at 37 °C under 10% CO_2. For RNA interference experiments, HeLa cells were grown in 6-well plates to 30% confluence on the day of transfection. The cells were transfected with luciferase double-stranded RNA as a control or WNK1 double-stranded RNA oligonucleotides using Oligofectamine (Invitrogen) according to the manufacturer's instructions. After 72 h, the cells were deprived of serum for 4 h before treatment.

Immunoblotting and Immunoprecipitation—For immunoblotting, proteins from the cell lysates were separated by SDS-PAGE followed by electrotransference to nitrocellulose membranes. The membranes were incubated with the indicated antibodies and developed using enhanced chemiluminescence. For immunoprecipitation, cell lysates were incubated with the respective antibody and protein A-Sepharose beads for 2 h at 4 °C. The beads were washed with either 1 M NaCl, 20 mM Tris-HCl (pH 7.4) (for the kinase assay) or 0.5 M NaCl, 10 mM Tris-HCl (pH 7.4), 5 mM $MgCl_2$ (for coimmunoprecipitation).

In Vitro Kinase Assays—Kinase assays were performed as described by Xu *et al.* (35). Most kinase reactions were in buffer containing 50 μM ATP; reactions with FLAG-MEKK3 included 10 μM ATP. To examine phosphorylation of FLAG-MEKK2/3 (kinase-dead) phosphorylation by His_6-WNK1-(198–491), FLAG-MEKK2/3 (kinase-dead) proteins immunoprecipitated from cell lysates were preincubated in 1× kinase buffer for 30 min at 30 °C prior to addition of His_6-WNK1-(198–491) and ATP.

RESULTS

Overexpression of WNK1 Activates ERK5 in HEK293 Cells—We reported previously that overexpression of WNK1-(1–555) did not activate cotransfected MAPKs in HEK293 cells (3). Subsequently, we identified an autoinhibitory domain in WNK1 located between residues 491 and 555 (9). Because WNK1-(1–491) had much higher catalytic activity than WNK1-(1–555) *in vitro*, we thought it was necessary to examine the more active form, WNK1-(1–491), for its possible effects on the activities of MAPKs. Thus, HA-tagged ERK2 or ERK5 was transfected into HEK293 cells along with either the vector or Myc-tagged WNK1-(1–491). Remarkably, ERK5 activity assayed using its substrate GST·MEF2C was increased significantly by WNK1-(1–491) compared with the vector control (Fig. 1*A*). In contrast, ERK2 activity was not affected by WNK1-(1–491) when assayed with myelin basic protein (Fig.

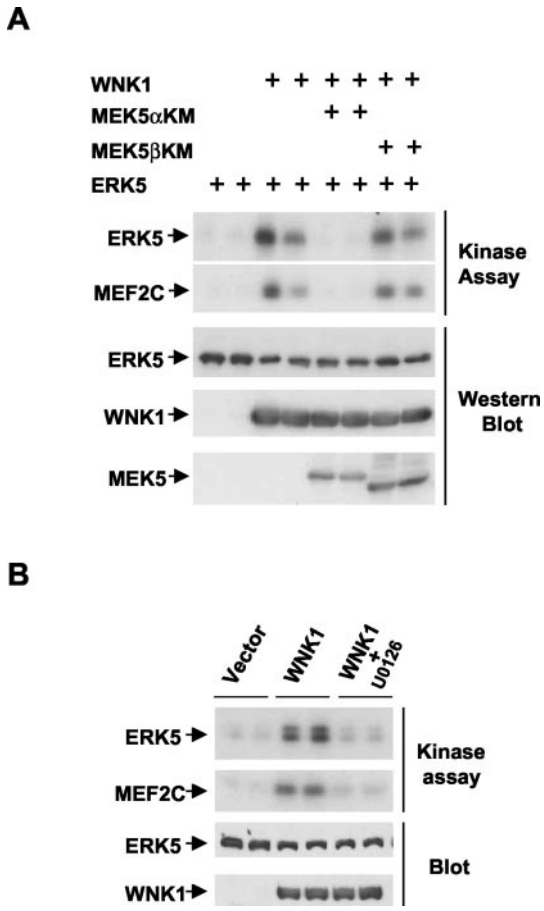

FIG. 2. **Activation of ERK5 by WNK1 requires MEK5.** HEK293 cells were transfected with pCEP4-HA-ERK5 along with pCMV5-Myc with or without WNK1-(1–491). ERK5 was immunoprecipitated and assayed as in Fig. 1. *A*, the cells were also transfected with either MEK5α K195M or MEK5β K106M. This is one of three experiments. *B*, cells cotransfected with WNK1 were either untreated or treated with 10 μM U0126 for 1 h before harvesting. This is one of five experiments. In both *panels*, ERK5 autophosphorylation is also shown. The lysates were immunoblotted with anti-HA and anti-Myc to detect ERK5 and WNK1 expression, respectively. In *A*, the lysates were also immunoblotted with anti-FLAG to detect expression of MEK5.

1*B*). Enhanced ERK5 autophosphorylation is another indicator of its activation state. As shown in Fig. 1*C*, WNK1-(1–491) increased ERK5 autophosphorylation as well as its activity toward GST·MEF2C. Activation of ERK5 was greater with wild type WNK1; a kinase defective mutant, WNK1-(1–491) K233M, did not stimulate ERK5 autophosphorylation or activity toward GST·MEF2C as well, although a small increase in ERK5 autophosphorylation was detected (Fig. 1*C*). We also found that expression of full-length WNK1 activated ERK5 (Fig. 1*D*). These results suggest that WNK1 might act as an upstream kinase in the ERK5 MAPK pathway.

Activation of ERK5 by WNK1 Requires MEK5 Activity—We next examined whether activation of ERK5 by WNK1 required the known MEK in the ERK5 pathway, MEK5. To address this question, we first used kinase-dead mutants (KM) of the two MEK5 isoforms, α and β. MEK5α K195M fully blocked activation of ERK5 by WNK1 (Fig. 2*A*). Both ERK5 autophosphorylation and activity toward GST·MEF2C were reduced to the control value. Unexpectedly, MEK5β K106M had no effect in the same experiment. In addition, we utilized the pharmacological compound U0126, which specifically inhibits the activities of MEK1, MEK2, and MEK5 but not other MAP2Ks (30). At 10 μM, U0126 efficiently blocked the activation of ERK5 by WNK1 in transfected cells treated for 1 h prior to harvest (Fig. 2*B*). These findings indicate that MEK5 activity is crucial for activation of ERK5 by WNK1.

Activation of ERK5 by WNK1 Is Dependent on MEKK2 and MEKK3—MEKK2 and MEKK3, the two known MAP3Ks in the ERK5 MAPK pathway, interact with MEK5 and activate the MEK5-ERK5 cascade (18, 19). To determine whether WNK1 acts upstream or downstream of MEKK2/3 in the ERK5 pathway, we examined the effects of dominant negative mutants of MEKK2/3 on ERK5 activation by WNK1. MEKK3 K391M prevented ERK5 activation by WNK1 (Fig. 3*A*). Both ERK5 autophosphorylation and activity toward GST·MEF2C decreased to basal levels if the MEKK3 K391M mutant was coexpressed. Similar results were also observed for MEKK2 K385M (Fig. 3*B*). On the other hand, a kinase-dead form of a MAP3K not known to be involved in the ERK5 pathway, TAO2-(1–993) D169A, did not affect the activation of ERK5 by WNK1 (Fig. 3*B*). Likewise, kinase-dead mutants of the MAP4K PAK1 and the MAP3K MEKK1 also failed to block ERK5 activation by WNK1 (data not shown). These data suggest that WNK1 most likely acts upstream of MEKK2 and MEKK3 in the ERK5 pathway.

Endogenous WNK1 Coimmunoprecipitates with MEKK2 and MEKK3—Because dominant negative mutants of MEKK2 and MEKK3 could block ERK5 activation by WNK1, we tested whether WNK1 and MEKK2/3 might exist in a complex in cells. HEK293 cells were transfected with Myc-tagged WNK1-(1–491) and HA-tagged MEKK3. WNK1 was immunoprecipitated with anti-Myc, and the precipitates were blotted with anti-HA. HA-MEKK3 was readily detected in the precipitates from lysates containing both WNK1 and MEKK3, but not from those containing only MEKK3 (Fig. 4*A*). The converse also revealed an association: MEKK3 was immunoprecipitated with anti-HA, and the precipitates were blotted with anti-Myc. Again, Myc-WNK1 was only detected in the precipitates from lysates containing both MEKK3 and WNK1 and not from those containing only WNK1 (Fig. 4*B*). To address the question of whether MEKK2 might also coimmunoprecipitate with WNK1-(1–491), HEK293 cells were transfected with either the vector or FLAG-tagged MEKK2/3 along with Myc-WNK1-(1–491). MEKK2/3 proteins were immunoprecipitated with anti-FLAG antibody and the precipitates were blotted with anti-Myc antibody to detect the presence of WNK1. MEKK2, like MEKK3, pulled down WNK1-(1–491) (Fig. 4*C*). The catalytic activities of MEKK2/3 were not required because the kinase-dead mutants also coimmunoprecipitated with WNK1 (Fig. 4*C*).

Next we wanted to examine whether the endogenous WNK1 could coimmunoprecipitate with MEKK2/3. HEK293 cells were transfected with FLAG-tagged MEKK2 or MEKK3. Endogenous WNK1 was immunoprecipitated from the cell lysates with the Q256 antibody, and the precipitates were blotted with anti-FLAG. As a control, the preimmune serum of Q256 was also used for immunoprecipitation. As shown in Fig. 4*D*, WNK1 immunoprecipitates contained significant amounts of MEKK2/3. Neither the preimmune serum nor a control antibody Y691 (anti-ERK1/2) pulled down comparable amounts of MEKK2. These results support the conclusion that MEKK2/3 and WNK1 are associated in cells.

WNK1 Phosphorylates the N Terminus of MEKK2 and MEKK3 in Vitro—Because WNK1 lies upstream of MEKK2/3 and they can exist in a complex in cells, we reasoned that MEKK2 and MEKK3 might be direct substrates of WNK1. To test this possibility, we used FLAG-tagged MEKK2/3 (KM) proteins immunoprecipitated from 293 cells as *in vitro* substrates for His-WNK1-(198–491). As shown in Fig. 5*A*, both MEKK2 and MEKK3 were phosphorylated by WNK1. We also expressed GST fusion proteins of MEKK2 and MEKK3 in bac-

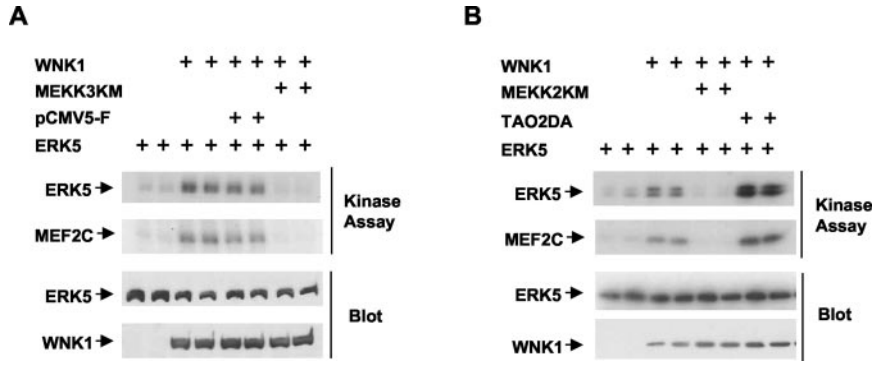

FIG. 3. **Activation of ERK5 by WNK1 is blocked by dominant negative mutants of MEKK3 and MEKK2.** *A*, HEK293 cells were transfected with HA-ERK5, Myc-WNK1-(1–491), and either pCMV5-Flag vector or FLAG-MEKK3 K391M. ERK5 was immunoprecipitated and assayed as in Fig. 1. The lysates were blotted with anti-HA to examine ERK5 expression and with anti-Myc to examine WNK1 expression. This is one of three experiments. *B*, HEK293 cells were transfected with HA-ERK5, Myc-WNK1-(1–491), and either FLAG-MEKK2 K385M or Myc-TAO2-(1–993) D169A. ERK5 was immunoprecipitated and assayed as in Fig. 1. The lysates were blotted with anti-HA to examine ERK5 expression and with anti-Myc to examine WNK1 expression. This is one of three experiments.

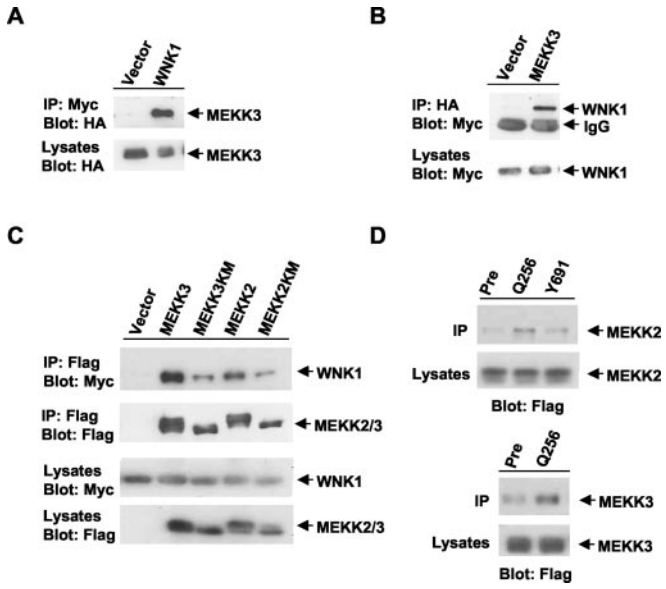

FIG. 4. **WNK1 coimmunoprecipitates with MEKK2 and MEKK3.** *A*, 293 cells were transfected with HA-MEKK3 and either pCMV5-Myc vector or Myc-WNK1-(1–491). The lysates were immunoprecipitated with anti-Myc, and the precipitates were blotted with anti-HA. The lysates were also blotted with anti-HA to detect MEKK3 expression. This is one of two experiments. *B*, 293 cells were transfected with Myc-WNK1-(1–491) and either pCMV5-HA vector or HA-MEKK3. The lysates were immunoprecipitated with anti-HA, and the precipitates were blotted with anti-Myc. The lysates were also blotted with anti-Myc to detect WNK1 expression. This is one of three experiments. *C*, 293 cells were transfected with Myc-WNK1-(1–491) and pCMV5-Flag vector or FLAG-MEKK2/3 (wild type or KM). The lysates were immunoprecipitated with anti-FLAG, and the precipitates were first blotted with anti-Myc, stripped, and then blotted with anti-FLAG. The lysates were blotted with anti-Myc and anti-FLAG to detect WNK1 or MEKK2/3 expression, respectively. This is one of three experiments. *D*, *top*, 293 cells were transfected with FLAG-MEKK2. The lysates were immunoprecipitated with Q256, its preimmune serum, or Y691, and the precipitates were blotted with anti-FLAG; *bottom*, 293 cells were transfected with FLAG-MEKK3. The lysates were immunoprecipitated with Q256 or its preimmune serum, and the precipitates were blotted with anti-FLAG. The lysates were also blotted with anti-FLAG to detect MEKK2/3 expression. This is one of four experiments.

teria to test as WNK1 substrates. N-terminal and C-terminal (KM) fragments of the two MAP3Ks were expressed, and in both cases, the N-terminal fragment, but not the C-terminal fragment, was phosphorylated by recombinant WNK1 (Fig. 5*B*) and also by endogenous WNK1 immunoprecipitated from cells treated with NaCl (Fig. 5*C*). These results are consistent with the idea that WNK1 is a MAP4K in the ERK5 pathway. However, the phosphorylation of MEKK2/3 by WNK1 does not appear to directly alter their catalytic activities because preincubation of MEKK2/3 with WNK1 in the presence of ATP neither increased nor decreased their kinase activities (data not shown).

Overexpression of WNK1 Activates Cotransfected MEKK3 in HEK293 Cells—To test whether WNK1 could affect the activity of MEKK3 in cells, we transfected 293 cells with either vector control or Myc-tagged WNK1-(1–491) along with FLAG-tagged MEKK3. MEKK3 was immunoprecipitated from cell lysates and assayed using His_6-MEK6 K82M as the substrate. Overexpression of WNK1-(1–491) increased the autophosphorylation of MEKK3 as well as its activity toward His_6-MEK6 K82M (Fig. 5*D*), showing that coexpression with WNK1 in cells stimulates MEKK3 activity. Interestingly, this activation is independent of the catalytic activity of WNK1, because a kinase-defective mutant of WNK1 also activated cotransfected MEKK3 to a similar extent (data not shown).

WNK1 Is Required for Activation of ERK5 by EGF in HeLa Cells—We have presented evidence that overexpression of WNK1 is sufficient to activate the ERK5 MAPK pathway. However, whether WNK1 is required for ERK5 activation under any physiological circumstances is still unknown. Growth factors such as EGF and stress stimuli are well documented activators of ERK5. Therefore, we tested whether WNK1 is required for ERK5 activation by EGF using RNA interference to knock down expression of endogenous WNK1 in HeLa cells. ERK5 activation by many agents including EGF leads to a decrease in its electrophoretic motility on gels (Fig. 6*A*), providing a simple assessment of its activity. We successfully reduced expression of endogenous WNK1 as shown in Fig. 6*B*. ERK5 activation by 1 ng/ml EGF was partially reduced by suppression of WNK1 expression, suggesting that WNK1 is required for ERK5 activation by EGF under these circumstances. With higher concentrations of EGF, the requirement for WNK1 became less pronounced (data not shown).

DISCUSSION

Since it was first cloned and characterized three years ago, the atypical protein kinase WNK1 has attracted considerable interest primarily because it has been linked to the regulation of blood pressure (3, 8). Although progress was made in the last 2 years in defining how WNK1 is regulated and in suggesting an effect of WNK1 on ion channels, the biochemical pathways regulated by WNK1 remain unknown. Here we provide evidence that WNK1 can activate the MAPK ERK5 through MEKK2/3.

The following observations suggest that WNK1 is a MAP4K

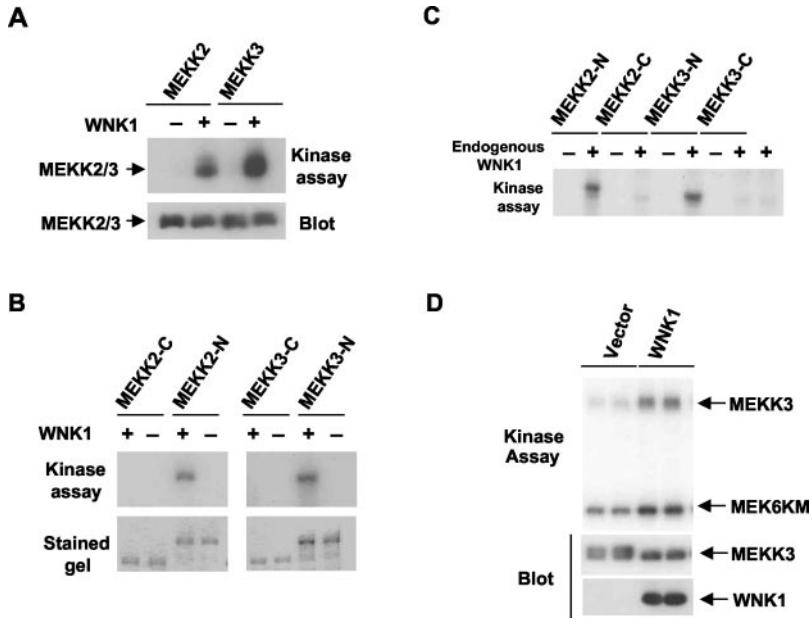

FIG. 5. **WNK1 phosphorylates MEKK2 and MEKK3 *in vitro*.** *A*, FLAG-MEKK2/3 (kinase-dead) proteins were immunoprecipitated from 293 cell lysates and used as *in vitro* substrates for His_6-WNK1-(198–491). The precipitates were blotted with anti-FLAG to compare the amounts of MEKK2/3. This is one of three experiments. *B*, the N terminus and C terminus of MEKK2/3 (kinase-dead) were expressed in *E. coli* as GST fusion proteins. 1 μg of each protein was then used as the *in vitro* substrate for His_6-WNK1-(198–491). Coomassie Blue-stained gel of GST-MEKK2/3 proteins is shown. This is one of two experiments. *C*, as in *B* above, except that endogenous WNK1 immunoprecipitated from NaCl-treated cells was used as the enzyme. This is one of two experiments. *D*, 293 cells were transfected with FLAG-MEKK3 and either pCMV5-Myc vector or WNK1-(1–491). MEKK3 was immunoprecipitated using anti-FLAG and its activity was assayed using His_6-MEK6 K82M as the substrate. The lysates were blotted with anti-FLAG to examine MEKK3 expression and with anti-Myc to examine WNK1 expression. This is one of four experiments.

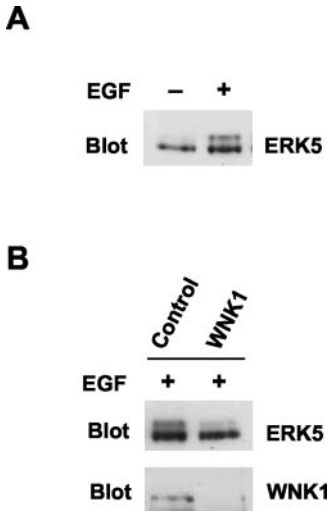

FIG. 6. **WNK1 is required for EGF activation of ERK5 in HeLa cells.** *A*, HeLa cells were either untreated (−) or treated (+) with 1 ng/ml EGF for 15 min prior to harvesting. The lysates were blotted with anti-ERK5. This is one of three experiments. *B*, HeLa cells transfected with either luciferase (*Control*) or WNK1 dsRNA were treated with EGF for 15 min prior to harvesting. The lysates were immunoblotted with Q256 and anti-ERK5. This is one of three experiments.

in the ERK5 pathway: 1) its activation of ERK5 can be blocked by kinase-dead mutants of MEKK2/3; 2) WNK1 interacts with MEKK2/3 in cells; 3) WNK1 phosphorylates MEKK2/3 *in vitro*; and 4) coexpression of WNK1 with MEKK3 activates it in cells. Nevertheless, *in vitro* experiments suggest that phosphorylation of MEKK2/3 by WNK1 apparently does not directly activate them. In cells, WNK1 activated MEKK3; however, WNK1 kinase activity was not required, because a kinase-dead mutant of WNK1 had the same stimulatory effect as the wild type protein. One possible explanation comes from the observation that WNK1 exists as a tetramer (9). The kinase-dead protein may interact with endogenous wild type WNK1, promoting activation of the MAP3Ks. Alternatively, protein-protein interactions could change the conformation of MEKK3 or its ability to form complexes. In contrast, activation of ERK5 by wild type WNK1 is greater than activation by kinase-dead WNK1. These apparently contradictory findings may be reconciled if WNK1 contributes two events toward ERK5 activation: stimulation of the MAP3K by a noncatalytic mechanism coupled with assembly of an ERK5 activation complex that requires phosphorylation of the MAP3K or some other component in the complex. If so, phosphorylation of MEKK2/3 by WNK1 may be important for transmitting the activation signal to ERK5 even though it is not required for activation of MEKK2/3.

Interestingly, our data suggest a role for only one of two isoforms of MEK5 in activation of ERK5 by WNK1. MEK5α has an additional 89 residues at its N terminus compared with MEK5β due to alternative splicing, whereas MEK5β appears to be more widely expressed (16). The inactive form of MEK5α was a very effective inhibitor, whereas the comparable mutant of MEK5β was not. A recent study has suggested that wild type MEK5β can act as a dominant negative to block ERK5 activation by EGF or by a constitutively active form of MEK5α (36). The mechanisms underlying this discrepancy are not known.

Significantly, we have demonstrated that WNK1 is required for ERK5 activation by EGF. We also found a partial requirement for WNK1 in the activation of ERK5 by H_2O_2 (data not shown). In contrast, WNK1 was not required for activation of ERK5 by either sorbitol or NaCl (data not shown). Surprisingly, there is a poor correlation of the requirement for WNK1 in ERK5 activation by these agents and the sensitivity of WNK1 itself to be activated by them. NaCl and sorbitol are significantly stronger WNK1 activators than H_2O_2, and we have thus far failed to reveal activation of WNK1 by EGF. Thus, the potential involvement of WNK1 in a pathway may not be obvious based on changes in its kinase activity alone. These results indicate that WNK1 participates in ERK5 activation by a subset of physiological ERK5 regulators.

There are four WNK homologs in mammals that share a high degree of identity within their kinase domains but significantly lower identity outside the kinase domains (4, 8). A recent study suggests that WNK1 and WNK4 might have opposite effects on channel regulation (12). Thus, it will be important to determine whether any of the other WNK family members also activate ERK5. Currently, we are testing WNK2 and WNK4 for their effects on the ERK5 pathway.

In summary, we demonstrated in this study that WNK1 activates the ERK5 MAPK pathway through MEKK2/3. The identification of potential WNK1 substrates other than myelin basic protein provides a starting point to map biochemical pathways that WNK1 regulates. Future studies should shed

more light on the important roles WNK1 plays in various cellular processes including ion transport.

Acknowledgments—We thank Anthony Anselmo and Tara Beers Gibson for critical suggestions and comments about the manuscript, Gray Pearson for helpful discussions, Wei Chen, Kathy McGlynn, and Svetlana Earnest for valuable reagents, and Dionne Ware for administrative assistance.

REFERENCES

1. Kostich, M., English, J., Madison, V., Gheyas, F., Wang, L., Qiu, P., Greene, J., and Laz, T. M. (2002) *Genome Biol.* http://www.genomebiology.com/2002/3/9/Research/0043
2. Manning, G., Whyte, D. B., Martinez, R., Hunter, T., and Sudarsanam, S. (2002) *Science* **298,** 1912–1934
3. Xu, B., English, J. M., Wilsbacher, J. L., Stippec, S., Goldsmith, E. J., and Cobb, M. H. (2000) *J. Biol. Chem.* **275,** 16795–16801
4. Verissimo, F., and Jordan, P. (2001) *Oncogene* **20,** 5562–5569
5. Murakami-Kojima, M., Nakamichi, N., Yamashino, T., and Mizuno, T. (2002) *Plant Cell Physiol.* **43,** 675–683
6. Nakamichi, N., Murakami-Kojima, M., Sato, E., Kishi, Y., Yamashino, T., and Mizuno, T. (2002) *Biosci. Biotechnol. Biochem.* **66,** 2429–2436
7. Morrison, D. K., Murakami, M. S., and Cleghon, V. (2000) *J. Cell Biol.* **150,** F57–F62
8. Wilson, F. H., Disse-Nicodeme, S., Choate, K. A., Ishikawa, K., Nelson-Williams, C., Desitter, I., Gunel, M., Milford, D. V., Lipkin, G. W., Achard, J. M., Feely, M. P., Dussol, B., Berland, Y., Unwin, R. J., Mayan, H., Simon, D. B., Farfel, Z., Jeunemaitre, X., and Lifton, R. P. (2001) *Science* **293,** 1107–1112
9. Xu, B., Min, X., Stippec, S., Lee, B. H., Goldsmith, E. J., and Cobb, M. H. (2002) *J. Biol. Chem.* **277,** 48456–48462
10. Zambrowicz, B. P., Abuin, A., Ramirez-Solis, R., Richter, L. J., Piggott, J., BeltrandelRio, H., Buxton, E. C., Edwards, J., Finch, R. A., Friddle, C. J., Gupta, A., Hansen, G., Hu, Y., Huang, W., Jaing, C., Key, B. W., Jr., Kipp, P., Kohlhauff, B., Ma, Z. Q., Markesich, D., Payne, R., Potter, D. G., Qian, N., Shaw, J., Schrick, J., Shi, Z. Z., Sparks, M. J., Van Sligtenhorst, I., Vogel, P., Walke, W., Xu, N., Zhu, Q., Person, C., and Sands, A. T. (2003) *Proc. Natl. Acad. Sci. U. S. A.* **100,** 14109–14114
11. Wilson, F. H., Kahle, K. T., Sabath, E., Lalioti, M. D., Rapson, A. K., Hoover, R. S., Hebert, S. C., Gamba, G., and Lifton, R. P. (2003) *Proc. Natl. Acad. Sci. U. S. A.* **100,** 680–684
12. Yang, C. L., Angell, J., Mitchell, R., and Ellison, D. H. (2003) *J. Clin. Investig.* **111,** 1039–1045
13. Chen, Z., Gibson, T. B., Robinson, F., Silvestro, L., Pearson, G., Xu, B., Wright, A., Vanderbilt, C., and Cobb, M. H. (2001) *Chem. Rev.* **101,** 2449–2476
14. Lewis, T. S., Shapiro, P. S., and Ahn, N. G. (1998) *Adv. Cancer Res.* **74,** 49–139
15. Zhou, G., Bao, Z. Q., and Dixon, J. E. (1995) *J. Biol. Chem.* **270,** 12665–12669
16. English, J. M., Vanderbilt, C. A., Xu, S., Marcus, S., and Cobb, M. H. (1995) *J. Biol. Chem.* **270,** 28897–28902
17. Yan, C., Luo, H., Lee, J. D., Abe, J., and Berk, B. C. (2001) *J. Biol. Chem.* **276,** 10870–10878
18. Chao, T. H., Hayashi, M., Tapping, R. I., Kato, Y., and Lee, J. D. (1999) *J. Biol. Chem.* **274,** 36035–36038
19. Sun, W., Kesavan, K., Schaefer, B. C., Garrington, T. P., Ware, M., Johnson, N. L., Gelfand, E. W., and Johnson, G. L. (2001) *J. Biol. Chem.* **276,** 5093–5100
20. English, J. M., Pearson, G., Hockenberry, T., Shivakumar, L., White, M. A., and Cobb, M. H. (1999) *J. Biol. Chem.* **274,** 31588–31592
21. Kamakura, S., Moriguchi, T., and Nishida, E. (1999) *J. Biol. Chem.* **274,** 26563–26571
22. Karihaloo, A., O'Rourke, D. A., Nickel, C. H., Spokes, K., and Cantley, L. G. (2001) *J. Biol. Chem.* **276,** 9166–9173
23. Kato, Y., Kravchenko, V. V., Tapping, R. I., Han, J., Ulevitch, R. J., and Lee, J. D. (1997) *EMBO J.* **16,** 7054–7066
24. Cavanaugh, J. E., Ham, J., Hetman, M., Poser, S., Yan, C., and Xia, Z. (2001) *J. Neurosci.* **21,** 434–443
25. Diaz-Meco, M. T., and Moscat, J. (2001) *Mol. Cell. Biol.* **21,** 1218–1227
26. Dong, F., Gutkind, J. S., and Larner, A. C. (2001) *J. Biol. Chem.* **276,** 10811–10816
27. Pearson, G. W., and Cobb, M. H. (2002) *J. Biol. Chem.* **277,** 48094–48098
28. Watson, F. L., Heerssen, H. M., Bhattacharyya, A., Klesse, L., Lin, M. Z., and Segal, R. A. (2001) *Nat. Neurosci.* **4,** 981–988
29. Dudley, D. T., Pang, L., Decker, S. J., Bridges, A. J., and Saltiel, A. R. (1995) *Proc. Natl. Acad. Sci. U. S. A.* **92,** 7686–7689
30. Favata, M. F., Horiuchi, K. Y., Manos, E. J., Daulerio, A. J., Stradley, D. A., Feeser, W. S., Van Dyk, D. E., Pitts, W. J., Earl, R. A., Hobbs, F., Copeland, R. A., Magolda, R. L., Scherle, P. A., and Trzaskos, J. M. (1998) *J. Biol. Chem.* **273,** 18623–18632
31. Blank, J. L., Gerwins, P., Elliott, E. M., Sather, S., and Johnson, G. L. (1996) *J. Biol. Chem.* **271,** 5361–5368
32. Chen, Z., Raman, M., Chen, L., Lee, S. F., Gilman, A. G., and Cobb, M. H. (2003) *J. Biol. Chem.* **278,** 22278–22283
33. Chen, Z., and Cobb, M. H. (2001) *J. Biol. Chem.* **276,** 16070–16075
34. Boulton, T. G., and Cobb, M. H. (1991) *Cell Regul.* **2,** 357–371
35. Xu, B., Wilsbacher, J. L., Collisson, T., and Cobb, M. H. (1999) *J. Biol. Chem.* **274,** 34029–34035
36. Cameron, S. J., Abe, J. I., Malik, S., Che, W., and Yang, J. (2004) *J. Biol. Chem.* **279,** 1506–1512

Neuron 50, 377–388, May 4, 2006 ©2006 Elsevier Inc. DOI 10.1016/j.neuron.2006.03.023

Pten Regulates Neuronal Arborization and Social Interaction in Mice

Chang-Hyuk Kwon,[1,3,4] Bryan W. Luikart,[1,4] Craig M. Powell,[2,4] Jing Zhou,[1] Sharon A. Matheny,[1] Wei Zhang,[1] Yanjiao Li,[1] Suzanne J. Baker,[3] and Luis F. Parada[1,*]

[1] Center for Developmental Biology and Kent Waldrep Foundation Center for Basic Neuroscience Research on Nerve Growth and Regeneration

[2] Departments of Neurology and Psychiatry University of Texas Southwestern Medical Center Dallas, Texas 75390

[3] Department of Developmental Neurobiology St. Jude Children's Research Hospital Memphis, Tennessee 38105

Summary

CNS deletion of *Pten* in the mouse has revealed its roles in controlling cell size and number, thus providing compelling etiology for macrocephaly and Lhermitte-Duclos disease. *PTEN* mutations in individuals with autism spectrum disorders (ASD) have also been reported, although a causal link between PTEN and ASD remains unclear. In the present study, we deleted *Pten* in limited differentiated neuronal populations in the cerebral cortex and hippocampus of mice. Resulting mutant mice showed abnormal social interaction and exaggerated responses to sensory stimuli. We observed macrocephaly and neuronal hypertrophy, including hypertrophic and ectopic dendrites and axonal tracts with increased synapses. This abnormal morphology was associated with activation of the Akt/mTor/S6k pathway and inactivation of Gsk3β. Thus, our data suggest that abnormal activation of the PI3K/AKT pathway in specific neuronal populations can underlie macrocephaly and behavioral abnormalities reminiscent of certain features of human ASD.

Introduction

Phosphatase and tensin homolog on chromosome ten (*PTEN*) is a tumor suppressor gene mutated in many human cancers (Ali et al., 1999). Individuals with germline *PTEN* mutations are prone to tumors but also display brain disorders, including macrocephaly, seizure, Lhermitte-Duclos disease, and mental retardation (Waite and Eng, 2002). *PTEN* mutations also have been reported in autistic individuals with macrocephaly (Butler et al., 2005; Goffin et al., 2001; Zori et al., 1998).

PTEN has lipid phosphatase activity against the 3′ phosphate of phosphatidylinositol 3,4,5 trisphosphate (Maehama and Dixon, 1998). Phosphatidylinositol 3-kinase (PI3K) catalyzes the reverse of this reaction, resulting in AKT activation. Upon activation, AKT phosphorylates a diverse spectrum of substrates, including *tuberous sclerosis complex 2* (*TSC2*) gene product tuberin, glycogen synthase kinase 3β (GSK3β), and the proapoptotic protein BAD (Luo et al., 2003).

Abnormalities in many components of the PI3K/AKT pathway have been associated with diverse brain disorders. For example, inactivating mutations in *PTEN* or activating mutations in *PI3K* are found in malignant brain tumors (Ali et al., 1999; Broderick et al., 2004), low AKT level is associated with schizophrenia (Emamian et al., 2004), and individuals with *TSC* mutations have CNS disorders, including autism (Wiznitzer, 2004). The PI3K/AKT pathway has also been linked to activity-dependent plasticity processes in the brain. Activation of the pathway was found in the amygdala in fear-conditioned rats (Lin et al., 2001). Components of the mTOR/S6K pathway, downstream of PI3K/Akt, are present in synapses and mediate synaptic plasticity through local protein synthesis (Tang et al., 2002).

Pten null mice die during embryogenesis, and heterozygotes are prone to tumors in the prostate, endometrium, and lymphoid system (Stiles et al., 2004). Conditional loss of *Pten* can have differing consequences depending on the cell type or its state of differentiation. Consistent with the frequent association of somatic mutations with cancer, *Pten* deletion in dividing T-lymphocytes, mammary epithelial cells, neural stem cells, and astrocytes induced hyperplasia (Fraser et al., 2004; Groszer et al., 2001; Li et al., 2002; Suzuki et al., 2001). *Pten* deletion in granule neurons, cardiomyocytes, and the cerebellum induced cellular hypertrophy (Crackower et al., 2002; Kwon et al., 2001). In primary neuron cultures, the PI3K pathway regulates cell survival, neurite growth, and dendritic arborization (Crowder and Freeman, 1998; Jaworski et al., 2005; Klesse and Parada, 1998; Markus et al., 2002). The above studies manipulated either mitotic cells or immature neurons. The in vivo role of the PI3K/PTEN/AKT pathway has been poorly studied in mature neurons where specialized properties including synapses and polarity are already established.

In the present study, we employed a *Neuron-specific enolase* (*Nse*) promoter-driven *cre* transgenic mouse line, in which cre activity is confined to discrete mature neuronal populations in the cerebral cortex and hippocampus (Kwon et al., 2006). The resulting conditional *Pten* mutant mice develop macrocephaly due to cre-specific neuronal hypertrophy. We identified abnormal dendritic and axonal growth and synapse number. The mice exhibit altered social behavior and inappropriate responses to sensory stimuli.

Results

Pten Is Inactivated in Differentiated Neurons

Cre activity in the brain of *Nse-cre* mice was limited to subsets of differentiated neurons, mostly in layers III to V of the cerebral cortex and in the CA3, dentate gyrus granular layer (GL), and polymorphic layer (PML) of the hippocampal formation (Kwon et al., 2006). By 4 weeks of age, roughly 30%–60% of the neurons in these

*Correspondence: luis.parada@utsouthwestern.edu

[4] These authors contributed equally to this work.

regions expressed functional β-galactosidase when crossed with *Rosa26-stop-lacZ* cre reporter (*Rosa26R* hereafter) (Soriano, 1999). A low level of sporadic cre activity was observed in a few neurons in the olfactory bulb, spinal cord, and cerebellar Purkinje cell layer. To confirm cre activity in differentiated neurons, we stained brain sections from 2-week-old mice for β-galactosidase and either a dendritic marker, microtubule-associated protein-2 (MAP2), or a neural stem cell marker, nestin. In the dentate gyrus at this age, active neurogenesis is still occurring in the subgranular zone (SGZ) between the GL and the PML (Shapiro and Ribak, 2005). Most granule neurons in the dentate gyrus are born in the SGZ and migrate and differentiate outward into the GL. In *Nse-cre*; *Rosa26R* brains, β-galactosidase colocalized with MAP2-expressing cells in the outer GL and the PML, but not in the inner GL or the SGZ. No β-galactosidase was detected in nestin-positive cells (Figure 1A). Consistent with this, postnatal day 15 (P15) *Nse-cre*; *Rosa26R* brains pulsed with bromodeoxyuridine (BrdU) at P14 did not show colocalization of BrdU and β-galactosidase (Figure 1B), indicating the absence of cre activity in dividing neuronal precursors. Chasing BrdU signal 4 weeks after the pulse revealed partial colocalization of BrdU and β-galactosidase in dentate granule neurons. Thus, cre activity is confined to subsets of differentiated neurons in *Nse-cre* mice.

Nse-cre; *Pten*$^{loxP/loxP}$ mice (mutant mice hereafter) were viable at birth and appeared normal until 4–5 weeks of age. Consistent with a previous report (Perandones et al., 2004), control mice showed Pten signal in most differentiated neurons, including those in the GL and PML of the dentate gyrus and cerebral cortex (Figures 1C and 1D, respectively). At 2 weeks of age, mutant dentate gyrus exhibited Pten-negative cells at the PML and the outer GL, similar to the cre activity of *Nse-cre*; *Rosa26R* brains. The same regions also showed increased phospho-Ser473-Akt (P-Akt), a marker for Akt activation. At 4 weeks of age, Pten-negative and P-Akt-positive cells increased in mutant dentate GL, indicating that *Pten* deletion accompanies differentiation of dentate granule neurons. *Pten* deletion and increased P-Akt signal were found in all sites of Nse-cre activity (Kwon et al., 2006), and the ratios of *Pten* deletion (55.89% ± 6.62% in dentate granule neurons; 44.88 ± 1.62% in sensory cortical layers III to V) coincided with the ratios predicted by the *Rosa26R* assays, indicating similar recombination efficiency for the *loxP-Pten* and *Rosa26* alleles.

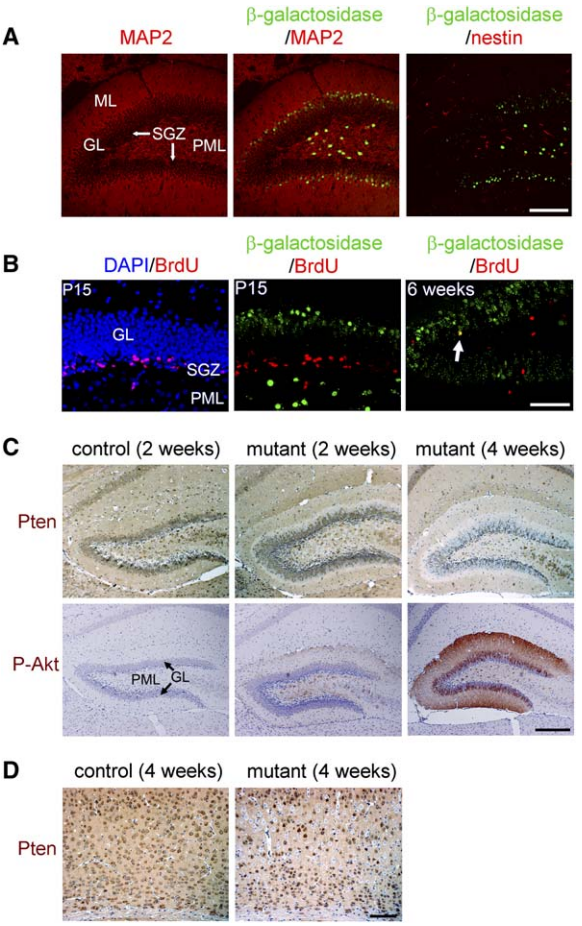

Figure 1. *Pten* Deletion Occurred in Differentiated Neurons

(A) In 2-week-old *Nse-cre*; *Rosa26R* mice, β-galactosidase signal was detected in MAP2-expressing neurons in the polymorphic layer (PML) and the outer granular layer (GL), close to the molecular layer (ML), in the dentate gyrus, but not in the inner GL, subgranular zone (SGZ), or in cells expressing nestin. Although a similar level and pattern of MAP2 or nestin immunoreactivity appeared in control (either without *cre* or *Rosa26R*), β-galactosidase was not detected (data not shown). Scale bar, 200 μm.

(B) P15 *Nse-cre*; *Rosa26R* mice injected with BrdU at P14 retained the BrdU signal mainly in the SGZ, which was absent in β-galactosidase-expressing cells in the outer GL and PML. Four weeks after the BrdU injection, BrdU signal was detected in the GL, and some of them colocalized with β-galactosidase-expressing granule neurons (arrow, for example). Scale bar, 100 μm.

(C) In mutant tissue at 2 weeks of age, similar to β-galactosidase activity in *Nse-cre*; *Rosa26R* brain, Pten-negative (blue), and P-Akt-positive signals (brown) were detected in the PML and the outer GL. At 4 weeks of age, the number of Pten-negative, P-Akt-positive cells increased in mutant dentate gyrus. Scale bar, 200 μm.

(D) In the sensory cortex layers III to VI, Pten (brown) was detected in most neurons in control. In mutant cortex, Pten-negative cells were mainly detected at layers III to V. Scale bar, 100 μm.

Behavioral Abnormalities in Social Interaction and Social Learning

Autistic spectrum disorders (ASD) have been reported in individuals with germline *PTEN* mutations (Butler et al., 2005; Goffin et al., 2001; Zori et al., 1998). Since the adult *Pten* mutant mice tended to be isolated from their littermates within the cage, we examined the colony using a series of established behavioral paradigms. We found that mutant mice exhibit a distinct pattern of behavioral abnormalities reminiscent of ASD.

Mice are a social species and display behavioral social interaction (Murcia et al., 2005). Thus, social interaction and nesting have been proposed as core paradigms to test autistic behavior in mice (Crawley, 2004) and have been used to measure autism-like behaviors in other mutant mouse models (Lijam et al., 1997; Moretti et al., 2005). As anticipated, control mice exposed to a novel conspecific juvenile exhibited typical behavior of approaching and sniffing, but such initial social interaction was profoundly decreased in mutant mice (Figure 2A). When re-exposed to the same juvenile after 3 days, control mice exhibited a typical decrease in social interaction compared to the initial interaction, indicating

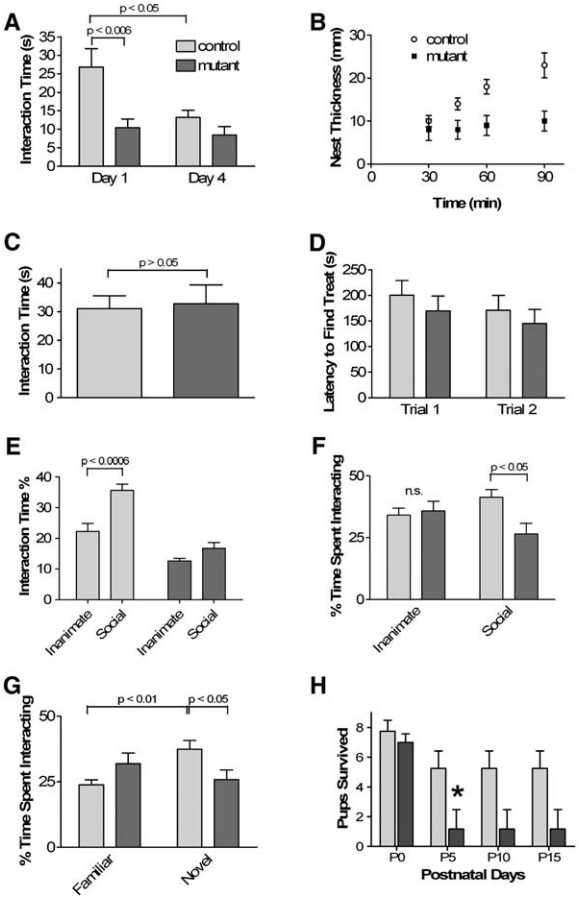

Figure 2. The *Pten* Mutant Mice Were Abnormal in Behavioral Tests for Social Interaction and Social Learning

(A) At day 1, mutants spent significantly less time interacting with a conspecific juvenile compared to controls (n = 12). Control mice spent significantly less time interacting with the same juvenile 3 days hence ($p < 0.05$), yet mutants did not decrease their interaction time ($p = 0.8$). Legend in this panel applies to all bar graphs.

(B) Mutant mice showed significant deficits in nest formation (n = 12). ANOVA revealed a significant effect of genotype ($F_{1,22} = 7.97$, $p = 0.01$), time ($F_{3,66} = 11.37$, $p < 0.00001$), and an interaction between genotype and time ($F_{3,66} = 6.26$, $p < 0.001$).

(C) Time spent interacting with a novel inanimate object under the same conditions as in (A) was not significantly affected by genotype (n = 12).

(D) Mutant mice did not show significant difference from control in latency to find a buried treat following overnight food deprivation (n = 12).

(E) When exposed to caged social and inanimate targets in an open field, controls showed normal preference for a social target over an inanimate target, while mutants spent similar time interacting with both targets (n = 12). Furthermore, mutant mice spent significantly less time interacting with a social target compared to controls ($p < 0.00001$). In this task, there was also a significant decrease in inanimate object interaction time between genotypes ($p < 0.01$), unlike in (C).

(F) In a social preference task, mutants spent less time with a social target compared to controls (n = 12). Time spent with an inanimate object was not significantly different in both groups.

(G) In a preference for social novelty task, controls showed a preference for social novelty, while mutants showed no preference between the social targets (n = 12). Mutants spent significantly less time interacting with a novel social target compared to controls.

(H) Mutant female mice delivered normal-sized pups. Mortality of pups between P0 and P5 was significantly higher in mutants (n = 6) compared to controls (n = 8). *$p < 0.05$ to controls and < 0.005 to P0.

recognition of the familiar juvenile and normal social learning. The mutant mice, however, did not decrease their interaction, indicating impaired social learning or inability to identify the juvenile due to the low level of initial interaction. We next examined nest formation, a test for home cage behavior (Lijam et al., 1997; Moretti et al., 2005). In contrast to the immediate activity of nest formation in control mice, mutant mice showed little nest-forming activity (Figure 2B). We do not attribute the abnormalities in social interaction and nest formation to deficiencies in general interest in novelty or olfactory sensation, since we did not detect significant difference between groups in tests for novel inanimate object interaction (Figure 2C) or olfaction (Figure 2D). Each of the above tests was fully replicated with equivalent significant results using a separate cohort of mice and performed by a different investigator, demonstrating the reproducibility of the results (data not shown).

Additional social tests gave similar results. For example, another social interaction test presents a test mouse with a caged adult mouse (social target) and an empty cage (inanimate target) in an open field. Control mice spent significantly more time interacting with the social target than with the inanimate target (Figure 2E). In contrast, *Pten* mutants showed decreased interaction with the social target compared to controls and spent a similar amount of time interacting with both targets. Another test for social novelty uses a three-roomed chamber. Initial interaction with the empty cage was similar in both groups, while interaction with the social target was significantly decreased in mutants compared to controls (Figure 2F). Subsequently, when mice were exposed to the familiar mouse versus a novel mouse, control mice showed a clear preference for the novel mouse over the familiar mouse as expected, while mutant mice did not show a preference for social novelty (Figure 2G). Additionally, mutants showed significantly less interaction with the novel target mouse compared to controls. In summary, the mutant mice exhibited decreased social interaction without change in novel object exploration or a preference for social novelty. Thus, the *Pten*-deficient mice display deficiencies in classic social interaction paradigms.

We also measured sexual and maternal behavior. While all naive control males made female mice pregnant, none of naive mutant males did. Although we do not exclude potential reproductive defects, we did not observe any active sexual behavior, such as mounting, from the mutant males. While mutant females could be fertilized by normal males, mortality of pups by P5 was higher than control group (Figure 2H), indicating defects in maternal care. Taken together, the *Pten* mutant mice exhibited abnormalities in social interaction, memory and preference, sexual behaviors, and maternal care in several different social paradigms.

Behavioral Abnormalities in Response to Sensory Stimuli, Anxiety, and Learning

By 6 weeks of age, mutant mice were also distinguishable from control mice in their response to novel sensory stimulation. When investigators handled mutant mice, they were unusually resistant to handling (n = 52). Consistent with this subjective observation, mutant mice exhibited normal locomotor activity in less stressful

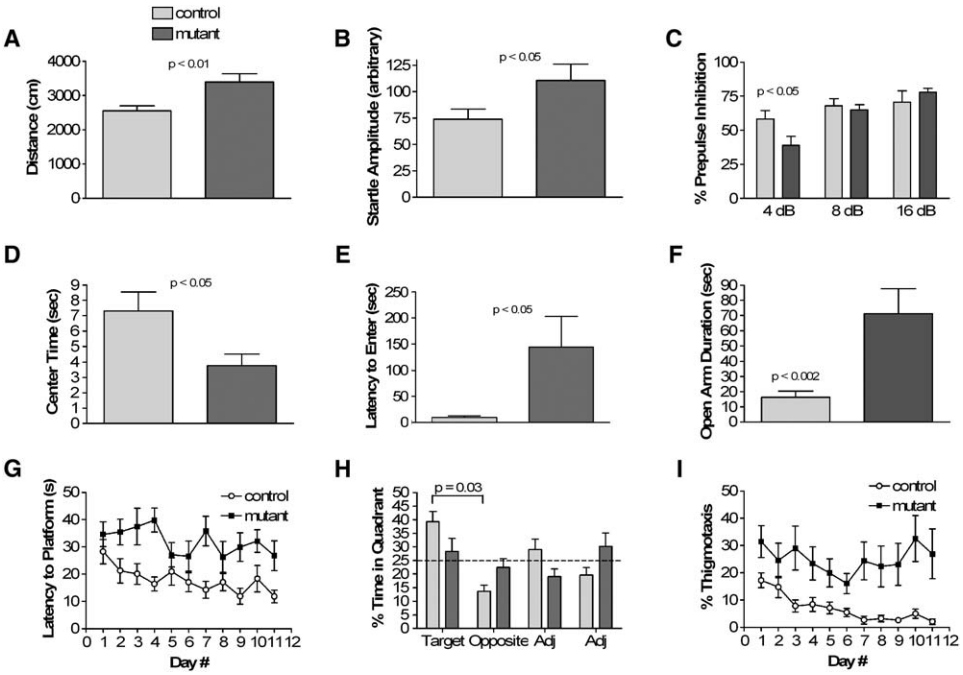

Figure 3. The *Pten* Mutant Mice Showed Abnormalities in Responses to Sensory Stimuli, Anxiety, and Learning

(A) Mutants exhibited increased locomotor activity in an open field test (n = 16 mutants, 17 controls). Average speed was 11.30 ± 0.84 cm/s for mutants and 8.51 ± 0.47 cm/s for controls (p = 0.006). Legend in this panel applies to all bar graphs.

(B) Initial startle response was significantly increased in mutants (n = 11 mutants, 14 controls). Data represent the average startle response to the first six presentations of a 40 ms, 120 dB white noise stimulus.

(C) In a prepulse inhibition test, mutants showed significantly impaired sensorimotor gating (n = 11 mutants, 14 controls).

(D) Mutants exhibited anxiety-like behavior as they spent significantly less time in the center zone of the open field apparatus (n = 16 mutants, 17 controls).

(E) The latency to enter the light side of the dark/light boxes was significantly elevated in mutants (n = 16 mutants, 17 controls).

(F) In elevated plus maze test, mutants exhibited significantly increased duration in open arm (n = 16 mutants, 17 controls).

(G) Mutants exhibited a significantly decreased learning curve in the submerged platform version of the water maze when latency to reach the platform was measured (n = 9 mutants, 12 controls). ANOVA revealed a main effect of genotype ($F_{1,17} = 11.17$, $p < 0.01$) and day number ($F_{10,170} = 2.21$, $p < 0.05$). Similar effect was seen in distance traveled to reach the platform (data not shown). Three mutant mice died during the water maze task due to seizure activity during training.

(H) Controls showed clear preference for target quadrant versus opposite whereas mutants showed no preference (n = 9 mutants, 12 controls).

(I) Mutant mice spent significantly increased time along the edge of the water maze (thigmotaxis, n = 9 mutants, 12 controls). ANOVA revealed a main effect of genotype ($F_{1,17} = 39.76$, $p < 0.00001$).

environments but hyperactivity under more stressful conditions. In the bright environment of the open field, mutants were hyperactive, traveling further (Figure 3A) at an increased average speed. However, in the dark/light boxes and in the enclosed, darker environments of the locomotor apparatus, locomotor activity was normal (see Figures S1A and S1B in the Supplemental Data available online). Additionally, mutants exhibited increased initial startle responses to a 120 dB white noise stimulus (Figure 3B). Upon repeated startle stimulation, mutants showed similar startle responses to controls, indicating normal habituation (Figure S1C). Sensorimotor gating, as measured with a prepulse inhibition paradigm, was also significantly impaired in mutant mice (Figure 3C). Thus, the mutants showed quantifiably increased activity in response to sensory stimuli.

Consistent with exaggerated response to stressful sensory stimuli, mutant mice also showed increased anxiety-like behavior in the open field test where they spent significantly less time in the center zone (Figure 3D) as well as a lower ratio of center versus periphery time (data not shown, p = 0.02). Similarly, in the dark/light apparatus, mutants showed longer latencies to enter the light side, spending the majority of their time on the dark side (Figure 3E). In a third anxiety-related test, the elevated plus maze, mutants did not show the increased anxiety-like behavior (Figure 3F). Indeed, there was an opposite effect in both the time spent in the open arms and the ratio of open arm entries to total arm entries (data not shown).

Because of the profound abnormalities in the dentate gyrus (described below), we tested the *Pten* mutant mice in the Morris water maze. Because of the abnormal anxiety, we habituated the mice to swimming in the maze for 4 days using a visible platform task. Mutant mice learned the visible platform task as well as controls, though there was a trend toward slower acquisition (Figure S1D). In the submerged platform version, measuring both latency to reach the platform and distance traveled to reach the platform, mutant mice did not learn as quickly as controls (Figure 3G). On the probe trial, control mice spent significantly more time in the target quadrant than the opposite quadrant, while mutants showed no significant preference (Figure 3H).

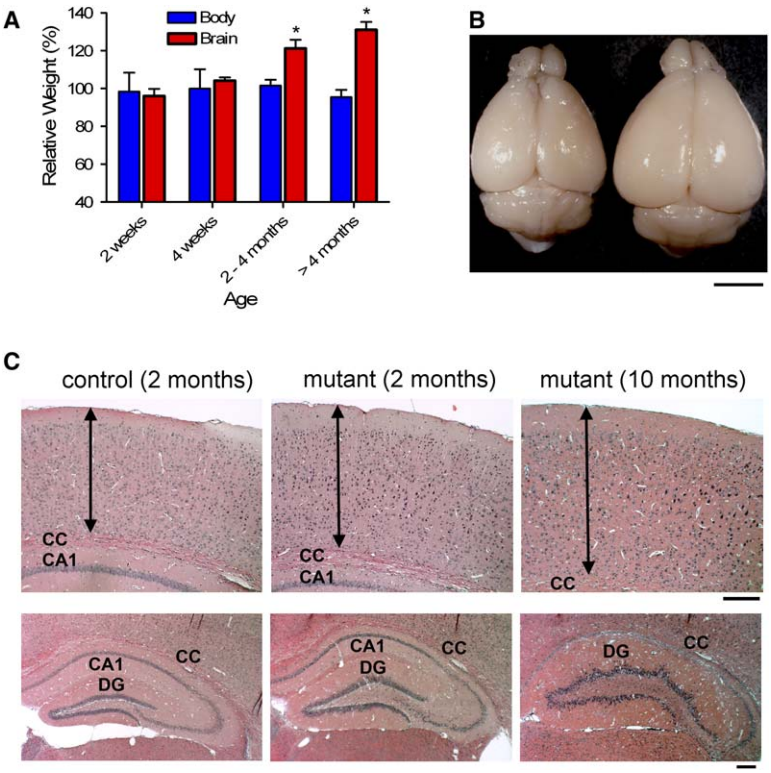

Figure 4. Progressive Macrocephaly and Regional Hypertrophy in the *Pten* Mutant Mice

(A) Relative sizes of mutant brain to control at different ages indicate progressive macrocephaly in mutant mice (n = 4 or more per group). *p < 0.005 versus control.

(B) A representative mutant brain at 10 months of age (right) is bigger than that from littermate control. Scale bar, 4 mm.

(C) H/E staining on coronal sections shows that the thickness of the cerebral cortex (arrows), the length between the pial surface and the corpus callosum (CC), increased in adult mutant brain (upper panels). In the hippocampus, progressively enlarged dentate gyri (DG) and compressed or absence of CA1 were seen in mutant brains (lower panels). Scale bars, 200 μm.

In addition, mutant mice exhibited a significantly greater tendency to swim along the edge of the maze (thigmotaxis) (Figure 3I), which is similar to their behavior in the open field test.

In addition to the behavioral abnormalities described, 6 of 52 mutant mice studied, including 3 of 12 during the water maze test, showed sporadic seizures (subjective observation). Further analysis using electroencephalogram/electromyogram (EEG/EMG) recording revealed that all mutant mice analyzed (n = 3) developed spontaneous seizures during the light phase, but no seizures were observed in any of control mice (Table S1). Repetitive spike-wave patterns were noted, sometimes accompanied by rhythmic slow activity. Continuous spike-wave bursting could also be seen. The incidence of seizures was 0.67 per mouse per day, and the mean duration was 10 min 50 s. Sound and tactile stimuli did not induce seizures in any mouse (data not shown). The relatively low incidence and short duration of seizure recorded in the subset of mutant mice is consistent with the low frequency by subjective observation. Given the relatively low incidence and short duration of seizures, it is unlikely that seizures bear on the robust behavioral abnormalities seen in all 52 mice. Consistent with this view, as described below, mutant mice did not show any deficit in tests for locomotor activity and strength. In the accelerating rotarod test, mutant mice exhibited normal coordination during the initial trials (Figure S1E). Interestingly, while both groups showed significant motor learning, during subsequent rotarod trials, mutant mice actually performed better on this repetitive test of motor coordination compared to controls. In vertical pole and dowel tests to measure strength and endurance, mutant mice performed as well as controls (Figures S1F and S1G). In addition, mutant mice did not show deficits in context- and cue-dependent fear conditioning (Figure S1H).

Progressive Macrocephaly and Soma Hypertrophy in Mutant Brain

Mouse strains with broad neuronal *Pten* deletion showed soma hypertrophy, macrocephaly, and premature death, occasionally with reduced body weight (Kwon et al., 2001, and unpublished observations). In the present study, the mutant mice appear to have a normal life span, presumably due to more restricted *Pten* deletion in subsets of postmitotic neurons. They also showed progressive macrocephaly, but without significant change in body weight (Figure 4A). The progressive macrocephaly was confined to the forebrain (cortex and hippocampus; Figures 4B and 4C), where most cre-mediated *Pten* deletion occurs (Kwon et al., 2006). Analysis of aging mice indicated eventual foliation of the DG and compression of the CA1 region (Figure 4C; lower right panel). Most dentate gyrus granule cells from wild-type mice expressed Pten and sustain relatively even soma diameter (Figure S2A). In contrast, Pten-negative neurons were larger than Pten-positive neurons at 4 weeks of age. The progressive increase in soma diameter and disorganized GL continued in mutant aging mice (Figures S2A and S2B). Such soma hypertrophy was also observed in the cortex and CA3 (Figure S2C) where cre activity is also present.

Regulation of Axonal Growth In Vivo

The Pten pathway is known to regulate neurite outgrowth in cell culture (Markus et al., 2002). Since *Nse-cre* drives *Pten* ablation only in differentiated neurons with established polarity, we examined the effects of Pten loss on existing neuronal processes. In the dentate

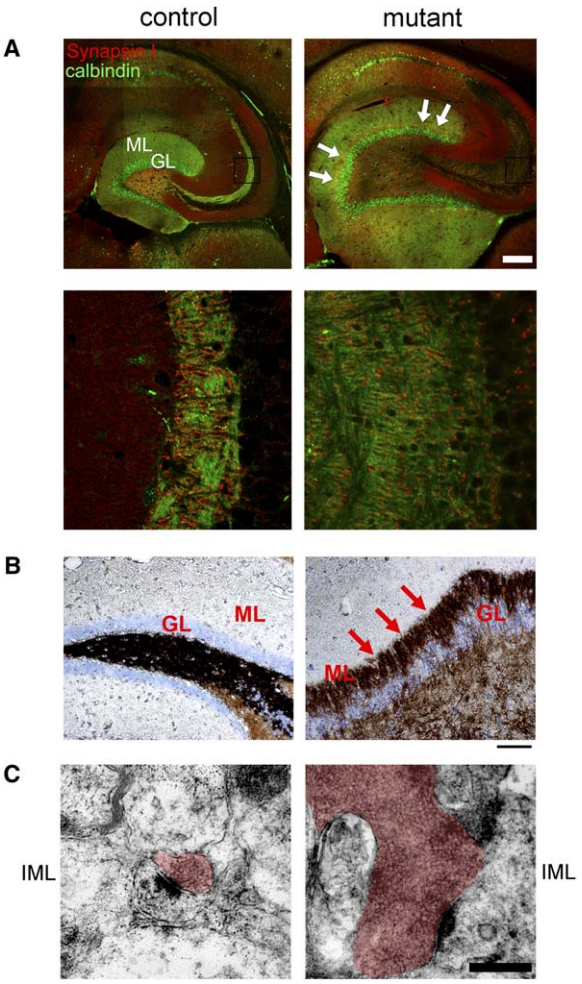

Figure 5. Hypertrophic and Ectopic Axonal Tract with Increased Synapses in *Pten*-Deleted Dentate Gyrus

(A) Horizontal floating sections from 10-month-old brains were stained for synapsin I (red) and calbindin (green). Confocal images showed that elongated and dispersed mossy fiber tract from the granular layer (GL) of mutant dentate gyrus and an ectopic layer of axonal signals (arrows) in the molecular layer (ML), compared to those of control (upper panels). Scale bar, 500 μm. High-magnification images revealed that the mossy fiber synapses spanned a larger area in mutant versus control animals (lower panels; from the boxes in upper panels).

(B) The inner ML of 7-month-old mutant dentate gyrus was positive for Timm staining (arrows), while such signals were absent in control ML. Scale bar, 100 μm.

(C) Electron microscopic analysis of the inner ML (IML) of dentate gyri revealed that the increased axonal staining in mutant was due to enlarged presynaptic varicosities (red highlight). The varicosities of mutant contained a large number of densely packed synaptic vesicles. Scale bar, 0.5 μm.

gyrus, granule neuron axons form the mossy fiber tract that projects from the GL through the PML to synapse with CA3 dendrites (Amaral, 1978). The extent of the mossy fiber tract was visualized by immunohistochemistry (IHC) using antibodies to synapsin I, a presynaptic marker, and to calbindin, which is expressed in the soma and processes of dentate granule neurons (Figure S3A). In adult mutants, the dentate gyrus showed a marked enlargement of the mossy fiber tract that progressed over time (Figures S3A and S3B). Confocal microscopy revealed that mutant axonal processes were more abundant and projected to a broader area (Figure 5A).

We also observed changes in the synapses of the mutant dentate gyrus. Synapsin I staining was increased in the inner molecular layer (ML) of aged mutants (arrows in Figure 5A). Normally, most synapses in this region are derived from mossy cells of the PML and express calretinin (Blasco-Ibanez and Freund, 1997). The increased synapsin I staining of the inner ML did not completely overlap with calretinin staining (Figure S3C). Instead, the abnormally localized axonal projections appear to push mossy cell axons out of the inner ML. In fact, the abnormal axonal projections were positive for Timm's staining (Figure 5B), which is specific for the mossy fiber tract of the dentate gyrus (Danscher et al., 2004), demonstrating ectopic positioning of granule axons in the mutant mice.

Ultrastructural examination of the inner ML of mutant animals indicated a dramatic increase in presynaptic vesicle number compared to control animals (Figure 5C). In support of the Timm's staining data, the large vesicle pools were apposed to multiple postsynaptic densities, thus exhibiting the morphological appearance of granule neuron mossy fiber synapses in the CA3 region with characteristic enlarged presynaptic terminals. Taken together, these results suggest that Pten inactivation in differentiated neurons causes increased axonal growth, ectopic axonal projections, and abnormal synapses.

Regulation of Dendrite Growth and Spine Density In Vivo

To more closely examine the morphology of dendrites in mutant brains, we used Golgi staining. In the cerebral cortex from 3-month-old mutant mice, we observed thickened or elongated processes (Figure 6A). There was obvious dendritic hypertrophy in adult mutant dentate gyrus (Figure 6B). Estimation of the thickness of MAP2-positive dentate ML revealed a significant increase in mutants that progressed with age (Figure 6C). We also observed a 24.9% increase in dendritic spine density within the ML of mutant versus control mice (Figure 6C).

Ectopic neuronal processes extending from the cell bodies into the PML were observed in mutant dentate gyri at 3 months of age (data not shown) when the behavioral phenotypes were fully developed. The ectopic neuronal processes were thin and spiny but could not be unambiguously distinguished as dendrites or axons at this age. At 8 months of age, the ectopic neuronal processes in *Pten* null neurons extending into the PML were longer and thicker with obvious spines (arrows in Figures 6B and 7A). IHC for MAP2 revealed that the ectopic processes were molecularly discernable as dendrites at 10 months of age (Figure 7B). Double labeling for MAP2 and P-Akt showed a layer of ectopic dendrites between the GL and the PML with increased P-Akt in mutant dentate gyrus at 10 months of age. Furthermore, confocal images showed that most granule neurons displaying dendritic ectopia had increased P-Akt, while neurons lacking P-Akt signal did not display dendritic ectopia (Figure 7C), indicating that the ectopia was due to cell-autonomous *Pten* deletion.

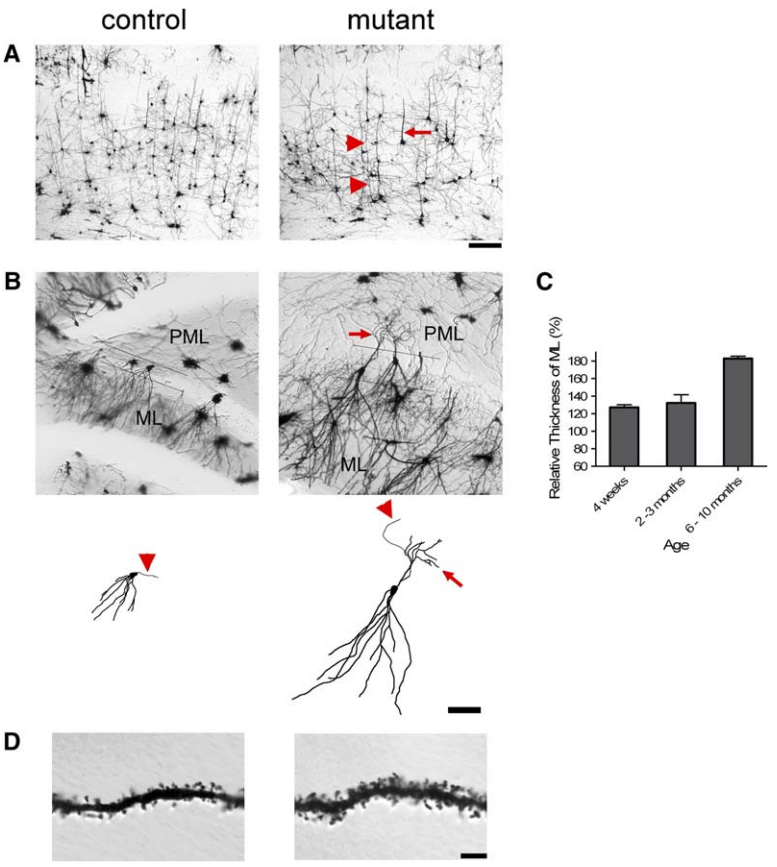

Figure 6. Golgi Stain Revealed Dendritic Hypertrophy, Ectopy, and Increased Spine Density in *Pten*-Deleted Brain

(A) Thickened or elongate neuronal processes (arrow and arrow heads, respectively) were present in mutant cerebral cortex compare to control at 3 months of age. Scale bar, 100 μm.

(B) At 8 months of age, increased length of the dendritic arbors in the molecular layer (ML) and ectopic neuronal processes (arrow) in the polymorphic layer (PML) were observed in mutant compare to control (upper panels). Reconstructions of single neurons made from image stacks emphasize the dendritic hypertrophy of the mutant neurons compare to control (lower panels). An axon can be seen emanating from both mutant and control neurons (arrowheads). Scale bar, 100 μm.

(C) Mutant ML was significantly thicker than that of control at all adult ages tested ($p < 0.05$).

(D) Higher-magnification images of dendrites in the ML revealed increased thickness and spine density in mutant (1.434 ± 0.064 spines/μm) versus control (1.077 ± 0.033 spines/μm) brains ($p < 0.000005$, $n = 23$ and 26 dendritic branches from three brains, respectively). Scale bar, 10 μm.

Molecular Correlates of Neuronal Hypertrophy and Abnormal Polarity

We next examined the status of downstream signaling components in *Pten*-deleted neurons. Previously, we reported that earlier *Pten* deletion in neurons increased P-Akt and phospho-Ser235/236-S6 (P-S6), markers for activation of the Akt and mTor/S6k pathways, respectively (Kwon et al., 2003). Here we show similar results when Pten is inactivated in differentiated neurons. We observed increased P-Akt and P-S6 in *Pten*-deleted, hypertrophic neurons, including the granule cells in the dentate gyrus at all ages tested (Figure 8A). Gsk3β is a direct target for Akt phosphorylation at Ser9, leading to functional inactivation (Cross et al., 1995). Both IHC and Western blot analysis demonstrate increased phospho-Ser9-Gsk3β (P-Gsk3β) in mutant tissues (Figure 8). Tuberin, the *Tsc2* product, is another direct target for Akt phosphorylation at Ser939 and an upstream regulator of the mTor/S6k pathway (Manning and Cantley, 2003). We detected increased phospho-Tuberin Ser939 (P-Tuberin) in the same tissues (Figure 8B). Thus, all tested downstream targets of Akt displayed increased phosphorylation in the *Pten*-deficient tissues.

Discussion

Through the use of cre-mediated recombination, we have deleted *Pten* and thus deregulated the PI3K pathway in subsets of differentiated neurons in the cortex and hippocampus.

Deregulation of Postmitotic Growth and Polarity of Neuronal Processes

At the time of *Pten* deletion, the dentate granule neurons already have established dendrites, extending over the full length of the ML, and axons projecting into the CA3 region. Furthermore, these neurons have already established synaptic connectivity. Our current findings indicate that Pten inactivation results in continued axonal and dendritic growth, with ectopic positioning of dentate axons to the ML and dendrites to the PML. Molecular markers for activation of the PI3K pathway were predictably detected. These data add to preceding reports of soma hypertrophy in *Pten*-deleted neurons (Backman et al., 2001; Kwon et al., 2001) and demonstrate that growth regulation by Pten extends to axons and dendrites.

Gsk3β was recently reported to be pivotal in controlling neuronal polarity in primary embryonic hippocampal neurons (Jiang et al., 2005; Yoshimura et al., 2005). In those studies, neurites destined to axons had more P-Gsk3β (inactive), and exogenous inactivation of Gsk3β resulted in formation of multiple axons. Conversely, expression of mutant Gsk3β insensitive to inactivation by Akt inhibited axon formation. Similar to the abnormal polarity in immature neurons, we observed hypertrophic axonal tracts and evidence of altered polarity of neuronal processes associated with inactivated Gsk3β in *Pten*-deleted, differentiated granule neurons. These results indicate that the PI3K/AKT/GSK3β pathway is critical not only for the establishment of polarity in

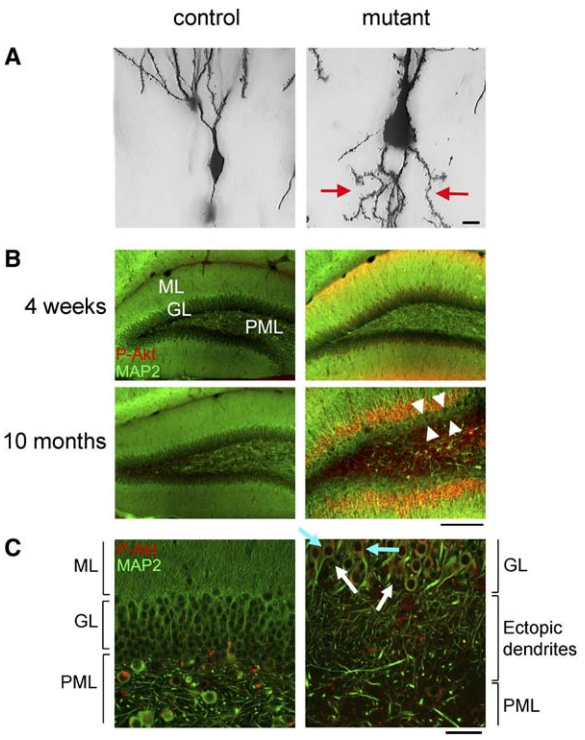

Figure 7. Ectopic Dendrites in *Pten*-Deleted Granule Neurons

(A) High-magnification images on Golgi-stained granule neurons in 8-month-old dentate gyri showed the presence of ectopic, spiny neuronal processes (arrows) in mutant, but not in control. Scale bar, 10 μm.

(B) Coronal floating sections were stained for MAP2 (green) and P-Akt (red). Increased P-Akt was apparent in the granular (GL) and molecular layers (ML) of mutant dentate gyri at all ages, but not in controls. Mutant dentate gyrus at 10 months of age had an ectopic layer of dendrites (arrow heads) between the GL and polymorphic layer (PML), which was absent at 4 weeks of age. Scale bar, 200 μm.

(C) Higher-magnification confocal images revealed that the ectopic dendrites were from P-Akt-positive granule neurons (light blue arrows, for example), but not from P-Akt-negative neurons (white arrows, for example). Scale bar, 50 μm.

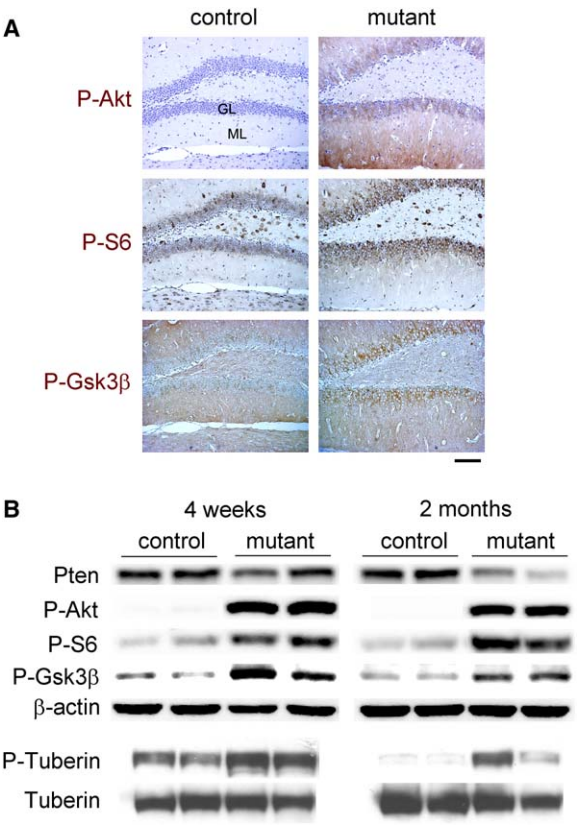

Figure 8. Molecular Signaling Downstream of *Pten*-Deleted Neurons

(A) At 2 months of age, mutant dentate gyri exhibited increased signal (brown) for P-Akt, P-S6 and P-Gsk3β, compared to those in control. The increased staining in mutants was apparent in the granular layer (GL) and inner molecular layer (ML) for P-S6 and in the GL for P-Gsk3β, whereas both the GL and ML displayed increased P-Akt. All sections were counterstained with hematoxylin, except for P-Gsk3β panels that were stained with methyl green. Scale bar, 200 μm.

(B) Western blot analysis showed decreased Pten and increased P-Akt, P-S6, P-Gsk3β, and P-Tuberin in mutant versus control at all ages tested. $p < 0.005$ for Pten at 2 months and P-Akt; $p < 0.1$ for P-S6, P-Gsk3β and P-Tuberin.

undifferentiated neurons in culture but also for maintenance in differentiated neurons in vivo.

Behavioral Abnormalities in Social Interaction and Anxiety

In our mouse model, cre-mediated recombination affects subsets of differentiated neurons in the hippocampus and cerebral cortex. This process is reproducible, and the anatomical and behavioral phenotypes are robust and fully penetrant. The *Pten* mutant mice appear to have normal life span, which allowed us to test paradigms proposed for autistic behaviors in mice (Crawley, 2004). Indeed, the mutant mice exhibited deficits in all social paradigms tested and also showed exaggerated reaction to sensory stimuli, anxiety-like behaviors, seizures, and decreased learning, which are features associated with ASD (American Psychiatric Association, 2000). The elevated plus maze gave different results compared to open field and dark/light boxes. This may reflect different aspects of anxiety-like behaviors and their controlling neural networks (Dawson and Tricklebank, 1995). Nonetheless, two of three tests clearly showed anxiety-like behavior in the mutant mice. Normal behaviors in many paradigms, including locomotor, motor coordination, and fear conditioning, indicate that the mutant mice were not globally impaired. It is worth noting that the behavioral abnormalities of the mutant mice appeared at a time when morphological abnormalities were subtle (6 weeks of age).

A Potential Link with Autism

ASD is a neuropsychiatric disorder characterized primarily by deficits in social interaction and repetitive behaviors (Baron-Cohen and Belmonte, 2005). Many genetic factors have been implicated in ASD, including 15q11-q13 duplication and mutations responsible for fragile X mental retardation syndrome (*FMR1*) and Rett syndrome (Andres, 2002; Muhle et al., 2004). Intriguingly, a few neurological disorders related to one another by harboring mutations in the PI3K pathway are also atypically associated with ASD. Individuals with tuberous sclerosis have mutations in the *TSC1/2* complex

and have a high incidence of ASD (25%–50%) (Asano et al., 2001; de Vries et al., 2005; Wiznitzer, 2004). In addition, the incidence of ASD patients who are subsequently diagnosed with neurofibromatosis type 1 (NF1) greatly exceeds epidemiological prediction (Marui et al., 2004; Mbarek et al., 1999). Finally, the recent preliminary association of *PTEN* mutations in ASD with macrocephaly (Butler et al., 2005) further points to abnormal activation of the PI3K pathway as one possible etiology. NF1, PTEN, and the TSC complex are negative regulators of the PI3K pathway, and inactivation of any of the proteins results in a hyperactive signal transduction in many circumstances (Hay, 2005; Klesse and Parada, 1998; Manning and Cantley, 2003).

Diverse anatomical and cellular abnormalities have been reported in brains from ASD individuals. For example, both macrocephaly and microcephaly have been described in autistic individuals, with a ratio of 15% and 20%, respectively (Fombonne et al., 1999). Similarly, enlarged amygdala in children and enlarged hippocampus in children and adolescents have been associated with ASD (Schumann et al., 2004). The sum of recent findings seems to approach a consensus that increased brain volume is a relatively common feature of autism (Cody et al., 2002). There have also been reports in autism cases of enlarged or abnormally oriented neurons, densely packed neuronal regions and isolated regions of atrophic neurons with reduced dendritic arborization (Bauman and Kemper, 2005; Murcia et al., 2005). Thus, diverse genetic and cellular changes are present in autistic brains. It is important to emphasize that causal versus ancillary abnormalities remain to be rigorously determined (Baron-Cohen and Belmonte, 2005; Cody et al., 2002; Dakin and Frith, 2005).

Similar to our mouse model, mice null for *FMR1* displayed deficits in social and anxiety behaviors and increased spine density, which is also reported in fragile X syndrome (Bagni and Greenough, 2005). Both FMR1 and the mTOR/S6K pathway regulate protein translation and synaptic plasticity (Tang et al., 2002; Zalfa et al., 2003). Given the known association of fragile X syndrome in ASD (Andres, 2002), aberrant regulation of synaptic protein translation and abnormal synaptic connectivity may be a common theme affecting social interaction and anxiety in the mouse models and potentially in subsets of ASD as well. Conversely, in Rett Syndrome and some reports of autism, neuronal atrophy and reduced dendritic spines have been reported (Zoghbi, 2003). It may be possible that synaptic imbalance resulting from excess or reduced connectivity could result in the similar abnormalities found in ASD.

Experimental Procedures

Mice and Histology

Pten^{loxP} mice (Suzuki et al., 2001) were a gift from Tak Mak (University of Toronto), and *Rosa26R* mice were from Jackson Lab (Bar Harbor, ME). To minimize transgenic variation due to genetic background, we maintained *Nse-cre*; *Rosa26R* or *Pten*^{loxP} mice in *C57/BL6* inbred background for at least three generations. For BrdU chasing, we injected subsets of 2-week-old *cre*; *Rosa26R* mice with BrdU as described (Fraser et al., 2004) and sacrificed them 1 day or 4 weeks after the injection. Mutant mice (*cre*; *Pten*$^{loxP/loxP}$) were born from breeding between *Pten*$^{loxP/loxP}$ mouse and *cre*; *Pten*$^{loxP/+}$ mouse or between *cre*; *Pten*$^{loxP/+}$ mice. Littermate controls used for this study were with a genotype of *cre*; *Pten*$^{+/+}$ or *Pten*^{loxP} mice without *cre*. For paraffin sectioning, we dissected out, processed, and sectioned brains as described (Fraser et al., 2004). For vibratome sectioning, we intracardially perfused the mice with ice-cold PBS followed by 4% (w/v) paraformaldehyde (PFA) in PBS. We dissected out the brain, post-fixed it in 4% PFA for overnight, and embedded it into 3% agarose. We made 50 μm thick coronal or horizontal sections by using a vibratome. All mouse protocols were approved by the Institutional Animal Care and Research Advisory Committee at University of Texas Southwestern Medical Center.

Immunostaining

We performed all IHC on triplicate sections per group. Based on anatomy, we chose matched sections from control and mutant. Antibodies used for IHC were against β-galactosidase (ICN, Aurora, OH), MAP2 (Sternberger Monoclonals, Lutherville, MA), nestin (BD Bioscience, San Jose, CA), BrdU (Dako, Carpinteria, CA), Pten (Neo-Markers, Winchester, MA), P-Akt, P-S6 (Cell Signaling, Beverly, MA), calbindin (Swant, Bellinzona, Switzerland), synapsin I, calretinin (Chemicon, Temecula, CA) or P-Gsk3β (Biosource, Camarillo, CA). For paraffin sections, we used microwave antigen retrieval for all antibodies, except that against P-Gsk3β. We visualized the primary antibodies by treating the sections with biotinylated secondary antibody and followed by amplification with peroxidase-conjugated avidin and DAB substrate. DAB-stained sections were counterstained with hematoxylin or methyl green (Vector Labs, Burlingame, CA). Alternatively, we detected the primary antibodies by secondary antibodies conjugated with Cy3 (Jackson Immunoresearch, West Grove, PA) or Alexa Fluor 488 (Molecular Probe, Eugene, OR) followed by counterstaining with DAPI (Vector Labs).

Cell Counting, Size Measurement, Golgi Staining, and Electron Microscopy

To measure the ratio of *Pten* deletion, we counted Pten-positive or -negative neurons in a 7 × 5 mm^2 area in the sensory cortex layers III to V and dentate GL by using MetaMorph software (Universal Imaging Corporation, West Chester, PA). We measured soma diameter of dentate granule neurons as described (Kwon et al., 2003), except for using the MetaMorph software. To estimate the length of the mossy fiber tract, we measured the center path of double-labeled signals for synapsin I and calbindin from the CA3 to the point at which two blades of dentate granular layer meet. Similarly, we estimated the thickest region of MAP2-positive dentate ML of either blade. We performed Golgi staining, image analysis, quantification of spine density, and electron microscopy as described (Luikart et al., 2005). Data were analyzed by Student's t test, except where noted, and displayed as mean ± SEM.

Behavioral Tests

Mutant mice were studied along with littermate controls in four cohorts of mice. Order of tests and cohorts are displayed in Table S2. Social interaction and social learning, interaction with a novel object, olfaction, strength tests by using vertical pole and dowel (Moretti et al., 2005), and nest formation (Lijam et al., 1997) were measured as described. Exceptions were performing social learning 3 days after the initial interaction test, placing one or two mice per cage in nest formation, overnight food deprivation before olfaction test, and using Student's t test in strength tests. Caged social interaction for social versus inanimate target (Moy et al., 2004) was performed in a 48 × 48 cm^2 white plastic arena using two 6.0 × 9.5 cm rectangular cages of wire mesh with or without adult mouse, allowing olfactory and minimal tactile interaction. Social preference for novelty was performed as described (Moy et al., 2004), except room and door dimensions were different (15 × 90 × 18.5 cm divided into three rooms of 15 × 29 cm separated by dividers with a central 3.8 × 3.8 cm door), and video tracking software from Noldus (Ethovision 2.3.19) replaced photobeams and direct observation. In the test, mice were initially allowed to explore the room for 10 min. Then mice were allowed to interact with an empty cage in one room versus a caged social target in the far room. Subsequently, mice were allowed to interact with the familiar caged target mouse versus a novel caged target mouse. The open field test was performed for 10 min in a brightly lit (~800 lux), 48 × 48 cm^2 white plastic arena using video tracking software with a center zone defined as a 15 × 15 cm^2 square. Elevated plus maze, dark/light behavior, locomotor activity, accelerating rotarod,

and Morris water maze were measured as described (Powell et al., 2004). Exceptions were scoring parameters by video tracking in elevated plus maze and allowing each mouse three sets of three trials per day with ~10 min between trials and 3 hr between sets in accelerating rotarod test. A variation on the startle reflex and prepulse inhibition protocol (Dulawa and Geyer, 2000) was used. Mice were subjected to five pseudorandomly presented trial types in a 22 min session with an average of 15 s (7–23 s) between trials: Pulse alone (40 ms, 120 dB, white noise pulse), three different Prepulse/Pulse trials (20 ms prepulse of 4, 8, or 16 dB above background noise level of 70 dB precedes the 120 dB pulse by 100 ms, onset to onset), and no stimulus. Context and cue-dependent fear conditioning was performed as described (Powell et al., 2004), except a different plexiglass box with clear walls (MedAssociates) was used and two pairings of a 2 s, 0.8 mA footshock and tone were delivered with 60 s between pairings. Freezing behavior was monitored at 10 s intervals by an observer blind to the genotype. To measure sexual behavior, naive male mice (n = 4) were caged with two sexually experienced female mice up to 30 days. We observed their sexual behavior about 1 hr at the first day and 10 min at next 4 days. To measure maternal behavior, we mated one or two naive female mice with a sexually experienced male mouse up to 30 days. We counted pups at P0, P5, P10, and P15.

EEG/EMG Recording

Pten mutants (n = 3) and controls (n = 4) at 8–9 months of age were anesthetized and surgically implanted for long-term EEG/EMG monitoring as described (Chemelli et al., 1999). Mice were housed individually under a 12 hr light-dark cycle at 25ºC, with food and water being replenished as necessary at CT 12:00 each day, but the mice were not otherwise disturbed. They were habituated to the recording conditions for 2 weeks before EEG/EMG signals were recorded over a period of 3 days, beginning at lights-off (CT 12:00). During the light period on the third day, sound and tactile stimuli were used to examine sensitivity to induced seizures. Mice were exposed to 10 min of an intense sound stimulus (a bunch of keys were shaken in the cage close to the mouse) followed by 3 min of tactile stimulus. Subsequently, the EEG/EMG record was visually screened for seizure epochs. Seizures were characterized as a spike-wave pattern on the EEG, typically accompanied by atonic periods or sustained rhythmic contractions on the EMG. Each seizure lasting for 2 s or more was noted.

Timm Staining

For Timm's staining, we intracardially perfused the mice with ice-cold 0.37% (w/v) sodium sulfide followed by 4% PFA. We dissected out the brain, postfixed it in 4% PFA for overnight, and cryoprotected in 30% (w/v) sucrose in PBS for 2–3 days. We made 16 μm thick coronal sections by using a cryostat. We performed a modified Timm staining as described (Danscher et al., 2004).

Western Blotting

We performed Western blotting as described (Kwon et al., 2003), except for loading 90 μg for P-Tuberin and Tuberin. Antibodies used for Western blotting were against Pten (NeoMarkers, Winchester, MA), P-Akt, P-S6, P-Gsk3β, P-Tuberin, Tuberin (Cell Signaling), or β-actin (Sigma, St. Louis, MO). We statistically analyzed chemiluminescence signals by using Kodak Image Station 2000R (Rochester, NY).

Supplemental Data

The Supplemental Data for this article can be found online at http://www.neuron.org/cgi/content/full/50/3/377/DC1/.

Acknowledgments

The authors thank Christopher Sinton and Shiori Ogawa for EEG/EMG analysis; Tak Mak for *Pten*^{loxP} mice; Junyuan Zhang, Xiaoyan Zhu, Steve McKinnon, Arash Khatami, Phillip Williams, David Theobald, Yajuan Liu, Ki-Woo Kim, and Jian Chen for technical assistance; and Gorm Danscher, Meredin Stoltenberg, Mark Lush, Douglas Benson, and Gary Westbrook for suggestions and helpful discussions. This work was supported in part by the American and Lebanese Associated Charities, NIH grant NS44172 (to S.J.B), and MH06597503 (to C.M.P.) NIH grant R37NS33199 and the American Cancer Society (to L.F.P.).

Received: August 12, 2005
Revised: February 15, 2006
Accepted: March 16, 2006
Published: May 3, 2006

References

Ali, I.U., Schriml, L.M., and Dean, M. (1999). Mutational spectra of PTEN/MMAC1 gene: a tumor suppressor with lipid phosphatase activity. J. Natl. Cancer Inst. *91*, 1922–1932.

Amaral, D.G. (1978). A Golgi study of cell types in the hilar region of the hippocampus in the rat. J. Comp. Neurol. *182*, 851–914.

American Psychiatric Association. (2000). Task Force on DMS-IV, Fourth edition (Washington DC: American Psychiatric Association).

Andres, C. (2002). Molecular genetics and animal models in autistic disorder. Brain Res. Bull. *57*, 109–119.

Asano, E., Chugani, D.C., Muzik, O., Behen, M., Janisse, J., Rothermel, R., Mangner, T.J., Chakraborty, P.K., and Chugani, H.T. (2001). Autism in tuberous sclerosis complex is related to both cortical and subcortical dysfunction. Neurology *57*, 1269–1277.

Backman, S.A., Stambolic, V., Suzuki, A., Haight, J., Elia, A., Pretorius, J., Tsao, M.S., Shannon, P., Bolon, B., Ivy, G.O., and Mak, T.W. (2001). Deletion of Pten in mouse brain causes seizures, ataxia and defects in soma size resembling Lhermitte-Duclos disease. Nat. Genet. *29*, 396–403.

Bagni, C., and Greenough, W.T. (2005). From mRNP trafficking to spine dysmorphogenesis: the roots of fragile X syndrome. Nat. Rev. Neurosci. *6*, 376–387.

Baron-Cohen, S., and Belmonte, M.K. (2005). Autism: a window onto the development of the social and the analytic brain. Annu. Rev. Neurosci. *28*, 109–126.

Bauman, M.L., and Kemper, T.L. (2005). Neuroanatomic observations of the brain in autism: a review and future directions. Int. J. Dev. Neurosci. *23*, 183–187.

Blasco-Ibanez, J.M., and Freund, T.F. (1997). Distribution, ultrastructure, and connectivity of calretinin-immunoreactive mossy cells of the mouse dentate gyrus. Hippocampus *7*, 307–320.

Broderick, D.K., Di, C., Parrett, T.J., Samuels, Y.R., Cummins, J.M., McLendon, R.E., Fults, D.W., Velculescu, V.E., Bigner, D.D., and Yan, H. (2004). Mutations of PIK3CA in anaplastic oligodendrogliomas, high-grade astrocytomas, and medulloblastomas. Cancer Res. *64*, 5048–5050.

Butler, M.G., Dasouki, M.J., Zhou, X.P., Talebizadeh, Z., Brown, M., Takahashi, T.N., Miles, J.H., Wang, C.H., Stratton, R., Pilarski, R., and Eng, C. (2005). Subset of individuals with autism spectrum disorders and extreme macrocephaly associated with germline PTEN tumour suppressor gene mutations. J. Med. Genet. *42*, 318–321.

Chemelli, R.M., Willie, J.T., Sinton, C.M., Elmquist, J.K., Scammell, T., Lee, C., Richardson, J.A., Williams, S.C., Xiong, Y., Kisanuki, Y., et al. (1999). Narcolepsy in orexin knockout mice: molecular genetics of sleep regulation. Cell *98*, 437–451.

Cody, H., Pelphrey, K., and Piven, J. (2002). Structural and functional magnetic resonance imaging of autism. Int. J. Dev. Neurosci. *20*, 421–438.

Crackower, M.A., Oudit, G.Y., Kozieradzki, I., Sarao, R., Sun, H., Sasaki, T., Hirsch, E., Suzuki, A., Shioi, T., Irie-Sasaki, J., et al. (2002). Regulation of myocardial contractility and cell size by distinct PI3K-PTEN signaling pathways. Cell *110*, 737–749.

Crawley, J.N. (2004). Designing mouse behavioral tasks relevant to autistic-like behaviors. Ment. Retard. Dev. Disabil. Res. Rev. *10*, 248–258.

Cross, D.A., Alessi, D.R., Cohen, P., Andjelkovich, M., and Hemmings, B.A. (1995). Inhibition of glycogen synthase kinase-3 by insulin mediated by protein kinase B. Nature *378*, 785–789.

Crowder, R.J., and Freeman, R.S. (1998). Phosphatidylinositol 3-kinase and Akt protein kinase are necessary and sufficient for the survival of nerve growth factor-dependent sympathetic neurons. J. Neurosci. *18*, 2933–2943.

Dakin, S., and Frith, U. (2005). Vagaries of visual perception in autism. Neuron *48*, 497–507.

Danscher, G., Stoltenberg, M., Bruhn, M., Sondergaard, C., and Jensen, D. (2004). Immersion autometallography: histochemical in situ capturing of zinc ions in catalytic zinc-sulfur nanocrystals. J. Histochem. Cytochem. *52*, 1619–1625.

Dawson, G.R., and Tricklebank, M.D. (1995). Use of the elevated plus maze in the search for novel anxiolytic agents. Trends Pharmacol. Sci. *16*, 33–36.

de Vries, P., Humphrey, A., McCartney, D., Prather, P., Bolton, P., and Hunt, A. (2005). Consensus clinical guidelines for the assessment of cognitive and behavioural problems in Tuberous Sclerosis. Eur. Child Adolesc. Psychiatry *14*, 183–190.

Dulawa, S.C., and Geyer, M.A. (2000). Effects of strain and serotonergic agents on prepulse inhibition and habituation in mice. Neuropharmacology *39*, 2170–2179.

Emamian, E.S., Hall, D., Birnbaum, M.J., Karayiorgou, M., and Gogos, J.A. (2004). Convergent evidence for impaired AKT1–GSK3beta signaling in schizophrenia. Nat. Genet. *36*, 131–137.

Fombonne, E., Roge, B., Claverie, J., Courty, S., and Fremolle, J. (1999). Microcephaly and macrocephaly in autism. J. Autism Dev. Disord. *29*, 113–119.

Fraser, M.M., Zhu, X., Kwon, C.H., Uhlmann, E.J., Gutmann, D.H., and Baker, S.J. (2004). Pten loss causes hypertrophy and increased proliferation of astrocytes in vivo. Cancer Res. *64*, 7773–7779.

Goffin, A., Hoefsloot, L.H., Bosgoed, E., Swillen, A., and Fryns, J.P. (2001). PTEN mutation in a family with Cowden syndrome and autism. Am. J. Med. Genet. *105*, 521–524.

Groszer, M., Erickson, R., Scripture-Adams, D.D., Lesche, R., Trumpp, A., Zack, J.A., Kornblum, H.I., Liu, X., and Wu, H. (2001). Negative regulation of neural stem/progenitor cell proliferation by the Pten tumor suppressor gene in vivo. Science *294*, 2186–2189.

Hay, N. (2005). The Akt-mTOR tango and its relevance to cancer. Cancer Cell *8*, 179–183.

Jaworski, J., Spangler, S., Seeburg, D.P., Hoogenraad, C.C., and Sheng, M. (2005). Control of dendritic arborization by the phosphoinositide-3′-kinase-Akt-mammalian target of rapamycin pathway. J. Neurosci. *25*, 11300–11312.

Jiang, H., Guo, W., Liang, X., and Rao, Y. (2005). Both the establishment and the maintenance of neuronal polarity require active mechanisms: critical roles of GSK-3beta and its upstream regulators. Cell *120*, 123–135.

Klesse, L.J., and Parada, L.F. (1998). p21 ras and phosphatidylinositol-3 kinase are required for survival of wild-type and NF1 mutant sensory neurons. J. Neurosci. *18*, 10420–10428.

Kwon, C.H., Zhu, X., Zhang, J., Knoop, L.L., Tharp, R., Smeyne, R.J., Eberhart, C.G., Burger, P.C., and Baker, S.J. (2001). Pten regulates neuronal soma size: a mouse model of Lhermitte-Duclos disease. Nat. Genet. *29*, 404–411.

Kwon, C.H., Zhu, X., Zhang, J., and Baker, S.J. (2003). mTor is required for hypertrophy of Pten-deficient neuronal soma in vivo. Proc. Natl. Acad. Sci. USA *100*, 12923–12928.

Kwon, C.H., Zhou, J., Li, Y., Kim, K.W., Hensley, L.L., Baker, S.J., and Parada, L.F. (2006). A neuron-specific enolase-cre line with cre activity in specific neuronal populations. Genesis *44*, 130–135.

Li, G., Robinson, G.W., Lesche, R., Martinez-Diaz, H., Jiang, Z., Rozengurt, N., Wagner, K.U., Wu, D.C., Lane, T.F., Liu, X., et al. (2002). Conditional loss of PTEN leads to precocious development and neoplasia in the mammary gland. Development *129*, 4159–4170.

Lijam, N., Paylor, R., McDonald, M.P., Crawley, J.N., Deng, C.X., Herrup, K., Stevens, K.E., Maccaferri, G., McBain, C.J., Sussman, D.J., and Wynshaw-Boris, A. (1997). Social interaction and sensorimotor gating abnormalities in mice lacking Dvl1. Cell *90*, 895–905.

Lin, C.H., Yeh, S.H., Lin, C.H., Lu, K.T., Leu, T.H., Chang, W.C., and Gean, P.W. (2001). A role for the PI-3 kinase signaling pathway in fear conditioning and synaptic plasticity in the amygdala. Neuron *31*, 841–851.

Luikart, B.W., Nef, S., Virmani, T., Lush, M.E., Liu, Y., Kavalali, E.T., and Parada, L.F. (2005). TrkB has a cell-autonomous role in the establishment of hippocampal Schaffer collateral synapses. J. Neurosci. *25*, 3774–3786.

Luo, J., Manning, B.D., and Cantley, L.C. (2003). Targeting the PI3K-Akt pathway in human cancer: rationale and promise. Cancer Cell *4*, 257–262.

Maehama, T., and Dixon, J.E. (1998). The tumor suppressor, PTEN/MMAC1, dephosphorylates the lipid second messenger, phosphatidylinositol 3,4,5-trisphosphate. J. Biol. Chem. *273*, 13375–13378.

Manning, B.D., and Cantley, L.C. (2003). United at last: the tuberous sclerosis complex gene products connect the phosphoinositide 3-kinase/Akt pathway to mammalian target of rapamycin (mTOR) signalling. Biochem. Soc. Trans. *31*, 573–578.

Markus, A., Zhong, J., and Snider, W.D. (2002). Raf and akt mediate distinct aspects of sensory axon growth. Neuron *35*, 65–76.

Marui, T., Hashimoto, O., Nanba, E., Kato, C., Tochigi, M., Umekage, T., Ishijima, M., Kohda, K., Kato, N., and Sasaki, T. (2004). Association between the neurofibromatosis-1 (NF1) locus and autism in the Japanese population. Am. J. Med. Genet. B Neuropsychiatr. Genet. *131*, 43–47.

Mbarek, O., Marouillat, S., Martineau, J., Barthelemy, C., Muh, J.P., and Andres, C. (1999). Association study of the NF1 gene and autistic disorder. Am. J. Med. Genet. *88*, 729–732.

Moretti, P., Bouwknecht, J.A., Teague, R., Paylor, R., and Zoghbi, H.Y. (2005). Abnormalities of social interactions and home-cage behavior in a mouse model of Rett syndrome. Hum. Mol. Genet. *14*, 205–220.

Moy, S.S., Nadler, J.J., Perez, A., Barbaro, R.P., Johns, J.M., Magnuson, T.R., Piven, J., and Crawley, J.N. (2004). Sociability and preference for social novelty in five inbred strains: an approach to assess autistic-like behavior in mice. Genes Brain Behav. *3*, 287–302.

Muhle, R., Trentacoste, S.V., and Rapin, I. (2004). The genetics of autism. Pediatrics *113*, e472–e486.

Murcia, C.L., Gulden, F., and Herrup, K. (2005). A question of balance: a proposal for new mouse models of autism. Int. J. Dev. Neurosci. *23*, 265–275.

Perandones, C., Costanzo, R.V., Kowaljow, V., Pivetta, O.H., Carminatti, H., and Radrizzani, M. (2004). Correlation between synaptogenesis and the PTEN phosphatase expression in dendrites during postnatal brain development. Brain Res. Mol. Brain Res. *128*, 8–19.

Powell, C.M., Schoch, S., Monteggia, L., Barrot, M., Matos, M.F., Feldmann, N., Sudhof, T.C., and Nestler, E.J. (2004). The presynaptic active zone protein RIM1alpha is critical for normal learning and memory. Neuron *42*, 143–153.

Schumann, C.M., Hamstra, J., Goodlin-Jones, B.L., Lotspeich, L.J., Kwon, H., Buonocore, M.H., Lammers, C.R., Reiss, A.L., and Amaral, D.G. (2004). The amygdala is enlarged in children but not adolescents with autism; the hippocampus is enlarged at all ages. J. Neurosci. *24*, 6392–6401.

Shapiro, L.A., and Ribak, C.E. (2005). Integration of newly born dentate granule cells into adult brains: hypotheses based on normal and epileptic rodents. Brain Res. Brain Res. Rev. *48*, 43–56.

Soriano, P. (1999). Generalized lacZ expression with the ROSA26 Cre reporter strain. Nat. Genet. *21*, 70–71.

Stiles, B., Groszer, M., Wang, S., Jiao, J., and Wu, H. (2004). PTEN-less means more. Dev. Biol. *273*, 175–184.

Suzuki, A., Yamaguchi, M.T., Ohteki, T., Sasaki, T., Kaisho, T., Kimura, Y., Yoshida, R., Wakeham, A., Higuchi, T., Fukumoto, M., et al. (2001). T cell-specific loss of pten leads to defects in central and peripheral tolerance. Immunity *14*, 523–534.

Tang, S.J., Reis, G., Kang, H., Gingras, A.C., Sonenberg, N., and Schuman, E.M. (2002). A rapamycin-sensitive signaling pathway contributes to long-term synaptic plasticity in the hippocampus. Proc. Natl. Acad. Sci. USA *99*, 467–472.

Waite, K.A., and Eng, C. (2002). Protean PTEN: form and function. Am. J. Hum. Genet. *70*, 829–844.

Wiznitzer, M. (2004). Autism and tuberous sclerosis. J. Child Neurol. *19*, 675–679.

Yoshimura, T., Kawano, Y., Arimura, N., Kawabata, S., Kikuchi, A., and Kaibuchi, K. (2005). GSK-3beta regulates phosphorylation of CRMP-2 and neuronal polarity. Cell *120*, 137–149.

Zalfa, F., Giorgi, M., Primerano, B., Moro, A., Di Penta, A., Reis, S., Oostra, B., and Bagni, C. (2003). The fragile X syndrome protein FMRP associates with BC1 RNA and regulates the translation of specific mRNAs at synapses. Cell *112*, 317–327.

Zoghbi, H.Y. (2003). Postnatal neurodevelopmental disorders: meeting at the synapse? Science *302*, 826–830.

Zori, R.T., Marsh, D.J., Graham, G.E., Marliss, E.B., and Eng, C. (1998). Germline PTEN mutation in a family with Cowden syndrome and Bannayan-Riley-Ruvalcaba syndrome. Am. J. Med. Genet. *80*, 399–402.

Cell Host & Microbe
Article

HSV-1 ICP34.5 Confers Neurovirulence by Targeting the Beclin 1 Autophagy Protein

Anthony Orvedahl,[1,2,9] Diane Alexander,[6,9] Zsolt Tallóczy,[8] Qihua Sun,[1] Yongjie Wei,[1] Wei Zhang,[3,4] Dennis Burns,[5] David A. Leib,[6,7] and Beth Levine[1,2,*]
[1] Department of Internal Medicine
[2] Department of Microbiology
[3] Center for Developmental Biology
[4] Kent Waldrep Foundation Center for Basic Neuroscience Research on Nerve Growth and Regeneration
[5] Department of Pathology
University of Texas Southwestern Medical Center, Dallas, TX 75390, USA
[6] Department of Ophthalmology and Visual Sciences
[7] Department of Molecular Microbiology
Washington University School of Medicine, St. Louis, MO 63110, USA
[8] Department of Neurology, Columbia University College of Physicians and Surgeons, New York, NY 10032, USA
[9] These authors contributed equally to this work.
*Correspondence: beth.levine@utsouthwestern.edu
DOI 10.1016/j.chom.2006.12.001

SUMMARY

Autophagy is postulated to play a role in antiviral innate immunity. However, it is unknown whether viral evasion of autophagy is important in disease pathogenesis. Here we show that the herpes simplex virus type 1 (HSV-1)-encoded neurovirulence protein ICP34.5 binds to the mammalian autophagy protein Beclin 1 and inhibits its autophagy function. A mutant HSV-1 virus lacking the Beclin 1-binding domain of ICP34.5 fails to inhibit autophagy in neurons and demonstrates impaired ability to cause lethal encephalitis in mice. The neurovirulence of this Beclin 1-binding mutant virus is restored in *pkr*$^{-/-}$ mice. Thus, ICP34.5-mediated antagonism of the autophagy function of Beclin 1 is essential for viral neurovirulence, and the antiviral signaling molecule PKR lies genetically upstream of Beclin 1 in host defense against HSV-1. Our findings suggest that autophagy inhibition is a novel molecular mechanism by which viruses evade innate immunity and cause fatal disease.

INTRODUCTION

Autophagy is an evolutionarily conserved process in which the cell packages cytosolic constituents in a double-membrane vesicle and delivers them to the lysosome for degradation (Levine and Klionsky, 2004). The digestion of intracellular contents by autophagy provides metabolic substrates during periods of starvation, contributes to tissue remodeling during differentiation and development, and removes protein aggregates and superfluous or damaged organelles. The dysregulation of autophagy may contribute to a number of diseases, including neurodegenerative disorders, aging, cancer, and infectious diseases (Shintani and Klionsky, 2004; Mizushima, 2005).

The first link between infection and autophagy, described in 1978, was the electron microscopic (EM) visualization of herpes simplex virus type 1 (HSV-1) and cytomegalovirus virions inside autophagosomes (Smith and de Harven, 1978). For decades thereafter, further evidence remained limited to EM observations of viruses and bacteria in autophagosome-like structures, colocalization of viruses and bacteria with endosomal/lysosomal and ER markers, or chemical manipulation of the autophagy pathway (Kirkegaard et al., 2004). More recently, the identification of evolutionarily conserved genes required for autophagy (Tsukada and Ohsumi, 1993, Thumm et al., 1994) has led to a growing body of molecular evidence indicating that cells deploy the autophagic machinery in defense against invading microorganisms (xenophagy) (Levine, 2005; Deretic, 2006; Schmid et al., 2006; Amano et al., 2006).

Xenophagy is important in innate immunity against viral infections (Kirkegaard et al., 2004; Seay et al., 2005; Levine, 2006). Neuronal overexpression of the mammalian autophagy protein Beclin 1 protects mice against lethal Sindbis virus encephalitis (Liang et al., 1998). In plants, the autophagy genes *BECLIN 1*, *ATG3*, and *ATG7* decrease viral replication and prevent the spread of programmed cell death during the tobacco mosaic virus-induced hypersensitive response (HR) (Liu et al., 2005). The antiviral, interferon-inducible PKR signaling pathway promotes autophagy in response to HSV-1 infection, and the HSV-1 neurovirulence protein ICP34.5 antagonizes this response (Tallóczy et al., 2002). These latter findings raise the possibilities that autophagy may also protect against HSV-1 infection and that HSV-1 ICP34.5-mediated blockade of autophagy may contribute to viral neurovirulence. However, the role of HSV-1 or other viral antagonism of autophagy in viral pathogenesis is not yet known.

We evaluated this question using a murine model of HSV-1 encephalitis. HSV-1, a 152 kb double-stranded DNA virus in the α-herpesvirus family, is an important human pathogen. It is the most common cause of sporadic encephalitis, with high rates of mortality and chronic neurological impairment in survivors (Tyler, 2004). The mouse model of HSV-1 encephalitis has provided important clues regarding the molecular determinants of HSV-1 neurologic disease. Most notably, Chou et al. first demonstrated that the virally encoded protein ICP34.5 is required for neurovirulence in mice (Chou et al., 1990). ICP34.5 is also required for neurologic disease in humans, since an ICP34.5-deleted virus can be used safely as an oncolytic agent to treat high-grade gliomas (Harrow et al., 2004).

ICP34.5 contains a GADD34 homology region (Chou and Roizman, 1994) that reverses eIF2α phosphorylation by recruiting protein phosphatase-1α (He et al., 1997). This observation has led to the proposal that ICP34.5 may function in neurovirulence by blocking eIF2α kinase signaling-dependent host translational arrest (Chou and Roizman, 1994). However, substitution of the corresponding domain from the murine homolog of GADD34 into ICP34.5 maintains the ability of HSV-1 to reverse eIF2α phosphorylation and prolong viral protein synthesis in vitro but results in a virus that is attenuated in vivo (He et al., 1996; Markovitz et al., 1997). Moreover, a second-site mutation in an ICP34.5-disrupted virus resulting in immediate-early expression of the US11 gene product restores the ability of the virus to reverse eIF2α phosphorylation and host-cell shutoff (Mulvey et al., 1999) but fails to restore neurovirulence (Mohr et al., 2001). Therefore, factors in addition to inhibition of host-cell translational shutoff likely contribute to ICP34.5-mediated neurovirulence.

In this study, we found that the HSV-1 ICP34.5 neurovirulence protein directly interacts with the mammalian autophagy protein Beclin 1. Beclin 1 was originally discovered in a yeast two-hybrid screen using Bcl-2 as a bait (Liang et al., 1998). Beclin 1 and its yeast ortholog, Atg6, are part of a class III PI3 kinase complex that recruits other autophagy proteins to the preautophagosomal membrane (Kihara et al., 2001a, 2001b). Orthologs of Beclin 1 regulate diverse homeostatic and developmental processes in model organisms (Levine and Klionsky, 2004). Beclin 1-mediated autophagy may also protect against different mammalian diseases, including Huntington's disease (Shibata et al., 2006; Jia et al., 2007), cancer (Liang et al., 1999; Qu et al., 2003; Yue et al., 2003; Degenhardt et al., 2006), and viral infections (Levine, 2006).

To investigate the functional significance of the HSV-1-ICP34.5/Beclin 1 interaction, we examined the ability of wild-type and Beclin 1-binding-deficient ICP34.5 mutants to antagonize Beclin 1-mediated autophagy in yeast and mammalian cells. Our results show that ICP34.5 can specifically antagonize Beclin 1-mediated autophagy and that the Beclin 1-binding domain, but not the GADD34 domain, is essential for this function. Furthermore, we show that a Beclin 1-binding-deficient ICP34.5 mutant virus is neuroattenuated in mice, suggesting that the ICP34.5/Beclin 1 interaction plays an important role in the pathogenesis of fatal HSV-1 encephalitis. The neurovirulence of this virus is restored in *pkr*$^{-/-}$ mice, providing genetic evidence for PKR-mediated autophagy in protection against HSV-1 disease. Our findings identify an as yet undefined mechanism of virulence: targeting of the autophagic machinery by a virally encoded protein.

RESULTS

HSV-1 ICP34.5 Inhibits Beclin 1-Dependent Autophagy in Yeast

In a yeast two-hybrid screen using HSV-1 ICP34.5 as a bait, one of the ICP34.5-interacting proteins identified was the mammalian autophagy protein Beclin 1 (B. Roizman, personal communication). Our laboratory confirmed that HSV-1 ICP34.5 interacts with human Beclin 1 in a yeast two-hybrid assay (Figure 1A). Unlike the interaction between Beclin 1 and cellular and viral Bcl-2 proteins (Pattingre et al., 2005; Liang et al., 2006), the N-terminal half of Beclin 1 is not sufficient for the interaction between Beclin 1 and ICP34.5. Full-length human Beclin 1, but not a truncation mutant encoded by nucleotides 1–708, binds to HSV-1 ICP34.5. Thus, the α-herpesvirus-encoded protein ICP34.5 binds to a region of Beclin 1 that is distinct from the region of Beclin 1 targeted by viral Bcl-2 proteins encoded by γ-herpesviruses.

Although mammalian Beclin 1 interacts with ICP34.5 in yeast, the yeast ortholog of Beclin 1, Atg6, does not interact with HSV-1 ICP34.5 (Figure 1A). Therefore, we used yeast disrupted of *ATG6* to examine the effects of ICP34.5 on Beclin 1-dependent autophagy. We measured autophagy by quantitative DIC microscopy of yeast following nitrogen starvation (Figures 1B and 1C). As reported previously (Liang et al., 1999; Melendez et al., 2003; Pattingre et al., 2005), human *beclin 1* transformation restores starvation-induced autophagy in autophagy-defective *atg6* null yeast. However, cotransformation of ICP34.5 with *beclin 1* abrogates the ability of Beclin 1 to rescue starvation-induced autophagy, decreasing levels to those observed in autophagy-deficient *atg6*Δ yeast (Figure 1B; $p < 0.0001$, Student's t test). ICP34.5 has no effect on the ability of *ATG6* transformation to rescue autophagy in *atg6*Δ yeast. Taken together, these results indicate that ICP34.5 is likely to inhibit autophagy by binding to Beclin 1.

ICP34.5 Inhibits Beclin 1-Dependent Autophagy in Mammalian Cells

Next, we sought to confirm the interaction between HSV-1 ICP34.5 and Beclin 1 in mammalian cells. In HEK293 cells transiently transfected with plasmids expressing Flag epitope-tagged Beclin 1 and HSV-1 ICP34.5, we found that Flag-Beclin 1 coimmunoprecipitated with ICP34.5 and that ICP34.5 coimmunoprecipitated with Flag-Beclin 1 (Figure 2A), indicating that Beclin 1 and ICP34.5 can interact in mammalian cells. To determine whether ICP34.5 does interact with endogenous Beclin 1 in virally infected cells, we performed coimmunoprecipitation studies of HSV-1-infected wild-type (*beclin 1*$^{+/+}$) embryonic stem

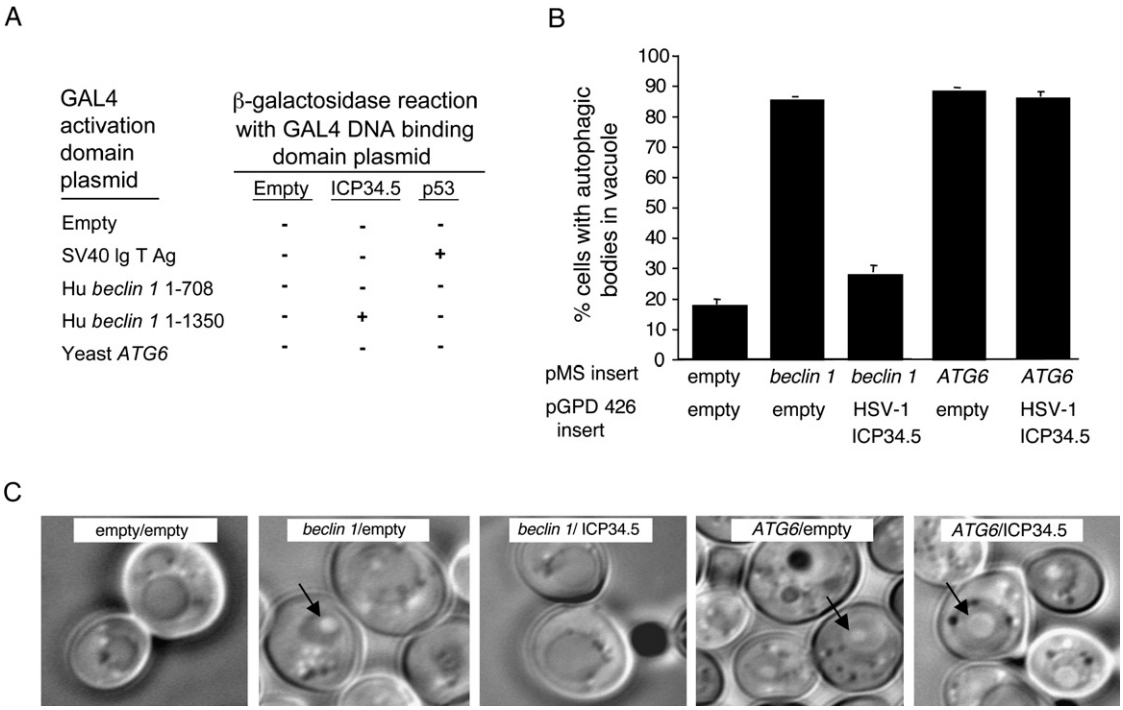

Figure 1. ICP34.5 Inhibits Beclin 1-Dependent Autophagy in Yeast

(A) Yeast two-hybrid interactions of ICP34.5 and Beclin 1. +, positive reaction within 8 hr; −, lack of positive reaction at 24 hr. Nucleotide position of genes fused to plasmid is indicated next to human *beclin 1* constructs.

(B) Quantitation of starvation-induced autophagy in *atg6*Δ yeast transformed with plasmids indicated below the x axis. Results represent mean ± SEM for triplicate samples. For each sample, a minimum of 100 cell profiles were analyzed, and cell profiles with one or more autophagosome within the vacuole were scored as positive. Similar results were obtained in five independent experiments.

(C) Representative DIC photomicrographs of *atg6*Δ yeast transformed with indicated plasmids following starvation for 4 hr. Arrows denote representative autophagosomes.

(ES) cells and HSV-1-infected ES cells containing a homozygous null mutation in *beclin 1* (*beclin 1*$^{-/-}$) (Figure 2B). We found that ICP34.5 coimmunoprecipitates with Beclin 1 in HSV-1-infected *beclin 1*$^{+/+}$ ES cells. No specific bands were observed in HSV-infected *beclin 1*$^{-/-}$ ES cells or in wild-type, *beclin 1*$^{+/+}$ ES cells infected with a previously characterized mutant strain of HSV-1 (17termA) (Bolovan et al., 1994) deleted of the entire ICP34.5 gene (Figure 2B). Thus, ICP34.5 interacts with endogenous Beclin 1 in virally infected mammalian cells.

To examine whether ICP34.5 antagonizes the autophagy function of Beclin 1 in mammalian cells, we used MCF7 human breast carcinoma cells stably transfected with human *beclin 1* (MCF7.*beclin 1* cells) or MCF7 cells stably transfected with empty vector (MCF7.control cells) (Liang et al., 2001). MCF7 cells express low levels of endogenous Beclin 1 and fail to increase autophagic activity in response to starvation unless Beclin 1 is ectopically expressed (Liang et al., 1999, 2001; Pattingre et al., 2005; Furuya et al., 2005). Therefore, we assessed the effects of HSV-1 ICP34.5 on the ability of *beclin 1* to rescue autophagy in MCF7 cells (Figures 2C and 2D).

To measure autophagy, we used the fluorescent autophagy marker GFP-LC3, which forms punctate dots upon proteolytic processing and lipidation during autophagy (Kabeya et al., 2000) (Figure 2D). Similar to previous reports, we found that MCF7.control cells fail to increase their autophagy activity in response to amino acid starvation, whereas MCF7.*beclin 1* cells undergo a significant increase in autophagic activity following starvation ($p = 0.003$ for MCF7.*beclin 1* cells in normal media versus starvation media, Student's t test) (Figure 2C). Transfection of an ICP34.5 expression plasmid significantly decreased starvation-induced autophagy in MCF7.*beclin 1* cells ($p = 0.008$, Student's t test) (Figure 2C). These data demonstrate that ICP34.5 can inhibit Beclin 1-dependent autophagy in mammalian cells.

Amino Acids 68–87 of ICP34.5 Are Required for Beclin 1 Binding and Inhibition of Beclin 1-Dependent Autophagy

Next, we performed a structure-function analysis to map the domain of ICP34.5 responsible for binding to Beclin 1 and inhibition of Beclin 1-dependent autophagy. To accomplish this, we performed coimmunoprecipitations of MCF7.*beclin 1* cells transfected with different myc-tagged ICP34.5 constructs and also assessed the ability of these ICP34.5 constructs to inhibit starvation-induced autophagy in MCF7.*beclin 1* cells.

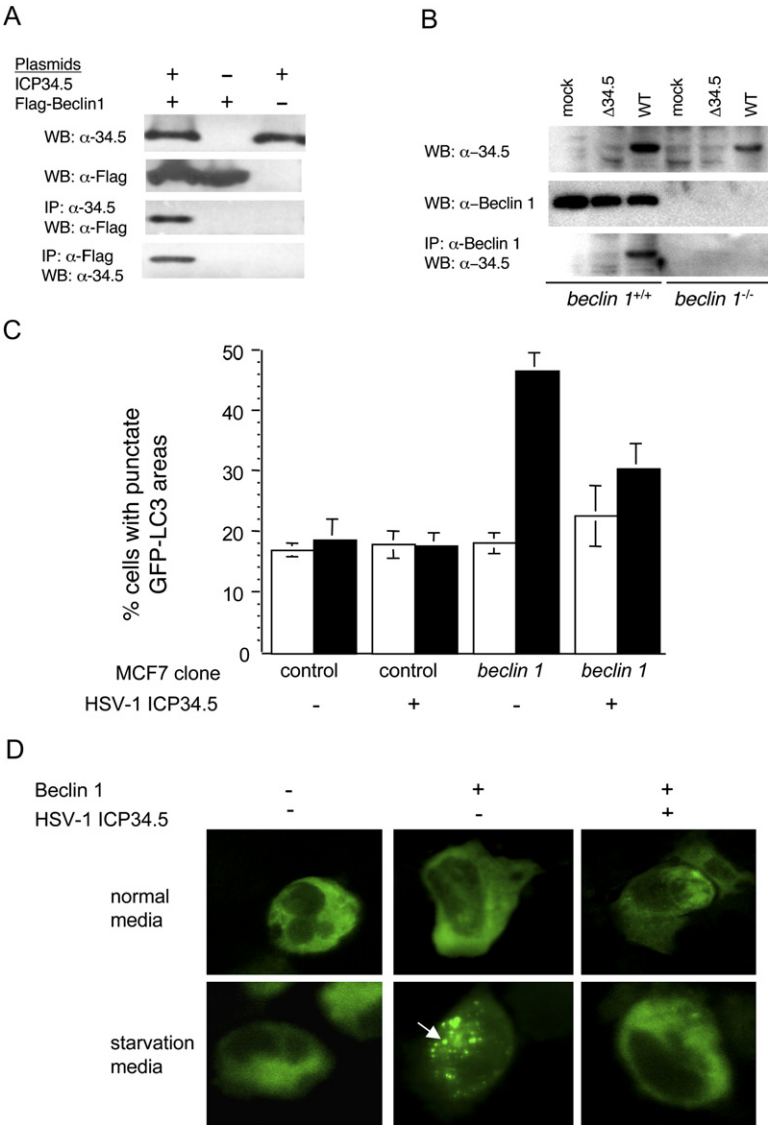

Figure 2. ICP34.5 Binds to Beclin 1 in Mammalian Cells and Inhibits Beclin 1-Mediated Autophagy

(A) Coimmunoprecipitation of Flag-tagged Beclin 1 with ICP34.5 in HEK293 cells transfected with the indicated plasmids.

(B) Coimmunoprecipitation of endogenous Beclin 1 with ICP34.5 in *beclin 1*$^{+/+}$ or *beclin 1*$^{-/-}$ mouse ES cells infected with the indicated virus.

(C) Quantitation of autophagy, as measured by GFP-LC3 punctations, in MCF7 cells transfected with plasmids expressing Beclin 1 and/or ICP34.5 during growth in normal media (open bars) or starvation media (filled bars). Results represent mean ± SEM for triplicate samples. For each sample, a minimum of 100 cells was analyzed. Similar results were obtained in five independent experiments.

(D) Representative photomicrographs of images used for quantitative analyses in (C). Arrow denotes representative punctate GFP-LC3 dot corresponding to an autophagosome.

ICP34.5 contains an N-terminal region, followed by a tripeptide repeat, and a C-terminal GADD34 homology domain (Figure 3A). Previous studies have shown that the GADD34 domain binds protein phosphatase-1α to dephosphorylate eIF2α and block eIF2α kinase signaling-dependent host-cell shutoff during HSV-1 infection (He et al., 1997). We found that wild-type ICP34.5 and ICP34.5 lacking the GADD34 domain (ICP34.5ΔGADD34) both immunoprecipitated with Flag-Beclin 1 in MCF7.*beclin 1* cells (Figure 3B). The lower levels of ICP34.5ΔGADD34 that coimmunoprecipitate with Beclin 1 are likely due to lower levels of expression of the ICP34.5ΔGADD34 protein (Figure 3B, see upper panel) rather than actual differences in binding affinity. Thus, the GADD34 domain of ICP34.5 that is required for antagonism of eIF2α phosphorylation is dispensable for Beclin 1 binding.

To further characterize the GADD34-independent interaction between ICP34.5 and Beclin 1, we constructed ICP34.5 mutants containing 20 amino acid deletions in the N-terminal half of the protein. Three ICP34.5 deletion mutants resulted in stable protein expression and could be used for further analyses, including mutants deleted of amino acids 48–67, 68–87, or 88–107 (herein referred to as ICP34.5Δ48–67, ICP34.5Δ68–87, and ICP34.5Δ88–107, respectively) (Figure 3B, and data not shown). Of these three deletion mutants, ICP34.5Δ48–67 and ICP34.5Δ88–107, but not ICP34.5Δ68–87, coimmunoprecipitated with Beclin 1 (Figure 3B, and data not shown). This indicates that deletion of the region spanning amino acids 68–87 (but not deletions of similar length in nearby flanking regions) abolishes the interaction between ICP34.5 and Beclin 1.

To evaluate the effect of ICP34.5 binding to Beclin 1 on Beclin 1-dependent, starvation-induced autophagy, we cotransfected MCF7.*beclin 1* cells with plasmids expressing HSV-1 ICP34.5 mutants and the autophagosome marker GFP-LC3 (Figure 3C). Consistent with the ability

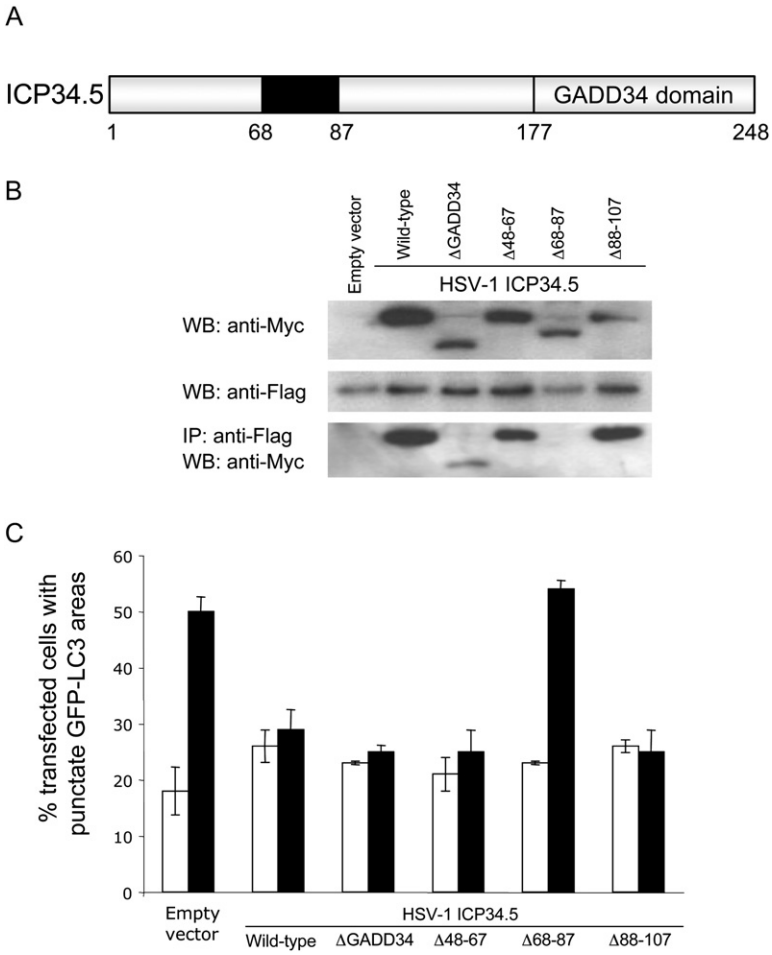

Figure 3. A Twenty-Amino-Acid Region of ICP34.5 Is Required for Beclin 1 Binding and Inhibition of Autophagy

(A) Schematic representation of ICP34.5 showing position of Beclin 1-binding region (amino acids 68–87) and GADD34 homology region.

(B) Coimmunoprecipitation of Myc-tagged wild-type or indicated mutant ICP34.5 and Flag-tagged Beclin 1 in MCF7.*beclin 1* cells.

(C) Quantitation of autophagy, as measured by GFP-LC3 punctate regions in MCF7.*beclin 1* cells transfected with the indicated HSV-1 ICP34.5 plasmids during growth in normal media (open bars) or starvation media (filled bars). Results represent mean ± SEM for triplicate samples. For each sample, a minimum of 100 cells was analyzed. Similar results were obtained in three independent experiments.

of ICP34.5ΔGADD34 to coimmunoprecipitate with Beclin 1 in MCF7.*beclin 1* cells, HSV-1 ICP34.5ΔGADD34 inhibits autophagy in these cells as effectively as wild-type ICP34.5 ($p = 0.3364$, Student's t test). Similarly, the 20 amino acid deletion mutants that retain the ability to interact with Beclin 1 (ICP34.5Δ48–67 and ICP34.5Δ88–107) also inhibit starvation-induced autophagy ($p = 0.4833$, Student's t test). In contrast, the mutant ICP34.5Δ68–87, which is unable to coimmunoprecipitate with Beclin 1, fails to inhibit starvation-induced autophagy in *MCF7.beclin 1* cells ($p = 0.0028$, Student's t test). This demonstrates that amino acids 68–87 are required not only for binding to Beclin 1 but also for inhibition of Beclin 1-dependent autophagy. The GADD34 domain of ICP34.5 is dispensable for this autophagy-inhibitory activity, suggesting that ICP34.5 can modulate host-cell functions through its interactions with Beclin 1 in a protein phosphatase-1α-independent manner.

Amino Acids 68–87 of ICP34.5 Are Not Required for Viral Growth In Vitro, Viral Blockade of eIF2α Phosphorylation, or Viral Blockade of Host-Cell Shutoff

To assess the functional significance of ICP34.5 inhibition of Beclin 1-mediated autophagy during viral infection, we constructed a mutant HSV-1 virus containing a deletion of amino acids 68–87 in ICP34.5 (referred to as HSV-1 34.5Δ68–87) and a marker rescue control (referred to as HSV-1 34.5Δ68–87R) (Figure S1 in the Supplemental Data available with this article online). HSV-1 34.5Δ68–87 expresses a protein of the predicted molecular weight (24.5 kDa) that reacts with a polyclonal anti-ICP34.5 antibody (Figure 4A). However, no ICP34.5Δ68–87 mutant protein coimmunoprecipitates with Beclin 1, indicating that deletion of amino acids 68–87 blocks the ability of ICP34.5 to bind to Beclin 1 in virally infected cells. The ICP34.5 protein expressed by the marker rescue virus HSV-1 34.5Δ68–87R coimmunoprecipitates with Beclin 1, confirming that the lack of interaction between ICP34.5Δ68–87 and Beclin 1 is not due to extragenic mutations.

In contrast to a mutant HSV-1 virus lacking the entire ICP34.5 gene (HSV-1 17termA), which displays a growth defect (Chou et al., 1990), HSV-1 34.5Δ68–87 replicates to the same levels as the wild-type marker rescue HSV-1 strain (HSV-1 34.5Δ68–87R) in human SK-N-SH neuroblastoma cells (Figure 4B). Previous studies have proposed that ICP34.5 is required for growth in SK-N-SH cells because of its ability to block virus-induced host-cell shutoff by dephosphorylating eIF2α. The mapping of this

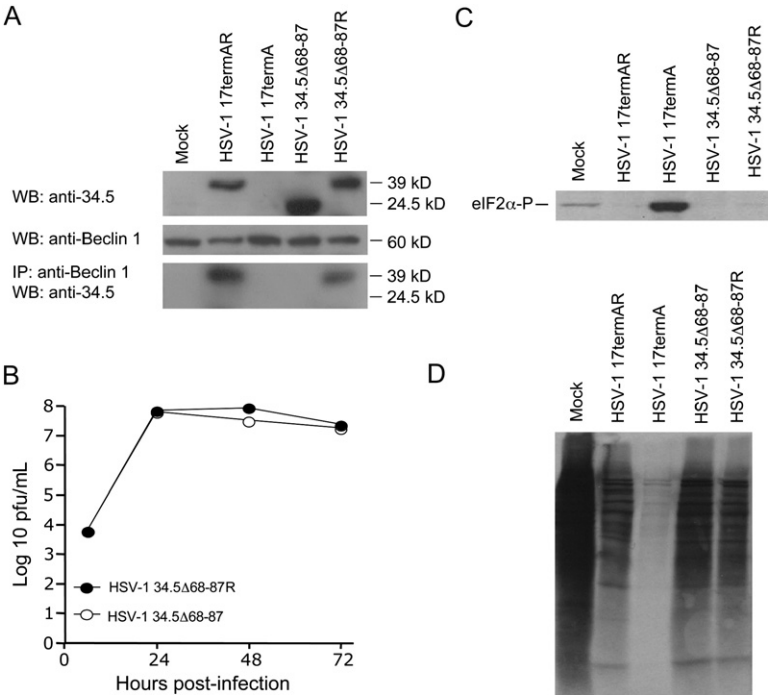

Figure 4. The Beclin 1-Binding Domain of ICP34.5 Is Dispensable for ICP34.5-Mediated Blockade of Host-Cell Shutoff

(A) Coimmunoprecipitation of endogenous Beclin 1 with ICP34.5 in SK-N-SH cells infected with HSV-1 ΔICP34.5 (17termA) or its marker rescue virus (17termAR), or HSV-1 34.5Δ68–87 or its marker rescue (HSV-1 34.5Δ68–87R).

(B) Viral replication of HSV-1 34.5Δ68–87 and HSV-1 34.5Δ68–87R in SK-N-SH neuroblastoma cells. Data shown represent mean ± SEM geometric titer.

(C) Western blot detection of the serine 51 phosphorylated form of eIF2α in SK-N-SH neuroblastoma cells 16 hr after infection with the indicated virus.

(D) ^{35}S-labeled cellular proteins in SK-N-SH cells 16 hr after infection with the indicated virus.

function of ICP34.5 to the GADD34 domain (which is not required for Beclin 1 binding), together with the wild-type levels of viral growth in HSV-1 34.5Δ68–87-infected SK-N-SH cells, suggested that HSV-1 34.5Δ68–87 should behave similarly to wild-type HSV-1 with respect to blockade of eIF2α phosphorylation and host-cell shutoff. Indeed, we found that HSV-1 34.5Δ68–87 blocked eIF2α serine 51 phosphorylation as effectively as its marker rescue control virus (HSV-1 34.5Δ68–87R) whereas significant eIF2α serine 51 phosphorylation was observed in SK-N-SH cells infected with HSV-1 17termA (Figure 4C). Furthermore, this blockade of eIF2α phosphorylation correlated with the ability of HSV-1 34.5Δ68–87 to maintain protein synthesis in virally infected SK-N-SH cells at levels similar to those observed in cells infected with wild-type marker rescue viruses (e.g., HSV-1 17termAR [Bolovan et al., 1994] or HSV-1 34.5Δ68–87R) in contrast to the marked host-cell shutoff observed in cells infected with HSV-1 17termA (Figure 4D). Together, these results demonstrate that amino acids 68–87 of ICP34.5 are dispensable for productive viral replication and inhibition of eIF2α phosphorylation and host-cell shutoff in SK-N-SH cells.

The Beclin 1-Binding-Deficient ICP34.5 Mutant Virus Is Defective in Autophagy Inhibition in Neurons

To evaluate whether HSV-1 34.5Δ68–87 can inhibit autophagy, we performed EM analyses of primary sympathetic neurons infected with HSV-1 34.5Δ68–87, HSV-1 34.5Δ68–87R, and HSV-1 17termA. We chose to use neurons because they are a natural target for HSV-1 infection in vivo, and previously we showed that HSV-1 lacking the entire ICP34.5 gene (HSV-1 17termA), but not wild-type HSV-1, induces autophagy in primary sympathetic neurons (Tallóczy et al., 2006). We found that HSV-1 34.5Δ68–87R-infected neurons (Figure 5A, upper right panel) exhibit levels of autophagy indistinguishable from those of mock-infected neurons (Figure 5A, upper left panel) (Figure 5B). In contrast, neurons infected with either the full ICP34.5 deletion mutant virus (HSV-1 17termA; Figure 5A, lower left panel) or the Beclin 1-binding-deficient ICP34.5 deletion mutant virus (HSV-1 34.5Δ68–87; Figure 5A, lower right panel) have significantly higher levels of autophagosome accumulation ($p < 0.0001$ for both mutants versus HSV-1 34.5Δ68–87R, Student's t test) (Figure 5B). These results, together with our results in neuroblastoma cells, demonstrate that ICP34.5 binds Beclin 1 and inhibits virus-induced autophagy in neurons and that this activity is independent from its role in antagonizing host-cell shutoff.

The Beclin 1-Binding-Deficient ICP34.5 Mutant Virus Is Neuroattenuated In Vivo

Our data with HSV-1 34.5Δ68–87 indicate that the Beclin 1-binding region of ICP34.5 is necessary for autophagy inhibition but not for ICP34.5-mediated blockade of host-cell translational arrest. To evaluate the significance of ICP34.5 antagonism of Beclin 1 function in viral neuropathogenesis, we compared the mortality of C57BL/6J mice infected intracerebrally with 5×10^5 pfu of either HSV-1 34.5Δ68–87 or HSV-1 34.5Δ68–87R (Figure 6A). Nearly 80% of mice succumbed to lethal HSV-1 34.5Δ68–87R infection within 10 days, whereas only 15% of mice infected with HSV-1 34.5Δ68–87 died within a 21 day observation period ($p < 0.0001$, log-rank test).

Consistent with reduced mortality, we observed a striking defect in viral replication in the brains of mice infected with HSV-1 34.5Δ68–87 (Figure 6B). Viral titers were similar in the brains of mice infected with HSV-1 34.5Δ68–87

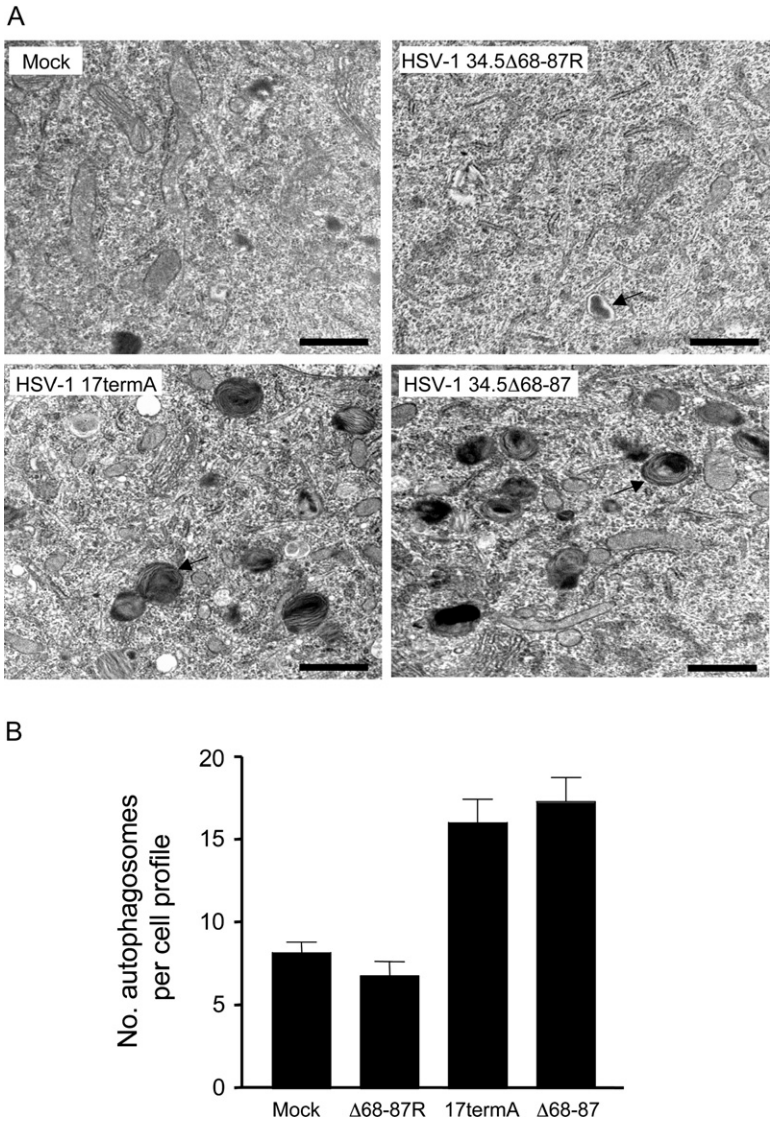

Figure 5. The Beclin 1-Binding Domain of ICP34.5 Is Required for Inhibition of Autophagy in Neurons

(A) Representative electron micrographs of primary sympathetic neurons infected with the indicated virus. Arrows denote representative autophagosomes that would be scored as positive in (B). Scale bars, 1 μm.

(B) Quantitation of the number of autophagosomes per cell profile in primary sympathetic neurons infected with the indicated virus. Results shown represent mean value ± SEM for 50 cells per experimental condition.

and HSV-1 34.5Δ68–87R at day 1 after infection. However, levels of infectious virus declined below the limit of detection within 5 days after infection in the brains of mice infected with HSV-1 34.5Δ68–87. In contrast, significant levels of infectious virus were recovered in the brains of mice infected with HSV-1 34.5Δ68–87R for at least 5 days, after which time the majority of mice succumbed to lethal disease.

Histopathological analyses of the brains of mice at days 1, 3, and 5 after infection revealed leptomeningeal, perivascular, and parenchymal inflammation (especially in the basal ganglia, brainstem, and hippocampus) in mice infected with both the HSV-1 34.5Δ68–87 and HSV-1 34.5Δ68–87R viruses, but the degree of parenchymal inflammation was more severe in mice infected with HSV-1 34.5Δ68–87R (Figure 6C, left panels, and data not shown). Very few HSV-1 immunoreactive neurons were observed in the brains of HSV-1 34.5Δ68–87-infected mice, whereas large regions of HSV-1 immunoreactive neurons were observed in the brains of HSV-1 34.5Δ68–87R-infected mice (Figure 6C, right panels). Furthermore, in HSV-1 34.5Δ68–87R-infected brains, there were numerous neurons with pyknotic nuclei and eosinophilic cytoplasm, whereas neuronal pathology was rarely observed in HSV-1 34.5Δ68–87-infected mice (Figure 6C, left panels). Thus, the brains of mice infected with HSV-1 34.5Δ68–87R demonstrate significantly more neuropathology than the brains of mice infected with HSV-1 34.5Δ68–87. Taken together, the mortality studies, CNS viral replication studies, and CNS histopathological analyses demonstrate that the Beclin 1-binding-deficient mutant virus is highly neuroattenuated in vivo.

Restoration of Neurovirulence of the Beclin 1-Binding-Deficient ICP34.5 Mutant Virus in Mice with a Homozygous Deletion in *pkr*

Previously, we have shown that PKR signaling is required for autophagy induction and autophagy-dependent virion

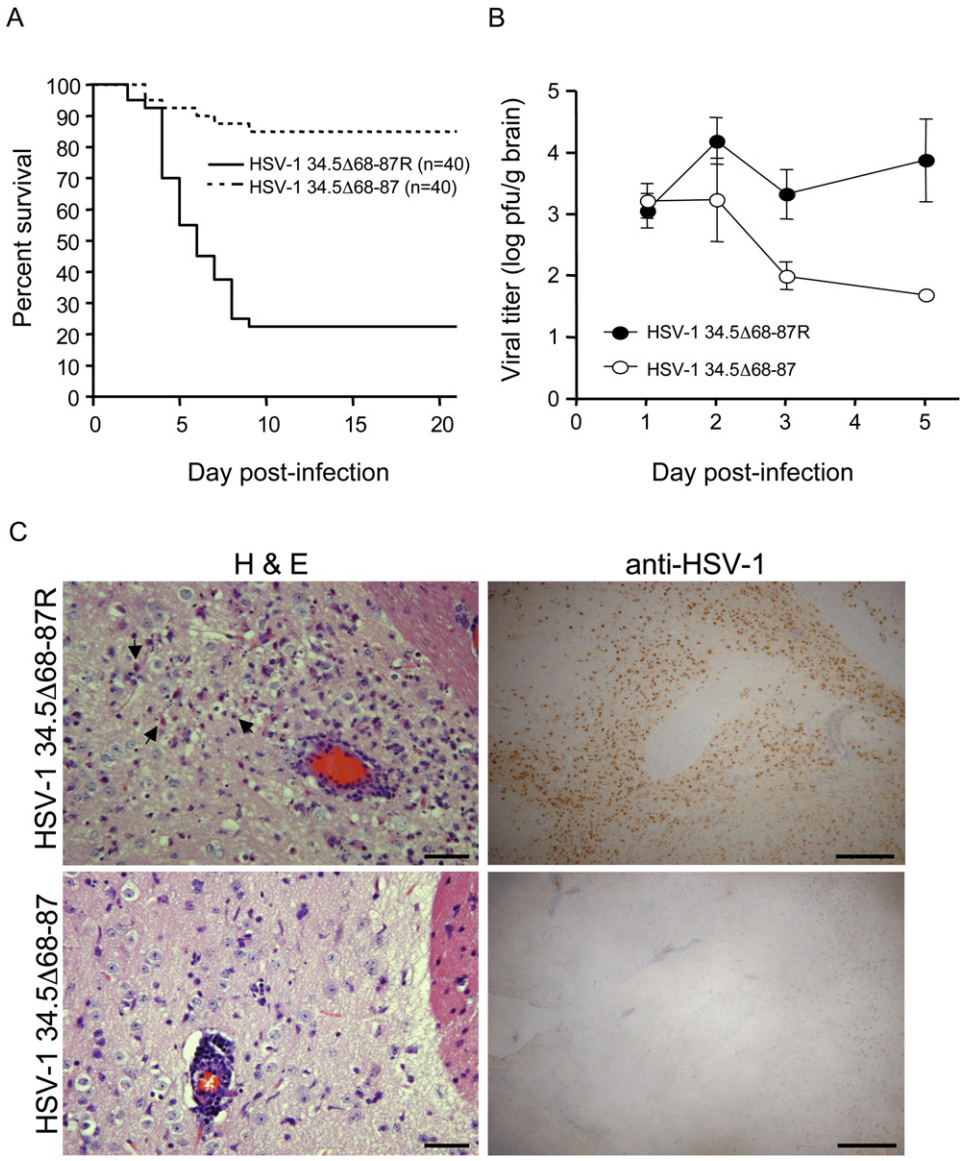

Figure 6. An HSV-1 Recombinant Virus Containing a Mutation in ICP34.5 that Abrogates Binding to Beclin 1 Is Neuroattenuated In Vivo

(A) Survival of C57BL/6J mice infected intracerebrally with 5×10^5 pfu of either HSV-1 34.5Δ68–87 or its marker rescue (HSV-1 34.5Δ68–87R). Results shown represent survival data combined from four independent infections. Similar results were observed in each experiment.

(B) Viral replication of HSV-1 34.5Δ68–87 and HSV-1 34.5Δ68–87R in brain tissue of infected mice at indicated time after infection. Lower limit of detection = 1.7. Data shown represent mean ± SEM geometric titer for seven to ten mice per experimental group per time point.

(C) Representative images of H&E staining (left panels) and HSV-1 antigen staining (right panels) in basal ganglia from mice infected with HSV-1 34.5Δ68–87R (upper panels) or HSV-1 34.5Δ68–87 (bottom panels) on day 5 postinfection. Arrows in upper left panel indicate eosinophilic, necrotic neurons with pyknotic nuclei. Scale bars, 50 μm in left panels and 200 μm in right panels.

degradation in murine embryonic fibroblasts (MEFs) and sympathetic neurons (Tallóczy et al., 2002, 2006). These findings raise the possibility that PKR signaling may lie genetically upstream of Beclin 1-dependent autophagy in HSV-1 antiviral host defense. To investigate this possibility, we evaluated whether the neurovirulence of the Beclin 1-binding ICP34.5 mutant virus is restored in 129 Ev/Sv mice containing a null mutation in *pkr* (herein referred to as $pkr^{-/-}$ mice).

Consistent with previously described mouse strain differences in susceptibility to HSV-1 infection (Kirchner et al., 1978), we found that 129 Ev/Sv mice are more susceptible to fatal HSV-1 infection than C57BL/6J mice (Figure 7A). However, similar to our findings in C57BL/6J mice, the HSV-1 34.5Δ68–87 mutant virus also results in significantly less mortality in wild-type 129 Ev/Sv mice as compared to the marker rescue control virus (Figure 7A; $p < 0.0001$, log rank test). In contrast, in $pkr^{-/-}$ mice, the

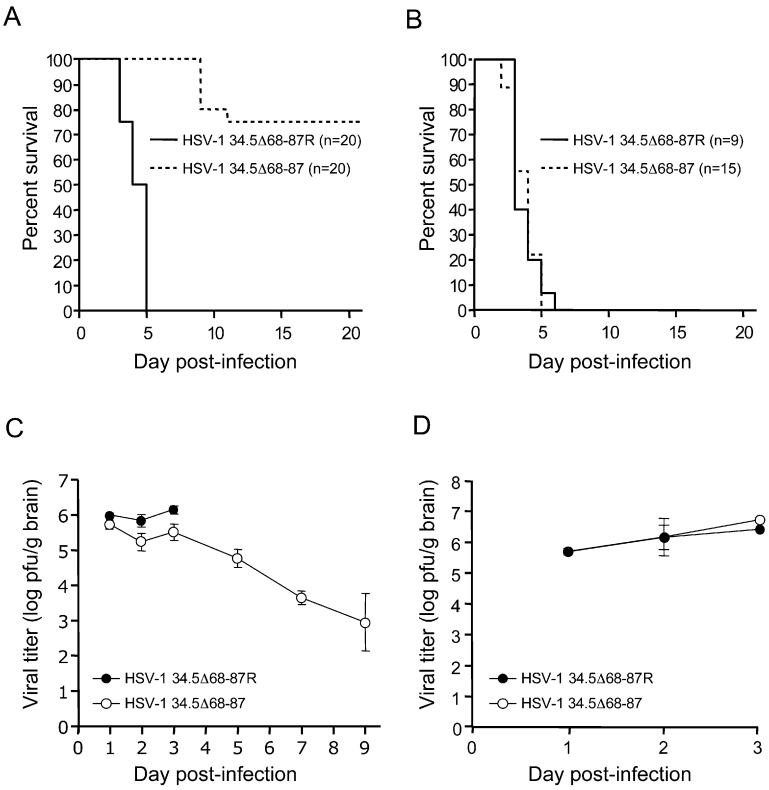

Figure 7. Restoration of Neurovirulence of a Beclin 1-Binding-Deficient Virus in *pkr*$^{-/-}$ Mice

(A) Survival of wild-type 129 Ev/Sv mice infected intracerebrally with 1 × 10^5 pfu of either HSV-1 34.5Δ68–87 or its marker rescue (HSV-1 34.5Δ68–87R). (B) Survival of 129 Ev/Sv *pkr*$^{-/-}$ mice infected intracerebrally with 1 × 10^5 pfu of either HSV-1 34.5Δ68–87 or its marker rescue (HSV-1 34.5Δ68–87R). (A and B) Results shown represent survival data combined from two to three independent infections. Similar results were observed in each experiment. (C) Viral replication of HSV-1 34.5Δ68–87 and HSV-1 34.5Δ68–87R in brain tissue of infected 129 Ev/Sv mice at indicated time after infection. (D) Viral replication of HSV-1 34.5Δ68–87 and HSV-1 34.5Δ68–87R in brain tissue of infected 129 Ev/Sv *pkr*$^{-/-}$ mice at indicated time after infection. For (C) and (D), data shown represent mean ± SEM geometric titer for three to five mice per experimental group per time point.

mortality of mice infected with HSV-1 34.5Δ68–87 was as high as the mortality of mice infected with HSV-1 34.5Δ68–87R (Figure 7B). Furthermore, in wild-type mice, HSV-1 34.5Δ68–87 replication in brain is significantly lower than HSV-1 34.5Δ68–87R replication (and HSV-1 34.5Δ68–87 infectious virus is gradually cleared) (Figure 7C), whereas in *pkr*$^{-/-}$ mice, HSV-1 34.5Δ68–87 replicates in brain to levels similar to those observed during infection with HSV-1 34.5Δ68–87R (Figure 7D). Together, these findings demonstrate that *pkr* deletion in vivo restores the virulence of the Beclin 1-binding-deficient ICP34.5 mutant virus. These findings suggest that PKR induction of Beclin 1-dependent autophagy is important for protection against HSV-1 encephalitis.

DISCUSSION

Here we provide evidence that an essential HSV-1 neurovirulence factor, ICP34.5, confers pathogenicity by binding to the mammalian autophagy protein Beclin 1 and antagonizing the host autophagy response. To the best of our knowledge, these findings represent the first description of a microbial virulence factor directly antagonizing the host autophagy machinery to elicit disease. Previous studies have demonstrated that certain bacterial and viral gene products can antagonize host autophagy in vitro. During *Shigella* infection, the bacterial encoded virulence factor *IcsB* blocks the induction of autophagy by *VirG* (Ogawa et al., 2005). In addition, viral Bcl-2 proteins encoded by the oncogenic γ-herpesviruses block autophagy induction by binding to Beclin 1 (Pattingre et al., 2005; Liang et al., 2006). However, in these examples, the significance of microbial antagonism of host autophagy in disease pathogenesis is not yet known. Our finding that the Beclin 1-binding domain of the HSV-1-encoded neurovirulence protein ICP34.5 is essential for lethal HSV-1 encephalitis demonstrates the importance of microbial evasion of autophagy in disease pathogenesis.

The requirement for HSV-1-mediated inhibition of autophagy in the pathogenesis of viral encephalitis provides strong evidence that autophagy is an important mechanism of innate immunity in vivo. Several studies have shown that autophagy genes restrict intracellular bacterial growth in cultured cells (Levine, 2005; Deretic, 2006; Amano et al., 2006); however, the role of autophagy in host defense against intracellular bacterial infections in vivo is not yet known. A previous study showed that enforced neuronal expression of Beclin 1 decreases Sindbis virus CNS replication, decreases Sindbis virus-induced neuronal apoptosis, and protects mice against lethal Sindbis virus encephalitis (Liang et al., 1998), raising the possibility that Beclin 1-dependent autophagy may play a role in innate antiviral immunity. In this study, we demonstrate that the Beclin 1-binding and autophagy-inhibitory domain of HSV-1 ICP34.5 is essential for neurological disease. This observation suggests that autophagy is an important mechanism of innate immunity that must be successfully countered for certain viruses to be pathogenic.

As a corollary, viral evasion of autophagy likely represents an important strategy that viruses use to outsmart

host antiviral defense. Previous studies have shown that HSV-1 ICP34.5 is required for neurovirulence (Chou et al., 1990; Harrow et al., 2004), that ICP34.5 blocks PKR-dependent autophagy (Tallóczy et al., 2002, 2006), and that blockade of PKR-dependent functions in vivo is essential for HSV-1 neurovirulence (Leib et al., 2000). However, since PKR activation also results in translational arrest in virally infected cells, the significance of the autophagy-inhibitory effects of ICP34.5 in viral virulence has been unclear. Our studies permitted us to genetically dissect the role of ICP34.5-mediated inhibition of autophagy in viral virulence from ICP34.5-mediated antagonism of other PKR-dependent functions by constructing a recombinant mutant virus that retains its GADD34 domain and ability to block PKR-dependent translational arrest but is defective in Beclin 1 binding and inhibition of autophagy in virally infected neurons. This mutant virus is highly neuroattenuated in vivo, suggesting that ICP34.5-mediated blockade of host-cell shutoff is not sufficient to confer neurovirulence but rather that ICP34.5-mediated blockade of Beclin 1-dependent autophagy is required for neurovirulence. Moreover, our findings in mice lacking *pkr*$^{-/-}$, demonstrating restoration of neurovirulence of a mutant strain of HSV-1 that is specifically impaired in Beclin 1-binding and autophagy-inhibitory activity, indicate that PKR lies genetically upstream of Beclin 1 in antiviral host defense in vivo. Since PKR is targeted by virulence factors encoded by many different viruses, including other medically important pathogens such as hepatitis C virus and influenza virus (Katze et al., 2002), it will be of interest to determine the role of autophagy evasion in the pathogenesis of diseases caused by such viruses.

One important question that arises is why ICP34.5 possesses two separate mechanisms for blocking host-cell autophagy, including blockade of PKR-dependent signaling and blockade of Beclin 1 function. Although we have previously shown that cells require *pkr* and the serine 51 phosphorylation site of eIF2α to undergo virus-induced autophagy (Tallóczy et al., 2002), it is possible that very low levels of phosphorylated eIF2α are sufficient to trigger autophagy in HSV-1-infected wild-type cells. If so, successful inhibition of autophagy may require a second mechanism, such as blocking a downstream autophagy effector protein. Indeed, we found that the GADD34 domain of ICP34.5, which is sufficient to antagonize PKR-dependent translational arrest, is not required to block autophagy in mammalian cells, whereas the Beclin 1-binding domain of ICP34.5 is required for autophagy inhibition. Thus, antagonism of PKR signaling, in the absence of antagonism of Beclin 1 function, is not sufficient to block host-cell autophagy (even though PKR and eIF2α serine 51 phosphorylation are required for autophagy induction).

The mechanism by which ICP34.5 inhibits Beclin 1-dependent autophagy is not yet known. Two major lines of evidence suggest that the binding of ICP34.5, either directly or indirectly, to Beclin 1 is required for its autophagy-inhibitory function. First, ICP34.5 fails to interact with the yeast ortholog Atg6 and has no inhibitory effect on the ability of *ATG6* transformation to rescue autophagy in *atg6* null yeast. In contrast, ICP34.5 binds to Beclin 1 in yeast and blocks the ability of *beclin 1* to rescue autophagy in *atg6* null yeast. Second, in mammalian cells, we observed a direct correlation between the ability of different mutants of ICP34.5 to coimmunoprecipitate with Beclin 1 and the ability to inhibit Beclin 1-dependent autophagy. Interestingly, the domain of Beclin 1 required for interacting with ICP34.5 appears to be distinct from that involved in binding to cellular and viral Bcl-2-like proteins or in binding to the class III PI3 kinase Vps34 (Liang et al., 1999; Pattingre et al., 2005; Furuya et al., 2005; and data not shown). Therefore, it is unlikely that ICP34.5 directly competes with Vps34 for binding to Beclin 1. Moreover, the lack of any structural similarity between HSV-1 ICP34.5 and γ-herpesvirus-encoded Bcl-2 proteins, coupled with the lack of conservation in regions of Beclin 1 required for binding to these proteins, indicates that different families of herpesviruses may have evolved diverse strategies to antagonize Beclin 1 activity in virally infected cells. The utilization of diverse strategies to target the same host autophagy protein by different virus families underscores the likely importance of Beclin 1 antagonism in viral pathogenesis and the likely importance of Beclin 1-dependent autophagy in antiviral host defense.

Beclin 1-dependent autophagy may function in antiviral host defense by several different mechanisms. There is now increasing evidence that cytoplasmic bacteria are targeted for lysosomal degradation by an autophagy gene-dependent pathway (xenophagy) (Levine, 2005; Amano et al., 2006), and it seems likely that a similar pathway is involved in the degradation of intracytoplasmic virions. Indeed, we previously found that HSV-1 virions are degraded inside autophagosomes in MEFs and in primary cultured neurons (Tallóczy et al., 2006). Based upon our CNS replication studies with the Beclin 1-binding-deficient ICP34.5 mutant virus, we speculate that xenophagy may also function to restrict HSV-1 replication in virally infected neurons in vivo. Autophagy may also play a direct role in promoting neuronal survival during viral infection. In support of this hypothesis, autophagy genes protect against programmed cell death in plant cells infected with tobacco mosaic virus (Liu et al., 2005), in mouse neurons infected with Sindbis virus (Liang et al., 1999), and in neurons subjected to noninfectious forms of cellular stress (Levine and Yuan, 2005).

It is interesting to note that basal autophagy in the mouse nervous system is critical to ensure protein quality control and the prevention of neurodegenerative diseases. Conditional deletion of either *atg5* or *atg7* in the central nervous system results in progressive accumulation of intraneuronal inclusion bodies, leading to neurodegeneration and motor deficits (Hara et al., 2006; Komatsu et al., 2006). Accordingly, it is possible that ICP34.5-mediated antagonism of autophagy may not only promote viral replication, increase neuronal death, and increase animal mortality during acute HSV-1 encephalitis, but also contribute to chronic cellular dysfunction in the neurons of survivors.

In conclusion, we have described a novel pathogen/host interaction that is required to elicit fatal neurological disease. An essential function of the virulence factor HSV-1 ICP34.5 is to target the host autophagy machinery component Beclin 1. Genetic disruption of PKR, an autophagy-inducing signaling molecule, completely restores the neurovirulence of an autophagy-inhibitory-defective mutant virus. These findings provide evidence that autophagy plays an important role in protection against viral infection and that successful viral evasion of autophagy plays a key role in disease pathogenesis.

EXPERIMENTAL PROCEDURES

Yeast Strains, Expression Vectors, and Assays

The *atg6*-disruped *S. cerevisiae* strain JCY3000 and wild-type strain SFY526 have been previously described (Seaman et al., 1997; Liang et al., 1998). For yeast two-hybrid studies, previously described plasmids were used, including full-length human *beclin 1* (1–1350 bp), a C-terminal truncation mutant of human *beclin 1* (1–708 bp), or yeast *ATG6* cloned into the GAL4 activation domain plasmid pGAD424 (Liang et al., 1998, 1999). The full-length open reading frame of HSV-1 strain F ICP34.5 cloned into pGBT9 β-galactosidase domain plasmid was provided by Bernard Roizman. Yeast two-hybrid analyses of these plasmids was performed in SFY526 cells as described (Liang et al., 1998). For autophagy studies, yeast expression vector constructs included empty vector pMS424, pMS424 encoding human *beclin 1* (Liang et al., 1999), pMS424 encoding *S. cerevisiae ATG6* (Seaman et al., 1997), empty vector pGPD426, and pGPD426 encoding HSV-1 strain 17 ICP34.5. Yeast autophagy was measured in JCY3000 cells during nitrogen starvation conditions by quantitative DIC microscopy as previously described (Liang et al., 1999, Tallóczy et al., 2002).

Mammalian Cell Lines

HEK293, MCF7, and SK-N-SH cell lines were obtained from the American Type Culture Collection (ATCC) and maintained according to ATCC instructions. The construction and maintenance of MCF7 cell lines stably transfected with tetracycline-repressible Flag-*beclin 1* has been previously described (Liang et al., 2001). Mouse *beclin 1*$^{-/-}$ and *beclin 1*$^{+/+}$ ES cells were provided by Nathaniel Heintz and cultured as described (Yue et al., 2003). ES cells were cultured without MEF feeder layers before experiments to ensure homogenous ES cell populations. Primary sympathetic neuron cultures were prepared from superior cervical ganglia of postnatal day 2 129 Ev/Sv mice using a modification of a previously described protocol (Easton et al., 1997).

Virus Strains

The HSV-1 ICP34.5 deletion mutant (17termA) and its marker-rescued virus (17termAR) were made in the background of strain 17 of HSV-1 and have been previously described (Bolovan et al., 1994; Leib et al., 2000). To construct an HSV-1 virus lacking the nucleotides encoding amino acids 68–87 of HSV-1 (termed HSV-1 ICP34.5Δ68–87) and its marker rescue control (HSV-1 ICP34.5Δ68–87R), we used our previously published BAC method (Gierasch et al., 2006). Please refer to Figure S1 for a schematic diagram and to the Supplemental Experimental Procedures for details of the construction of these viruses.

Viral Growth Curves

Viral growth in SK-N-SH neuroblastoma cells was measured during infection with HSV-1 34.5Δ68–87 or HSV-1 34.5Δ68–87R at an MOI of 0.01 pfu/cell by performing plaque assay titration of freeze-thawed lysates on Vero cells. For in vivo viral replication studies, mice were sacrificed at the indicated time points after infection, and frozen brain tissue homogenates were used for plaque assay titration on Vero cells.

Coimmunoprecipitation and Western Blot Analyses

For coimmunoprecipitation studies, HEK293 cells were cotransfected with pCR3.1 plasmids expressing N-terminal Flag epitope-tagged Beclin 1 and ICP34.5, and MCF7.*beclin 1* cells were transfected with C-terminal Myc-tagged HSV-1 strain 17 ICP34.5 full-length or deletion mutants using Lipofectamine 2000 (Invitrogen) according to the manufacturer's instructions. Coimmunoprecipitation of virally expressed ICP34.5 and endogenous Beclin 1 was performed on SK-N-SH and ES cells infected with the indicated virus at an MOI of 5. Beclin 1 was immunoprecipitated and detected in Western blot analyses using either anti-Flag (HEK293 cells, MCF7.*beclin 1* cells) (Sigma F3165; 1:100 dilution) or anti-Beclin 1 (Novus Biologicals or Santa Cruz; 1:100 dilution), and ICP34.5 was detected in cell lysates and coimmunoprecipitates using either anti-Myc (MCF7.*beclin 1* cells) (Novus ab9106; 1:10,000 dilution) or a rabbit polyclonal anti-ICP34.5 antibody raised against GST-purified N-terminal 69 amino acids of the Patton strain 34.5 protein (HEK293 cells, ES cells, SK-N-SH cells) (generously provided by I. Mohr; 1:1000 dilution). EIF2α phosphorylation in SK-N-SH was detected by Western blot analysis as described previously (Tallóczy et al., 2002) using anti-phospho-specific eIF2α Ab (1:100 dilution) (Research Genetics). Please refer to the Supplemental Experimental Procedures for details of lysis conditions for coimmunoprecipitation experiments.

Mammalian Cell Autophagy Assays

Quantitative GFP-LC3 light microscopy autophagy assays were performed in MCF7.*beclin 1* cells cotransfected with a GFP-LC3-expressing plasmid, pEGFP-C1 (Kabeya et al., 2000), and a pCR3.1 construct expressing full-length or deletion mutants of C-terminal Myc-tagged HSV-1 strain 17 ICP34.5 as described (Pattingre et al., 2005). Quantitative EM autophagy assays were performed as previously described (Tallóczy et al., 2002) in primary sympathetic neurons pretreated with 100 IU/ml recombinant mouse IFN-α (Sigma) for 18 hr, infected with HSV-1 17termA, HSV-1 34.5Δ68–87, or HSV-1 34.5Δ68–87R at an MOI of 5, and fixed 24 hr after infection.

Host-Cell Shutoff Assays

Host-cell shutoff assays were performed as previously described (Chou and Roizman, 1992), using SK-N-SH cells infected at an MOI of 5 and incubated at 16 hr after infection with [^{35}S]methionine (specific activity 1175 Ci/mmol; 1Ci = 43.5 TBq; MP Biomedicals, Inc) for 1.5 hr in media lacking methionine.

Animal Experiments

Four- to eight-week-old C57BL/6J mice (Jackson Laboratory), and *pkr*$^{-/-}$ or wild-type 129 Ev/Sv backcrossed control mice (Leib et al., 2000) of either sex were used in all studies. For HSV-1 encephalitis mortality studies, mice were anesthetized, injected intracerebrally with 1–5 × 10^5 pfu of virus in 30 μl HBSS, and followed daily for 3 weeks for survival. All animal procedures were performed in accordance with Institutional Animal Use and Care Committee policies.

Histopathological Analyses

At serial time points after infection, mice were euthanized, and the left cerebral hemispheres were fixed by immersion in 4% paraformaldehyde. Serial paraffin-embedded sections were stained with H&E and subjected to immunohistochemical analysis using a rabbit polyclonal antibody to HSV-1 (1:6000 dilution) in conjunction with a MACH 4 Universal HRP-polymer detection system (Dako).

Supplemental Data

The Supplemental Data include Supplemental Experimental Procedures and one supplemental figure and can be found with this article online at http://www.cellhostandmicrobe.com/cgi/content/full/1/1/23/DC1/.

ACKNOWLEDGMENTS

This work was supported by NIH grants RO1 AI051367 (B.L.), T32 AI007520 (A.O.), RO1 EY09083 (D.A.L.), and T32 EY13360-06 (D.A.); an Ellison Medical Foundation Senior Scholars Award in Infectious Diseases (B.L., A.O.); a Lew Wasserman Scholarship from Research to Prevent Blindness (D.A.L.); and core grants to the Department of Ophthalmology from the NIH (P30-EY02687) and Research to Prevent Blindness (D.A.L.). We thank Bernard Roizman for sharing unpublished data and reagents; Luis Parada, Bin He, and Sangita Sinha for helpful advice; Ian Mohr and Richard Thompson for providing antibodies and virus strains; Kristy Brown for assistance with electron microscopy; Yajuan Liu and Zhongju Zou for excellent technical assistance; and Frederick Scott and Renee Talley for administrative assistance.

Received: November 6, 2006
Revised: December 4, 2006
Accepted: December 15, 2006
Published: March 14, 2007

REFERENCES

Amano, A., Nakagawa, I., and Yoshimori, T. (2006). Autophagy in innate immunity against intracellular bacteria. J. Biochem. (Tokyo) *140*, 161–166.

Bolovan, C.A., Sawtell, N.M., and Thompson, R.L. (1994). ICP34.5 mutants of herpes simplex virus type 1 strain 17syn+ are attenuated for neurovirulence in mice and for replication in confluent primary mouse embryo cell cultures. J. Virol. *68*, 48–55.

Chou, J., and Roizman, B. (1992). The γ_1(34.5) gene of herpes simplex virus 1 precludes neuroblastoma cells from triggering total shutoff of protein synthesis characteristic of programmed cell death in neuronal cells. Proc. Natl. Acad. Sci. USA *89*, 3266–3270.

Chou, J., and Roizman, B. (1994). Herpes simplex virus 1 $\gamma_1$34.5 gene function, which blocks the host response to infection, maps in the homologous domain of the genes expressed during growth arrest and DNA damage. Proc. Natl. Acad. Sci. USA *91*, 5247–5251.

Chou, J., Kern, E.R., Whitley, R.J., and Roizman, B. (1990). Mapping of herpes simplex virus-1 neurovirulence to $\gamma_1$34.5, a gene nonessential for growth in culture. Science *250*, 1262–1266.

Degenhardt, K., Mathew, R., Beaudoin, B., Bray, K., Anderson, D., Chen, G., Mukherjee, C., Shi, Y., Gelinas, C., Fan, Y., et al. (2006). Autophagy promotes tumor cell survival and restricts necrosis, inflammation, and tumorigenesis. Cancer Cell *10*, 51–64.

Deretic, V. (2006). Autophagy as an immune defense mechanism. Curr. Opin. Immunol. *18*, 375–382.

Easton, R.M., Deckwerth, T.L., Parsadanian, A.S., and Johnson, E.M., Jr. (1997). Analysis of the mechanism of loss of trophic factor dependence associated with neuronal maturation: A phenotype indistinguishable from Bax deletion. J. Neurosci. *17*, 9656–9666.

Furuya, N., Yu, J., Byfield, M., Pattingre, S., and Levine, B. (2005). The evolutionarily conserved domain of Beclin 1 is required for Vps34 binding, autophagy and tumor suppressor function. Autophagy *1*, 46–52.

Gierasch, W.W., Zimmerman, D.L., Ward, S.L., Vanheyningen, T.K., Romine, J.D., and Leib, D.A. (2006). Construction and characterization of bacterial artificial chromosomes containing HSV-1 strains 17 and KOS. J. Virol. Methods *135*, 197–206.

Hara, T., Nakamura, K., Matsui, M., Yamamoto, A., Nakahara, Y., Suzuki-Migishima, R., Yokoyama, M., Mishima, K., Saito, I., Okano, H., and Mizushima, N. (2006). Suppression of basal autophagy in neural cells causes neurodegenerative disease in mice. Nature *441*, 885–889.

Harrow, S., Papanastassiou, V., Harland, J., Mabbs, R., Petty, R., Fraser, M., Hadley, D., Patterson, J., Brown, S.M., and Rampling, R. (2004). HSV1716 injection into the brain adjacent to tumour following surgical resection of high-grade glioma: Safety data and long-term survival. Gene Ther. *11*, 1648–1658.

He, B., Chou, J., Liebermann, D.A., Hoffman, B., and Roizman, B. (1996). The carboxyl terminus of the murine MyD116 gene substitutes for the corresponding domain of the $\gamma_1$34.5 gene of herpes simplex virus to preclude the premature shutoff of total protein synthesis in infected human cells. J. Virol. *70*, 84–90.

He, B., Gross, M., and Roizman, B. (1997). The $\gamma_1$34.5 protein of herpes simplex virus 1 complexes with protein phosphatase 1α to dephosphorylate the α subunit of the eukaryotic translation initiation factor 2 and preclude the shutoff of protein synthesis by double-stranded RNA-activated protein kinase. Proc. Natl. Acad. Sci. USA *94*, 843–848.

Jia, K., Hart, A.C., and Levine, B. (2007). Autophagy genes protect against disease caused by polyglutamine expansion proteins in *Caenorhabditis elegans*. Autophagy *3*, 21–25.

Kabeya, Y., Mizushima, N., Ueno, T., Yamamoto, A., Kirisako, T., Noda, T., Kominami, E., Ohsumi, Y., and Yoshimori, T. (2000). LC3, a mammalian homologue of yeast Apg8p, is localized in autophagosome membranes after processing. EMBO J. *19*, 5720–5728.

Katze, M.G., He, Y., and Gale, M. (2002). Viruses and interferon: A fight for supremacy. Nat. Rev. Immunol. *2*, 675–687.

Kihara, A., Kabeya, Y., Ohsumi, Y., and Yoshimori, T. (2001a). Beclin-phosphatidylinositol 3-kinase complex functions at the trans-Golgi network. EMBO Rep. *2*, 330–335.

Kihara, A., Noda, T., Ishihara, N., and Ohsumi, Y. (2001b). Two distinct Vps34 phosphatidylinositol 3-kinase complexes function in autophagy and carboxypeptidase Y sorting in *Saccharomyces cerevisiae*. J. Cell Biol. *152*, 519–530.

Kirchner, H., Kochen, M., Munk, K., Hirt, H.M., Mergenhagen, S.E., and Rosenstreich, D.L. (1978). Differences in susceptibility to herpes simplex virus infection of inbred strains of mice. IARC Sci. Publ. 783–788.

Kirkegaard, K., Taylor, M.P., and Jackson, W.T. (2004). Cellular autophagy: Surrender, avoidance and subversion by microorganisms. Nat. Rev. Microbiol. *2*, 301–314.

Komatsu, M., Waguri, S., Chiba, T., Murata, S., Iwata, J., Tanida, I., Ueno, T., Koike, M., Uchiyama, Y., Kominami, E., and Tanaka, K. (2006). Loss of autophagy in the central nervous system causes neurodegeneration in mice. Nature *441*, 880–884.

Leib, D.A., Machalek, M.A., Williams, B.R., Silverman, R.H., and Virgin, H.W. (2000). Specific phenotypic restoration of an attenuated virus by knockout of a host resistance gene. Proc. Natl. Acad. Sci. USA *97*, 6097–6101.

Levine, B. (2005). Eating oneself and uninvited guests: Autophagy-related pathways in cellular defense. Cell *120*, 159–162.

Levine, B. (2006). Autophagy in antiviral host defense. In Autophagy in Immunity and Infection, V. Deretic, ed. (Weinheim, Germany: Wiley-Vch), pp. 227–241.

Levine, B., and Klionsky, D.J. (2004). Development by self-digestion: Molecular mechanisms and biological functions of autophagy. Dev. Cell *6*, 463–477.

Levine, B., and Yuan, J. (2005). Autophagy in cell death: An innocent convict? J. Clin. Invest. *115*, 2679–2688.

Liang, X.H., Kleeman, L., Jiang, H.H., Gordon, G., Goldman, J.E., Berry, G., Herman, B., and Levine, B. (1998). Protection against fatal Sindbis virus encephalitis by Beclin, a novel Bcl-2-interacting protein. J. Virol. *72*, 8586–8596.

Liang, X.H., Jackson, S., Seaman, M., Brown, K., Kempkes, B., Hibshoosh, H., and Levine, B. (1999). Induction of autophagy and inhibition of tumorigenesis by *beclin 1*. Nature *402*, 672–676.

Liang, X.H., Yu, J., Brown, K., and Levine, B. (2001). Beclin 1 contains a leucine-rich nuclear export signal that is required for its autophagy and tumor suppressor function. Cancer Res. *61*, 3443–3449.

Liu, Y., Schiff, M., Czymmek, K., Tallóczy, Z., Levine, B., and Dinesh-Kumar, S.P. (2005). Autophagy regulates programmed cell death during the plant innate immune response. Cell *121*, 567–577.

Liang, C., Feng, P., Ku, B., Dotan, I., Canaani, D., Oh, B.H., and Jung, J.U. (2006). Autophagic and tumour suppressor activity of a novel Beclin 1-binding protein UVRAG. Nat. Cell Biol. *8*, 688–699.

Markovitz, N.S., Baunoch, D., and Roizman, B. (1997). The range and distribution of murine central nervous system cells infected with the $\gamma_1$34.5- mutant of herpes simplex virus 1. J. Virol. *71*, 5560–5569.

Melendez, A., Tallóczy, Z., Seaman, M., Eskelinen, E.-L., Hall, D.H., and Levine, B. (2003). Autophagy genes are essential for dauer development and life-span extension in *C. elegans*. Science *301*, 1387–1391.

Mizushima, N. (2005). The pleiotropic role of autophagy: From protein metabolism to bactericide. Cell Death Differ. *12* (*Suppl 2*), 1535–1541.

Mohr, I., Sternberg, D., Ward, S., Leib, D., Mulvey, M., and Gluzman, Y. (2001). A herpes simplex virus type 1 γ34.5 second-site suppressor mutant that exhibits enhanced growth in cultured glioblastoma cells is severely attenuated in animals. J. Virol. *75*, 5189–5196.

Mulvey, M., Poppers, J., Ladd, A., and Mohr, I. (1999). A herpesvirus ribosome-associated, RNA-binding protein confers a growth advantage upon mutants deficient in a GADD34-related function. J. Virol. *73*, 3375–3385.

Ogawa, M., Yoshimori, T., Suzuki, T., Sagara, H., Mizushima, N., and Sasakawa, C. (2005). Escape of intracellular *Shigella* from autophagy. Science *307*, 727–731.

Pattingre, S., Tassa, A., Qu, X., Garuti, R., Liang, X.H., Mizushima, N., Packer, M., Schneider, M.D., and Levine, B. (2005). Bcl-2 antiapoptotic proteins inhibit Beclin 1-dependent autophagy. Cell *122*, 927–939.

Qu, X., Yu, J., Bhagat, G., Furuya, N., Hibshoosh, H., Troxel, A., Rosen, J., Eskelinen, E.L., Mizushima, N., Ohsumi, Y., et al. (2003). Promotion of tumorigenesis by heterozygous disruption of the *beclin 1* autophagy gene. J. Clin. Invest. *112*, 1809–1820.

Schmid, D., Dengjel, J., Schoor, O., Stevanovic, S., and Munz, C. (2006). Autophagy in innate and adaptive immunity against intracellular pathogens. J. Mol. Med. *84*, 194–202.

Seaman, M.N., Marcusson, E.G., Cereghino, J.L., and Emr, S.D. (1997). Endosome to Golgi retrieval of the vacuolar protein sorting receptor, Vps10p, requires the function of the VPS29, VPS30, and VPS35 gene products. J. Cell Biol. *137*, 79–92.

Seay, M., Dinesh-Kumar, S., and Levine, B. (2005). Digesting oneself and digesting microbes: Autophagy as a host response to viral infection. In Modulation of Host Gene Expression and Innate Immunity by Viruses, P. Palese, ed. (Dordrecht, The Netherlands: Springer), pp. 245–279.

Shibata, M., Lu, T., Furuya, T., Degterev, A., Mizushima, N., Yoshimori, T., MacDonald, M., Yankner, B., and Yuan, J. (2006). Regulation of intracellular accumulation of mutant Huntingtin by Beclin 1. J. Biol. Chem. *281*, 14474–14485.

Shintani, T., and Klionsky, D.J. (2004). Autophagy in health and disease: A double-edged sword. Science *306*, 990–995.

Smith, J.D., and de Harven, E. (1978). Herpes simplex virus and human cytomegalovirus replication in WI-38 cells. III. Cytochemical localization of lysosomal enzymes in infected cells. J. Virol. *26*, 102–109.

Tallóczy, Z., Jiang, W., Virgin, H.W., IV, Leib, D.A., Scheuner, D., Kaufman, R.J., Eskelinen, E.L., and Levine, B. (2002). Regulation of starvation- and virus-induced autophagy by the eIF2α kinase signaling pathway. Proc. Natl. Acad. Sci. USA *99*, 190–195.

Tallóczy, Z., Virgin, H.W., IV, and Levine, B. (2006). PKR-dependent autophagic degradation of herpes simplex virus type 1. Autophagy *2*, 24–29.

Thumm, M., Egner, R., Koch, B., Schlumpberger, M., Straub, M., Veenhuis, M., and Wolf, D.H. (1994). Isolation of autophagocytosis mutants of *Saccharomyces cerevisiae*. FEBS Lett. *349*, 275–280.

Tsukada, M., and Ohsumi, Y. (1993). Isolation and characterization of autophagy-defective mutants of *Saccharomyces cerevisiae*. FEBS Lett. *333*, 169–174.

Tyler, K.L. (2004). Herpes simplex virus infections of the central nervous system: Encephalitis and meningitis, including Mollaret's. Herpes *11* (*Suppl 2*), 57A–64A.

Yue, Z., Jin, S., Yang, C., Levine, A.J., and Heintz, N. (2003). Beclin 1, an autophagy gene essential for early embryonic development, is a haploinsufficient tumor suppressor. Proc. Natl. Acad. Sci. USA *100*, 15077–15082.

Development/Plasticity/Repair

Neurotrophin-Dependent Dendritic Filopodial Motility: A Convergence on PI3K Signaling

Bryan W. Luikart,[1,2]* Wei Zhang,[1]* Gary A. Wayman,[2] Chang-Hyuk Kwon,[1] Gary L. Westbrook,[2] and Luis F. Parada[1]

[1]Department of Developmental Biology and Kent Waldrep Foundation Center for Research on Nerve Growth and Regeneration, University of Texas Southwestern Medical School, Dallas, Texas 75390-9133, and [2]The Vollum Institute, Oregon Health & Science University, Portland, Oregon 97239

Synapse formation requires contact between dendrites and axons. Although this process is often viewed as axon mediated, dendritic filopodia may be actively involved in mediating synaptogenic contact. Although the signaling cues underlying dendritic filopodial motility are mostly unknown, brain-derived neurotrophic factor (BDNF) increases the density of dendritic filopodia and conditional deletion of tyrosine receptor kinase B (TrkB) reduces synapse number *in vivo*. Here, we report that TrkB associates with dendritic growth cones and filopodia, mediates filopodial motility, and does so via the phosphoinositide 3 kinase (PI3K) pathway. We used genetic and pharmacological manipulations of mouse hippocampal neurons to assess signaling downstream of TrkB. Conditional knock-out of two downstream negative regulators of TrkB signaling, Pten (phosphatase with tensin homolog) and Nf1 (neurofibromatosis type 1), enhanced filopodial motility. This effect was PI3K-dependent and correlated with synaptic density. Phosphatidylinositol 3,4,5-trisphosphate (PIP3) was preferentially localized in filopodia and this distribution was enhanced by BDNF application. Thus, intracellular control of filopodial dynamics converged on PI3K activation and PIP3 accumulation, a cellular paradigm conserved for chemotaxis in other cell types. Our results suggest that filopodial movement is not random, but responsive to synaptic guidance molecules.

Key words: BDNF; TrkB; filopodia; spine; PIP3; PIP2

Introduction

The establishment of appropriate synaptic connections between neurons during development is a prerequisite for normal nervous system function, beginning with contact between presynaptic elements and motile dendritic filopodia (Dailey and Smith, 1996; Ziv and Smith, 1996; Fiala et al., 1998; Niell et al., 2004). Neural activity in developing networks must involve extracellular cues that guide filopodial motility. Activity-dependent release of brain-derived neurotrophic factor (BDNF), a 13.5 kDa neurotrophin, is an attractive candidate for this purpose. *In vitro* application of BDNF elicits filopodia and spine formation (Dunaevsky et al., 1999; Eom et al., 2003; Ji et al., 2005). Furthermore, conditional ablation of the high affinity BDNF receptor, tyrosine receptor kinase B (TrkB), reduces synaptic density indicating its participation in hippocampal synapse formation *in vivo* (Luikart et al., 2005). Thus, the interaction of BDNF with TrkB could drive activity-dependent synaptic morphogenesis (Patapoutian and Reichardt, 2001; Poo, 2001; Cohen-Cory, 2002).

TrkB activation drives signaling through the phospholipase Cγ (PLCγ), phosphoinositide 3 kinase (PI3K), and Ras pathways. These signaling pathways are highly regulated and mediate context-dependent cellular responses including differentiation, survival, growth, and synaptic potentiation. For example, the neurofibromatosis type 1 (Nf1) tumor suppressor, functions as a Ras GTPase-activating protein (GAP) that negatively regulates Ras signaling (Zhu et al., 2001). The loss of Nf1 results in neurotrophin-independent survival of neurons (Vogel et al., 1995). The lipid phosphatase, phosphatase with tensin homolog (Pten) opposes PI3K signaling by catalyzing the conversion of phosphatidylinositol 3,4,5-trisphosphate (PIP3) into phosphatidylinositol 4,5-bisphosphate (PIP2). Pten overexpression inhibits neurotrophin-dependent growth and differentiation (Musatov et al., 2004), whereas conditional deletion of Pten in the hippocampus and cortex results in neuronal hypertrophy and behavioral abnormalities reminiscent of human autism (Kwon et al., 2006). These observations and the fact that mutations in BDNF, TrkB, Pten, and Nf1 are associated with impaired cognitive function in humans could indicate a convergence on a common mechanism (North et al., 1997; Yeo et al., 2004; Butler et al., 2005).

Despite extensive knowledge of downstream TrkB signaling, the molecular pathways underlying dendritic filopodial motility and synapse formation are unknown. To identify the signaling pathways involved in TrkB-mediated synapse formation, we imaged dendritic filopodia and synapses in hippocampal neuronal cultures. To alter molecules involved in TrkB signaling, we over-

Received Jan. 15, 2008; revised May 19, 2008; accepted May 24, 2008.

This work was supported by National Institutes of Health Grant R37NS33199, Department of Defense Grant W81XWH-05-1-0265-01, National Institute of Neurological Disorders and Stroke Center Grant P50 NS 052606, The Simons Foundation, and National Institutes of Health Grants F32MH079548 (B.W.L.) and MH46613 (G.L.W.). L.F.P. is an American Cancer Society Research Professor. We thank Peter Devreotes for the PH-GFP construct and David Kaplan for the TrkB point mutant constructs.

*B.W.L. and W.Z. contributed equally to this work.

Correspondence should be addressed to Luis F. Parada, Department of Developmental Biology and Kent Waldrep Foundation Center for Research on Nerve Growth and Regeneration, University of Texas Southwestern Medical School, 6000 Harry Hines Boulevard, Dallas, TX 75390-9133. E-mail: Luis.Parada@utsouthwestern.edu.

G.A. Wayman's present address: Department of Veterinary and Comparative Anatomy, Pharmacology, and Physiology, Washington State University, Pullman, WA 99164.

DOI:10.1523/JNEUROSCI.0195-08.2008

 0270-6474/08/287006-07$15.00/0

expressed TrkB mutant cDNAs, and used cre-mediated knockdown of TrkB, Pten, or Nf1 in neurons cultured from loxp generated germline alleles. We also used pharmacological inhibitors to complement the genetic studies. Deletion of TrkB, Pten, or Nf1 all caused abnormal dendritic filopodial motility, and altered excitatory synapse formation by a common PI3K-dependent mechanism.

Materials and Methods

Mice. *TrkB*$^{flox/flox}$, *NF-1*$^{flox/flox}$, and *Pten*$^{flox/flox}$ mice have all been described previously (Zhu et al., 2001; Luikart et al., 2005; Kwon et al., 2006). Mutant mice were generated by crossing parents that were homozygous for the floxp alleles. All mouse procedures used in were approved by institutional animal care and advisory committees at the University of Texas Southwestern Medical Center and Oregon Health & Sciences University.

Constructs. TrkB cDNAs including point mutations were PCR cloned from previously described adenoviral genomic DNA or plasmids (Atwal et al., 2000) (sense, ACC ATG TCG CCC AGG TGG CAT; TrkB wild type (WT), TrkB Y490F, and TrkB K538N antisense, GTC GAC CCT AGG ATG TCC AGG AA; TrkB Y785F and TrkB Y785/490F antisense, GTC GAC CCT AGG ATG TCC AGG TA). PCR products were cloned into pGEM-T easy (Promega), removed with *Eco*RI/*Sal*I, and cloned into the same sites of pEYFP-N1 (Clontech).

Primary cell culture and live imaging. Serum-containing dissociated hippocampal cultures were prepared from postantal day 1 (P1) to P3 mouse pups and transfected at 4–6 d *in vitro* (DIV) using calcium phosphate as described previously (Luikart et al., 2005). Live imaging at 10–11 DIV was performed using the 63× objective of the LSM510 confocal microscope equipped with a motorized stage, objective heater (temperature control mini, 37.5°C), stage heater (temperature control, 37°C), and humidified climate control chamber (temperature overheat, 1.5°C, CTI controller 3700, 5% CO_2). With these settings, the neurons were maintained at an actual temperature of 37°C. All imaging was performed without changing cell-culture media. Images of up to eight cells were captured per imaging session using LSM510 software with the MultiTime Module at a resolution of 640 × 480, an electronic zoom of 2.5×, and a scan speed of 2.56 μm/s. For each neuron, a Z-stack of seven images (Z-step, 0.6 μm) was captured using 1–4% argon laser power with a pinhole of 2.4 μm. Thus, protrusions appeared in at least two images of the stack, and the entire dendritic region remained in the plane of the Z-stack. All equipment was from Zeiss.

Organotypic hippocampal slice cultures. Slice cultures were prepared from P5 Sprague Dawley rats and transfected using the Helios Gene Gun (Biorad) as described previously. Live imaging was performed using the 63× water-immersion objective with an Axioskop 2 FS microscope (Zeiss) equipped with a motorized stage (Applied Scientific Instrumentation), inline solution heater (Warner Instruments; bath temp, 35°C), spinning disk unit (Solamere Technology), and an XR/Mega10 CCD camera (Stanford Photonics). Imaging was performed in a solution containing (in mM) 125 NaCl, 25 $NaHCO_3$, 2.5 KCl, 1.25 NaH_2PO_4, 2.0 $CaCl_2$, 1.0 $MgCl_2$, and 25 D-glucose, bubbled with 95% O_2/5% CO_2. Images of a single field of view were captured per imaging session using QED In Vivo software. For each neuron, a Z-stack of 20–30 images (Z-step, 0.4 μm) was captured using a 33 ms exposure time and signal averaging of four images. Thus, protrusions appeared in at least two images of the stack and the entire dendritic region remained in the plane of the Z-stack.

Imaging quantification. We imaged the cultures at a time (10 DIV) when spine formation has not yet occurred and filopodia are the predominant dendritic protrusion. We thus defined filopodia as any dendritic protrusion under 10 μm in length. We quantified filopodial turnover as the average of the sum of new filopodia appearing and the number of filopodia eliminated per dendrite length every 5 min for a total of 30 min. This measurement was performed manually using the manual object counting feature of MetaMorph. Filopodial motility was calculated as the average of the absolute value of the sum of changes in filopodial lengths per dendrite length every 5 min for a total of 30 min. The length of each filopodia was measured by manually tracing using MetaMorph. The relative fluorescence of dendritic versus filopodial pleckstrin homology (PH)-green fluorescent protein (GFP) was quantitated by manually tracing the parent dendrite, and filopodia arising from this dendrite, and using the color profiler plugin for Image J. The fluorescence index was defined as filopodial 488/568 ratio divided by the dendritic 488/568 ratio. Measurements were performed by an investigator blind to experimental conditions.

Immunocytochemistry. Neurons were prefixed with 4% paraformaldehyde in PBS at a 1:1 ratio with cell culture media (37°, 2 min) followed by a change into 37°C 4% paraformaldehyde for 5 min. Using this protocol, we observed minimal filopodial collapse; however, no fixation protocol completely maintained filopodia as observed in the living cells. After fixation, cells were washed for 5 min with PBS, 5 min with 0.3% Triton X-100 in PBS, and blocked with 6% NGS in PBS for 30 min. Primary antibodies were applied overnight at 4°C in blocking solution. All antibodies were used at the following concentrations: postsynaptic density-95 (PSD-95; Affinity Bioreagents; MA1-046) at 1:400; synaptophysin (Zymed; 18-0130) at 1:800; and anti-TrkB at 1:100 (a gift from David Kaplan, Hospital for Sick Children, Toronto, Ontario, Canada). Secondary Cy3 anti-mouse and Cy5 anti-rabbit antibodies were applied for 30 min (The Jackson Laboratory). Cells were washed 3 × 5 min after each antibody application.

Results

TrkB containing puncta traffic to dendritic growth cones and filopodia

To gain insight into the cellular functions of TrkB during synaptogenesis, we examined TrkB dynamics using an enhanced-yellow fluorescent protein (YFP)-tagged TrkB fusion protein. Furthermore, we reduced the signaling contribution of the endogenous TrkB receptors by cotransfecting TrkB-YFP and cre-dsRed into cultured hippocampal neurons from mice homozygous for the conditional TrkB flox allele. Both dsRed and YFP colocalized in a diffuse pattern throughout the cell. In addition to the diffuse signal, TrkB-YFP was also found concentrated in highly motile puncta. TrkB-YFP puncta within the shafts of primary dendrites of 10–11 DIV neurons were transported in both anterograde and retrograde directions (Fig. 1*A*,*B*, supplemental Video 1, available at www.jneurosci.org as supplemental material). We confirmed that the puncta indeed expressed TrkB using immunohistochemistry (supplemental Fig. 1, available at www.jneurosci.org as supplemental material). These puncta were rarely stable, traveling anterograde at 1.008 ± 0.082 μm/s and retrograde at 0.988 ± 0.071 μm/s (mean ± SEM; $n = 50$ and 51 puncta from 6 cells, respectively). Transport appeared to be saltatory with brief pauses in movement followed by rapid transport. TrkB-YFP puncta traveled in and out of dendritic growth cones and filopodia (Fig. 1*C*,*D*, supplemental Video 2, available at www.jneurosci.org as supplemental material) at considerably slower velocities. For secondary dendrites with growth cones and in filopodia TrkB-YFP, puncta moved at 0.015 ± 0.002 μm/s (mean ± SEM; $n = 85$ puncta from 3 cells). Thus, movement of TrkB was reduced in dendritic growth cones and filopodia compared with primary dendrites suggesting that TrkB is trafficked to and from these dynamic structures. The velocities measured for TrkB motility within the primary dendrite are within the ranges defined as active transport by kinesin and dynein (Hill et al., 2004).

TrkB signaling mediates filopodial motility

To examine TrkB signaling, we used mutant cDNAs fused in frame with enhanced-YFP that disrupt specific downstream pathways (Atwal et al., 2000). The relative activity of mutant proteins was assessed by transfection of the TrkB-YFP fusion proteins into NG108 cells in the presence of BDNF (50 ng/ml, 10

min) (supplemental Fig. 2, available at www.jneurosci.org as supplemental material). As anticipated, TrkB-YFP increased phosphorylation of mitogen-activated protein kinase (MAPK), AKT, and PLC-γ, whereas a kinase dead receptor, incapable of binding ATP (TrkB K538N-YFP), did not support phosphorylation of these downstream effectors. Mutation of the TrkB Shc/FRS-2 binding site (TrkB Y490F-YFP) selectively inhibited phosphorylation of extracellular signal-regulated kinase (ERK) and AKT, whereas mutation of the PLC-γ binding site (TrkB Y785F-YFP) abolished PLC-γ phosphorylation and the double mutant TrkB Y490F/Y785F abolished all BDNF-induced phosphorylation.

To test whether TrkB puncta in dendritic growth cones and filopodia influence structural dynamics, we analyzed filopodial motility (Fig. 2, Table 1), which is enhanced by BDNF (50 ng/ml). Overexpression of wild-type TrkB cDNA (TrkB-YFP) increased filopodial motility, whereas the kinase dead receptor reduced filopodial motility below the level of wild-type cells, consistent with a dominant negative activity (Table 1). The expression of the kinase dead receptor was also characterized by decreased filopodial density (0.31/μm TrkB-YFP vs 0.09/μm TrkB K538N; $p < 0.00004$) and increased filopodial length (2.66 μm TrkB-YFP vs 5.04 μm TrkB K538N; $p < 0.0004$. To examine which signaling pathways were responsible for the effect of TrkB on dendritic filopodia, we expressed the TrkB mutants in cre-dsRed-positive *TrkB*$^{flox/flox}$ hippocampal neurons so that we could blunt background effects of the wild-type receptor (supplemental Videos 3–7, respectively, available at www.jneurosci.org as supplemental material). We found that, whereas introduction of the PLCγ signaling mutant had similar enhancement of filopodial motility compared with TrkB-YFP, overexpression of the Ras/MAPK/PI3K signaling-deficient TrkB cDNA did not support the enhancement of motility (Table 1). These data confirm the TrkB activity in filopodial motility and refine its signaling requirement for the Ras pathway.

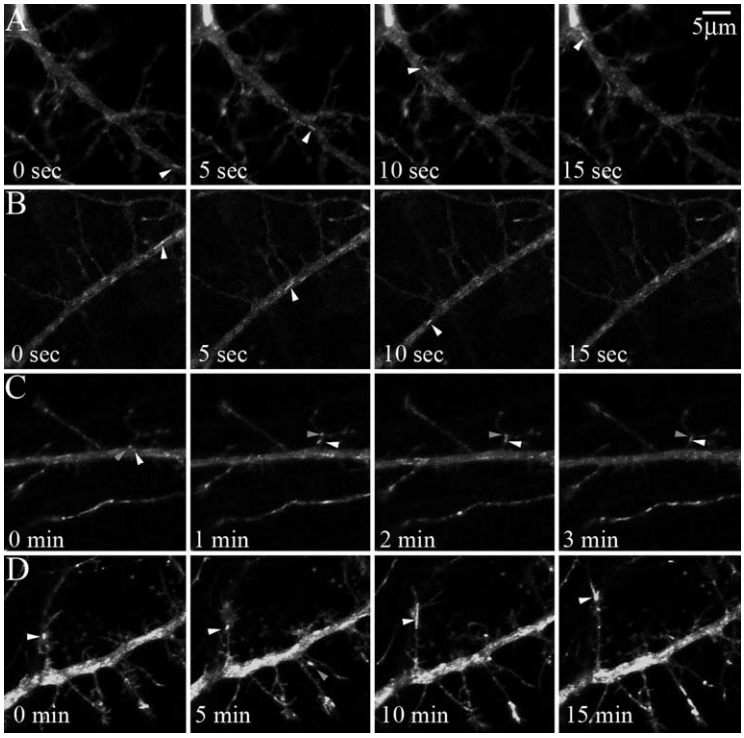

Figure 1. TrkB-YFP puncta are rapidly transported within primary dendrites and stable in dendritic growth cones and filopodia. ***A***, ***B***, We observed TrkB puncta being rapidly transported in both the retrograde (***A***, arrowheads) and anterograde (***B***, arrowheads) directions. Within primary dendrites, TrkB puncta traveled at an average velocity of 1.008 ± 0.082 μm/s in the anterograde and 0.988 ± 0.071 μm/s in the retrograde direction (mean ± SEM; $n = 50$ and 51 puncta from 6 cells, respectively). ***C***, ***D***, At longer time intervals (1 and 5 min), we resolved that TrkB puncta were less mobile in immature dendritic branches, growth cones, and filopodia (arrowheads). In these structures, TrkB puncta moved at an average velocity of 0.015 ± 0.002 μm/s (mean ± SEM; $n =$ 85 puncta from 3 cells).

TrkB Y490 has two major bifurcating effector pathways: PI3K and Raf/ERK (Atwal et al., 2000). To distinguish between these downstream pathways, we used specific pharmacological inhibitors (Vlahos et al., 1994; Alessi et al., 1995). The ERK inhibitor [2-(2-amino-3-methyoxyphenyl)-4*H*-1-benzopyran-4-one (PD98059), 10 μM] had no effect on TrkB-mediated filopodial motility, whereas block of PI3K signaling (LY294002 [2-(4-morpholinyl)-8-phenyl-4*H*-1-benzopyran-4-one], 10 μM) completely prevented TrkB-mediated enhancement of filopodial motility (Table 1). Thus, consistent with the TrkB mutant studies, the Ras pathway is critical, but Raf/ERK signaling is dispensable whereas PI3K signaling is required.

To examine the *in vivo* relevance of our observations, we turned to genetic systems using mouse conditional knock-outs. The Nf1 tumor suppressor encodes a Ras-GAP that is a known negative regulator of Trk family receptor signaling (Dasgupta and Gutmann, 2003) and the Pten tumor suppressor negatively regulates PI3K signaling (Wu et al., 1998). Thus, elimination of either of these two tumor suppressors results in constitutive activation of the Ras and PI3K pathways, respectively. We reasoned that if reduction of TrkB activity diminished filopodial motility, then genetic activation of the Ras/PI3K pathway should have an apposing effect. We cultured hippocampal neurons from *Nf1*$^{flox/flox}$ and *Pten*$^{flox/flox}$ mice to examine the consequence of genetic ablation on filopodial motility (Backman et al., 2001; Zhu et al., 2001). GFP-cre mediated recombination of either Nf1 or Pten resulted in increased filopodial motility (Table 1). Thus, genetic activation of the PI3K pathway demonstrates its role in filopodial motility downstream of TrkB.

We next examined the activity of pharmacological inhibitors on genetically modified neurons. The PI3K antagonist eliminated the enhanced filopodial motility that resulted from Nf1 or Pten ablation. Conversely, ERK pathway inhibition had no discernible effect when compared with Nf1 or Pten knock-out neurons (Table 1). Thus, both our pharmacologic and genetic data converge to identify the requirement for PI3K activity in mediating neuronal filopodial motility.

Synaptic marker density correlates with filopodial motility

Filopodial motility and turnover can be associated with synapse formation (Ziv and Smith, 1996). We therefore examined whether the observed changes in filopodial motility correlated with synapse number as assessed by immunocytochemical overlap of presynaptic and postsynaptic proteins (synaptophysin and PSD-95). TrkB overexpression increased synaptic density when

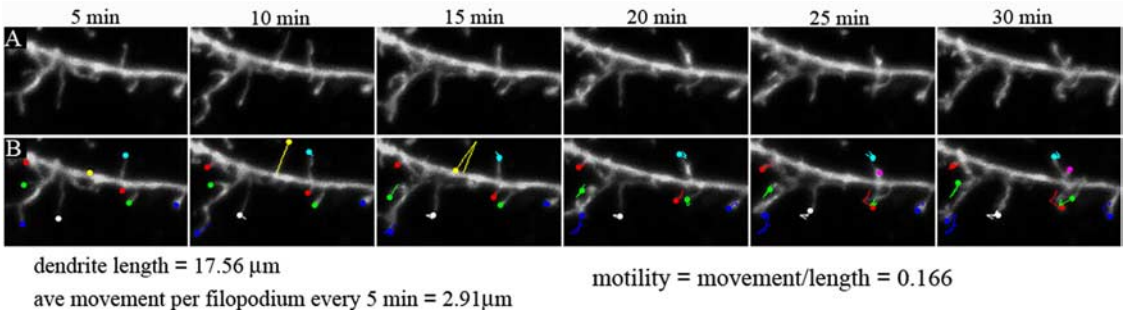

Figure 2. Dendritic filopodial motility quantitation. ***A***, Time-lapse images of dendrites from neurons expressing GFP. ***B***, Filopodial motility was calculated as the average of the absolute value of the sum of changed filopodial lengths per dendrite length every 5 min for a total of 30 min. The colored dots represent the tip of each filopodium and the corresponding line shows the distance the filopodium travels over time. For this example, the dendritic segment is 17.56 μm long. The average distance each filopodium moves every 5 min is 2.91 μm, and the motility is 0.166 (2.91/17.56).

Table 1. PI3K mediates dendritic filopodial motility

	Motility mean ± variance (*n*)	*p* value	% of control	Implicated pathway
GFP	0.218 ± 0.008 (27)			
GFP + BDNF (50 ng/ml)	0.386 ± 0.019 (11)	6.11×10^{-4}**	177%	PLCγ, ERK, PI3K
TrkB WT	0.354 ± 0.015 (8)	2.76×10^{-2}*	162%	PLCγ, ERK, PI3K
TrkB Y490/785F	0.178 ± 0.017 (7)	9.75×10^{-1}	82%	PLCγ, ERK, PI3K
TrkB K538N	0.094 ± 0.004 (7)	4.93×10^{-2}*	43%	PLCγ, ERK, PI3K
TrkB Y490F	0.215 ± 0.011 (10)	1.00	99%	ERK, PI3K
TrkB Y785F	0.346 ± 0.027 (8)	4.66×10^{-2}*	158%	Not PLCγ
GFP + DMSO	0.246 ± 0.017 (24)			
TrkB WT + DMSO	0.468 ± 0.010 (7)	1.76×10^{-4}**	190%	PLCγ, ERK, PI3K
Nf1 KO + DMSO	0.368 ± 0.012 (12)	2.87×10^{-2}*	150%	ERK, PI3K
Pten KO + DMSO	0.474 ± 0.018 (14)	2.32×10^{-6}**	193%	PI3K
TrkB WT + PD98059 (10 μM)	0.409 ± 0.025 (9)	4.19×10^{-3}**	166%	Not ERK
Nf1 KO + PD98059 (10 μM)	0.356 ± 0.010 (13)	5.56×10^{-2}	144%	Not ERK
Pten KO + PD98059 (10 μM)	0.439 ± 0.009 (11)	1.11×10^{-4}**	178%	Not ERK
TrkB WT + LY294002 (10 μM)	0.154 ± 0.004 (12)	1.83×10^{-1}	63%	PI3K
Nf1 KO + LY294002 (10 μM)	0.194 ± 0.025 (13)	7.97×10^{-1}	79%	PI3K
Pten KO + LY294002 (10 μM)	0.156 ± 0.004 (15)	1.39×10^{-1}	63%	PI3K

The average filopodial motility values for all genetic and pharmacological manipulations performed on the dissociated hippocampal neurons are shown. Compared with the GFP control, both the application of exogenous BDNF and overexpression of TrkB WT enhanced filopodial motility, implicating the PLCγ, Erk, and PI3K pathways in motility regulation. Expression of TrkB Y785F, but not TrkB Y490F, supported enhanced motility, indicating that the PI3K or ERK pathways (not PLCγ) are primarily responsible for this effect. The expression of the kinase dead point mutation (TrkB K538N) resulted in a reduction of filopodial motility indicating the dominant negative role of this receptor. Compared with control, the overexpression of TrkB WT, knock-out of Nf1, and knock-out of Pten all supported an increase in filopodial motility. In the presence of the Erk inhibitor PD98059 these genetic manipulations still support an increase in filopodial motility. However, in the presence of the PI3K inhibitor LY294002, this increase was completely abolished. Together, these results indicate that PI3K signaling mediated enhanced dendritic filopodial motility (statistics using a one-way ANOVA and Dunnett's *post hoc* test against either the GFP or GFP + DMSO control).

*Significant at the 5% level; **significant at the 1% level.

compared with neurons expressing GFP alone (0.287 ± 0.023 synapses/μm^2 vs 0.218 ± 0.021 synapses/μm^2, respectively; $p < 0.05$ using a two-tailed two-sample equal-variance Student's *t* test). Consistent with our observations using TrkB mutant cDNAs in filopodial motility, the PI3K deficient mutant, but not the PLCγ deficient mutant, resulted in decreased PSD-95/synaptophysin overlap (Fig. 3). Thus, changes in synapse density paralleled changes in filopodial motility in a TrkB-dependent manner. These data were further validated in similar studies using conditional Pten and Nf1 neurons in which synaptic density was enhanced. We next examined synapse formation *in vivo*. In the CNS dendritic spines are considered to reflect synaptic density. Using the Golgi technique, we examined dendritic spine density in the dentate gyrus of mice with conditional hippocampal ablation of TrkB (Luikart et al., 2005), Pten (Kwon et al., 2006), and Nf1 (Zhuo et al., 2001). We found that TrkB ablation resulted reduced dendritic spines, whereas Pten and Nf1 abated brains exhibited increased numbers of spines. Thus, *in vivo*, TrkB and downstream effector activity governs normal dendritic spine formation (supplemental Fig. 3, available at www.jneurosci.org as supplemental material).

Accumulation of PIP3 in filopodia

PI3K and Pten direct the spatial accumulation of PIP3 and, thus, actin polymerization in *Dictyostelium discoideum* during chemotaxis (Iijima and Devreotes, 2002). To test whether a similar focal accumulation of PIP3 accompanies filopodial motility, we examined the cellular localization of the PIP3 indicator, PH-GFP (Jin et al., 2000). For these experiments, we used biolistic gene transfer into organotypic hippocampal cultures. We used the ratio of PH-GFP and monomeric Cherry fluorescent protein (mCherry) as a measure of PIP3 accumulation. To address whether this ratio was altered between filopodia and the parent dendrite, we defined the fluorescence index as the filopodial GFP/cherry ratio divided by the dendritic GFP/cherry ratio. We found a significant accumulation of PH-GFP in dendritic filopodia (1.349 ± 0.0261) compared with GFP (1.028 ± 0.0236, mean ± SEM; $p < 1.0 \times 10^{-5}$) (Fig. 4). Treatment of slice cultures with BDNF produced a 1.682 ± 0.0442-fold increase in filopodial PH-GFP (mean ± SEM; $p < 1.0 \times 10^{-5}$, BDNF-treated versus untreated slices) (Fig. 4). Thus, PI3K activity downstream of TrkB increased PIP3 within dendritic filopodia indicating activity of the receptor within this dynamic structure.

Discussion

TrkB localization

TrkB is necessary for the normal development of synaptic connectivity of the hippocampus *in vivo* (Luikart et al., 2005). We first examined the cellular localization of TrkB-YFP in primary hippocampal cultures during synaptogenesis. In agreement with the study by Gomes et al. (2006), TrkB was trafficked in anterograde and retrograde directions through both dendrites and axons. Furthermore, once in filopodia and dendritic growth cones, TrkB receptors appeared to stabilize. Using antibodies specific to the extracellular domain of TrkB, Gomes et al. (2006) reported that puncta in dendritic growth cones and filopodia are exposed to the extracellular environment. Therefore, it appears that these receptors are poised to transduce signals in response to extracellular BDNF. Our calculated velocity of TrkB puncta movement in dendrites was faster than that observed by Gomes et al. (2006) in axons. This difference is not unexpected as we performed live

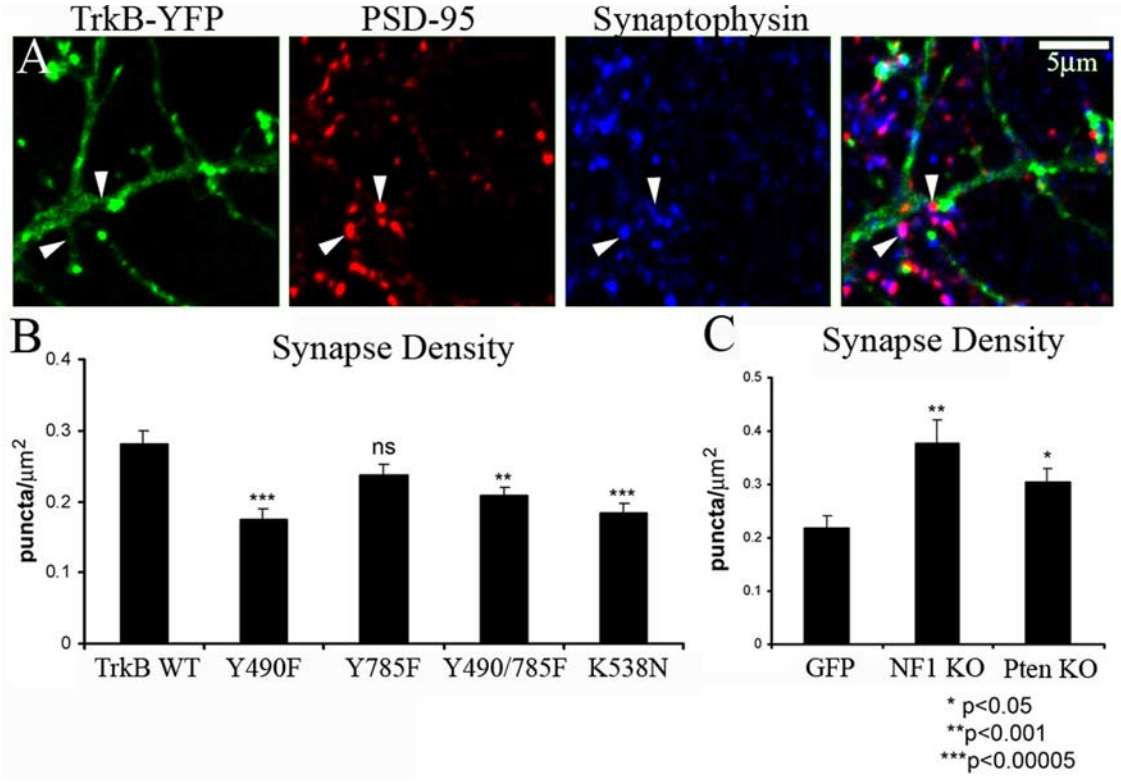

Figure 3. Synapse density in TrkB, Nf1, and Pten mutant hippocampal neurons. ***A***, Immunohistochemistry for PSD-95 (red) and synaptophysin (blue) in neurons expressing the TrkB-YFP fusion protein (green). Synapses were identified for quantitation as points at which the red, green, and blue signals overlapped (***A***, arrowheads). Synaptic density was measured for TrkB-YFP (WT; $n = 80$ neurons), TrkB Y490F-YFP ($n = 79$), TrkB Y785F-YFP ($n = 77$), TrkB Y490/785F-YFP ($n = 78$), and TrkB K538N-YFP (KD, $n = 77$). The Y490F, Y490/785F, and K538N mutations resulted in a significant decrease in synapse number when compared with TrkB-YFP. ***B***, However, TrkB Y785F-YFP was not significantly different from TrkB-YFP. Synapse density was measured for neurons from Nf1 flox and Pten flox animals transfected with GFP or GFP-cre. ***C***, The deletion of both Nf1 ($n = 30$ neurons) and Pten ($n = 30$) resulted in a significant increase in synaptic density when compared with GFP ($n = 34$; p values calculated using two-sample equal variance t test).

imaging at 37°C whereas they recorded at room temperature. Our results demonstrate that TrkB is associated with dendritic growth cones and filopodia, and is thus in position to regulate dynamics of those structures.

PI3K signaling and filopodial motility

Our results demonstrate that PI3K is the mediator of TrkB-dependent filopodial motility. The mechanism by which PI3K activity is linked to cytoskeletal dynamics has been studied in cellular chemotaxis (Song and Poo, 2001; Van Haastert and Devreotes, 2004; Sasaki and Firtel, 2006). In response to extracellular guidance molecules, the cellular distribution of PI3K and Pten regulates the spatial distribution of PIP3 in *Dictyostelium* (Iijima and Devreotes, 2002; Huang et al., 2003). Accumulation of PIP3 results in actin polymerization and forward movement of the cell. In dendritic filopodia, the accumulation of PIP3 and the regulation of motility by Pten and PI3K suggests that filopodial dynamics use an analogous mechanism. Trk receptors form complexes with components of the PI3K signaling cascade (Howe et al., 2001) and associate with dendritic filopodia. BDNF application results in filopodial PIP3 accumulation, increased motility, and increased filopodial number. BDNF is a synaptically released molecule with limited diffusion capability *in vivo*, suggesting that its dendritic growth promoting properties are likely localized. Furthermore, the molecular machinery underlying BDNF enhancement of filopodial motility has been conserved in chemotaxis indicating that it may elicit directional movements of dendritic filopodia. This chemoattractive aspect of BDNF has been documented for growing axons (Song and Poo, 2001). However, this is the first study to link spatially restricted TrkB signaling to PI3K activation, PIP3 accumulation, and dendritic filopodial motility.

Although it is unclear how PI3K activity and PIP3 accumulation may lead to actin polymerization, it is ultimately the activation of Rac, Rho, and Cdc42 that mediate actin dynamics (Etienne-Manneville and Hall, 2002) and dendritic growth (Threadgill et al., 1997). PI3K is required for Rac activation and critical for the activation of Rac by Ras (Cantrell, 2001; Innocenti et al., 2003). T-cell lymphoma invasion and metastasis 1 (Tiam1), the Rac1-GEF (guanine-nucleotide exchange factor) that mediates activity-dependent dendritic elaboration, is regulated directly by TrkB, PIP3, and calcium through NMDA receptor activation (Innocenti et al., 2003; Fleming et al., 2004; Miyamoto et al., 2006). Thus, an attractive model would place Tiam1 as the nexus for neurotrophin and glutamate regulation of dendritic growth.

Filopodial motility and synapse formation

The enhancement of filopodial motility resulting from the overexpression of TrkB, or reduction of Pten and Nf1, correlated with increased synaptic density. In our studies, enhancement of motility correlates positively with ultimate stabilization of synaptic contacts. BDNF-dependent activation of TrkB promoted dendritic filopodial motility and synapse formation via the activation of PI3K. For synaptogenesis to occur, there must not only be contact between neurons, but also stabilization of contacts and accumulation of synaptic proteins (Akins and Biederer, 2006). Although our data addresses the molecular pathways by which TrkB mediates enhanced filopodial motility and synapse forma-

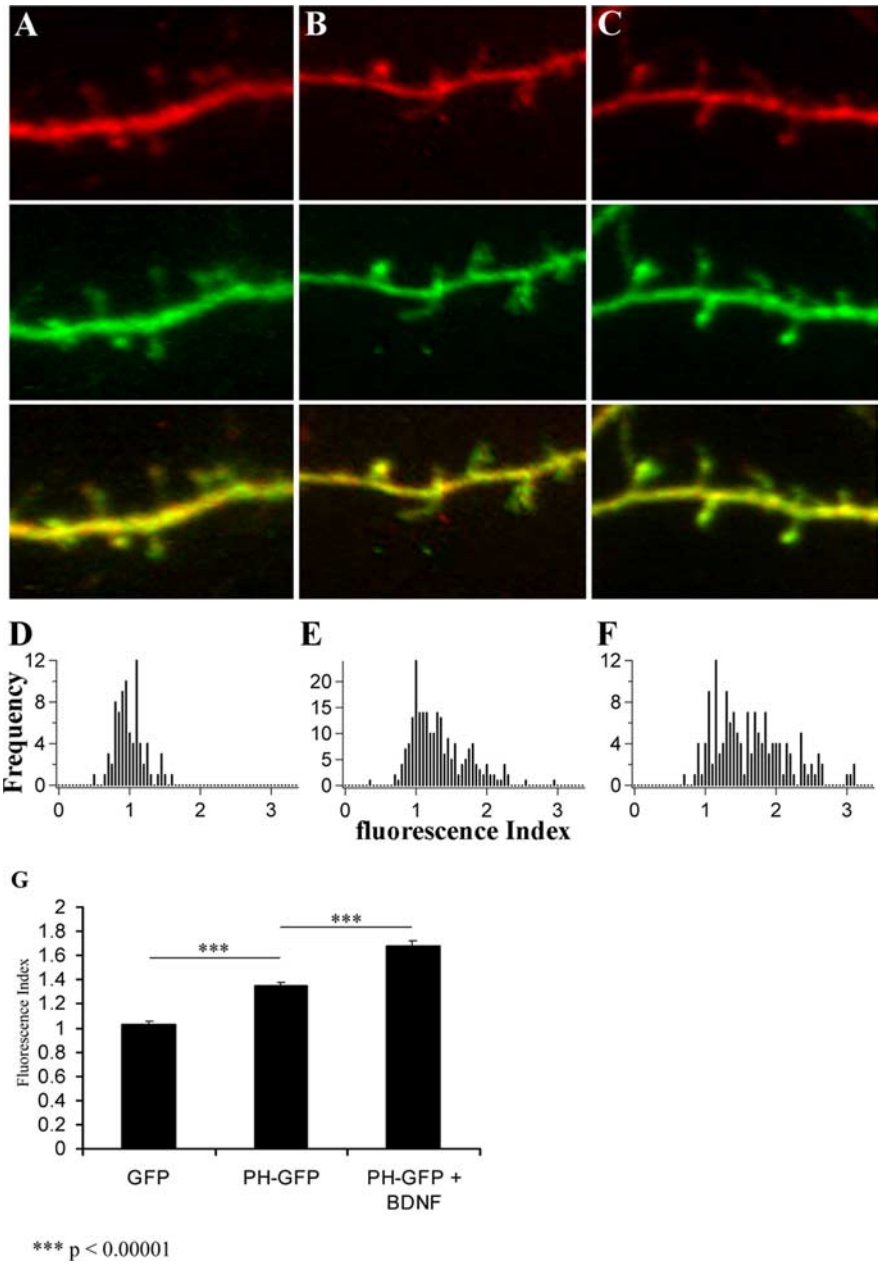

Figure 4. BDNF-dependent accumulation of PH-GFP in dendritic filopodia. ***A–C***, Representative images of dendritic segments expressing GFP and mCherry (***A***), PH-GFP and mCherry (***B***), and PH-GFP and mCherry from BDNF-treated (50 ng/ml for 4–6 h) slices (***C***). The distribution of GFP fluorescence in filopodia relative to dendrites was quantified as the filopodial 488/568 ratio divided by the dendritic 488/568 ratio (fluorescence index). Thus, numbers >1 indicate increased relative GFP fluorescence in the filopodia versus dendrites. ***D–F***, The distribution of these values was plotted for GFP (***D***; $n = 79$ filopodia), PH-GFP (***E***; $n = 230$ filopodia), and BDNF treated PH-GFP (***F***; $n = 151$ filopodia). The equal distribution of GFP and mCherry between dendrites and filopodia is indicated by the distribution of the fluorescence index around 1. The shift in this distribution toward numbers >1 in the PH-GFP condition indicates accumulation of PIP3 in dendritic filopodia. Application of BDNF further increased the filopodial PIP3 levels when compared with untreated cells (*p* values calculated using the Newman–Keuls test).

tion, it does not address mechanisms by which TrkB may contribute to the stabilization of synaptic contacts. Nonetheless, it appears that Trk signaling does contribute to stabilization (Vaillant et al., 2002; Hu et al., 2005).

The PI3K pathway has been highly conserved throughout evolution, mediating chemoattractive responses in *Dictyostelium*, neutrophil chemotaxis, wound healing, and tumor cell metastasis (Merlot and Firtel, 2003; Van Haastert and Devreotes, 2004). This paradigm suggests that BDNF not only enhances filopodial motility, but may use chemoattractive molecular pathways allowing for directed movement of filopodia toward sites of BDNF release. BDNF synthesis and secretion is regulated by neuronal activity (Patterson et al., 1992; Hartmann et al., 2001; Kohara et al., 2001). Thus, filopodial motility may not be random, but influenced by extracellular cues allowing for the activity-dependent sculpting of neuronal connectivity during development and activity-dependent remodeling of synaptic connectivity in the adult (Luikart and Parada, 2006). Indeed, recent evidence suggests that filopodia are not distributed randomly with respect to mature synaptic boutons (Nägerl et al., 2007; Toni et al., 2007). Although BDNF is an attractive candidate to mediate this extracellular targeting, other neuromodulators also influence PI3K-dependent and -independent pathways that are important for dendritic development. For example, glutamate and GABA influence dendritic development through non-PI3K pathways. Thus, a variety of extracellular influences likely converge on intracellular pathways mediating directional growth and movement. The modulation of dendritic development and synapse formation can have global consequences on CNS function. Accordingly, human mutations in the TrkB, Pten, and Nf1 genes cause cognitive impairment (North et al., 1997; Yeo et al., 2004; Butler et al., 2005). Our data provide a putative link between the function of these genes and normal synaptic development.

References

Akins MR, Biederer T (2006) Cell–cell interactions in synaptogenesis. Curr Opin Neurobiol 16:83–89.

Alessi DR, Cuenda A, Cohen P, Dudley DT, Saltiel AR (1995) PD 098059 is a specific inhibitor of the activation of mitogen-activated protein kinase kinase in vitro and in vivo. J Biol Chem 270:27489–27494.

Atwal JK, Massie B, Miller FD, Kaplan DR (2000) The TrkB-Shc site signals neuronal survival and local axon growth via MEK and P13-kinase. Neuron 27:265–277.

Backman SA, Stambolic V, Suzuki A, Haight J, Elia A, Pretorius J, Tsao MS, Shannon P, Bolon B, Ivy GO, Mak TW (2001) Deletion of Pten in mouse brain causes seizures, ataxia and defects in soma size resembling Lhermitte-Duclos disease. Nat Genet 29:396–403.

Butler MG, Dasouki MJ, Zhou XP, Talebizadeh Z, Brown M, Takahashi TN, Miles JH, Wang CH, Stratton R, Pilarski R, Eng C (2005) Subset of individuals with autism spectrum disorders and extreme macrocephaly associated with germline PTEN tumour suppressor gene mutations. J Med Genet 42:318–321.

Cantrell DA (2001) Phosphoinositide 3-kinase signalling pathways. J Cell Sci 114:1439–1445.

Cohen-Cory S (2002) The developing synapse: construction and modulation of synaptic structures and circuits. Science 298:770–776.

Dailey ME, Smith SJ (1996) The dynamics of dendritic structure in developing hippocampal slices. J Neurosci 16:2983–2994.

Dasgupta B, Gutmann DH (2003) Neurofibromatosis 1: closing the GAP between mice and men. Curr Opin Genet Dev 13:20–27.

Dunaevsky A, Tashiro A, Majewska A, Mason C, Yuste R (1999) Developmental regulation of spine motility in the mammalian central nervous system. Proc Natl Acad Sci USA 96:13438–13443.

Eom T, Antar LN, Singer RH, Bassell GJ (2003) Localization of a β-actin messenger ribonucleoprotein complex with zipcode-binding protein modulates the density of dendritic filopodia and filopodial synapses. J Neurosci 23:10433–10444.

Etienne-Manneville S, Hall A (2002) Rho GTPases in cell biology. Nature 420:629–635.

Fiala JC, Feinberg M, Popov V, Harris KM (1998) Synaptogenesis via dendritic filopodia in developing hippocampal area CA1. J Neurosci 18:8900–8911.

Fleming IN, Batty IH, Prescott AR, Gray A, Kular GS, Stewart H, Downes CP (2004) Inositol phospholipids regulate the guanine-nucleotide-exchange factor Tiam1 by facilitating its binding to the plasma membrane and regulating GDP/GTP exchange on Rac1. Biochem J 382:857–865.

Gomes RA, Hampton C, El-Sabeawy F, Sabo SL, McAllister AK (2006) The dynamic distribution of TrkB receptors before, during, and after synapse formation between cortical neurons. J Neurosci 26:11487–11500.

Hartmann M, Heumann R, Lessmann V (2001) Synaptic secretion of BDNF after high-frequency stimulation of glutamatergic synapses. EMBO J 20:5887–5897.

Hill DB, Plaza MJ, Bonin K, Holzwarth G (2004) Fast vesicle transport in PC12 neurites: velocities and forces. Eur Biophys J 33:623–632.

Howe CL, Valletta JS, Rusnak AS, Mobley WC (2001) NGF signaling from clathrin-coated vesicles: evidence that signaling endosomes serve as a platform for the Ras-MAPK pathway. Neuron 32:801–814.

Hu B, Nikolakopoulou AM, Cohen-Cory S (2005) BDNF stabilizes synapses and maintains the structural complexity of optic axons in vivo. Development 132:4285–4298.

Huang YE, Iijima M, Parent CA, Funamoto S, Firtel RA, Devreotes P (2003) Receptor-mediated regulation of PI3Ks confines PI(3,4,5)P3 to the leading edge of chemotaxing cells. Mol Biol Cell 14:1913–1922.

Iijima M, Devreotes P (2002) Tumor suppressor PTEN mediates sensing of chemoattractant gradients. Cell 109:599–610.

Innocenti M, Frittoli E, Ponzanelli I, Falck JR, Brachmann SM, Di Fiore PP, Scita G (2003) Phosphoinositide 3-kinase activates Rac by entering in a complex with Eps8, Abi1, and Sos-1. J Cell Biol 160:17–23.

Ji Y, Pang PT, Feng L, Lu B (2005) Cyclic AMP controls BDNF-induced TrkB phosphorylation and dendritic spine formation in mature hippocampal neurons. Nat Neurosci 8:164–172.

Jin T, Zhang N, Long Y, Parent CA, Devreotes PN (2000) Localization of the G protein betagamma complex in living cells during chemotaxis. Science 287:1034–1036.

Kohara K, Kitamura A, Morishima M, Tsumoto T (2001) Activity-dependent transfer of brain-derived neurotrophic factor to postsynaptic neurons. Science 291:2419–2423.

Kwon CH, Luikart BW, Powell CM, Zhou J, Matheny SA, Zhang W, Li Y, Baker SJ, Parada LF (2006) Pten regulates neuronal arborization and social interaction in mice. Neuron 50:377–388.

Luikart BW, Parada LF (2006) Receptor tyrosine kinase B-mediated excitatory synaptogenesis. Prog Brain Res 157:15–24.

Luikart BW, Nef S, Virmani T, Lush ME, Liu Y, Kavalali ET, Parada LF (2005) TrkB has a cell-autonomous role in the establishment of hippocampal Schaffer collateral synapses. J Neurosci 25:3774–3786.

Merlot S, Firtel RA (2003) Leading the way: Directional sensing through phosphatidylinositol 3-kinase and other signaling pathways. J Cell Sci 116:3471–3478.

Miyamoto Y, Yamauchi J, Tanoue A, Wu C, Mobley WC (2006) TrkB binds and tyrosine-phosphorylates Tiam1, leading to activation of Rac1 and induction of changes in cellular morphology. Proc Natl Acad Sci USA 103:10444–10449.

Musatov S, Roberts J, Brooks AI, Pena J, Betchen S, Pfaff DW, Kaplitt MG (2004) Inhibition of neuronal phenotype by PTEN in PC12 cells. Proc Natl Acad Sci USA 101:3627–3631.

Nägerl UV, Köstinger G, Anderson JC, Martin KA, Bonhoeffer T (2007) Protracted synaptogenesis after activity-dependent spinogenesis in hippocampal neurons. J Neurosci 27:8149–8156.

Niell CM, Meyer MP, Smith SJ (2004) In vivo imaging of synapse formation on a growing dendritic arbor. Nat Neurosci 7:254–260.

North KN, Riccardi V, Samango-Sprouse C, Ferner R, Moore B, Legius E, Ratner N, Denckla MB (1997) Cognitive function and academic performance in neurofibromatosis. 1: consensus statement from the NF1 Cognitive Disorders Task Force. Neurology 48:1121–1127.

Patapoutian A, Reichardt LF (2001) Trk receptors: mediators of neurotrophin action. Curr Opin Neurobiol 11:272–280.

Patterson SL, Grover LM, Schwartzkroin PA, Bothwell M (1992) Neurotrophin expression in rat hippocampal slices: a stimulus paradigm inducing LTP in CA1 evokes increases in BDNF and NT-3 mRNAs. Neuron 9:1081–1088.

Poo MM (2001) Neurotrophins as synaptic modulators. Nat Rev Neurosci 2:24–32.

Sasaki AT, Firtel RA (2006) Regulation of chemotaxis by the orchestrated activation of Ras, PI3K, and TOR. Eur J Cell Biol 85:873–895.

Song H, Poo M (2001) The cell biology of neuronal navigation. Nat Cell Biol 3:E81–88.

Threadgill R, Bobb K, Ghosh A (1997) Regulation of dendritic growth and remodeling by Rho, Rac, and Cdc42. Neuron 19:625–634.

Toni N, Teng EM, Bushong EA, Aimone JB, Zhao C, Consiglio A, van Praag H, Martone ME, Ellisman MH, Gage FH (2007) Synapse formation on neurons born in the adult hippocampus. Nat Neurosci 10:727–734.

Vaillant AR, Zanassi P, Walsh GS, Aumont A, Alonso A, Miller FD (2002) Signaling mechanisms underlying reversible, activity-dependent dendrite formation. Neuron 34:985–998.

Van Haastert PJ, Devreotes PN (2004) Chemotaxis: signalling the way forward. Nat Rev Mol Cell Biol 5:626–634.

Vlahos CJ, Matter WF, Hui KY, Brown RF (1994) A specific inhibitor of phosphatidylinositol 3-kinase, 2-(4-morpholinyl)-8-phenyl-4H-1-benzopyran-4-one (LY294002). J Biol Chem 269:5241–5248.

Vogel KS, Brannan CI, Jenkins NA, Copeland NG, Parada LF (1995) Loss of neurofibromin results in neurotrophin-independent survival of embryonic sensory and sympathetic neurons. Cell 82:733–742.

Wu X, Senechal K, Neshat MS, Whang YE, Sawyers CL (1998) The PTEN/MMAC1 tumor suppressor phosphatase functions as a negative regulator of the phosphoinositide 3-kinase/Akt pathway. Proc Natl Acad Sci USA 95:15587–15591.

Yeo GS, Connie Hung CC, Rochford J, Keogh J, Gray J, Sivaramakrishnan S, O'Rahilly S, Farooqi IS (2004) A de novo mutation affecting human TrkB associated with severe obesity and developmental delay. Nat Neurosci 7:1187–1189.

Zhu Y, Romero MI, Ghosh P, Ye Z, Charnay P, Rushing EJ, Marth JD, Parada LF (2001) Ablation of NF1 function in neurons induces abnormal development of cerebral cortex and reactive gliosis in the brain. Genes Dev 15:859–876.

Zhuo L, Theis M, Alvarez-Maya I, Brenner M, Willecke K, Messing A (2001) hGFAP-cre transgenic mice for manipulation of glial and neuronal function in vivo. Genesis 31:85–94.

Ziv NE, Smith SJ (1996) Evidence for a role of dendritic filopodia in synaptogenesis and spine formation. Neuron 17:91–102.